ABSTRACT

The problems of developing turbulent flow and heat transfer in the simultaneously developing regions of concentric annuli were studied both analytically and experimentally. For the analytical study, solutions were obtained from an integral viewpoint with a modified Reichardt's expression of the eddy diffusivity for momentum and a turbulent Prandtl number which was correlated from the present experimental work.

In the analytical study, it was assumed that the flow within the boundary layer was turbulent everywhere and in the experimental work, the flow was tripped at the starting position of the boundary layer. The fluid properties in the analysis were taken to be independent of temperature.

Experiments have been conducted on the effects of various factors on both the turbulent flow and heat transfer in the developing regions of concentric annuli. Air which had a Prandtl number of about 0.71 and represented gas flow in general, was used as the working fluid. Four annuli having radius ratios of 1.61, 2.31, 3.83 and 15.32 were used over a range of Reynolds numbers between about 20,000 and 110,000. The maximum axial lengths available for the experiment were between about 50 and 100 equivalent diameters depending on the respective radius ratios. All core tubes which were instrumented for temperature and power measurements were heated electrically to provide uniform heat fluxes throughout the test section.

The analytically and experimentally obtained velocity profiles for both the developing and fully developed flows through concentric

annuli confirmed that the conventional universal velocity profile of pipe flow can not be applied in the case of flow in non-circular ducts. Velocity profiles in the inner region of a concentric annulus were significantly affected by the Reynolds number, radius ratio and entrance length.

The hydrodynamic entrance lengths based on friction measurements were obtained for about 6 to 12 equivalent diameters from the present experimental work and these values were in good agreement with the prediction. However, the experimental values based on the fully developed velocity profile were between about 20 and 42 equivalent diameters. The entrance lengths evaluated from the axial turbulence intensity measurements were somewhere between those based on friction factor and velocity profile. Agreement between the proposed model of the eddy diffusivity for momentum and the experimental results was, in general, good.

The fully developed heat transfer was attained from both the analytical and experimental studies generally in an entrance length of less than 40 equivalent diameters for the air flow. For the very small Prandtl numbers, "pseudo thermal entrance length" was predicted. This showed that, even though the thermal boundary layer had extended itself across the flow duct, the generalized temperature profile continued to change until the flow was hydrodynamically fully developed. The values of Nusselt number for the case of the inner wall alone heated were always larger than those for the outer wall alone heated condition.

ACKNOWLEDGEMENT

The author is greatly indebted to Dr. Y. Lee who supervised and initiated the present work and also gave him valuable help and guidance throughout the course of the present study.

The author wishes to extend his gratitude to Dr. A. Feingold, Chairman, and other staff members of the Department of Mechanical Engineering, for their interest and encouragement throughout his stay in the Department.

Sincere thanks are also due to Mr. G. Toth and his technical staff, Department of Mechanical Engineering, and to the staff of the University Computing Center for their generous assistance.

The financial support of the National Research Council of Canada under the Grant No. NRC A-5175 is gratefully acknowledged.

A special debt of gratitude is due to the author's wife for her understanding and perseverance under the extremely difficult condition.

TABLE OF CONTENTS

LIST OF TABLES

INDEX OF FIGURES

NOMENCLATURE

A, A^+	=	function defined by Eq. (3. 38) and (3. 39), respectively
b	=	outside thickness of pitot tube
B, B^+	=	function defined by Eq. (3. 38) and (3. 39), respectively
C	=	constant
D	=	diameter
D^+	=	dimensionless function defined by Eq. (3. 41)
E	=	voltage
E^+	=	dimensionless function defined by Eq. (3. 41)
F^+	=	dimensionless function defined by Eq. (A. 2. 3)
G^+	=	dimensionless function defined by Eq. (A. 2. 4)
f	=	friction factor
F	=	force
G	=	mass flow rate
h	=	convective heat transfer coefficient
H	=	velocity profile shape factor defined by Eq. (2. 6)
I	=	amperage
k	=	mixing length constant; thermal conductivity
K	=	function defined by Eq. (2. 4)
L	=	heated length
m	=	function defined by Eq. (2. 4)
M_1	=	dimensionless mass flux defined by Eq. (A. 3. 5)
M_2	=	dimensionless momentum flux defined by Eq. (A. 3. 6)
n	=	constant
p	=	pressure; function defined by Eq. (2. 7)
q, Q	=	heat flux, Btu/hr. $ft.^2$ and Btu/hr. ft , respectively
q'	=	heat generation
q^+	=	dimensionless heat flux parameter

r	=	radial distance
r^+	=	dimensionless radial distance parameter, $r \cdot u^*/\nu$
r_1^{++}	=	dimensionless radial distance parameter, $r_1 \cdot u_2^*/\nu$
r_2^{++}	=	dimensionless radial distance parameter, $r_2 \cdot u_1^*/\nu$
R	=	radial distance defined by Eq. (3.21); result defined by Eq. (5.6); radius
R^+	=	dimensionless radial distance parameter, $R \cdot u^*/\nu$
R_2^{++}	=	dimensionless radial distance parameter, $R_2 \cdot u_1^*/\nu$
s	=	dimensionless parameter defined by Eq. (3.33)
t	=	temperature, °F
T, T_j^+	=	absolute temperature, °R; temperature defined by Eq. (3.53)
u	=	velocity in x direction
u^*	=	friction velocity, $(\tau_w/\rho)^{0.5}$
u^+	=	dimensionless velocity parameter, u/u^*
u_2^{++}	=	dimensionless velocity parameter, u_2/u_1^*
U^+	=	modified velocity parameter defined by Eq. (2.1)
v	=	velocity in radial direction
w	=	velocity in azimuthal direction, uncertainty in the independent variable
x	=	distance in flow direction from the entrance
y	=	distance from the wall
y^+	=	dimensionless distance parameter, $y \cdot u^*/\nu$
y_1^{++}	=	dimensionless distance parameter, $y_1 \cdot u_2^*/\nu$
y_2^{++}	=	dimensionless distance parameter, $y_2 \cdot u_1^*/\nu$
Y	=	modified wall distance defined by Eq. (2.1)
Y^+	=	modified distance parameter defined by Eq. (2.1)
c_p	=	specific heat at constant pressure
De	=	equivalent diameter of annulus, $2(r_2 - r_1)$
De^+	=	dimensionless equivalent diameter, $De \cdot u^*/\nu$

F_g	=	radiation geometry factor
F_ϵ	=	surface emissivity
Nu	=	Nusselt number
Pr	=	Prandtl number
Re	=	Reynolds number based on De
Re_d	=	Reynolds number based on D
Re_x	=	Reynolds number based on x
Re_θ	=	function defined by Eq. (2. 7)
St	=	Stanton number
V_B	=	anemometer output voltage
$V_{z'}$	=	anemometer bridge voltage at zero velocity
V_z	=	corrected voltage of V_z
w_R	=	uncertainty in the result

Greek Symbols

α	=	radius ratio, r_2/r_1
δ	=	thickness of hydrodynamic boundary layer
δ_j^*	=	dimensionless parameter, $\delta_j/\lvert r_m - r_j\rvert$ for adiabatic flow; $\delta_{tj}/(r_2 - r_1)$ for diabatic flow
δ_j^+	=	dimensionless hydrodynamic boundary layer thickness parameter, $\delta_j \cdot u_j^*/\nu$
δ_1^{++}	=	dimensionless hydrodynamic boundary layer thickness parameter, $\delta_1 \cdot u_2^*/\nu$
δ_2^{++}	=	dimensionless hydrodynamic boundary layer thickness parameter, $\delta_2 \cdot u_1^*/\nu$
δ_t	=	thickness of thermal boundary layer
δ_{tj}^+	=	dimensionless thermal boundary layer thickness parameter, $\delta_{tj} \cdot u_j^*/\nu$
Δ	=	displacement of pitot tube
ϵ	=	eddy diffusivity; emissivity

η	=	dimensionless parameter defined by Eq. (3.33)
θ	=	time
κ	=	thermal diffusivity
μ	=	viscosity
ν	=	kinematic viscosity
ρ	=	density
σ	=	eddy diffusivity ratio, $\varepsilon_H/\varepsilon_M$; Boltzmann constant
τ	=	shear stress
φ	=	function; azimuthal coordinate
φ_1, φ_2	=	functions defined by Eq. (2.2)
Ψ	=	dimensionless parameter defined by Eq. (3.36)

Superscripts

'	=	fluctuating component
—	=	mean

Subscripts

1	=	inner wall or inner wall region of annulus
2	=	outer wall or outer wall region of annulus
b	=	bulk
cr	=	critical
d	=	fully developed; based on diameter
e	=	entrance
H	=	heat
i	=	instantaneous; inner wall heated
j	=	refers to region 1 or 2 for k, r, T, u, y, De, ε, τ; refers to i or o for h, q, Nu, x/De
ℓ	=	value at the edge of the laminar sublayer

m	=	maximum
M	=	momentum
o	=	outer wall heated
p	=	purely thermal; pseudo developed for very small Pr
T	=	thermal
w	=	wall
x	=	local
δ	=	at the edge of the hydrodynamic boundary layer
δt	=	at the edge of the thermal boundary layer
max	=	maximum

CHAPTER 1

INTRODUCTION

A duct of circular cross section is a convenient geometry from an engineering point of view and, therefore, is of considerable practical importance. For this reason, many studies dealing with fluid flow and heat transfer in circular tubes have been made. However, the use of non-circular ducts is often necessary due to design requirements other than fluid flow.

An annular cross-section has wide engineering application and its fully developed flow cases, both laminar and turbulent, have been the subject of many analytical and experimental studies. In contrast, very few works on turbulent flow and heat transfer in the entrance regions of concentric annuli having constant cross-sectional areas can be found in the literature. However, this problem is of practical importance because the design of many heat transfer systems requires a detailed knowledge of flow conditions, heat transfer characteristics, geometry, etc.

As a fluid flows through a duct or channel, its velocity profile undergoes a change from its initial entrance form to that of a fully developed profile at some axial location downstream from the entrance. In addition to this, if a fluid flowing adiabatically into a duct or channel, enters a region having a wall temperature different from that of the fluid, thermal entrance effects are also present. This new temperature distribution takes various forms depending on the heat flux boundary conditions and past history of the fluid.

In this thesis, the problems of the developing turbulent flow and heat transfer in concentric annuli are studied analytically from an integral view-point based on a model of Reichardt's expression for the eddy diffusivity of momentum(1)* together with a new turbulent Prandtl number obtained from the present experimental work. Solutions are found for the case of adiabatic turbulent flow and for the case of heat transfer where one surface is uniformly heated and the other is insulated.

The aims of the present study, therefore, are to introduce a new model of the eddy diffusivity of momentum and to extend it to heat transfer; to test the analytical prediction based on the model against experimental results, and finally to draw some conclusions from it.

During the course of the present studies, a heat exchanger was designed and constructed to conduct the experimental studies. Although the results from the experimental works can not be as exhaustive as those of the analysis, the aims are to obtain sufficient experimental results to allow comparison with the analytical predictions and to verify certain assumptions made in the course of deriving the basic equations.

Throughout the analysis, the fluid properties are considered constant: to approach this idealization experimentally, the test data are to be obtained in such a way that the extrapolation of the data to a zero heating rate condition will be possible. Other conditions for both the analysis and the experiments are steady, constant wall heat flux, radial symmetry, and uniform free stream velocity and temperature distributions with the effects of natural convection and axial

---

* Numbers in parentheses designate the References at the end of the thesis.

conduction kept negligible. The flow will be tripped at the starting position of the boundary layer to be in accord with the analysis.

CHAPTER II

LITERATURE SURVEY

Until recently, the studies of flow and heat transfer in circular and non-circular ducts have been concerned primarily with three groups of problems.

The first group dealt with the development of the velocity profile in the entrance region of a duct with no heat transfer. The fluid is assumed to enter the duct at a uniform velocity. As the fluid moves down the duct, a boundary layer begins forming at the entrance and grows on the wall surface due to the fact that the fluid immediately adjacent to the wall has a velocity of zero. The fully developed velocity profile exists when the two edges of the boundary layers coincide.

The second group was concerned with the flow in which the velocity profile of the fluid is already fully developed but enters a section of duct having a wall temperature different from the temperature of the entering fluid. This is the problem of a purely thermal entrance region.

Finally, the third group was concerned with the so-called fully developed problems in which the heat transfer and friction parameters do not change along the length of the duct. The results can be applied to long ducts. For obvious reasons, the nature of turbulent flow and heat transfer under the fully developed condition has been studied extensively by many investigators over the last few decades.

Only recently has some attention been given to the case of simultaneous development of velocity and temperature profiles in the entrance region of circular ducts or annuli. Understanding of the flow characteristics and heat transfer in this region is of practical importance as these configurations are the most widely occuring. In technical applications, we are often more concerned with the development of the hydrodynamic and thermal boundary layers together, rather than merely the thermal boundary layer alone.

2.1 STUDIES OF HYDRODYNAMIC ENTRANCE REGION

As a fluid flows through a duct its velocity profile undergoes a change from its initial entrance form to that of a fully developed profile at an axial location far down-stream from the entrance. However, the fully developed flow cases,both laminar and turbulent, have been the subject of many analytical and experimental studies mainly because of their greater simplicity and wider engineering applications.

Since turbulent flow in circular tubes is the type usually encountered in practice, it has been studied extensively. One of the most rigorous studies of turbulent flow in a circular pipe was carried out by Deissler(2). Some studies have been made with hot-wire anemometers to determine velocity fluctuations, correlation coefficients, and the spectrum of turbulence. An investigation by Laufer(3) covers the structure of turbulent pipe flow quite thoroughly. Cremers and Eckert(4) measured the turbulence correlations with hot-wire anemometer in a triangular duct, and recently Clark(5) also used the hot-wire anemometer to study the turbulent boundary layers.

The problems of fully developed turbulent flow in a concentric annulus have been studied experimentally or analytically by many workers: Barrow[6], Lee and Barrow[7], Brighton and Jones[8], Rothfus et al.[9], Levy[10], Quarmby[11, 12], Michiyoshi and Nakajima[13], Wilson and Medwell[14], and Randhava[15]. The study of turbulent flow in rough surface ducts has been made by Kjellström and Hedberg[16], and Robertson et al.[17].

In contrast, little work on developing turbulent flow in a duct has been done. The earliest analytical studies on the entrance region of the turbulent flow in a circular duct appear to be those of Deissler[18] and Holdhusen[19]. Deissler used Von Karman integral techniques with his own logarithmic velocity distributions. Also in the works of Ross[20], Shapiro and Smith[21], and Bowlus and Brighton[22], there are studies of turbulent flow in the entrance region of a tube. More recently, Barbin and Jones[23] reported their measurements of mean velocities, turbulence intensities and Reynolds stresses in the inlet region of a smooth circular tube. Data are presented for the first 40 diameters of pipe length. They reported, however, that the fully developed flow was not attained in this length for a Reynolds number of 388, 000 but the wall shear stress and the static pressure gradient attained their fully developed values within the first 15 diameters. They also reported that velocity profiles at successive sections in the entrance region are not similar.

The influence of entrance configuration on turbulent velocity profiles was observed by Knudson and Katz[24]. The entrance region problems in the parallel plate configuration were studied analytically by Wang and Longwell[25].

The only studies of the turbulent flow of a fluid in the entrance region of a concentric annulus found in the literature have been reported by Rothfus et al.[26], Olson and Sparrow[27], Okiishi and Serovy[28], and Sridhar et al.[29].

Results of Rothfus et al.[26] (with annuli having radius ratios of 1.78 and 2.97) based on the ratio of the local apparent shear stress to the fully developed value,indicate an entrance region behavior which is quite different from that for turbulent flows in circular tubes and between parallel plates. The entrance lengths appear to be larger by a factor of ten than the typical circular tube entrance lengths and to be strongly affected by the Reynolds number. Since a circular tube and a parallel plate channel are special cases of the annulus, it is not clear why the results from concentric annuli should be so different.

To explore this apparent anomaly, Olson and Sparrow[27] investigated the entrance region by measuring the wall static pressure, for water flowing in annuli. They found that the length required to approach to within 5% of the fully developed pressure gradient was about 15 to 20 hydraulic diameters which are in general accord with entrance length results for tubes and parallel plates.

Okiishi and Serovy[28] studied the flow in the inlet region of two annular configurations using both square-edged and rounded entrances. With their apparatus they reported that they were able to obtain the fully developed turbulent flow based on the local velocity profile approaching its limiting value only for the case of the square-edged entrance. For the case of the rounded entrance, however, they reported that the length of the apparatus was insufficient.

Their maximum available test length was 35 equivalent diameters. Sridhar et al.[29], on the other hand, reported that the entrance lengths, based on the core velocity reaching a constant value, for the annuli with square-edged entrances were between 25 and 35 diameters, but the entrance lengths for the bellmouth entrances were about 10 to 15 equivalent diameters more than those of the square-edged entrances. Therefore, it can only be concluded that there is not the same consistency and good agreement among the different investigations as there is for the plain circular tube.

The flow in the entrance region of a duct or channel is obviously dependent on the shape of the inlet section, and possibly on the turbulence level outside the boundary layers. The flow in an entrance with a rounded inlet section is not the same as the flow existing in an entrance with a square-edged inlet section, as shown by experiments[27,28,29]. For a rounded entrance, a reasonably uniform velocity exists at the entrance and one can expect that the boundary layer will progress from laminar to turbulent. If the boundary layer is tripped right at the entrance using suitable tripping wires, it becomes turbulent without being preceded by a laminar boundary layer. To study the entrance region problems analytically, a variety of methods have been employed for the determination of the flow characteristics in this region. An overwhelming majority of these methods employ the usual boundary layer assumptions. (However, even in the case of laminar flow, difficulties have been encountered in obtaining solutions mainly because of the nonlinear terms in the momentum equation.) The value of such solutions depends very much upon the accuracy of the description of the eddy diffusivity for momentum along and across the duct.

Previous formulations for the fully developed regions of concentric annuli, e.g., Reynolds et al.[30], Quarmby[12, 31], Barrow and Lee[32], and Lee[33] have included certain assumptions which seem to be in fair agreement with experimental works.

Semi-empirical analyses on the prediction of the mean flow quantities near the hydrodynamic entrance, which resembles boundary layer over a flat plate, have been given[34], but a thorough treatment of the entire flow field from entrance to fully developed region is lacking. The free stream in the entrance region of a circular duct accelerates as the thickness of boundary layer grows unlike that in zero stream pressure gradient boundary layer flow and it loses its identity downstream as the boundary layer thickness becomes a value equal to the radius. Most of the reported velocity measurements in the entrance regions of circular pipes were by-products of studies of fully developed flow. For the case of concentric annuli, no measurement on eddy diffusivity distribution and turbulence could be found in the published works.

2.2 STUDIES OF THERMAL ENTRANCE REGION

It is a well known fact that thermal entrance effects are always present when a fluid flowing adiabatically into a duct enters a region having a wall temperature different from that of the fluid. On entering the heated section, a new temperature distribution will be set up within the fluid; this may take various forms depending upon the heat flux boundary conditions and past history of the fluid. At the cross section where heating commences, the temperature gradient in the fluid near the wall is theoretically infinite and decreases in the direction of fluid flow until a constant value is reached if constant fluid properties are assumed.

The thermal entrance region has been defined, either as that distance required for the local heat transfer coefficient to approach that of the fully developed value or, as the distance from the entrance to the cross section where the non-dimensionalized temperature profile becomes independent of the flow direction. Since velocity profile of the fluid entering a heat transfer passage is already fully developed, it is often called a "purely thermal entrance region" to distinguish it from a simultaneously developing entrance region.

Some of the theoretical and experimental studies on turbulent fluid flow and heat transfer in the entrance region of a circular tube can be found in the works cited in References 35 ~ 49. Thermal entry region studies between parallel plates were reported by Schlinger[(50)], Barrow and Lee[(51)], and Hatton and Quarmby[(52)].

For the purely thermal entrance region problem in the entrance regions of concentric annuli, the only pertinent analytical studies to date are those of Lee[(33)], Kays and Leung[(34)], Quarmby and Anand[(53, 54)], and Chen and Yu[(55)]. Some results of experimental works on the thermal entrance region heat transfer in annuli are reported by Farman and Beckmann[(56)], and Quarmby[(57)].

Kays and Leung[(34)] utilized empirical measurements to deduce temperature solutions for four radius ratios (5.22, 3.92, 2.66, 2.0) and for a number of Reynolds numbers. However, since their results were based on experimental measurements made with air, the solutions are, of course, limited to a fluid with Prandtl number 0.7 and are restricted to the particular radius ratios and Reynolds numbers of the tests.

Lee[33] studied the problem by means of momentum and energy integral equations along with a modified universal velocity profiles which were substantiated by his previous experimental work[58]. The modified universal velocity profile equation which he used was:

$$U^{+} = 2.5 \ln (1 + 0.4 Y^{+}) + 7.8 \left[1 - \exp\left(-\frac{Y^{+}}{11}\right) - \left(\frac{Y^{+}}{11}\right) \cdot \exp(-0.33 Y^{+})\right] \qquad (2.1)$$

$$(Y^{+} \geq 0)$$

where

$$Y^{+} = \frac{r_2^{+2} - r_m^{+2}}{r_2} - \left[\left(\frac{r_2^{+2} - r_m^{+2}}{r_2^{+}}\right)^2 - r_2^{+2} + r^{+2} + 2r_m^{+2} \ln\left(\frac{r_2^{+}}{r^{+}}\right)\right]^{0.5}$$

He derived the momentum eddy diffusivity, ε_M, from the universal velocity profile given by Eq. (2.1) and the momentum equation:

$$\varepsilon_{M/\nu} = \left[\tau(r)/\varphi_1 (Y^{+}) \cdot \varphi_2 (r^{+})\right] - 1 \qquad (2.2)$$

where

$$\varphi_1 (Y^{+}) = \frac{1}{1 + 0.4 Y^{+}} + \frac{7.8}{11} \left[\exp\left(-\frac{Y^{+}}{11}\right) - \exp(-0.33 Y^{+}) + 0.33 Y^{+} \cdot \exp(-0.33 Y^{+})\right]$$

and

$$\varphi_2(r^+) = - \frac{\left(\frac{r^{+2} - r_m^{+2}}{r^+}\right)}{\left[\left(\frac{r_2^{+2} - r_m^{+2}}{r_2^+}\right)^2 - r_2^{+2} + r^{+2} + 2r_m^{+2} \cdot \ln\left(\frac{r_2^+}{r^+}\right)\right]^{0.5}}$$

The results indicate that the heat transfer coefficient attains its fully developed value in less than 30 equivalent diameters and that the thermal entrance length is moderately dependent upon radius ratio, Reynolds number and Prandtl number.

Farman and Beckmann(56) reported their experimental study of entrance region heat transfer in an annulus. Water was used as the heat transfer medium and the radius ratio of the annular test section was 1.35. Measurements were made to determine the variation of heat transfer coefficient with flow for heat transfer sections of different length. From their investigation, the following empirical correlation was proposed:

$$Nu = 0.051 \ Re^{0.78} \ Pr^{0.4} \ (1/a)^{0.45} \ (L/De)^{\varphi} \qquad (2.3)$$

where

$$\varphi = -(1.39/Re^{0.196}) \text{ and } L \text{ is heated length.}$$

Recently Quarmby and Anand(53, 54) have studied the problem of thermal entrance region with two boundary conditions, i.e., either one wall has a constant temperature while the other is insulated or there is uniform heat flux at one annular surface. For both of the sublayers the momentum eddy diffusivity was evaluated from Deissler's expression(18). However, for the core region of the outside sublayers, they used the modified eddy diffusivity of Reichardt[1] which was used by Kays and Leung[34]. The eddy diffusivity of heat, ε_H, was obtained from ε_M through the Jenkins' expression for the ratio[59]. The solutions were given for four different radius ratios with Reynolds numbers from 20,000 to 40,000 and for Pr = 0.01, 0.7 and 1,000.

A similar type of study was carried out more recently by Chen and Yu[55]. However, they were mainly concerned with fluids having low Prandtl numbers, (e.g., liquid metals), for which the effects of variations in boundary conditions may be very important, and especially for the case of axially varying heat fluxes. Very recently, an experimental study in the entrance region of an annulus was given by Farber et al.[60]. High pressure carbon dioxide was their working fluid and two annuli (α = 1.47 and 1.96) were studied. Correlated heat transfer results were proposed with the form:

$$St = K \; Re^{-n} \; Pr^{-0.6} \; (T_w/T_b)^{-m} \tag{2.4}$$

where

$$n = 0.2$$

$$m = 0.31 \left[1 - \exp(-0.15 \cdot x/De)\right]$$

$$K = 0.024 \left[1 + 0.43 \exp(-0.35 \cdot x/De)\right] \quad \text{for } \alpha = 1.47$$

$$K = 0.026 \left[1 + 0.19 \exp(-0.35 \cdot x/De)\right] \quad \text{for } \alpha = 1.96$$

The nature of turbulent flow and heat transfer under fully developed conditions has been studied extensively by many investigators over the last three decades. Turbulent heat transfer in smooth circular tubes with variable fluid properties was studied by Deissler[61].

Corcoran et al.[62] measured experimental values of temperature and velocity gradients for the flow between parallel plates. More recently, Haberstroh and Baldwin[63], Lawn[64] and Gowen and Smith[65] reported the studies of fully developed turbulent heat transfer in the pipe flow.

Extensive experimental results for air flowing in a smooth annulus with a constant heat flux from the inner core tube under the fully developed conditions have been reported by many workers such as in References 6, 7 and 57.

Pickering[66] studied heat transfer experimentally with water flowing in an annulus. He also reviewed and compared the results of the theoretical and experimental works on heat transfer to turbulently flowing fluids in annuli. He concluded that the theoretical predictions of Maloney * exhibited a particularly good correlation with his experimental results. Some more studies on the heat transfer under the fully established turbulent flow condition with uniform internal heat flux in concentric annulus can be found in such studies as in Refs.[67, 68, 69, 70].

Reynolds et al.[30] tried to generalize the problems of heat transfer in concentric annuli and indicated the possibilities for superposition of their four fundamental solutions. These fundamental solutions were specified by the heat flux or wall temperature boundary conditions of the annuli. Only limited cases such as the fully developed heat transfer and thermal entrance region problems with arbitrarily prescribed heat flux have been solved.

---

* From Ref. 66.

2.3 STUDIES OF SIMULTANEOUSLY DEVELOPING ENTRANCE REGION

All of the thermal entry region solutions so far considered have been based on the idealization that the velocity profile is fully developed. Since heat transfer often occurs near the actual entrance of a tube or an annulus, the velocity profile is not developed but rather developing. Frequently the flow conditions or the design of a heat transfer section are such that the effects of the simultaneously developing region are significant. On the other hand, with very long flow passages, the entry length is only a small fraction of the whole length and then the effect can be negligible. However, with certain fluid and thermal boundary conditions, these entry effects might be very important and cognizance of them must be taken.

Since the emphasis of the present study is on the simultaneously developing entrance region, it is in order to make a brief review for the case of laminar flow through a duct for completeness.

One of the earliest analytical studies on the combined entry-length problem of laminar flow and heat transfer in a circular tube appears to be that of Kays(71). He obtained a numerical solution for Prandtl number of 0.71, employing Langhaar's velocity profiles(72). He reported the relationships for the mean and local Nusselt numbers for the three different boundary conditions.

The problem of laminar heat transfer in the entrance section of flat rectangular ducts has been studied by Sparrow(73). The flat ducts considered were two parallel planes with heat being transferred through each plane. He solved the two dimensional energy equation for laminar heat transfer using a parabolic velocity profile given as:

$$\frac{u}{u_\delta} = 2\frac{y}{\delta} - \left(\frac{y}{\delta}\right)^2 \qquad (2.5)$$

where u_δ is velocity at the edge of the boundary layer,
δ is the thickness of the boundary layer,
and y is the distance from wall where velocity is u.
Nusselt numbers were reported for the range of Prandtl numbers from 0.01 to 50.

The solutions for the family of circular tube and annuli for laminar flow with constant heat flux and various Prandtl numbers were given by Heaton et al.[74]. They linearized the energy equation by an approximation first introduced by Langhaar[72] in connection with the hydrodynamic problem, and they were then able to obtain a generalized entry region temperature profile which could be used in the energy integral equation.

The effects of various factors on the turbulent heat transfer and friction in the entrance regions of smooth passages were investigated analytically by Deissler[75]. He used integral heat transfer and momentum equations for calculating the thickness of the thermal and velocity boundary layers. The influence of Reynolds number, Prandtl number, initial velocity distribution, wall-boundary condition, and of variable fluid properties were studied. His results indicate that approximately fully developed heat transfer and friction are, in general, attained in an entrance length less than 10 diameters. The effect of initial velocity distribution on heat transfer in the entrance region was that the values of (Nu_x/Nu_d) for a uniform initial velocity distribution were higher than those for a fully developed velocity distribution. This result might be expected because of higher friction in the case of uniform initial velocity profile.

Recently a rather different procedure was employed by Barrow[76] and Roberts[77] for the turbulent heat transfer in the entry region of a pipe and a concentric annulus respectively. They used the concept of an "equivalent immersed body". However, the analyses were entirely based on experimental correlation, viz.: (1) a correlation for the velocity of the potential core; (2) a local skin friction correlation; (3) a modified Reynolds analogy factor; and (4) a shape factor of the turbulent velocity profile.

His predicted relation for the pipe[76] is,

$$Nu = \frac{0.258\ Re\ [1 + 0.008\ (x/D)]}{\left[\log_{10}\left(\frac{0.00815\ Re \cdot x/D}{H}\right)\right]^2} - 0.1432\ (1 + 0.008 \cdot x/D)\ (x/D) \tag{2.6}$$

where H is the velocity profile shape factor and equal to 1.4. The local bulk Nusselt number for annuli[77] was given by

$$Nu = \frac{Re\, Pr^{\frac{1}{3}}\ (1 + 0.01 \cdot x/De)\ \varphi_1}{1 - \left[\frac{4\,\varphi_1\ (1 + 0.01 \cdot x/De)}{Pr^{2/3}\ (1 + a)}\right] \cdot x/De} \tag{2.7}$$

where

$$\varphi_1 = 0.0065\ (Re_\theta)^{-1/6}$$

$$Re_\theta = \frac{Re\ (0.01 \cdot x/De)\ (p^2 - 1)}{4\,H\ (a - 1)}$$

and

$$p = \left[\frac{1 + a^{1-n}}{1 + \left(\frac{1}{a}\right)^n}\right] \quad \text{with} \quad n = 0.343$$

$H \simeq 1.4$

The correlation given by Eq. (2. 7) will be compared with those obtained from the present study in Chapter 6. Since the boundary layer-potential stream model is no longer applicable near the fully developed core region, the analysis does not permit the determination of Nu_d or entry length. They also made experimental investigations with air in the entry region of internally heated annuli using two radius ratios. The effects of boundary layer tripping wire size on the wall temperature distribution and local heat transfer coefficient were given in their studies.

The very recent work of Wilson and Medwell[78], which was reported during the closing stage of the present study[79, 80], relies upon the eddy distribution suggested by Levy[10] for fully developed turbulent annular flow with a constant universal mixing constant identical to that used in circular tubes. This assumption is not at all in agreement with the findings of both the analytical and experimental investigations of many workers even for the fully developed case[8, 10, 81]. Levy[10] himself did not use a universal mixing length constant for the inner region of concentric annuli.

It is apparant from the above review of studies on the turbulent flow and heat transfer in the developing region of a concentric annulus that the case in which velocity and temperature profiles are developing simultaneously has, generally speaking, not been completely investigated in most cases. The knowledge of velocity and temperature fields in the developing boundary layers is most important in understanding the problems of turbulent flow and heat transfer in a duct.

CHAPTER 3

ANALYTICAL STUDIES

3.1 BASIC EQUATIONS

In cylindrical coordinates, let r denote the radial direction, while φ and x denote the azimuthal and axial coordinates. The velocities corresponding to these coordinates are v, w, and u respectively. For the case of incompressible fluid flow, the Navier-Stokes equations for the cylindrical coordinates could be expressed in the following form(82):

$$\rho\left(\frac{\partial u}{\partial \theta} + u\frac{\partial u}{\partial x} + v\frac{\partial u}{\partial r} + \frac{w}{r}\frac{\partial u}{\partial \varphi}\right) = F_x - \frac{\partial p}{\partial x} + \mu\nabla^2 u \qquad (3.1.a)$$

$$\rho\left(\frac{\partial u}{\partial \theta} + u\frac{\partial u}{\partial x} + v\frac{\partial v}{\partial r} + \frac{w}{r}\frac{\partial v}{\partial \varphi} - \frac{w^2}{r}\right) = F_r - \frac{\partial p}{\partial r}$$

$$-\mu\left(\frac{v}{r^2} + \frac{2}{r^2}\frac{\partial w}{\partial \varphi}\right) + \mu\nabla^2 v \qquad (3.1.b)$$

$$\rho\left(\frac{\partial w}{\partial \theta} + u\frac{\partial w}{\partial x} + v\frac{\partial w}{\partial r} + \frac{w}{r}\frac{\partial w}{\partial \varphi} + \frac{vw}{r}\right) =$$

$$F_\varphi - \frac{1}{r}\frac{\partial p}{\partial \varphi} - \mu\left(\frac{w}{r^2} - \frac{2}{r^2}\frac{\partial v}{\partial \varphi}\right) + \mu\nabla^2 w \qquad (3.1.c)$$

The corresponding energy equation, if the properties c_p and k can be assumed independent of temperature, has the following form:

$$\rho \, c_p \, \frac{DT}{D\theta} = k \, \nabla^2 \, T + \frac{Dp}{D\theta} + q' + \mu \left(\frac{\partial u}{\partial r}\right)^2 \tag{3.2}$$

where

$$\nabla^2 = \frac{\partial^2}{\partial x^2} + \frac{\partial^2}{\partial r^2} + \frac{1}{r} \frac{\partial}{\partial r} + \frac{\partial}{r^2} \frac{\partial^2}{\partial \varphi^2} \ ,$$

$\frac{DT}{D\theta}$ is the substantial derivative of T, and q' is heat generation.

The continuity equation for incompressible steady flow is:

$$\frac{\partial u}{\partial x} + \frac{\partial v}{\partial r} + \frac{1}{r} \frac{\partial w}{\partial \varphi} + \frac{v}{r} = 0 \tag{3.3}$$

Even though flow is turbulent, the momentum and energy equations are still applicable if instantaneous values for the velocity, pressure and temperature are used. Since the fluctuations are random and chaotic, it is evident that the solution of the equations for turbulent flow is impossible at the present. Reynolds[83] modified the momentum equation by introducing the mean fluctuating values of the flow quantities in place of the instantaneous values. As the instantaneous velocity component is the sum of the mean component and fluctuating velocity component in the same direction, the transformation of the above Navier-Stokes equation due to Reynolds can be obtained by introducing:

$$u_i = u + u', \quad v_i = v + v', \quad w_i = w + w' \text{ and } p_i = p + p'.$$

Now Reynolds equation in cylindrical coordinates for incompressible steady flow in a straight duct of uniform cross section neglecting the body force have the following form:

$$\rho\left(u\frac{\partial u}{\partial x}+v\frac{\partial u}{\partial r}+\frac{w}{r}\frac{\partial u}{\partial \varphi}\right)=-\frac{\partial p}{\partial x}$$

$$-\left[\frac{\partial}{\partial x}\left(\rho\,\overline{u'^2}\right)+\frac{1}{r}\frac{\partial}{\partial r}\left(r\,\rho\,\overline{u'v'}\right)+\frac{1}{r}\frac{\partial}{\partial \varphi}\left(\rho\,\overline{u'w'}\right)\right]$$

$$+\mu\,\nabla^2 u \qquad (3.4.a)$$

$$\rho\left(u\frac{\partial u}{\partial x}+v\frac{\partial v}{\partial r}+\frac{w}{r}\frac{\partial v}{\partial \varphi}-\frac{w^2}{r}\right)=-\frac{\partial p}{\partial r}$$

$$-\left[\frac{\partial}{\partial x}\left(\rho\,\overline{u'v'}\right)+\frac{1}{r}\frac{\partial}{\partial r}\left(r\,\rho\,\overline{v'^2}\right)+\frac{1}{r}\frac{\partial}{\partial \varphi}\left(\rho\,\overline{v'w'}\right)-\frac{\rho\,\overline{w'^2}}{r}\right]$$

$$+\mu\left(\nabla^2 v-\frac{v}{r^2}-\frac{2}{r^2}\frac{\partial w}{\partial \varphi}\right) \qquad (3.4.b)$$

$$\rho\left(u\frac{\partial w}{\partial x}+v\frac{\partial w}{\partial r}+\frac{w}{r}\frac{\partial w}{\partial \varphi}+\frac{vw}{r}\right)=-\frac{1}{r}\frac{\partial p}{\partial \varphi}$$

$$-\left[\frac{\partial}{\partial r}\left(\rho\,\overline{u'w'}\right)+\frac{\partial}{\partial r}\left(\rho\,\overline{v'w'}\right)+\frac{1}{r}\frac{\partial}{\partial \varphi}\left(\rho\,\overline{w'^2}\right)-\frac{2(\rho\,\overline{v'w'})}{r}\right.$$

$$+\mu\left(\nabla^2 w+\frac{2}{r_2}\frac{\partial w}{\partial \varphi}-\frac{w}{r^2}\right) \qquad (3.4.c)$$

The corresponding equation for heat transfer in turbulent flow is:

$$u\frac{\partial T}{\partial x}+v\frac{\partial T}{\partial r}+\frac{w}{r}\frac{\partial T}{\partial \varphi}=\kappa\,\nabla^2 T$$

$$-\left(\frac{\partial}{\partial x}\overline{u'T'}+\frac{1}{r}\frac{\partial}{\partial r}r\,\overline{v'T'}+\frac{1}{r}\frac{\partial}{\partial \varphi}\overline{w'T'}\right) \qquad (3.5)$$

In Eq. (3, 4), the three normal stresses $-\rho\,\overline{u'^2}$, $-\rho\,\overline{v'^2}$, and $-\rho\,\overline{w'^2}$ and three shear stresses, $-\rho\,\overline{u'v'}$, $-\rho\,\overline{v'w'}$ and $-\rho\,\overline{u'w'}$ are called the Reynolds stresses or eddy stresses. The problem under consideration here is that of a developing steady, incompressible, constant cross-sectional duct flow. Therefore, all of the derivatives with respective to time, θ, and the body force are neglected.

In the absence of secondary flow, Eq. (3, 4, a) is sufficient for determining the axial velocity distribution. In most situations, axial thermal conduction and eddy diffusion are either zero or negligibly small, and terms $\frac{\partial^2 T}{\partial x^2} - \frac{\partial}{\partial x}(\overline{u'T'})$ can be ignored. For further simplification of Eq. (3, 4, a), the boundary layer approximation is applied, so that terms $\frac{\partial^2 u}{\partial x^2}$, and $\frac{\partial \overline{u'^2}}{\partial x}$ are also ignored.

Now for the axisymmetric flow (e. g. , pipe or concentric annulus), the appropriate equations of momentum are:

$$u\frac{\partial u}{\partial x} + v\frac{\partial u}{\partial r} + \frac{1}{\rho}\frac{\partial p}{\partial x} = \frac{\nu}{r}\frac{\partial}{\partial r}\left(r\frac{\partial u}{\partial r}\right) - \frac{1}{r}\frac{\partial}{\partial r}\left(r\,\overline{u'v'}\right) \tag{3.6}$$

and the equation of energy is:

$$u\frac{\partial T}{\partial x} + v\frac{\partial T}{\partial r} = \frac{\kappa}{r}\frac{\partial}{\partial r}\left(r\frac{\partial T}{\partial r}\right) - \frac{1}{r}\frac{\partial}{\partial r}\left(r\,\overline{v'T'}\right) \tag{3.7}$$

In Eq. (3, 7), the last term (barred term) represents the turbulent heat convection and it is analogous to Reynolds stress. Using the concept of eddy diffusivity, ε, the turbulence terms $-\overline{v'u'}$ and $-\overline{v'T'}$ are often expressed as $\varepsilon_M\,(\partial u/\partial r)$ and $\varepsilon_H\,(\partial T/\partial r)$ respectively. The turbulent shearing stress and that of the heat transfer is usually described as a flux of heat. Unlike its molecular counter-part (ν or κ), however, the eddy diffusivity is not a fluid property because it is a function of position and flow conditions[82]. Now with:

$$-\overline{u'v'} = \epsilon_M \left(\frac{\partial u}{\partial r}\right)$$

and,

$$-\overline{v'T'} = \epsilon_H \left(\frac{\partial T}{\partial r}\right)$$

equations (3. 6) and (3. 7) yield:

$$u\frac{\partial u}{\partial x} + v\frac{\partial u}{\partial r} + \frac{1}{\rho}\frac{\partial p}{\partial x} = \frac{1}{r}\frac{\partial}{\partial r}\left[r\ (\nu + \epsilon_M)\frac{\partial u}{\partial r}\right] \tag{3.8}$$

and,

$$v\frac{\partial T}{\partial r} + u\frac{\partial T}{\partial x} = \frac{1}{r}\frac{\partial}{\partial r}\left[r\ (\kappa + \epsilon_H)\frac{\partial T}{\partial r}\right] \tag{3.9}$$

Corresponding equations for the rectangular coordinates are:

$$u\frac{\partial u}{\partial x} + v\frac{\partial u}{\partial y} + \frac{1}{\rho}\frac{\partial p}{\partial x} = \frac{\partial}{\partial y}\left[\nu + \epsilon_M)\frac{\partial u}{\partial y}\right] \tag{3.10}$$

$$u\frac{\partial T}{\partial x} + v\frac{\partial T}{\partial y} = \frac{\partial}{\partial y}\left[(\kappa + \epsilon_H)\frac{\partial T}{\partial y}\right] \tag{3.11}$$

In the present study, we are concerned with the determination of velocity and temperature profiles in the developing region of a concentric annulus shown in Figs. 3. 1(a), 3. 1(b), and 3. 1(c). In the calculation of fluid frictions, entrance length and heat transfer, the velocity distribution must be determined from the momentum equation and used in the energy equation to solve the temperature profiles for the specified boundary conditions.

3.2 PHYSICAL MODEL

The physical model selected for a study of the development of the velocity and temperature profiles in the entrance region of a concentric annuli is the following:

(1) The flow is turbulent at all points along the ducts (within the boundary layer) and steady.

(2) The flow is of an incompressible Newtonian fluid and the fluid properties are constant.

(3) The velocity and temperature profiles are uniform across the entrance section, and the hydrodynamic boundary layer and thermal boundary layer thicknesses are zero at the entrance section.

(4) At the radius where the local mean velocity is a maximum, the shear stress is zero.

(5) The flow in the region outside the inner and outer boundary is a potential flow.

(6) While one wall heated and the other wall insulated.

(7) The usual boundary layer conceptions[82, 84]:

$$\frac{\partial u}{\partial y} \gg \frac{\partial u}{\partial x}, \quad \frac{\partial v}{\partial x}, \quad \frac{\partial v}{\partial y}$$

$$\frac{\partial p}{\partial x} \simeq \frac{dp}{dx}, \quad \frac{\partial p}{\partial y} \simeq 0 \quad \text{and}$$

$$\frac{\partial T}{\partial y} \gg \frac{\partial T}{\partial x}$$

will be applied and also, it is assumed that the viscous dissipation and work of compression are negligible compared with heat conduction.

Even for moderately higher Reynolds numbers, the flow in the vicinity of the inlet is preceded by a laminar boundary layer. According to Prandtl[85], in the presence of a laminar boundary layer near the entrance of a duct, the turbulent portion of the boundary layer behaves as if the boundary layer were turbulent all the way from the entrance. In experimental work, this idealization can be achieved by using a boundary layer tripping device at the entrance of the duct.

The turbulent fluid flow in the entrance region of a duct, compared with that in the fully developed region, is further complicated by the entrance configuration. For the rounded entrance, however, a reasonably uniform mean velocity is expected for a concentric annulus, in which the boundary layers grow on the inner and outer walls in the presence of a favorable pressure gradient. For the sharp-edged entrance, on the other hand, flow separation can be expected near the inlet. Therefore, the analytical studies will be attempted only for the former case.

It is not necessarily true that the radius of maximum velocity coincides with the point of zero shear stress[16, 58]. On the other hand, to calculate theoretically the zero shear radius or the shear stress at the radius of maximum velocity is not possible. However, the radius of zero shear will very likely be a radius not too different from the radius of the maximum velocity for a smooth concentric annulus. This point will be further discussed in Section 6.1.1.

3.3 MOMENTUM AND ENERGY EQUATIONS IN THE DEVELOPING REGION

The solution of the basic equations in the developing region is essentially one of finding the velocity and temperature distributions.

However, even though these equations, Eq. (3. 6) and Eq. (3. 7), can be greatly simplified, it is still extremely difficult if not impossible to solve because of non-linearities involved in the equations.

Here, we are studying the problems of annuli for the case in which the hydrodynamic and thermal boundary layers are developing simultaneously in the entrance region. The problem will be studied from an integral view-point based on a modified model of Reichardt's expression[1] for the eddy diffusivity of momentum and a new proposed turbulent Prandtl number.

Two boundary conditions will be considered for the heat transfer solutions, i. e. , the thermal boundary conditions on this solution are that one wall has a constant heat flux while the other is insulated. In axisymmetric flow, the distribution of the shear stress, τ, and heat flux, q, can be derived from the equations of momentum and energy.

The forces acting on the annular fluid element for the entrance region described in Fig. 3. 1(a) yields:

$$[p_x - (p_x + \frac{\partial p_x}{\partial x} dx)]\ 2\pi r\ dr + (\tau + \frac{\partial \tau}{\partial r}\ dr)\ 2\pi\ (r + dr)\ dx$$

$$- 2\pi r\ \tau\ dx = [- \frac{\partial p}{\partial x} + \frac{1}{r} \frac{\partial}{\partial r} (\tau \cdot r)]\ 2\pi r\ dr\ dx \qquad (3.12)$$

The time rate change of momentum in the cylindrical volume is:

$$\rho \frac{d}{d\theta} \left\{[(u + \frac{\partial u}{\partial x}\ dx) - u] + [(u + \frac{\partial u}{\partial r}\ dr) - u]\right\} 2\pi r\ dr\ dx$$

$$= \rho\ (u \frac{\partial u}{\partial x} + v \frac{\partial u}{\partial r})\ 2\pi r\ dr\ dx \qquad (3.13)$$

Employing the momentum theorem, the rate of creation of momentum is equal to the external forces, i. e. :

$$- \frac{\partial p_x}{\partial x} + \frac{1}{r} \frac{\partial}{\partial r} (\tau \cdot r) = \rho\ (u \frac{\partial u}{\partial x} + v \frac{\partial u}{\partial r}) \qquad (3.14)$$

Rearranging, we obtain:

$$\left(u\frac{\partial u}{\partial x} + v\frac{\partial u}{\partial r}\right) + \frac{1}{\rho}\frac{\partial p}{\partial x} = \frac{1}{\rho}\frac{1}{r}\frac{\partial}{\partial r}(\tau \cdot r) \tag{3.15}$$

Now the heat balance of a cylindrical fluid element in the developing region [See Fig. 3.1(b)] gives:

$$-2\pi r\, dr\, \rho u\, c_p \frac{\partial T}{\partial x} dx - 2\pi r\, dr\, \rho\, v\, dx \frac{\partial T}{\partial r} dr$$

$$= 2\pi\, dx \left\{ (r + dr)\left(q + \frac{\partial q}{\partial r} dr\right) - q \cdot r \right\} \tag{3.16}$$

Rearranging,

$$u\frac{\partial T}{\partial x} + v\frac{\partial T}{\partial r} = -\frac{1}{c_p \rho r}\frac{\partial}{\partial r}(q \cdot r) \tag{3.17}$$

Eqs. (3.15) and (3.17) in combination with Eqs. (3.8) and (3.9) yield:

$$\frac{\tau}{\rho} = (\nu + \epsilon_M)\frac{\partial u}{\partial r} \tag{3.18}$$

and,

$$-\frac{q}{c_p \rho} = (\kappa + \epsilon_H)\frac{\partial T}{\partial r} \tag{3.19}$$

The velocity and temperature distributions, u and T, for a given wall heat flux and fluid flow may be determined from Eqs. (3.18) and (3.19) if ϵ_M and ϵ_H are both known. To obtain the velocity profiles in the developing regions of concentric annular ducts, a model of eddy diffusivity for momentum is proposed. The proposed model, is, in principle, based on the model of Reichardt for a circular tube[1], but taking into account the radius ratio of the two ducts as well as the similarity of the function for ϵ_M in the direction of flow. An empirical correlation function is obtained from the experimental studies for the calculation of the thermal eddy diffusivity, ϵ_H.

3.4 ADIABATIC TURBULENT FLOW IN THE DEVELOPING REGIONS

In the previous section, the momentum and energy equations were derived which can be used in calculating turbulent flow for the concentric annuli.

In this section we shall modify the Reichardt's expression for the eddy diffusivity of momentum, so that it can be applied to the entire developing turbulent regions of a concentric annulus. Then, we shall proceed to the solutions for the turbulent velocity distributions in the entrance regions. The momentum integral equation of the developing turbulent boundary layer will be developed in a general manner, so that, from it, we can deduce the hydrodynamic entrance length. Finally the local friction factors will be obtained from the usual definitions.

Whenever a fluid enters a duct, the boundary layers start to develop. The fully developed velocity profiles exist after the two edges of the boundary layers coincide if properties remain constant. The flow in the entrance section is obviously dependent on the shape of inlet section.

3.4.1. Eddy Diffusivity for Momentum and Velocity Profile

The analysis of the entrance region problems requires a solution for velocity profile and the value of such a solution depends very much upon the accuracy of the description of the eddy diffusivity for momentum along and across the duct. The most interesting feature of the study on turbulent fluid flow in a concentric annular duct is the complete failure in application of the conventional "universal velocity profile" or "law-of-the-wall"[8, 11, 81].

Since the assumption of an eddy diffusivity of zero at the pipe center line is not realistic, Reichardt[1] proposed the following expression for ϵ_M, based on experimental data for the turbulent core in a smooth pipe:

$$\frac{\epsilon_M}{\nu} = \frac{kR^+}{6}\left[1 - \left(\frac{r}{R}\right)^2\right]\left[1 + 2\left(\frac{r}{R}\right)^2\right] \qquad (3.20)$$

where k is a constant and equals to 0.4.

Integration of Eq. (3.18) with Eq. (3.20) and the linear variation of the time-averaged shear stress yields a velocity profile which is in excellent agreement with experimental results for the turbulent core flow[84].

Levy[10] and Roberts[86] both derived expressions for the velocity profiles in turbulent flow through the fully developed region of a concentric annulus, assuming that the expression of Eq. (3.20) would be applicable in a modified form.

Their expressions seem to be valid for both the inner and outer wall regions of a concentric annulus (with appropriate values being given to the constant k for the inner wall regions).

In the present study, we further postulate that Reichardt's expression for the eddy diffusivity of momentum can be applicable to the entire developing turbulent flow regions on both sides of the concentric annulus with proper modification for the regions remote from the wall, thus:

$$\left(\frac{\varepsilon_M}{\nu}\right)_j = \frac{k_j}{6}\left|R_j^+ - r_j^+\right|\left[1 - \left(\frac{R_j - r}{R_j - r_j}\right)^2\right]\left[1 + 2\left(\frac{R_j - r}{R_j - r_j}\right)^2\right] \qquad (3.21)$$

where j refers to region 1 or 2:

$$R_j = r_1 + \delta_1 \quad \text{or} \quad r_2 - \delta_2$$

$$r = r_1 + y_1 \quad \text{or} \quad r_2 - y_2$$

For regions close to each wall, we retain Deissler's expression for the eddy diffusivity[75] given by:

$$\left(\frac{\varepsilon_M}{\nu}\right)_j = n^2 u_j^+ y_j^+ \left[1 - \exp\left(-n^2 u_j^+ y_j^+\right)\right] \qquad (3.22)$$

where

$$n^2 = 0.0154.$$

Now that the eddy diffusivities, $\left(\frac{\varepsilon_M}{\nu}\right)_j$, are established for the entire developing fluid flow regions, the velocity profiles within the developing boundary layers can be derived using the assumption that zero shear stress occurs at the radius of maximum velocity (see Section 3.2) or at the edges of the boundary layers. Hence, equating the eddy diffusivities at the plane of zero shear (or at $y_j = \delta_j$), we obtain:

$$\left(\frac{k_2}{k_1}\right)_x = \frac{\delta_1}{\delta_2} \left(\sqrt{\frac{\tau_{w1}}{\tau_{w2}}}\right)_x \tag{3.23}$$

and,

$$\left(\frac{k_2}{k_1}\right)_d = \frac{r_m - r_1}{r_2 - r_m} \left(\sqrt{\frac{\tau_{w1}}{\tau_{w2}}}\right)_d \tag{3.24}$$

If it is assumed that the pressure is constant in the radial direction, force balance on annular fluid elements between r_1 and δ_1, and between δ_2 and r_2 yield the following equations:

$$\left(\frac{\tau_{w1}}{\tau_{w2}}\right)_x = \frac{r_2}{r_1} \frac{\left(2r_1\delta_1 + \delta_1^2\right)}{\left(2r_2\delta_2 - \delta_2^2\right)} \tag{3.25}$$

and,

$$\left(\frac{\tau_{w1}}{\tau_{w2}}\right)_d = \frac{r_2}{r_1} \frac{\left(r_m^2 - r_1^2\right)}{\left(r_2^2 - r_m^2\right)} \tag{3.26}$$

Therefore, Eqs. (3.23) and (3.24) in combination with Eqs. (3.25) and (3.26) give the following relation:

$$\left(\frac{k_2}{k_1}\right)_x = \frac{\delta_1}{\delta_2} (\alpha)^{\frac{1}{2}} \left(\frac{2r_1\delta_1 + \delta_1^2}{2r_2\delta_2 - \delta_2^2}\right)^{\frac{1}{2}} \tag{3.27}$$

and,

$$\left(\frac{k_2}{k_1}\right)_d = \left(\frac{r_m - r_1}{r_2 - r_m}\right)^{3/2} (\alpha)^{\frac{1}{2}} \left(\frac{r_m + r_1}{r_2 + r_m}\right)^{\frac{1}{2}} \tag{3.28}$$

Eqs. (3.27) and (3.28) give the relation between k_1 and boundary layer thickness for the given radius ratio in the entrance region or developed condition.

Now the shear-stress distribution within the boundary layers on both walls can be obtained from a force balance on an annular fluid element and expressed thus:

$$\left(\frac{\tau}{\tau_{wj}}\right)_x = \frac{r_j}{r} \left| \frac{r^2 - R_j^2}{r_j^2 - R_j^2} \right| \tag{3.29}$$

The basic governing equation, Eq. (3.18) can be rewritten incorporating non-dimensional parameters as:

$$\left(\frac{\tau}{\tau_{wj}}\right)_x = \left[1 + \left(\frac{\epsilon_M}{\nu}\right)_j\right] \left(\frac{du^+}{dy^+}\right)_j \tag{3.30}$$

For the regions near both walls, the integration of Eq. (3.30) with substitution of Eq. (3.22) gives:

$$u_j^+ = \int_o^{y_j^+} \frac{dy_j^+}{1 + n^2 u_j^+ y_j^+ \left[1 - \exp\left(-n^2 u_j^+ y_j^+\right)\right]} \tag{3.31}$$

where $\qquad y_j^+ \leq 26$

and the variation of shear stress is neglected.

For the turbulent regions remote from "wall" influence, the substitution of Eqs. (3.21) (3.29) into Eq. (3.30) gives:

$$\frac{r_j}{r} \left| \frac{r^2 - R_j^2}{r_j^2 - R_j^2} \right| = \left\{1 + \frac{k_j}{6} \left| R_j^+ - r_j^+ \right| \left[1 - \left(\frac{R_j - r}{R_j - r_j}\right)^2\right] \left[1 + 2\left(\frac{R_j - r}{R_j - r_j}\right)^2\right]\right\} \left(\frac{du^+}{dy^+}\right)_j \tag{3.32}$$

The integration of Eq. (3.32) gives the following expression for the velocity distribution in the turbulent fluid flow of the developing regions in concentric annuli[10, 79].

$$u_j^+ = \frac{1}{k_j} \ln\left[1.5\, y^+ \frac{1+\eta_j}{1+2\eta_j^2}\right] + \frac{2 s_j (1-s_j)}{k_j (1+s_j)(2s_j - 1)} \ln \frac{1+\eta_j}{2}$$

$$+ \frac{1}{2} \frac{s_j (1-s_j)(1-3s_j)}{k_j (1+s_j)\left[s_j^2 + \frac{1}{2}(1-s_j)^2\right]} \ln\left(\frac{1+2\eta_j^2}{3}\right)$$

$$+ \frac{6}{k_j (1+s_j)} \frac{\ln\left[\eta_j (1-s_j) + s_j\right]}{\left[\left(\frac{1-s_j}{s_j}\right)^2 - 1\right]\left[2\left(\frac{s_j}{1-s_j}\right)^2 + 1\right]}$$

$$+ \frac{\sqrt{2}}{k_j} \frac{(1-s_j)\, s_j}{1+s_j} \frac{\tan^{-1}\sqrt{2} - \tan^{-1}\eta_j\sqrt{2}}{s_j^2 + \frac{1}{2}(1-s_j)^2} + C_j \qquad (3.33)$$

where $\eta_j = \dfrac{\delta_j^+ - y_j^+}{\delta_j^+}$

and $s_j = R_j^+ / r_j^+$

For the fully developed flow case, the general expression so obtained from Eq. (3.33) is identical to that of Levy[10] as expected.

In Eq. (3.32), the true shear stress distribution given by Eq. (3.29) was used. However, as long as the choice of the shear stress distribution is consistent with one that agrees well with experimental results for the pipe flow case, a function of shear stress distribution which would lead to a much simpler and more convenient velocity profiles than those given by Eq. (3.33) would seem to be more practical. According to Deissler's study[75], the variations across the flow boundary layers of the shear stress τ have a negligible effect on the velocity distributions.

Therefore, as an alternative to Eq. (3.29), the local shear stress within the boundary layers is assumed to be proportional to the distance as:

$$\left(\frac{\tau}{\tau_w}\right)_j = \frac{\delta_j - y_j}{\delta_j} \tag{3.34}$$

The substitution of Eqs. (3.21) and (3.34) in Eq. (3.30) give:

$$\frac{\delta_j - y_j}{\delta_j} = \left\{1 + \frac{k_j}{6} \left| R_j^+ - r_j^+ \right| \left[1 - \left(\frac{R_j - r}{R_j - r_j}\right)^2\right]\left[1 + 2\left(\frac{R_j - r}{R_j - r_j}\right)^2\right]\right\}\left(\frac{du^+}{dy^+}\right)_j \tag{3.35}$$

Integration of Eq. (3.35) gives the following expression for the velocity distribution in the turbulent flow of the developing region as an alternative of Eq. (3.33) (See Appendix 1 for the derivation):

$$u_j^+ = -\frac{3}{\psi}\,\delta_j^+ \ln\left| \frac{k_j \delta_j^+ - 4 k_j \delta_j^+ \eta_j^2 - \psi}{k_j \delta_j^+ - 4 k_j \delta_j^+ \eta_j^2 + \psi} \right| + C_j \tag{3.36}$$

where

$$\psi = \left(9 k_j^2 \delta_j^{+2} + 48 k_j \delta_j^+\right)^{\frac{1}{2}}$$

Now to determine the constant C_j for Eq. (3.33) and Eq. (3.36), each velocity profile is forced through a point which is found most suitable for joining the u_1^+ and u_2^+ based on the experimental works of the present study. The points were found to be $u_j^+ = 12.8$ and $y_j^+ = 26$.

While a value of 0.4 for $k_2 = \varphi(x)$ was found in the analysis because it has been shown[10, 80] that the mechanism of the flow outside of the radius of maximum velocity is very similar to that occuring in pipe flow, the value of $k_1(x)$ is to be calculated from Eq. (3.33) or Eq. (3.36) from known boundary conditions.

3.4.2 Momentum Integral Equation

The momentum integral equation for the developing hydrodynamic boundary layer in a concentric annulus can be written from the diagram described in Fig. 3.1.(a) in the idealized model. Applying the momentum principle, the relation between flow boundary layer thickness and distance along the duct is determined.

Since the force acting on the fluid in a space is equal to the rate of flow of momentum out of the space, the momentum equation for flow boundary layers can be written as:

$$d F_x = \left[\int_0^{\delta_j} \rho\, u_j^2\, 2\pi r\, dy_j\right]_2 - \left[\int_0^{\delta_j} \rho\, u_j^2\, 2\pi r\, dy_j\right]_1$$

$$+ \left\{\left[\int_0^{\delta_j} \rho\, u_j\, 2\pi r\, dy_j\right]_2 - \left[\int_0^{\delta_j} \rho\, u_j\, 2\pi r\, dy_j\right]_1\right\} u_{\delta j} \qquad (3.37.a)$$

where 1 and 2 refer to the planes indicated. Some rearrangement gives:

$$\tau_{wj}\, r_j\, dx + \tfrac{1}{2}\,(R_j^2 - r_j^2)\, dp = u_{\delta j}\, d\left[\int_0^{\delta_j} \rho\, u_j\, r\, dy_j\right]$$

$$- d\left[\int_0^{\delta_j} \rho\, u_j^2\, r\, dy_j\right] \qquad (3.37.b)$$

There is no shear force at δ_j because the velocity gradient is, from the definition, zero at the edge of the boundary layer.

Now, from the items, (1), (3), and (5), of the physical model in Section 3. 2, we have:

(1) the flow outside of the boundary layer is frictionless, i. e., $dp = - \rho \, u_{\delta j} \, du_{\delta j}$

(2) the boundary layer thickness is taken as zero at $x = 0$, and

(3) the flow is turbulent everywhere, $x \geq 0$.

Integration of Eq. (3. 37) with the assumption (1) above between $x = 0$ and $x = x$ with some rearrangement gives:

$$x_j = \int_{u_e}^{u_{\delta j}} \frac{\delta_j (R_j + r_j) \, \rho}{2 \, \tau_{wj} \, r_j} \, u_{\delta j} \, du_{\delta j} - \int_o^A \frac{dA}{\tau_{wj} \, r_j}$$

$$+ \int_o^B \frac{u_{\delta j} \, d\,B}{\tau_{wj} \, r_j} \qquad (3.38)$$

where

$$A = \int_o^{\delta_j} \rho \, u_j^2 \, r \, dy_j \qquad \text{and,}$$

$$B = \int_o^{\delta_j} \rho \, u_j \, r \, dy_j$$

Eq. (3. 38) can be made more general by stating it in terms of dimensionless parameters, as:

$$\left(\frac{x}{De}\right)_{M,j} = \int_{u_e^+}^{u_{\delta j}^+} \frac{\delta_j^+ \, (R_j^+ + r_j^+)}{2 \, r_j^+ \, (De^+)_j} \, u_{\delta j}^+ \, du_{\delta j}^+$$

$$-\int_{o}^{A^+} \frac{dA^+}{r_j^+ (De^+)_j} + \int_{o}^{B^+} \frac{u_{\delta j}^+ \, dB^+}{r_j^+ (De^+)_j} \tag{3.39}$$

where

$$A^+ = \int_{o}^{\delta_j^+} u_j^{+2} \, r^+ \, dy_j^+ \quad ,$$

$$B^+ = \int_{o}^{\delta_j^+} u_j^+ \, r^+ dy_j^+ \quad \text{and}$$

$$(De^+)_j = 2 r_1^+ (\alpha - 1), \quad \text{or} \quad 2 r_2^+ (1 - \alpha^{-1})$$

Now the Reynolds number is defined, as:

$$Re = \frac{\rho \, u_e \, De}{\mu} \tag{3.40.a}$$

and in terms of the non-dimensional parameters,

$$Re = (u_e^+)_j \, (De^+)_j \tag{3.40.b}$$

Substituting Eq. (3.40) into Eq. (3.39), and after some rearrangement, we obtain:

$$\left(\frac{x}{De}\right)_{M,j} = \int_{\frac{Re}{2}}^{E^+} \left[\frac{\delta_j^+ (R_j^+ + r_j^+)}{r_j^+ (De^+)_j^2} \, u_{\delta j}^+ - \frac{2}{r_j^+ (De^+)_j^2} \int_{o}^{\delta_j^+} u_j^+ \, r^+ \, dy_j^+ \right] dE^+$$

$$+ \int_{o}^{D^+} \frac{dD^+}{r_j^+ (De^+)_j} \tag{3.41}$$ *

---

* Detailed derivations are given in Appendix 2.

where

$$D^{+} = \int_{o}^{\delta_j^{+}} (u_{\delta j}^{+} - u_j^{+})\, u_j^{+}\, r^{+}\, dy_j^{+} \ ,$$

and,

$$E^{+} = \tfrac{1}{2}\, u_{\delta j}^{+}\, (De^{+})_j$$

One can compute $(x/De)_x$ for the given δ_j^{+} and Re from Eq. (3.41). The value of Re for a given r_1^{+} and δ_j^{+} will be obtained in the next section.

3.4.3. Friction Factor

The local friction factor based on the local shear stress at the wall and excluding momentum changes* due to a developing velocity profile is defined by:

$$f_j = \frac{\tau_{wj}}{\frac{1}{2}\,\rho\, u_b^2} \tag{3.42}$$

The local friction factor for the outer wall can be stated in dimensionless parameters which have been derived in the preceding section as:

$$f_{2x} = \frac{2}{(u_{b2}^{+2})_x} \tag{3.43}$$

Since it is assumed that the pressure is constant in the radial direction, force balance on the developing boundary layers yields the following equation:

---

* The effect of momentum flux changes on the friction factor for the developing boundary layers is discussed in Appendix 3.

$$\frac{dp}{dx} \cdot \left[(r_2^2 - R_2^2) + (R_1^2 - r_1^2) \right] = 2\,\bar{\tau}\,(r_1 + r_2) \tag{3.44}$$

Also for the outer boundary layer:

$$\frac{dp}{dx} \cdot (r_2^2 - R_2^2) = 2\,\tau_{w2}\, r_2 \tag{3.45}$$

Then, from Eq. (3.44) with Eq. (3.45), we have:

$$f_x = \frac{r_2\,(2\,r_2\,\delta_2 - \delta_2^2 + 2\,r_1\,\delta_1 + \delta_1^2)}{(2\,r_2\,\delta_2 - \delta_2^2)\,(r_1 + r_2)}\; f_{2x} \tag{3.46}$$

or, in dimensionless quantity, the average local friction factor f_x is:

$$f_x = \frac{r_2^+\,(2\,r_2^+\,\delta_2^+ - \delta_2^{+2} + 2\,r_1^{++} \cdot \delta_1^{++} + \delta_1^{++2})}{(2\,r_2^+\;\delta_2^+ - \delta_2^{+2})\,(r_1^{++} + r_2^{++})}\;\frac{2}{(u_{b2}^{\;+2})_x} \tag{3.47}$$

where the superscript ++ indicates that the parameters of the inner region are made dimensionless using the local shear velocity of the outer region for parameter conformity.

Therefore, the average local friction factor, f_x, can be calculated from the velocity profile given by either Eq. (3.33) or Eq. (3.36).

Bulk velocity is defined as:

$$u_b = \frac{\int_{dA} u\,dA}{\int_{dA} dA} \tag{3.48}$$

which can be written in dimensionless form for the entrance region as:

$$(u_{b2}^{+})_x = \frac{2}{r_2^{+2}\,(1-\alpha^{-2})}\left(\int_o^{\delta_1^{++}} u_1^{++}\, r^{++}\, dy_1^{++} + \tfrac{1}{2}\, u_{\delta 2}^{+}\,(R_2^{+2} - R_1^{++2}) + \int_o^{\delta_2^{+}} u_2^{+}\, r^{+}\, dy_2^{+}\right) \tag{3.49}$$

The Reynolds number defined by Eq. (3.40.a) can now be written as:

$$Re = \frac{4}{r_2\,(1+\alpha^{-1})\,\nu}\int_{r_1}^{r_2} u\, r\, dr \tag{3.50}$$

and in dimensionless parameters, as:

$$Re = 2\, r_2^{+}\,(u_{b2}^{+})\,(1-\alpha^{-1}),\ \text{ or }\ 2\, r_1^{+}\,(u_{b1}^{+})\,(\alpha - 1) \tag{3.51}$$

Now Eqs. (3.49) and (3.51) give the relation between Re and δ_j^+ or $u_{\delta j}^+$ for a given value of r_j^+.

3.4.4 Method of Solution and Results

With Eqs. (3.33), (3.36), (3.41), (3.47) and (3.51), the remainder of the calculation is entirely numerical.

To obtain u_j^+ (y, x/De, Re), $(x/De)_{x,M}$ and f_x for developing turbulent flow velocity profiles in a smooth concentric annulus, we proceed as follows:

1. Values of α and r_1^+ are prescribed.

2. Values of $u^+_{j,\ell}$ and $y^+_{j,\ell}$ based on the experimental works of the present study are found to be 12.8 and 26, respectively. From these values, C_j in Eq. (3.33) or Eq. (3.36) is obtained. Also a value of r_m^+ is assumed.

3. Knowing α, R_1^+ and r_m^+, compute k_1 from Eq. (3.27) for given values of δ_1^+ and δ_2^+. Here, it is assumed that the thickness ratio of the developing boundary layers equals that of the fully developed.

4. The results computed are substituted into Eq. (3.33) or Eq. (3.36), with C_j calculated from step (2) above and the calculations are continued until the boundary conditions satisfy Eq. (3.33) or Eq. (3.36).

5. For prescribed values of step (1) above, Re, $(x/De)_M$ and f_x are computed from Eqs. (3.41), (3.46) and (3.51) with the known velocity profiles obtained from step (4).

The results of the "mixing length" constant k_1 for the inner region of the developing turbulent flow in the concentric annuli are presented in Table 3.1 and plotted in Figs. 3.2 to 3.4. The relationship between r_1^+ and Reynolds number for various radius ratios is given in Fig. 3.5 with radius ratio as parameter.

The eddy diffusivities for momentum calculated from the proposed model are plotted in Figs. 5.44, 5.45 and 5.46 for the entrance region, and compared with the present experimental results. In Figs. 5.47, 5.48 and 5.49, the predicted eddy diffusivities are presented along with the present experimental results for the fully developed turbulent flow for three radius ratios of 1. 61, 2. 31 and 3. 83 with Reynolds number as the variable parameter.

The results of analytical velocity profiles are plotted in Figs. 3. 6 to 3. 11 for the various radius ratios and Reynolds numbers. In Fig. 3. 11, a comparison is given of the present analysis and some other correlations[7, 8, 12] for the radius ratio of 2. 31. There is reasonable agreement.

A typical boundary layer development in the entrance region is shown in Fig. 3. 12 for the radius ratio 2. 31 and Reynolds number 44, 000. The results of Eq. (3. 41) are presented in Fig. 3. 13 for the various Reynolds numbers with radius ratio as parameter. The results of the average friction factors and the entrance lengths in the developing region are plotted in Figs. 3. 14, 3. 15 and also tabulated in Table 3. 2 for the various radius ratios. The fully developed friction factors are given in Fig. 3. 16.

3.5 DIABATIC TURBULENT FLOW IN THE DEVELOPING REGIONS

In section 3.4, the turbulent flow velocity profiles in the entrance regions of a concentric annulus were developed from a new modified eddy diffusivity of momentum. In this section, we shall consider the problems of the combined hydrodynamic and thermal boundary layer development in the entrance regions where both the fluid velocity and temperature profiles are uniform. Employing the proposed empirical correlation of turbulent Prandtl number, the temperature distribution in these regions will be developed. The ratio of eddy diffusivities for momentum and for heat will be discussed in some detail. The energy integral equation will be then applied and the relation between boundary layer thickness and entrance length will be obtained in the similar manner as we considered in section 3.4.2. Finally, the local Nusselt numbers will be obtained for the various Reynolds numbers, Prandtl numbers and radius ratios.

3.5.1. Eddy Diffusivity for Heat

The ratio of eddy diffusivity of heat and momentum, ϵ_H/ϵ_M, which is often called the turbulent Prandtl number, plays an important role in most analytical studies to predict heat transfer coefficients in turbulent convective heat transfer[24]. To simplify the mathematical manipulation, many of these analytical results are based on the assumption that this ratio is equal unity. This simple assumption, $\epsilon_H/\epsilon_M = 1$, is equivalent to Reynolds' analogy. According to the experimental works reported in References, 7, 87, 88, 89 and also from the present experimental study, it appears that the ratio ϵ_H/ϵ_M is not equal to unity, but has a rather complicated relationship with other variables such as y, Pr, Re, α, etc.

From these works, it is at least clear that the ratio of eddy diffusivity for momentum and for heat, ϵ_H/ϵ_M is:

(1) greater than unity for air, and

(2) less than unity for liquid metal.

However, it must be pointed that the available experimental evidence is not sufficiently consistent to arrive at any concrete conclusion.

Consequently, some workers such as Leung and his associates [90] in their analysis on the heat transfer with turbulent flow in concentric annuli with constant and variable heat flux used the theoretical treatment of Jenkins[59]. Jenkins considered the heat conduction to or from an element of an eddy during its transverse to the main flow direction and from this consideration, a correlation for ϵ_H/ϵ_M was obtained. However, Leung et al. used a multiplying factor of 1.2 to fit the expression better to their experimental data.

Lee[33] divided the annular passage into two regions in his study of thermal entrance problems and then allowed the variation of ϵ_H/ϵ_M based on his previous experimental measurement as follows:

(1) $\epsilon_H/\epsilon_M = 1.4 - \frac{Y^+}{75}$ for $0 < Y^+ \leq 30$

(2) $\epsilon_H/\epsilon_M = 1.0$ for $Y^+ > 30$

where Y^+ is defined by Eq. (2.1)

Axial variation of the ratio of eddy diffusivity for momentum and for heat, $\varepsilon_H/\varepsilon_M$, in the thermal entrance region of a circular duct seems to be very little, according to Abberch and Churchill[40] from their experimental work; but the work of Hanratty[91] indicates that at smaller values of axial distance x, the values of eddy diffusivity for heat near the center of the pipe are seen to decrease for air. However, for the axisymmetric case as in the present study, this difference in the eddy diffusivity obtained by the two workers from their experiments is of little importance, since the heat flux is already small in the outer region. The present study shows also little effect on the variation with (x/De). Therefore, it is assumed in this study that $\varepsilon_H/\varepsilon_M$ variation in the entrance region of the concentric annulus is independent of the length, x.

Consequently, it appears that the problem of turbulent Prandtl number is still subject to further studies, both experimentally and analytically. The effects of turbulence structure, fluid properties and wall characteristics on eddy motion must be taken into consideration.

For the present study, an empirical correlation of turbulent Prandtl number, $\varepsilon_H/\varepsilon_M$, is formulated as a function of y_j^+ and radius ratio, α from the results of the present experimental work, as:

$$\sigma\,(y_j^+) = \frac{\varepsilon_H}{\varepsilon_M}\,(y_j^+) = 0.968\,\alpha^{0.045}\;y_j^{+0.031} \qquad (3.52)$$

In the analysis Eq. (3.52) is used for the case of Prandtl number greater than 0.5 because the experimental results were obtained using air as the working fluid.

In their very recent experimental work with flow ($Pr = 6 \sim 40$) in a rectangular duct, Mizushina and his co-workers[89] concluded that the effect of Prandtl number was not noticed for the range of Reynolds number between 10,000 and 24,000.

3.5.2. Temperature Profile

Temperature profile can be derived from the energy equation, given by Eq. (3.19), if the functions for the heat flux and the eddy diffusivity for heat are known. Eq. (3.19) in non-dimensional parameters can be given, as:

$$\frac{q}{q_i} = \left(\frac{1}{P_r} + \frac{\epsilon_H}{\nu}\right) \frac{\partial T_j^+}{\partial y_j^+} \tag{3.53}$$

where

$$T_j^+ = \frac{(T_w - T_j)\,\rho\, c_p\, u_j^*}{q_i} \quad \text{or} \quad \frac{(T_w - T_j)\,\rho\, c_p\, u_j^*}{q_o}$$

In Eq. (3.53), q_i refers to the uniform heat flux from the inner core tube, and in the case of outer wall heating, the subscript i in Eq. (3.53) is changed to o.

To solve Eq. (3.53), the distribution of heat flux across the flow section, $q^+ (y_j^+)$ must be known. Strictly speaking, in order to express the local heat flux, q, in terms of the known wall value, q_i, or q_o, it is not necessary to make any assumptions concerning the velocity distribution, because the local mass flow rate at any point, r, in the cross section can be calculated using the velocity profile given by Eq. (3.33). However, the expression for q resulting from this procedure is formidably complicated.

It has been shown by Barrow[92] that the choice of function for velocity profile to obtain the heat flux distribution across the annular space for the case of assymmetric heating has a minor effect on the final heat transfer calculation. To express the local heat flux q in terms of q_i in a concentric annulus, he assumed firstly that the local velocity is constant and equal to the bulk velocity. Secondly, he assumed a seventh power law velocity profile across the annular space in order to study the effect of a more realistic velocity distribution and the resulting expression was compared with the first case. The comparison showed that the more realistic velocity distribution predicted heat fluxes in the outer region of the maximum velocity of the annulus smaller than those calculated from the first case. However, since the heat fluxes are already very small in the outer region of the annulus, the assumption concerning the velocity field is not critical to the evaluation of local heat flux in the region of greatest importance.

Lee[33] further extended Barrow's contention in his study of the thermal entrance region, as:

$$q^+ (r^+)_x = \left(\frac{q}{q_i}\right)_x = \frac{r_1^+}{r^+} \left(\frac{r_{\delta t1}^{+2} - r^{+2}}{r_{\delta t1}^{+2} - r_1^{+2}}\right) \tag{3.54}$$

The **simplification** of the function for q is, therefore, not vital to the analysis but the variation given by Eq. (3.54) is closer to that in the real situation and is analogous to Eq. (3.36) in lieu of Eq. (3.33). In the present analysis, the function of q given by Eq. (3.54) will be retained for the reason just stated above. [See Appendix 4 for the derivation of Eq. (3.54)].

With the function for heat flux distribution known, the combination of Eq. (3. 21) or (3. 22) with Eqs. (3. 52) and (3. 53) yields the temperature profile upon integration. However, in the present heat transfer analysis, two fundamental boundary conditions are considered as mentioned in section 3. 2:

(A) The inner core tube alone heated at a uniform rate with the other tube wall insulated, and

(B) The outer tube alone heated at a uniform rate with the inner core tube wall insulated.

Therefore, Eq. (3. 54) for the boundary condition (A) becomes

$$(q_i^+)_x = \left(\frac{q}{q_i}\right)_x = \frac{r_1^+}{r^+}\left(\frac{r_{\delta t1}^{+2} - r^{+2}}{r_{\delta t1}^{+2} - r_1^{+2}}\right) \qquad (3.55.a)$$

and for the boundary condition (B)

$$(q_o^+)_x = \left(\frac{q}{q_o}\right)_x = \frac{r_2^+}{r^+}\left(\frac{r^{+2} - r_{\delta t2}^{+2}}{r_2^{+2} - r_{\delta t2}^{+2}}\right) \qquad (3.55.b)$$

where

$$r_{\delta tj} = r_1 + \delta_{t1} \quad \text{or} \quad r_2 - \delta_{t2}$$

Temperature Profile for the region very closed to the wall.

From Eqs. (3.22), (3. 52), and (3. 53) the temperature profile becomes

$$T_j^+ = \int_o^{y_j^+} \frac{dy_j^+}{\frac{1}{P_r} + n^2 u_j^+ y_j^+ \left[1 - \exp\left(-n^2 u_j^+ y_j^+\right)\right] \sigma\left(y_j^+\right)} \tag{3.56}$$

where $n^2 = 0.0154$

In deriving Eq. (3.56), it is assumed $q_j^+ = 1.0$. Eq. (3.56) is applicable to the both boundary conditions, (A) and (B).

Temperature Profile for the region away from the wall.

The temperature profiles in these regions must be considered separately for the two different boundary conditions (A) and (B) because the nature of the flow is affected by the flow regions, and they will be derived individually for each boundary condition.

For Boundary Condition (A):

Combination of Eq. (3.21) with Eqs. (3.52) and (3.53) yields:

$$T_1^+ = \int_{26}^{y_1^+} \frac{\frac{r_1^+}{r^+} \left(\frac{r_{\delta t1}^{+2} - r^{+2}}{r_{\delta t1}^{+2} - r_1^{+2}}\right) dy_1^+}{\frac{1}{Pr} + \frac{k_1}{6} \delta_1^+ \left(1 - \eta_1^2\right)\left(1 + 2\eta_1^2\right) \sigma\left(y_1^+\right)} + \text{Eq. (3.56)} \tag{3.57}$$

for $26 < y_1^+ < \delta_{m1}^+$,

and

$$T_1^+ = \int_{y_2^{++}}^{\delta_2^{++}} \frac{\frac{r_1^+}{r^+}\left(\frac{r_{\delta t1}^{+2} - r^{+2}}{r_{\delta t1}^{+2} - r_1^{+2}}\right) dy_2^{++}}{\frac{1}{Pr} + \frac{k_2}{6}\,\delta_2^{++}\,(1-\eta_2^2)\,(1+2\eta_2^2)\,\sigma\,(y_2^{++})} + \text{Eq. (3.57)} \tag{3.58}$$

$$\text{for } 26 < y_2^{++} < \delta_{m2}^{++}$$

where the superscript ++ indicates that the parameters of the outer region are made dimensionless using the local shear velocity of the inner for parameter conformity.

<u>For Boundary Condition (B):</u>

The same procedure as above gives:

$$T_2^+ = \int_{26}^{y_2^+} \frac{\frac{r_2^+}{r^+}\left(\frac{r^{+2} - r_{\delta t2}^{+2}}{r_2^{+2} - r_{\delta t2}^{+2}}\right) dy_2^+}{\frac{1}{Pr} + \frac{k_2}{6}\,\delta_2^+\,(1-\eta_2^2)(1+2\eta_2^2)\,\sigma\,(y_2^+)} + \text{Eq. (3.56)} \tag{3.59}$$

$$\text{for } 26 < y_2^+ < \delta_{m2}^+ ,$$

and

$$T_2^+ = \int_{y_1^{++}}^{\delta_1^{++}} \frac{\frac{r_2^+}{r^+}\left(\frac{r^{+2} - r_{\delta t2}^{+2}}{r_2^{+2} - r_{\delta t2}^{+2}}\right) dy_1^{++}}{\frac{1}{Pr} + \frac{k_1}{6}\,\delta_1^{++}\,(1-\eta_1^2)\,(1+2\eta_1^2)\,\sigma\,(y_1^{++})} + \text{Eq. (3.59)} \tag{3.60}$$

$$\text{for } 26 < y_1^{++} < \delta_{m1}^{++}$$

where the superscript ++ indicates that the parameters of the inner region are made dimensionless using the local shear velocity of the outer region for parameter conformity.

3.5.3 Energy Integral Equation

The energy integral equation for the thermal boundary layer that build up on a heated surface of a concentric annulus while the other surface is insulated can be written from an idealized model described in Fig. 3.1(b), as:

$$2\pi r_j q_j \, dx + \left(\int_o^{\delta_{tj}} c_p t \rho u \, 2\pi r \, dy \right)_1 +$$

$$c_p t_{\delta tj} \left[\left(\int_o^{\delta_{tj}} \rho u 2\pi r \, dy \right)_2 - \left(\int_o^{\delta_{tj}} \rho u 2\pi r \, dy \right)_1 \right]$$

$$= \left(\int_o^{\delta_{tj}} c_p t \rho u \, 2\pi r \, dy \right)_2 \tag{3.61}$$

where the subscripts on the parentheses refer to planes 1 and 2 in the diagram and the axial conduction neglected. Some rearrangement gives:

$$2\pi r_j q_j \, dx = d\left[\int_o^{\delta_{tj}} c_p t \rho u \, 2\pi r \, dy \right]$$

$$= 2\pi \; c_p t_{\delta tj} \; d\left[\int_o^{\delta_{tj}} \rho u r \, dy \right] \tag{3.62}$$

The physical model used here, as described in Section 3.2, is:

(1) $\delta = \delta_{tj} = 0$ at $x = 0$,

(2) $dq_{wj}/dx = 0$, and

(3) the flow is turbulent everywhere, $x \geq 0$.

An integration of Eq. (3.62) gives with these assumptions, as:

$$\left(\frac{x}{De}\right)_{x,T,j} = \frac{1}{De\, r_j q_j} \int_o^{\delta_{tj}} (T - T_{\delta t j})\; c_p \rho u r\, dy \tag{3.63}$$

Eq. (3.63) is completely general for both Boundary Condition (A) and (B); however, for the actual computation, Eq. (3.63) is now transformed into dimensionless forms utilizing various non-dimensional parameters explained as follows:

<u>For Boundary Condition (A)</u>

$$\left(\frac{x}{De}\right)_{x,T,i} = \frac{1}{2r_1^{+2}(\alpha-1)} \left[\int_o^{\delta_{t1}^+} (T_{\delta t 1}^+ - T_1^+)\, u_1^+ (y_1^+ + r_1^+)\, dy_1^+\right] \tag{3.64}$$

for $\delta_1^+ \geq \delta_{t1}^+$

and,

$$\left(\frac{x}{De}\right)_{x,T,i} = \frac{1}{2r_1^{+2}(\alpha-1)} \left[\int_o^{\delta_1^+} (T_{\delta t 1}^+ - T_1^+)\, u_1^+ (y_1^+ + r_1^+)\, dy_1^+\right.$$

$$+ u^+_{\delta 1} \int_{\delta_1^+}^{\delta_{t1}^+} (T^+_{\delta t1} - T^+_1)(y^+_1 + r^+_1)\ dy^+_1 \Big] \tag{3.65}$$

$$\text{for } \delta_1^+ < \delta_{t1}^+ .$$

For Boundary Condition (B)

$$\left(\frac{x}{De}\right)_{x,T,o} = \frac{1}{2r_2^{+2}(1-\alpha^{-1})} \left[\int_o^{\delta_{t2}^+} (T^+_{\delta t2} - T^+_2) u^+_2 (r^+_2 - y^+_2)\ dy^+_2\right] \tag{3.66}$$

$$\text{for } \delta_2^+ \geq \delta_{t2}^+$$

and,

$$\left(\frac{x}{De}\right)_{x,T,o} = \frac{1}{2r_2^{+2}(1-\alpha^{-1})} \Big[\int_o^{\delta_2^+} (T^+_{\delta t2} - T^+_2) u^+_2 (r^+_2 - y^+_2)\ dy^+_2$$

$$+ u^+_{\delta 2} \int_{\delta_1^+}^{\delta_{t2}^+} (T^+_{\delta t2} - T^+_2) u^+_2 (r^+_2 - y^+_2)\ dy^+_2 \Big] \tag{3.67}$$

$$\text{for } \delta_2^+ < \delta_{t2}^+ .$$

Eqs. (3.64) to (3.67) give the relation between $(x/De)_{x,T,j}$ and δ^+_{tj} for concentric annuli with the specified Boundary Conditions (A) and (B). For the solution of these equations both values of δ^+_j and δ^+_{tj} at the given section are required. The calculation procedure is presented in Section 3.5.5.

3.5.4 Heat Transfer

The local heat transfer coefficient and Nusselt number are defined in the usual way, as:

$$h_{x,j} = \frac{q_{x,j}}{(T_w - T_b)_{x,j}} \tag{3.68}$$

and

$$(Nu)_{x,j} = \frac{h_{x,j}\ De}{k} \tag{3.69}$$

In dimensionless form, Eq. (3.69) becomes;

$$(Nu)_{x,j} = \frac{(De^+)_j\ Pr}{(T_b^+)_{x,j}} \tag{3.70}$$

where

$$De_1^+ = 2r_1^+(\alpha - 1), \quad \text{and} \quad De_2^+ = 2r_2^+(1-\alpha^{-1})$$

Eq. (3.70) can be determined using the appropriate δ_{tj}^+ and by finding the local bulk temperature, $(T_b^+)_{x,j}$, of the fluid at any given value of (x/De).

Now the bulk temperature, $(T_b)_{x,j}$, is defined as:

$$(T_b)_{x,j} = \left(\frac{\int_{dA} T\,u\,dA}{\int_{dA} u\ dA} \right)_{x,j} \tag{3.71}$$

and, in terms of dimensionless parameters, as:

$$(T_b^+)_{x,j} = \left(\frac{\int_{r_1^+}^{r_2^+} T^+ u^+ r^+ dr^+}{\int_{r_1^+}^{r_2^+} u^+ r^+ dr^+} \right)_{x,j} \tag{3.72}$$

For Boundary Condition (A), the dimensionless local bulk temperature is:

$$(T_b^+)_{x,1} = \frac{2}{r_1^{+2} (\alpha^2 - 1) u_{b1}^+} \left[\int_o^{\delta_1^+} T_1^+ u_1^+ r^+ dy_1^+ \right.$$

$$\left. + \tfrac{1}{2} T_{\delta t1}^+ u_{\delta 1}^+ \left(R_2^{++2} - R_1^{+2} \right) + T_{\delta t1}^+ \int_o^{\delta_2^{++}} u_2^{++} r^+ dy_2^{++} \right] \tag{3.73}$$

$$\text{for } \delta_1^+ = \delta_t^+ ,$$

$$(T_b^+)_{x,1} = \frac{2}{r_1^{+2} (\alpha^2 - 1) u_{b1}^+} \left[\int_o^{\delta_1^+} T_1^+ u_1^+ r^+ dy_1^+ + u_{\delta 1}^+ \int_{\delta_1^+}^{\delta_{t1}^+} T_1^+ r^+ dy_1^+ \right.$$

$$\left. + \tfrac{1}{2} u_{\delta 1}^+ T_{\delta t1}^+ \left(R_2^{++2} - r_{\delta t1}^{+2} \right) + T_{\delta t1}^+ \int_o^{\delta_2^{++}} u_2^{++} r^+ dy_2^{++} \right] \tag{3.74}$$

$$\text{for } \delta_1^+ < \delta_{t1}^+ ,$$

$$\left(T_b^+\right)_{x,1} = \frac{2}{r_1^{+2}(\alpha^2 - 1)\, u_{b1}^+}\left[\int_0^{\delta_{t1}^+} T_1^+ u_1^+ r^+ dy_1^+ + T_{\delta t1}^+ \int_{\delta_{t1}^+}^{\delta_1^+} u_1^+ r^+ dy_1^+\right.$$

$$\left. + \tfrac{1}{2} u_{\delta 1}^+ T_{\delta t1}^+ \left(R_2^{++2} - R_1^{+2}\right) + T_{\delta t1}^+ \int_0^{\delta_2^{++}} u_2^{++} r^+ dy_2^{++}\right] \qquad (3.75)$$

$$\text{for } \delta_1^+ > \delta_{t1}^+$$

Likewise, the corresponding equations for the Boundary Condition (B) can be written with appropriate changes in the subscripts.

3.5.5 Method of Solution and Results

To obtain T_j^+ (y, x/De, Re, Pr), $(x/De)_{x,T,j}$, and $Nu_{x,j}$ for the simultaneously developing thermal boundary layer in a smooth concentric annulus, the following calculation procedures are used:

i. Values of α, r_1^+ and Pr are prescribed.

ii. To calculate u_j^+, $(x/De)_{x,M}$ and Re, steps (2) to (5) described in Section 3.4.4 are followed.

iii. Since the momentum boundary layer thickness, δ_j, is known at a given $(x/De)_{x,M}$ from step (ii) above, we now assume a certain value for δ_{tj} as the thermal boundary layer thickness.

iv. Temperature distributions are computed from Eq. (3.56) with Eqs. (3.57) and (3.58) for Boundary Condition (A) and with Eqs. (3.59) and (3.60) for Boundary Condition (B).

v. Thermal entrance length $(x/De)_{x,T,j}$ is then calculated from the assumed value of δ_{tj}, and the values of $(x/De)_{x,T,j}$ is compared to that of $(x/De)_{x,M}$.

vi. Repeat from step (iii) to step (v) until arriving at the condition $(x/De)_{x,M} \simeq (x/De)_{x,T,j}$.

vii. For prescribed values of step (i) above, Re, $(T_b^+)_{x,j}$, $(x/De)_{x,T,j}$ and $Nu_{x,j}$ are computed from the appropriate equations with the known values of δ_j^+ and δ_{tj}^+ obtained from step (vi).

The results of predicted temperature profiles, for the Boundary Condition (A), are plotted in Figs. 3.17 to 3.24 and the results for the Boundary Condition (B) in Figs. 3.25 and 3.26. The comparison of temperature profiles for the different Boundary Conditions is shown in Fig. 3.27. In Figs. 3.28, the typical developments of the temperature profiles are given for the radius ratio 2.31 and Reynolds number 44,000 for the Prandtl number 0.001.

The results of Nusselt numbers and the entrance lengths, $(x/De)_{x,T,j}$, are tabulated in Table 3.3 to 3.7 and local Nusselt numbers are plotted in Figs. 3.29 to 3.37 for various conditions. The predicted fully developed Nusselt numbers are shown in Figs. 3.38 to 3.41. In Fig. 3.42, the typical developments of the hydrodynamic and thermal boundary layers are given for the radius ratio 2.31 and Reynolds number 44,000. The effects of Prandtl number, radius ratio, Reynolds number and boundary condition on the $(x/De)_{d,T,j}$ are also shown in Figs. 3.43 to 3.45.

CHAPTER 4

EXPERIMENTAL STUDIES

In the previous chapter, the theoretical analysis was presented and the predicted velocity profiles, local friction factors, temperature profiles, Nusselt numbers, and both the hydrodynamic and thermal entrance lengths for the simultaneously developing regions of concentric annuli were evaluated.

The main object of the present study is to obtain experimentally momentum and heat transfer characteristics for turbulent fluid flow through a concentric annulus where both the velocity and thermal boundary layers develop simultaneously in the entrance region. The case of a uniform heat flux at the inner core surface is chosen as this is a more frequently imposed boundary condition. The problem is of practical importance because the design of many heat transfer systems requires a detailed knowledge of flow conditions, heat transfer characteristics, geometry, etc.

The main annulus assembly and instrumentation which were used in the present investigation are described in the following sections. Some details of calibration methods of orifice, pitot tubes, thermocouples, and hot-wire anemometers are also described. Finally, an experimental procedure for determining various local flow and heat transfer characteristics in the entrance region of an annulus are presented.

4.1 APPARATUS

The main annulus assembly used in the present investigation is shown in Fig. 4.1 schematically and in 4.2 (a). The essential dimensions are included in Table 4.1 and Fig. 4.1.

The outer tube has an inside diameter of 3.834 inches and this, together with four different sizes of inner core tubes, provides four annuli with radius ratios of 1.61, 2.31, 3.83 and 15.32.

The available dimensionless test length, x/De, should be long enough to ensure a fully developed flow both hydrodynamically and thermally. At the stage of designing this main heat exchanger, the available literature such as Refs.[27, 28, 33, 57] was examined carefully. From a summary of these works, it was concluded that the hydrodynamic entrance length of a concentric annulus was about 10 to 40 equivalent diameters, and the purely thermal entrance length was about 10 to 50 diameters for the ranges of moderate radius ratios and Reynolds numbers. Since it is deduced that the entrance length of the simultaneously developing region could not be very much different from that of the purely thermal entrance region, the available test lengths of the present annulus assembly (about 50 to 100 equivalent diameters) were considered to be long enough.

Air is drawn through a flow measuring orifice, 3.15 inches B.S. orifice[93], into a settling chamber and through a bell-mouthed contraction section into the test section by a blower located at the extreme down stream end as seen in Fig. 4.1. The settling chamber consists of filters, screens and flow straighteners, and a temperature measuring device is also provided inside. The bell-mouthed section is machined from a 12" x 12" x 8" plexiglas block and the blower fan is rated 300 cfm at 20 in. of water. The details of the annular entrance section are shown in Fig. 4. 3.

Along the test section, provision is made for the measurement of pressure drops and detailed exploration of the velocity and temperature field at various sections in the developing region. The locations of measuring sections and static pressure tappings are shown in Fig. 4. 4. Also, in Fig. 4. 5 are shown the positions of thermocouples on the surface of 3 core tubes. A specially designed traversing mechanism as shown in Fig. 4. 2 (b), carries the measuring instrument such as thermocouple or hot-wire probe so that the measurement of local flow and temperature fields will be possible. With this mechanism, the radial displacement of a probe is measured within 0. 001 inches by the electrical contact.

The electrically heated core tubes are supported at three points by electrically insulated 3-point carriers which provide radial adjustment of the core tube. To minimize flow disturbance in the developing flow region, one of these carriers is made of a fine stainless-steel wire. Figs. 4. 6 (a) and 4. 6 (b) show the details of a wire and a rod support mechanism. A revolving steel ball is provided at the tip of each rod support to accomodate the axial expansion of the core tube when it is heated.

The position of the core tube relative to the outer tube is determined by a depth micrometer gauge through several openings along the length and around the circumference of the test sections. In this way, the maximum eccentricity of the annulus was less than 3%. To minimize the axial misalignment, all the flanges are clamped together and then drilled and reamed simultaneously during the manufacturing stage. The entire outside section of the outer tube is covered with 4 inches I. D. and 6 inches O. D. fiberglass insulation to minimize the radial heat loss. The eventual heat loss through the insulation is measured by means of heat-meters consisting of two thermocouples whose hot junctions are set at a known radial distance apart. Three such heat-meters are used along the length of the test sections. Also provision is made for the measurement of conduction heat loss from the core heater tube to the electric lead cable. Two pairs of thermocouples are located at each known position of the cable near each tube end.

The assembled test section is mounted horizontally on several supports. Provision is made on the feet of these supports to provide a fine adjustment of height by screw mechanisms. Thus the horizontal alignment of the whole assembly could be easily accomplished by adjusting these screws. The horizontal alignment was checked by a surveying level. The maximum misalignment was 0.125 inches per 18 feet.

To minimize the pressure loss and the vibration effect from the blower, a conical diffuser and a flexible tube were used to connect the assembly annulus to the blower (See Fig. 4.1).

The inlet geometry as shown in Fig. 4.3 was constructed as close as possible to correspond to the idealized model as illustrated in Figs. 3.1(a) to 3.1(c). Boundary layer tripping wires were used on the entrance surfaces at $x = 0$.

The approximate size for these wires were calculated from the assumption that the dimensionless thickness of the laminar sublayer extends to about y_j^+ of 30. With this value known, several different wire gauges were tried and it was found that steel music wire of A. W. G. 23 gave the best performance for the test annuli with the radius ratio of 1. 61 and 15. 32, and of A. W. G. 30 for the radius ratio of 2. 31 and 3. 83 respectively.

4. 2 INSTRUMENTATION

4. 2. 1 Hot-wire Anemometry

A DISA 55D00 series hot-wire anemometer system in conjunction with miniature hot-wire probes (DISA 55F31) was used to detect the longitudinal turbulence level and to measure some of the local time-averaged flow velocity. The probe wire was platinum-plated tungsten, 5 microns in diameter and 1. 25 mm long. Its electrical resistance was 3. 5 ohms. *

To allow minimum disturbance of the flow, the smallest size of hot-wire probe and probe support were chosen. The longitudinal turbulence only was measured with a single wire probe because in the present study, we are mainly interested in the variation of the turbulence intensity in the flow direction. The initial turbulence intensity of the free stream air flow was also measured with a miniature hot-wire probe near the bell-mouth.

The signal from the constant temperature hot-wire probe was fed to the Anemometer, DISA 55D01, which was in turn connected to the Auxiliary Unit, DISA 55D25, and the output signal was fed to the Linearizer, DISA 55D10. The linearized turbulence signal was then integrated by RMS Voltmeter, DISA 55D35, and finally root mean

---

* Detailed technical data of hot-wire probes are given in DISA Probe Catalog No. 603.

squared values were either read on the dial of RMS meter, DISA 55D35, or on DVM, DISA 55D30, or on DVM, HP 2401C. The typical combination of the turbulence measurement system is shown in Fig. 4.7.

For the measurement of the time averaged velocity component, the signal from the Auxiliary Unit is directly fed to the integrated DVM, DISA 55D30 or HP 2401C.

4.2.2 Total Tube Probe and Pressure Measurement System

A total pressure tube probe was manufactured from a stainless steel hypodermic needle of 0.032 inches O. D. by 0.027 inches I. D. with a flattened tip as shown in Fig. 4.8 (a). For flow field investigation, both the total tube and the hot-wire probe were used. In order to minimize flow interference, it was desirable to make the total tube probe diameter small with respect to the annulus passage dimensions. However, at low velocities and with small tube diameters, the effects of viscosity cause an error in the total pressure reading[94, 95] which is difficult to correct for. (See Appendix 5 for this correction). Taking these facts into consideration the above dimensions were chosen.

To measure the main stream velocity profiles with the total tube probe at each section of the entrance region, 16 measuring ports of 0.14 inches diameter were provided as shown in Fig. 4.4. Also provided were 16 static pressure tappings of 1/16 inches in diameter along the outer tube. These were made by drilling through the wall from the outside and by carefully removing the burrs on the inside. A short length (3/8 inches) of about 1/4 inches O. D. brass tubing was then carefully soldered over the each hole.

Pressure was read on either a differential micro-manometer or a long alcohol manometer depending on the heads of the pressures. The micro-manometer used was DISA 55D41/42 Calibration Unit and it was rated to be accurate within about 0.001 inches of the manometer fluid, the specific gravity of which in the present study was 0.80.

4.2.3 Temperature Measurement System

Enamel and cotton insulated copper and constantan wires manufactured by Honeywell Inc. were used to make thermocouples which were used in connection with calibrated precision mercury-in-glass thermometers.

The junction of thermocouple probes was made by fusion welding of two ends of wires in the T/C Welder, Fisher 416. In the welding process, helium gas was used to prevent the oxidation on the junction of the thermocouples. A shiny clean metal surface which would minimize radiation error was obtained by this method.

The traversing thermocouple probe was made of a 40 S. W. G. Cu-constantan thermocouple junction mounted across a gap of 0.075 inches fork as shown in Fig. 4.9. The fork was made of epoxy resin to reduce the heat transfer along the metal stem of the probe. The nearest approach of the thermocouple hot junction to the heated surface was about 0.020 inches. The relative position of the probe to the heated surface was also obtained by electrical contact with the boundary.

To measure the axial wall temperature distribution in the entrance region, twelve thermocouples were embedded in the wall of the heating core tube. The locations of the thermocouples are shown in Fig. 4.5. At two out of the 16 foot-long sections as shown in Fig. 4.5, three pairs of thermocouples were installed to check the possible circumferential variation of wall temperature. All the thermocouple junctions along the test heaters were made by using a "split hot junction" method[58] which is illustrated in Fig. 4.8 (b). By this method, the shorting of the two thermocouple wires in the tube could be prevented. However, for the annulus having a radius ratio of 15.32, the inside diameter of the core heater tube, which was 0.152 inches, was too small to install more than two pairs of thermocouple in the downstream end of the annulus.

The ambient and settling box temperatures were also recorded using thermocouples. All the thermocouples were connected to the E. M. F. measurement devices such as N. R. Model 8687 potentiometer or HP 2401C DVM via two N. R. Model 8248, 16 points rotary selector switches for convenience and rapidity of temperature measurement.

Thermocouples were used with a common cold junction maintained in an ice-water mixture. The E. M. F. from thermocouples was also recorded by a two channel strip chart recorder, HP 4100B, and during the latter stage of study, a modified Hewlett Packard 2010K high speed Data Acquisition System was used. The accuracy of the system was rated as $\pm 0.01\%$ of the reading for 100 mv range with a resolution of 1 μv. Details of typical temperature measuring circuits are shown in Fig. 4.10.

4.2.4 Power and Its Measurement System

The wall of the inner core tube acts as a resistant heating element. Because of the high electric current required, the power to the test heater tube was applied via two transformers, a power-stat (variable transformer 13.4 KVA Super Electric Co.), and a step-down transformer (Dry Type 15KVA Marcus Co.). The power supply and instrumentation circuits are illustrated in Fig. 4.11.

The power dissipated in the heated core tube was determined by measuring the voltage drop across the two points of known distance along the test section and current. For the voltage drop measurement, the copper wires of the wall thermocouples were utilized. The voltage drops were read by a vacuum-tube voltmeter, HP 427A, with full-scale sensitivities ranging from 10 mv to 300 V A.C. which was rated with a measuring accuracy of $\pm$ 2% of full scale.

An ammeter, Yokogawa M015L124, with 10 ampere (full scale of 6 inches dial) was used to measure the electric current of the heater core tube in conjunction with a current transformer (GE JP-1) because of its high current flow (up to 700 Amp.). An Amprobe (RS-100) was also used to make a quick check of the current flow.

4.2.5 Orifice Plate

To measure mean velocity in each run, a B.S. 3.15 inches orifice[93] was manufactured. The orifice was calibrated against the total tube traversing of the flow across the annulus. The orifice plate was placed at the inlet section of the settling chamber as shown in Figs. 4.1 and 4.2 (a). The calibration of the orifice plate is described in the following section.

4.3 CALIBRATION OF INSTRUMENTS

All the instruments which were used in the present experimental study were described in the previous section and their functions and sensitivities were also explained. To check all those instruments against known standards is obviously very important to reduce error involved in any measurement.

Calibration can be accomplished by a comparison of the particular instrument with either (a) a primary standard, (b) a secondary standard with a higher accuracy than the instrument to be calibrated, or (c) a known input **source**.

In this section, the methods of calibration which were applied in the present study are described.

4.3.1 Calibration of Orifice Plate

The mean flow velocities measured from the pitot tube traversing were used to calibrate the orifice. The velocity distribution measurements were taken from five to nine cross sections along each annulus and also along the outer tube without the inner core for the wide range of Reynolds number. The results of calibration are shown in Fig. 4.12. The accuracy of the orifice was, therefore, estimated $\pm$ 1% for the range of Reynolds numbers studied.

4.3.2 Calibration of Hot-wire Probe

One of the most versatile instruments employed in fluid-dynamic measurements is the hot-wire anemometer, using as a transducer either a hot-wire, hot-film, or thermistor probe. With the constant temperature hot-wire anemometer which was used in the present experiment, the current is supplied to the bridge circuit from a direct-coupled amplifier and then the unbalance of the bridge due to fluctuations experienced by the hot-wire is applied to the input of the amplifier. The wire is kept at constant resistance by an electronic servo system and the instantaneous value of the current applied may therefore be assumed to equal the instantaneous thermal loss to the surroundings. If only the velocity is varied, the probe current will be a direct measure of the velocity. The constant-temperature anemometer is particularly well suited to studying phenomena requiring high frequency response[83].

The output voltage of a constant-temperature anemometer, as is well known, is a non-linear function of the flow velocity under measurement. This nonlinearity is not very important in measurements of small degrees of turbulence, in which case a small section of the calibration curve may be considered sufficiently linear. At a higher degree of turbulence, the distortion caused by the curvature of the calibration curve becomes noticeable and measurements at a wide range of mean flow velocities are difficult because of the consequent treatment of results obtained in both cases is not a very satisfactory solution and an electronic circuit is usually adopted to take care of the linearization problem[96].

Two limitations of the hot-wire anemometer require careful consideration. One is thermal inertia lag of the sensing element; the other is the nonlinear conversion of velocities to electrical signals. The hot-wire sensing element is usually of tungsten or platinum wire about 5 microns in diameter and a time constant of the order of 1 msec may be obtained. However, a recent feed-back system employed in practice such as in a DISA system may raise the upper frequency limit of the anemometer by a factor equal to maximum 400 k Hz[97].

In the present study, the calibration curves of a DISA 55F22 miniature hot-wire probe were made either using an electronic linearizer, DISA 55D10 or without using it. Two typical calibration curves are shown in Figs. 4.13 and 4.14.

During the calibration, the probe was placed in an air flow of known velocity which was measured by means of a total tube and a static pressure tap. DISA calibration unit (Type 55D 41/42) was used for this purpose along with a vertical adapter (DISA 55A67). Details of the operation of this equipment are given in the DISA service manual[97].

A calibration curve can be plotted in a variety of ways. One of the simplest methods is to plot the anemometer output voltage, V_B, as a function of velocity, u. Since this calibration curve is non-linear, plots are made of $(V_B/V'_z)^2 - 1$ vs. u, which provide nearly a straight-line, by a proper choice of V'_z [96, 97]. The value of V'_z may be obtained by multiplying 0.925 to the bridge voltage V_z at zero velocity. One can see a typical straight calibration curve from Fig. 4.13 in which the curve is plotted on a log-log scale.

If a linearizer is used, the output voltage of the anemometer can be linearized by making proper compensations for exponent and temperature changes. For this purpose, DISA 55D10 Linearizer was used.

Fig. 4.14 shows a typical calibration curve using a linearizer, from which one can read a local velocity, u, directly from the anemometer output voltage V_B.

4.3.3 Calibration of Thermocouple

All temperatures were measured with copper-constantan thermocouples. The thermocouples that were used in this study were calibrated by means of "fixed" points and interpolation, and also by direct reference to a secondary thermometer. Boiling distilled water, and well mixed water and ice made of the same distilled water were used as "fixed" points of 212°F and 32°F, and, also, the same ice-water mixture was taken as a cold junction reference point. A precision mercury-in-glass thermometer set, Fisher Nr. 15-155, was used as a secondary thermometer, a constant temperature oil bath with a temperature controlled heater and an agitator was used. In fact, the constant temperature oil bath used here was the part of a viscometer, M & L Test Equipment 4510.

A typical calibration curve of the thermocouples is shown in Fig. 4.15. Also shown in Fig. 4.15 are values from B.S. 1828 copper vs. constant thermocouple table.

4.4 EXPERIMENTAL PROCEDURE

The present experimental study has been made in two stages; (i) the developing adiabatic turbulent flow and (ii) the developing diabatic turbulent flow in four concentric annuli.

Before the annuli tests were made, an extensive preliminary test was carried out without any inner core tube. Then, four annuli having radius ratios of 1.61, 2.31, 3.83 and 15.32 were studied over a Reynolds number range of about 20,000 to 110,000 with air. According to Bankston[98], the laminarization due to the diabatic condition is found to occur at the Reynolds number well in excess of the minimum number for fully turbulent adiabatic flow, and the resulting heat transfer coefficients are much lower than those associated with fully turbulent flow at the same Reynolds number. However, the lowest Reynolds number used in the present study is about 20,000 which is well above that limit.

All the experimental work refers to the steady state which was attained in about 1 to 3 hours. A number of the tests were run a second time to affirm the reproducibility of the experimental results.

In the following section, some detailed procedures for the preliminary, adiabatic turbulent flow and diabatic turbulent flow tests will be given.

4.4.1 Preliminary Test

The outer tube was operated without a core tube in the preliminary test. The main purposes of this initial procedure were:

(1) to test for the apparatus by checking the friction and velocity data in the fully developed region against the well-established circular tube data,

(2) to establish a basis for comparison of the data, such as that for the turbulence, friction factors, velocity profiles, which would be obtained in subsequent experiments,

(3) to check the size of turbulent tripping wire so that the turbulent flow will start at the beginning of the inlet section, and finally

(4) to test the experimental technique to be used.

Having reached a steady condition, the settling box and the ambient room temperatures were recorded, and then, the static pressure, the complete velocity profiles and the turbulent velocities at each test section were explored by the static pressure taps, total tube and hot-wire probe for the entire developing region. The Reynolds numbers covered were about 20,000 to 150,000.

4.4.2 Velocity Profile and Friction Measurements

After the test sections were assembled and aligned, the concentricity of the core relative to the outer tube was checked by a depth gauge whose contact to the core tube was detected with an AVO-meter. The core tubes were supported by 3-point carriers as mentioned in Section 4.1 so that radial adjustments of the core tubes were easily accomplished. The eccentricity due to the lack of straightness of the tubes was negligible in most cases, but a maximum of 3% was noted with the annulus whose radius ratio was 1.61. The eccentricity of the order of 3% has no effect on the flow and heat transfer characteristic for the fully developed region of an annulus[7,27].

The velocity profiles obtained from all four annuli throughout the experiment were numerically integrated and used for calculating Reynolds numbers and also for the calibration of the orifice as discussed in Section 4.3.1.

Steady state conditions were maintained for at least one-half hour before any measurement was taken. The apparatus was considered to have reached a steady state in velocity measurement when the reading on the manometer for the orifice was unchanged for a reasonable time. Then, the settling chamber and the ambient room temperatures were recorded. The room temperature was recorded continuously by a strip chart recorder and efforts were made to keep it constant by adjusting the room ventilation system. The average ambient room temperature variation was within $\pm$ 1°F for each test. The range of Reynolds numbers studied were about 20,000 to 110,000.

4.4.3 Turbulence Measurement

The mean velocity and RMS values of the axial components of the velocity fluctuations were measured by the constant temperature hot-wire anemometer mentioned Section 4.2.1. Before the measurements were made, the hot-wire probes were calibrated as described in Section 4.3.2. The turbulence measurements were carried out only at late in night to avoid disturbances in the surroundings. The vibrations from the blower were damped out by connecting the annulus assembly to the blower with a flexible tubing.

The room temperature and inlet temperature were continuously recorded. Since the hot-wire systems were very sensitive to temperature changes, extreme care was taken to maintain a constant ambient room temperature. The room temperature was able to be kept nearly constant with $\pm$ 0.5°F during each test.

To maintain a steady condition, the blower was kept running for at least one-half hour and the hot-wire system was allowed about one or two hours warming up time before measurements were made.

To obtain uniform turbulence at the entrance section, five sets of fine wire grids were used in the settling chambers. (See Fig. 4.3). The probe was supported by a radial traversing mechanism. The range of Reynolds number covered in the test was between about 20,000 and 80,000.

4.4.4 Temperature Profile and Heat Transfer Measurement

The heat transfer runs were conducted with the fluid flow rate adjusted to give a particular Reynolds number. The power input to the heater tube was adjusted so that the maximum difference between the temperature of the heater wall and inlet temperature was about 20 to 120°F. Initially the annuli were allowed to run for a certain interval of time to reach a thermally steady state. This was detected by continuously recording the temperature of the heater on the strip chart recorder. A length of one to two hours was normally required. The room temperature was also held fairly constant for the test period. The average temperature change during the test was usually less than 1°F.

The following quantities were measured during the test:

(1) Temperature profiles in the developing region at four to seven cross sections,

(2) Axial and circumferential wall temperatures,

(3) Power dissipation in the heater core tube,

(4) Heat losses through the insulation and lead cables,

(5) Static pressures along the test length,

(6) Air flow rate,

(7) Room and inlet air temperature.

The procedure for temperature traversing was similar to that used in measuring flow velocities.

Throughout the analysis, the fluid properties were considered constant; to approach this idealization experimentally, several sets of experiments were conducted for each radius ratio, viz.: the heat flux of the heater core tube was changed from a certain minimum value to a certain upper value for a given Reynolds number.

The tests were studied over a Reynolds number range of about 20,000 to 110,000 for all four annuli. For the radius ratio of 15.32, the heat transfer measurements were confined to the fully developed condition, because of physical dimension of the core tube as mentioned in Section 4.2.3. A number of the test were run a second time to test the reproducibility of the experimental results.

The lower limit of the Reynolds number was fixed at about 20,000 to ensure fully turbulent flow and the upper limits of Reynolds number were governed by the capacity of the blower used. The experimental error is discussed in Section 5.4 and the sample calculations are given in Appendix 6.

CHAPTER 5

EXPERIMENTAL RESULTS

The experimental results of the present studies are presented in graphical and tabulated forms.

In order to test experimental apparatus in general, a series of tests on a single pipe were performed and the data obtained were carefully examined against the existing correlations for circular tubes to establish confidence in the apparatus and instrumentation to be used in the forthcoming experiments. The preliminary results obtained for the friction factor and velocity distribution in the circular pipe without a core tube were in good agreement with the circular pipe correlations readily available in the literature[23, 24, 75]. This agreement verified that the apparatus was reliable for further experiments. No constant error of sufficient magnitude to affect the results appeared to exist in the apparatus.

The results of the preliminary tests, and the experimental works for developing adiabatic and diabatic turbulent flow through concentric annuli are presented in the following sections.

5.1 PRELIMINARY TESTS

Extensive velocity profiles in a single tube (3.834" I. D.) were obtained in the developing region for a range of Reynolds number between about 30,000 and 150,000. Fig. 5.1 shows the velocity profiles at different sections in the entrance region for a Reynolds number of 29,400. The velocity measurements taken in the developing region of the circular tube are also plotted on u^+ vs. y^+ along with the analytical prediction of Deissler[75] in Fig. 5.2. Fig. 5.3 shows the variation of static pressure along the tube for the four different Reynolds numbers, where $(p_e - p)/(\rho u_b^2)$ is plotted versus (x/De). The experimental results of friction factors with and without trip wires in the entrance region of the tube are also shown in Figs. 5.4, 5.5 and 5.6 in which they are compared with previous correlations for circular tubes[75, 82, 84].

The results of turbulence measurements at five different locations in the developing region of a circular tube are also shown in Fig. 5.7.

5.2 ADIABATIC TURBULENT FLOW IN THE DEVELOPING REGIONS

5.2.1 Velocity Profile

Velocity distributions were measured for a range of Reynolds number between about 20,000 and 110,000 in concentric annuli with radius ratios of 1.61, 2.31, 3.83 and 15.32. The experimental Reynolds numbers are calculated with the equivalent diameter and the observed average velocities. Figs. 5.8 to 5.11 are the plots of some of the experimental velocity profiles obtained, where the ratio of u/u_b is plotted versus non-dimensional distance $(r-r_1)/(r_2-r_1)$. The theoretical result (Eq. 3.36) is also included in these figures for comparison. In order to determine the average velocity in the annulus, these local velocity profiles were numerically integrated around the annulus. Dividing the result by the cross-sectional area of the annulus gives the average velocity. These average velocities were also used for the calibration of the orifice as discussed in Section 4.3.1.

When the pitot tube is located very close to solid walls, where the local velocity changes rapidly, it does not sense the stagnation pressure at the center of the pitot tube opening. Correction for this is discussed in Appendix 5.

The velocity measurements taken in the inner and outer regions of each annulus are also plotted on u_j^+ versus y_j^+ coordinates in Figs. 5.12 to 5.19, inclusively. Figs. 5.12 to 5.15 show the comparison of experimental results with the predicted velocity profiles in the entrance region at the Reynolds number of 23,000. Typical non-dimensional velocity profiles for the fully developed annular flow are given along with the predicted in Figs. 5.16 to 5.19 for the Reynolds numbers ranging from about 23,000 tc 110,000 and for the radius ratios of 1.61, 2.31, 3.83 and 15.32, respectively.

To obtain the hydrodynamic entrance length (which will be discussed in Section 6.1.3) based on the local velocity profile, the variation of non-dimensionalized core velocity along the entry length of the annuli are plotted in Figs. 5.20 and 5.21 for Reynolds numbers between 23,000 and 110,000, and in Fig. 5.22, the variation of the velocity at the different radial location is plotted.

5.2.2 Pressure Drop and Friction Factor

The precise location of maximum velocity, r_{max}, within the annulus is important as the values of wall shear stresses depend on the square of this quantity. However, it must be pointed out that this is based on the assumption that the radius of maximum velocity coincides with the position of zero shear. (See Section 6.1.2 for the further discussion on this assumption).

The flatness of velocity profiles in the vicinity of the maximum velocity makes it difficult to locate r_{max} accurately. The radius of maximum velocity is usually obtained from a plot of velocity gradients against the radial distance. The velocity gradient, du/dy, is computed from the velocity profile measurements by the numerical differentiation method based on the principles of the Lagrangian interpolation of polynormials[99, 100]. The typical velocity gradient curves in the vicinity of maximum velocity are shown in Fig. 5.23. The radii of maximum velocity so obtained are summarized in Fig. 5.24.

The variations of static pressure measured along the annulus test sections are plotted in Figs. 5.25 to 5.28, where $(p_e - p)/(\rho u_b^2)$ is plotted versus (x/De) for Reynolds number ranging between 23,000 and 110,000. The overall friction factors obtained from the annuli installed with the appropriate boundary layer tripping wires are plotted in Figs. 5.29 to 5.33 along with those predicted in the present study. The experimental results of Olson et al.[27] and Okiish et al.[28] are also compared with the present work in Fig. 5.31. In Figs. 5.32 and 5.33, the effects of the Reynolds number and radius ratio on the distributions of the local average friction factor are shown along with the theoretical results. The results of the fully developed friction factors are also plotted in Figs. 5.34 and 5.35. Included in Figs. 5.34 and 5.35 are: (1) the prediction according to the hydraulic radius concept using the previous pipe correlations, (2) the analytical results of Lee[58] and (3) the present theoretical friction factors, given by Eq. (3.47). Fig. 5.36 shows the effect of radius ratio on friction factors for the fully developed region at the Reynolds number of 23,000.

5.2.3 Hydrodynamic Entrance Length

In general, the entrance length can be defined in the experimental work in terms of the length of duct needed for one of the following to approach its limiting value:

(a) the local pressure gradient or local wall shear stress,

(b) the local velocity profile,

(c) the local turbulent intensity distribution.

In the present study, a bell-mouth with a boundary layer tripping device was provided at the entrance of the annulus, and therefore, the velocity at the entrance was close to uniform and the velocity within the boundary layer was everywhere turbulent.

The experimental hydrodynamic entrance lengths based on the local friction factor, f_x, are presented in Figs. 5.37 and 5.38 along with the predicted results from Eq. (3.41) for four annuli having the radius ratios of 1.61, 2.31, 3.83 and 15.32. Also in Fig. 5.39, the experimental results on the hydrodynamic entrance lengths based on both the local friction factors and velocity profiles are plotted and compared the analysis. For the entrance length based on the local turbulent intensity distribution, the hot-wire anemometry was used and their results are presented in the following section.

5.2.4 Turbulence Intensity

In the present study, only the axial turbulence intensities were measured along the annuli passage at Reynolds numbers between about 20,000 and 80,000.

Fig. 5.40 shows the variation of the axial turbulence at five different axial positions along the annulus having a radius ratio of 3.83. Reynolds number was about 23,000 and the value of $(\sqrt{\overline{u'^2}}/u_2^*) \times 100$ is plotted vs. the dimensionless distance $(r-r_1)/(r_2-r_1)$. The results from the annulus having a radius ratio of 15.32 are also shown in Fig. 5.41 where Reynolds number is 42,000.

The effect of Reynolds number on the axial turbulence intensities in the fully developed region are plotted in Fig. 5.42 for Reynolds numbers ranging between 23,000 and 78,000, and the effect of radius ratio on the turbulence intensities is shown in Fig. 5.43. The non-dimensionalized radii of maximum velocity measured from the experimental velocity gradients are also included in each figure.

5.2.5 Eddy Diffusivity for Momentum

The experimental eddy diffusivities for momentum, ε_M, for the developing turbulent flow in the concentric annulus were evaluated from the experimentally obtained velocity profiles and pressure gradients.

From Eq. (3.18), the dimensionless eddy diffusivity for momentum, ε_M/ν, can be expressed, as:

$$\left(\frac{\varepsilon_M}{\nu}\right)_j = \left[\frac{(\tau/\rho)/\nu}{(du/dr)_j}\right] - 1.0 \qquad (5.1)$$

and the wall shear stress from the measured pressure gradient, as:

$$\tau_j = -(dp/dx)\left|\frac{r_m^2 - r^2}{2r}\right|_j \qquad (5.2)$$

From these two Eqs. (5.1) and (5.2), the experimental value of ε_M/ν, can be calculated knowing the velocity and pressure gradients. These gradients were determined by applying a numerical differential method based on the principles of the Lagrangian interpolation of polinomials[100] on the experimental results for velocity and static pressure.

Shown in Figs. 5.44, 5.45 and 5.46 are plots of experimental eddy diffusivities for momentum in the entrance region for the three annuli having radius ratios of 1.61, 2.31 and 3.83. The predicted values from the analysis are also included for comparison. In Figs. 5.47, 5.48 and 5.49, the predicted and experimental eddy diffusivities are compared in the case of the fully developed turbulent flow for the annuli having radius ratios of 1.61, 2.31 and 3.83 with Reynolds number as the variable parameter. The effect of radius ratio on the momentum eddy diffusivity is shown in Fig. 5.50.

Near the edge of the boundary layer or in the near vicinity of the radius of maximum velocity, it is extremely difficult to obtain accurate velocity gradients, because the local velocity gradient there becomes nearly zero and at the limit ε_M would become indeterminate. Experimental results are scattered much more in the developing region, but this is because the experimental evaluation of eddy diffusivity for momentum is very sensitive to any small discrepancy in the derivative of the actual velocity profile.

5.3 DIABATIC TURBULENT FLOW IN THE DEVELOPING REGIONS

5.3.1 Temperature Profile and Eddy Diffusivity for Heat

The variation of wall temperature along the axial direction in the entrance region of annuli having radius ratios of 1.61, 2.31, and 3.83 are shown in Figs. 5.51, 5.52 and 5.53, respectively. It was observed that the circumferential variation of wall temperature at the given sections was negligibly small for each heater core. The typical experimental radial temperature profiles at various values of (x/De) in the simultaneously developing region are plotted in dimensionless forms in Figs. 5.54(a) and (b) along with the predicted temperature profiles.

From these experimental temperature profiles, the experimental eddy diffusivity of heat, $\varepsilon_H/(Pr \cdot \kappa)$, can now be evaluated using the equation (3.19), as:

$$\left(\frac{\varepsilon_H}{Pr \cdot \kappa}\right)_j = \left[\frac{q/(c_p \cdot \mu)}{(dt/dy)_j}\right] - \frac{1}{Pr} \tag{5.3}$$

In using Eq. (5.3), the radial heat flux distribution at a given axial location must be known, and this has been extensively discussed in Section 3.5.2 of the present thesis. Therefore, the radial heat flux distribution given by Eq. (3.54) which was rearranged as:

$$q = q_i \frac{r_1}{r} \left(\frac{r_{\delta t1}^2 - r^2}{r_{\delta t1}^2 - r_1^2}\right) \tag{5.4}$$

was used in the evaluation of the eddy diffusivity for heat, ε_H.

Even the heat flux distribution is accurately prescribed (which is not impossible to obtain) the approximate nature of the radial heat flux distribution given by Eq. (5. 4) does not affect the evaluation of ϵ_H, especially in the outer region of the maximum velocity of the annular with assymetric heat from the inner core tube. This is because the heat fluxes are already small in that region. The determination of eddy diffusivity for heat is still less reliable than that for momentum as, with the experimental setup used in the present experiment, the local temperature measurement involves a larger margin of experimental error than in the case of local velocity measurement. Therefore, the values of $\epsilon_H/(Pr \cdot \kappa)$ were treated with care because of these uncertainties concerning the temperature gradient and local heat flux.

The temperature gradients in Eq. (5. 3) were determined applying the numerical differentiation method mentioned in the previous section on the experimental temperature profile. In Figs. 5. 55 and 5. 56, the experimental values of eddy diffusivities for heat in the entrance region obtained by Eqs. (5. 3) and (5. 4) are shown for two annuli having radius ratios of 2. 31 and 3. 83. Experimental eddy diffusivities for heat in the fully developed regions for the same annuli are plotted in Figs. 5. 57 and 5. 58 with Reynolds number as the variable parameter.

The measurement for the temperature gradients near the boundary layer edge is extremely difficult, therefore, the values taken for $\epsilon_H/(Pr \cdot \kappa)$ in this region are least reliable. However, in the fully developed region, the values of $\epsilon_H/(Pr \cdot \kappa)$ may be more reliable than those of ϵ_M/ν at the radius of maximum velocity where the latter becomes indeterminate.

5.3.2 Ratio of Eddy Diffusivity for Heat to Eddy Diffusivity for Momentum

The equations making use of the link between momentum and heat transfer require the information between two eddy diffusivities, ε_H and ε_M. This ratio which is sometimes called "turbulent Prandtl number", has been a subject of considerable investigation in the field of pipe flow. However, the information concerning this ratio in a concentric annulus is very little.

In Figs. 5.59 (a) and (b), the experimental values of $\varepsilon_H/\varepsilon_M$ in the fully developed region area shown for the two annuli having radius ratios of 2.31 and 3.83, in which the ratio, $\varepsilon_H/\varepsilon_M$, are plotted against y_j^+. The hatched areas are the approximate limit of about 95% of the experimental results obtained from the data reduction of the experimental work. It appears that this ratio is a function of α, Re, Pr as well as radial position in the flow[7, 87, 88, 89]. By cross plotting the experimental results of different radius ratios and Reynolds numbers, attempts have been made to correlate the ratio, $\varepsilon_H/\varepsilon_M$, for the developing and fully developed flows in the concentric annuli. Although the correlation so obtained is approximate, at least, even in the fully developed flow, it was thought that they can be applicable in the developing flow since the general shapes of ε_M/ν and $\varepsilon_H/(Pr \cdot \kappa)$ within the developing boundary layers are much alike with those in the fully developed region as seen from Figs. 5.45 and 5.55.

The broken lines in the Figs. 5.59 (a) and (b) are the correlation:

$$\frac{\varepsilon_H}{\varepsilon_M} = 0.0968\ \alpha^{0.045}\ y_j^{+0.031} \qquad (5.5)$$

which was used in the analysis, Section 3. 5. 1. Strictly speaking, Eq. (5. 5) is valid only for the radius ratio up to 16, but in the present analysis it is assumed that this correlation can be used up to $\alpha = 30$.

5. 3. 3 Heat Transfer Coefficient

Throughout the theoretical analysis, the properties are considered constant; to approach this idealization experimentally, the test data were obtained in such a way that the extrapolation of the experimental results to zero heating rate condition was possible, as previously stated in Section 4. 4. 4.

Fig. 5. 60 shows the effect of heat flux on the Nusselt numbers in which the fully developed Nusselt numbers, Nu_d, is plotted against heat flux, q_i, for the four annuli having radius ratios of 1. 61, 2. 31, 3. 83 and 15. 32 at the Reynolds numbers of 23, 000 and 77, 000. A smooth curve is drawn along the experimental points and finally it is extrapolated to the zero heat flux. The effect of heat flux on the surface temperature at a given axial position in the annuli is seen in Fig. 5. 61 for the Reynolds number of 77, 000.

The experimental heat transfer coefficient in terms of Nusselt number in the entrance region where both the temperature and velocity profiles are simultaneously developing are shown in Figs. 5. 62, 5. 63 and 5. 64 as a function of (x/De) for three annuli having radius ratios 1. 61, 2. 31 and 3. 83. The Reynolds number covered was between about 20, 000 and 110, 000.

For the purpose of comparison with analytical results, the figures are plotted along with the values extrapolated to zero heat flux from the experimental Nusselt numbers. The experimental heat transfer coefficients are also plotted in Figs. 5.65 and 5.66 as (Nu_x/Nu_d) vs. (x/De) for a wide range of Reynolds number and for three annuli with different radius ratios, respectively. In Fig. 5.65, the effect of Reynolds number on the values of (Nu_x/Nu_d) in the entrance region for a given annulus is seen, while the effect of radius ratio is seen in Fig. 5.66.

The experimental Nusselt numbers obtained in the fully developed region for the annulus having radius ratio of 2.31 are plotted against Reynolds number in Fig. 5.67 as an example. They are compared with those predicted or correlated by other investigators, namely, Davis[101], Walger[102], Kays and Leung[34] and Lee[33]. Also included are the prediction given by Eq. (3.70) and the values extrapolated to zero heat flux from the experimental results.

5.3.4 Thermal Entrance Length

The entrance length required for simultaneous development of both the velocity and thermal boundary layers was measured from the cross-plots of local Nusselt number distributions along the annulus. However, to determine the value of $(x/De)_{d,T}$ from these curves was extremely difficult since the spread of experimental data in the heat transfer field is usually high. In Fig. 5.68, the entrance lengths obtained from these cross-plots of the local Nusselt number are plotted with the approximate range of the experimental uncertainity experience in the data deduction. The solid lines indicate the predicted value from the present analysis, Eq. (3.65). The radius ratios of the three annuli were 1.61, 2.31 and 3.83 and the range of Reynolds number was between 20,000 and 120,000. The experimental data of Quarmby[57] are also plotted in the figure for comparison with the present study.

5.4 ESTIMATION OF EXPERIMENTAL UNCERTAINTIES

The experimental uncertainty is estimated using the method described by Kline and McClintock[103] with the estimates based on odds of 20 to 1. An estimate is made here of the probable error in the experimental results of fluid flow and heat transfer parameters presented in the experimental study. Only the major parameters, such as friction factor, Reynolds number, turbulent intensity and Nusselt number will be considered.

The results, R, is a given function of n independent variables $x_1, x_2, x_3, \ldots\ldots, x_n$, then,

$$R = R(x_1, x_2, x_3, \ldots\ldots, x_n) \tag{5.6}$$

Let w_R be the uncertainty in the result and $w_1, w_2, \ldots\ldots, w_n$ be the uncertainties in the independent variables. If the uncertainties in the independent variables are given with same odds, then the uncertainty in the result having these odds is given by Kline and McClintock[103] as:

$$w_R = \left[\left(\frac{\partial R}{\partial x_1} w_1 \right)^2 + \left(\frac{\partial R}{\partial x_2} w_2 \right)^2 + \ldots + \left(\frac{\partial R}{\partial x_n} w_n \right)^2 \right]^{\frac{1}{2}} \tag{5.7}$$

When $(\partial R/\partial x_i)$ terms in each parameter such as Re, f, $\sqrt{\overline{u'^2}}/u_b$, Nu, etc. were evaluated and substituted in Eq. (5.11), the following results were obtained.

(a) $$Re = \frac{De \cdot u_b}{\nu}$$

where the estimated uncertainties in each terms are:

De, $\pm$ 0.2%

u_b, $\pm$ 1.6%

$\nu^{(90)}$, $\pm$ 1.5%

Then, we have:

$$\left(\frac{w_R}{R}\right)_{Re} = 2.2\%$$

(b) $$f = \frac{\bar{\tau}}{\frac{1}{2}\rho u_b^2}$$

$$\left(\frac{w_R}{R}\right)_f = 3.5\%$$

(c) $$\text{Turbulence Intensity} = \sqrt{\overline{u'^2}}/u_b$$

$$\left(\frac{w_R}{R}\right)_{Turb} = 1.9\%$$

(d) $$Nu = \frac{q_i \cdot De}{k\,(t_w - t_b)}$$

$$\left(\frac{w_R}{R}\right)_{Nu} = 5.5\%$$

CHAPTER 6

DISCUSSION

Results from both the analytical and experimental studies described in the previous chapters enable us to evaluate the various characteristics of turbulent flow and heat transfer in the developing region of a concentric annulus. In the experimental study, it is essential to investigate in detail the local flow mechanism with particular emphasis on the velocity and temperature distributions, because not only can a check be made on the nature of the flow but the data so obtained would justify the underlying assumptions used in the analysis of heat transfer.

In order to test the experimental apparatus in general, and to refine the experimental technique to be used throughout the study, a series of tests on a single pipe were performed. The data so obtained were carefully compared with existing correlations for that case to establish confidence in the apparatus and instrumentation to be used. It can be seen from Fig. 5.1 that reasonably symmetrical velocity profiles were obtained from both the developing and fully developed regions. In Fig. 5.2, the experimental data from the single pipe are compared with Deissler's pipe flow correlation[75]. These results are also compared in the figure with the predicted velocity profile in the outer region of a concentric annulus to test a fundamental assumption made in the analytical work of Section 3.4 (page 35). The assumption was that the mechanism of the flow outside of the radius of maximum velocity in a concentric annulus is very similar to that occuring in pipe flow. It can be seen from the comparison in Fig. 5.2 that this assumption is reasonably justified.

The results of static pressure measurement along the test tube with a suitable tripping wire are shown in Fig. 5.3. The linear variation of the static pressure in the fully developed region can be seen. The friction factors from the pressure measurement are also shown in Figs. 5.4 and 5.6. The results are compared with Deissler's correlation[75] for the pipe flow. The results shown in Fig. 5.4 are those obtained in the developing region of the tube with a boundary layer tripping wire of W. G. 28 installed at the bell-mouthed entrance. The agreement between the experiment and Deissler's prediction is excellent. Because of the tripping wire at the entrance, the flow seems to be turbulent everywhere within the boundary layer without being preceded by a laminar boundary layer. On the other hand, as seen in Fig. 5.5, the results of friction factors obtained from the tube without the tripping wire installed exhibit the fluctuations near the entrance. The fluctuation pattern is affected significantly by Reynolds number. This is expected because there must be a fixed critical Reynolds number based on the length from the entrance, x, for a given tube and a flow condition. If $Re_{x,cr}$ is fixed, it can be shown that

$$\left(\frac{x}{D}\right)_{cr} = \frac{Re_{x,cr}}{Re_d} \qquad (6.1)$$

Therefore, with large Re_d, the length required for flow transition from laminar to turbulent becomes shorter and this trend is definitely observable in Fig. 5.5.

In Fig. 5.6, the fully developed friction factors are compared with the existing correlations widely used. The agreement between the present experimental results and the correlations is excellent.

The results of the axial turbulence intensity measurement are also shown in Fig. 5.7. The agreement between the present work and that of Barbin and Jones[23] is very good.

These agreements of the present work with previous investigation in the circular pipe without any core tube verify that the apparatus is reliable and the experimental procedure and data deduction method used are correct for further annular experiments. No constant error of sufficient magnitude to affect the results appeared to exist in the apparatus.

6.1 ADIABATIC TURBULENT FLOW IN THE DEVELOPING REGIONS

6.1.1. Velocity Profile

From the "mixing length constants" for the inner region of the developing turbulent flow in the concentric annuli as presented in Figs. 3.2, 3.3, 3.4, and in Table 3.1, it can be seen that, unlike $k_2 = 0.4$ for the outer regions of annuli of different radius ratios, k_1 is very sensitive to radius ratio α, Reynolds number, and axial distance x. Increase in the radius ratio at a given Reynolds number and location results in a large value of k_1, which could have been affected by the increase in the radial convexity of the flow boundary. As the flow approaches its fully developed form, the constant k_1 becomes smaller and at $\delta^* = 1$ it must be almost identical to the values Levy[10] also used in his work.

The velocity profiles predicted with the constant, k_1, shown in Figs. 3.6 to 3.10 illustrate the effects of various parameters, i.e., δ^*, α and Re. These analytical results are compared with the present experimental velocity measurement in Figs. 5.8 to 5.19 and these figures substantiate the basic assumptions made in the analysis for the developing velocity profile in a concentric annulus.

The velocity profiles in the outer wall regions vary almost not at all with radius ratio at a given value of (x/De) and are similar to those found in circular pipes. However, the velocity profiles for the inner wall region vary with radius ratio and Reynolds number at a given value of (x/De). Their difference from those for the outer wall regions becomes greater as the radius ratio, α, is increased.

To test the accuracy of the present analysis based on the modified eddy diffusivity for momentum given by Eq. (3.21), the predicted velocity profile was compared with those reported by other investigators[8, 12, 58] in Fig. 3.11. These velocity profiles are all for the fully developed flow in a concentric annulus. The good agreement of the present prediction with those of three other works indicates the soundness of the model of ε_M based on Eq. (3.21) in the fully developed flow.

It is interesting to note from Figs. 3.6 to 3.8 and also from Figs. 5.12 to 5.14 that within the boundary layer the dimensionless velocity profiles are almost independent of the axial distance for a given α, but are sensitive to the radius ratio, α. The velocity profile calculated from Eq. (3.36) which is based on the linear variation of shear stress distribution within the boundary layer is almost indistinguishable from that calculated from Eq. (3.33). Therefore, for practical purposes, Eq. (3.36) is sufficient and simpler to use than the complex expression of Eq. (3.33).

The fully developed velocity profiles, both the predicted and experimentally obtained, as shown in Figs. 5.16, 5.17, 5.18 and 5.19 illustrate that the velocity profiles in the outer region vary little with radius ratio and are very similar to the circular tube $u^+ - y^+$ logarithmic law in all four annuli. This has been also demonstrated previously in Fig. 5.2.

The velocity field in the inner region deviated with changes in radius ratio. The deviation of the inner portion from the outer is greater with larger radius ratio, and the trend is generally in accord with previous work[6, 7, 8, 10, 11]. This deviation of the velocity profiles for the inner regions from those for the outer regions could be explained as a result of the increased radial convexity associated with an increase in the radius ratio. It seems that the change in the concavity affects the turbulent mechanism of the flow very little but that this is not true for the convex boundary. These experimental velocity profiles were obtained with trip wires placed at $x \simeq 0$. The wire gauges of the steel music wire used were 23 for α of 1.61 and 15.32, and 30 for α of 2.31 and 3.83, respectively. With these boundary layer tripping wires placed at the entrance, the repeatability of flow development was very consistent throughout the experimental work. The axial turbulence intensities at the inlet ($x \simeq 0$) were as follows:

α	1.61	2.31	3.83	15.32
$\frac{\sqrt{\overline{u'^2}}}{u_e}$	0.016-0.019	0.005-0.018	0.002-0.01	0.003-0.005

The axial variation of the velocity at a given radial distance from the wall, especially at $r = r_{max}$, plotted in Fig. 5.20 to 5.22 will be discussed in Section 6.1.3.

In the present analysis, the radius of maximum velocity for the fully developed turbulent flow was predicted from Eq. (3.36) with appropriate boundary condition. The predicted values are compared with the experimental results of the present study and also with those of other workers[8, 34] in Figs. 5.23 and 5.24. The analytical values for r_{max} agree very well with the empirical correlation proposed by Kays and Leung[34]. Considering the difficulties in measuring the precise velocity distributions across a cross section, the agreement between the present experimental results and the prediction are thought good. Some improvement on the analysis could be made by modifying the assumption for the "mixing length constant", k_2.

It is often assumed, without any justification, that the position of zero shear coincides with the radius of maximum velocity. The shear stress for the fully developed flow in the axial direction is, from Eq. (3.4):

$$\tau_{x,r} = \mu \frac{du}{dr} - \rho \overline{u'v'} \qquad (6.2)$$

Thus the assumption of zero shear where $du/dr = 0$ is based on the assumption that $\overline{u'v'} = 0$. This cannot be accepted immediately for a general case although, of course, it must be true for some duct geometries for reasons of symmetry. The eddy diffusivity for momentum, ϵ_M, is defined as:

$$\varepsilon_M = - \frac{\overline{u'v'}}{\frac{\partial u}{\partial r}} \tag{6.3}$$

Since cases where $\overline{u'v'} \neq 0$ where $du/dr = 0$ seem possible, it is not necessarily true that the radius of the maximum velocity coincides with the point of the zero shear stress(7). Consequently it is not possible to calculate theoretically the zero shear radius nor the shear stress at the radius of maximum velocity. It has been shown(7,16) that the assumption, viz.: the position of zero shear coincides with the radius of maximum velocity, is not necessarily true for turbulent flow in all annuli.

The experimental results of Kjellström and Hedberg(16) show that, for the smooth annulus, there appeared to be no difference between the radius of the maximum velocity and the point of zero shear. However, for partially roughened annuli, there was a small but significant difference. One of the boundary conditions of the present study is hydrodynamically smooth. Therefore, in the present study, it is assumed that the radius of maximum velocity coincides with the position of zero shear.

6.1.2 Friction Factor

The variation of static pressure measurements along the four annuli plotted in Figs. 5.25 to 5.28 indicates the linear variation of the axial pressure drop in the fully developed region. The pressure drops in the developing region are non-linear and include the pressure drop due to the changes in momentum. The effect of the momentum change on the "apparent pressure drop"(84) is discussed in some detail in Appendix 3.

The predicted friction factor calculated from Eq. (3.47) is compared with the experimental friction factors in Figs. 5.29 to 5.36. The agreement between the analysis and the experiment is good. In Fig. 5.31, the experimental results of Okiishi and Serovy[28] and Olson and Sparrow[27] are also compared with the present work. In their experiment, Okiishi and Serovy did not use a boundary layer tripping device in the rounded entrance. Their results are very similar to those observed in the pipe flow without any boundary layer tripping wire as shown in Fig. 5.5 of the present study. Olson and Sparrow, who used both the rounded and squared annular entrance geometries, observed that there were fluctuations in the flow with the rounded entrance without any boundary layer trip and that their pressure drop measurements exhibited similar trends to those observed by Okiishi and Serovy. However, when they placed a thin circular band in contact with the inner surface at the rounded entrance, flow stability was improved and monotonically decreasing pressure gradients were obtained as shown in Fig. 5.31. In the present experimental work, the same trend was also found to be true; however, since the analysis is based on the assumption that the flow is everywhere turbulent ($x>0$, within the boundary layer), only the results obtained from the annuli having tripping wires are compared with the analysis.

In the present experimental study, only two sizes of the boundary layer tripping wire were used. It could be that, for a given annulus, these two sizes were too small to be effective if Reynolds numbers were too small. On the other hand, above a certain range of Reynolds numbers for a given annulus, the wire sizes used were too large and probably have behaved like a square edged entrance. (See the results for $\alpha = 1.61$ and 2.31 in Table 5.1).

Hence, when we consider only appropriate ranges of Reynolds numbers for each radius ratio for the particular tripping wire size, the agreement between the experimental results and those predicted is excellent as shown in Figs. 5.29 and 5.30. This is not surprising since the friction factor is calculated from the predicted velocity profiles given by Eq. (3.33) which were verified by the results of the experimental work already shown in Figs. 5.8 to 5.19.

The predicted effects of Reynolds number and the radius ratio on the distributions of the local average friction factor observed in Figs. 3.14 and 3.15 are compared with the experimental results in Figs. 5.32 and 5.33. The agreement between the experimental results and the predicted results is good in view of the difficulty associated with the measurement of the static pressure. In the determination of the wall shear stress, only the static pressure gradient was used because calculations with a Reynolds number of 44,000 and a radius ratio of 3.83 indicated that the error introduced by neglecting the variation of the momentum flux in the developing region of the flow was 0.018% at $(x/De) = 5$ as demonstrated in Appendix 3. Although the error increases with smaller values of (x/De) because of the uncertainty involved in the analysis for the region $(x/De) < 1$, this would not have produced any marked effect on the variation of the friction factor.

The experimental results of the fully developed friction factor for the four annuli agree with the present analytical prediction very closely as seen in Figs. 5.34 and 5.35 in which the various recommended correlations are also compared. In the range of radius ratio between 1.61 and 15.32 and Reynolds number studied, the largest friction factor was associated with the radius ratio of 3.83.

The analytical friction factor predicted this as shown in Fig. 5.36. It is interesting to note that once the radius ratio is larger than a certain value, the friction factor starts to decrease.

The prediction of Lee[58], deviates slightly from the present analysis for the radius ratio 15.32, but this is understandable, as he himself concluded in his paper, since the Lamb's radius of maximum velocity, r_m, used in his theoretical derivation can not be correlated for the higher radius ratio.

As shown in Figs. 5.34 to 5.36, the use of the circular tube correlations with the hydraulic diameter of an annulus as the characteristics dimension is inadequate.

6.1.3 Hydrodynamic Entrance Length

The results of the analysis on the hydrodynamic entrance length for developing turbulent flow in the concentric annuli are shown in Figs. 5.37 to 5.39. Also shown in Figs. 5.39 are the experimental entrance lengths obtained from the measurement of the velocity and friction factor distributions. Before going into any further discussion, attention must now be brought to the different definitions of hydrodynamic entrance length used by different investigators in the experimental work. In general, the entrance length is defined in terms of the length of duct needed for one of the following to approach its limiting value;

(a) the local pressure gradient or local wall shear stress,

(b) the local velocity profile,

(c) the local turbulent intensity distribution.

The definition in terms of (b) above can also be stated in another way as the length required for the potential core to disappear. The three lengths defined by the three different quantities are not necessarily the same. Also, because the influence of the viscosity in the boundary layer decreases asymptotically outwards[82], these local values in the flow direction tend asymptotically to their limiting values. Therefore, again according to different investigators, the definition of the fully developed flow is different. For example, Olson and Sparrow[27], whose definition of the entrance length is based on (a), took a value within 5% of its limiting value to be a fully developed flow, whereas, Lana and Christiansen[104], who used (b) above for their definition of the entrance length, assumed that a value within 1.0% of the limiting, fully developed value constituted fully developed flow. It was not possible to find any example in the literature which used (c) for the definition of the entrance length. In the present study, all three definitions were examined. Of course, the analysis is based on definition (b).

Experimental results are compared with the analysis as shown in the figures and it can be seen that the experimental data of f_x/f_d = 100% and $(u_{max})_x/(u_{max})_d$ = 95$\sim$99% for the present ranges of the radius ratio and Reynolds number agree well with those of the prediction. The values of (f_x/f_d) were obtained from plots similar to those in Figs. 5.29 and 5.30 and $(u_{max})_x/(u_{max})_d$ from the plots represented in Figs. 5.20, 5.21 and 5.22. However, the difference between the analysis and experimental values based on $(u_{max})_x/(u_{max})_d$ = 100% is great. This phenomenon was also observed with developing turbulent flow in a circular smooth pipe by Barbin and Jones[23]. The explanation for this could, perhaps, be that while the wall shear stress which is very sensitive to the velocity field near the wall is approaching its limiting value, a further change in the velocity profile away from the wall continues asymptotically.

The measurement of turbulent intensity in the flow direction is represented in Fig. 5.40 to 5.43. Here, the local turbulent intensity distribution reaches its limiting value at the values of (x/De) somewhere between those based on $(u_{max})_x/(u_{max})_d = 1.0$ and $(f_x/f_d) - 1.00$.

The agreement between the present results and those of Sridhar et al.[29] based on $(u_{max})_x/(u_{max})_d = 1.00$ is good as seen in Fig. 5.39. The results in a circular pipe have not been compared with those of the present study as the wall boundary conditions are different.

From the above discussions, it can be concluded that the present analysis from the integral viewpoint using a velocity profile based on the modified Reichardt's eddy diffusivity for momentum satisfactorily predicts the characteristics of the developing turbulent flow in concentric annuli.

6.1.4 Eddy Diffusivity for Momentum

The typical distributions of the eddy diffusivity for momentum, ε_M, predicted from the model given by Eq. (3.21) are compared in Figs. 5.44, 5.45, and 5.46 with measured results of the present experimental work for developing turbulent flow in a concentric annulus. The experimental eddy diffusivity for momentum, ε_M, was computed from the mean velocity measurements through the definition of ε_M given by Eq. (3.18). The velocity gradient was determined by using a numerical differentiation method based on the principles of the Lagrangian interpolation of polynomials as mentioned in Section 5. 2. 2. The examination of both the predicted values and the experimental results indicates that the eddy diffusivity increases to a peak on both regions of the flow streams and then decreases slightly near the boundary layer edge or near the radius of maximum velocity, but does not go to zero. Near the edge of the boundary layer it is extremely difficult to obtain accurate velocity gradients and, therefore, the experimental results in these regions are less reliable. However, within the boundary layer, the agreement is generally good. In Figs. 5. 47, 5. 48 and 5. 49, the predicted eddy diffusivities and the experimental results are compared for the fully developed turbulent flow for a radius ratio of 1. 61, 2. 31 and 3. 83 respectively at different Reynolds numbers.

Fig. 5. 50 shows the effect of radius ratio on the eddy diffusivity. The predicted values and experimental results are plotted for the three radius ratios, 1. 61, 2. 31 and 3. 83, and for Reynolds number 44, 000 in the fully developed region. The experimental results are in good agreement with the model used. From Fig. 5. 50 it seems that the radius ratio has little effect on the momentum eddy diffusivity distribution.

6. 2 DIABATIC TURBULENT FLOW IN THE DEVELOPING REGIONS

6. 2. 1 Temperature Profile, Eddy Diffusivity for Heat and Ratio, $\varepsilon_H/\varepsilon_M$

The dimensionless temperature profile, T_1^+, predicted in the entrance region of a concentric annulus for the uniform heat flux at the core tube calculated from Eqs. (3. 56) to (3. 58) and plotted in Figs. 3.17 to 3.20 on semi-logarithmic coordinates indicated that the temperature profile is not only a function of the axial position from the entrance, (x/De), but also of the radius ratio, α, Reynolds number, Re and Prandtl number, Pr. The effect of Prandtl number on the temperature profile was also demonstrated in Fig. 3. 24 in which the temperature was plotted on a $T_1^+/T_{\delta t 1}^+$ vs. $(r - r_1)/(r_2 - r_1)$ plane for the Reynolds number of 44,000 and radius ratio 2. 31.

The representative dimensionless temperature profiles for the case of uniform heat flux at the outer tube and the inner core tube insulated [Boundary Condition (B)] were shown in Figs. 3.25 and 3. 26 from which the effects of δ^* and α could be observed. When the plots in Figs. 3. 25 and 3. 26 are compared with those in Figs. 3.17 and 3.18, some difference in the effects of both δ^* and α due to the heating boundary condition can be observed. For a given α and Prandtl number at a given Reynolds number, it can be seen from these figures that the local bulk temperature $T_{b,x,j}$ for the boundary condition (A) [See page 48 for the definition of (A) and (B)] is smaller than that for (B). Therefore, it can be deduced from Eq. (3. 70) that $Nu_{x,i}$ is always greater than $Nu_{x,o}$. This is shown in Figs. 3. 40 and 3. 41 and it will be again discussed in Section 6. 2. 2. The comparison of the temperature ratio $T_j^+/T_{\delta t j}^+$ for the conditions (A) and (B) is made in Fig. 3. 27.

The temperature profile development for the flow of very low Prandtl number shown in Fig. 3. 28 exhibits a very interesting phenomenon. Even though the thermal boundary layer reaches the other side of the annulus, because of the velocity profile which is still developing, the temperature profile continues to change until the fully developed fluid flow is established. However, the effect of the developing flow seems to be very small.

The experimental wall temperature curves in the entrance regions shown in Figs. 5.51 to 5.53 for the three annuli for a wide range of Reynolds number illustrate very steep axial temperature gradients in the developing region especially at very near the entrance and it can be seen that they become linear some distance in the downstream direction. The linear wall temperature gradient, $dt_w/dx = 0$, indicates that the fully developed condition is reached.

The typical temperature profiles in the entrance region obtained in the experiment are compared with those predicted in Figs. 5.54(a) and (b), it is evident that the agreement is good. In these figures, the temperature distributions are plotted as $T_1^+/T_{\delta t1}^+$ against the normalized wall distance, $(r - r_1)/(r_2 - r_1)$. In this way, the use of wall heat flux, q, can be avoided and this is a distinct advantage since the accurate determination of heat loss in the calculation of heat flux in the experiment is extremely difficult.

The typical experimental eddy diffusivity for heat, $\varepsilon_H/(Pr \cdot \kappa)$. in the entrance region of annuli is shown in Figs. 5.55 and 5.56. As in the case of the eddy diffusivity for momentum, it was extremely difficult to determine the accurate temperature gradient near the edge of the thermal boundary layer from the temperature profile. However, it appears from Figs. 5.55 and 5.56 for the entrance regions and from Figs. 5.57 and 5.58 for the fully developed regions of the annuli that the eddy diffusivity for heat, ε_H, does not decrease at the edges of the thermal boundary or at the radius of the maximum velocity which is quite contrary to the trends observed in the case of the eddy diffusivity for momentum as shown in Figs. 5.44 to 5.50. This may be due to the asymmetric condition of heating from the core tube in the present study. Inspection of the curves in Figs. 5.57 and 5.58 indicates an increase in $\epsilon_H/(Pr \cdot \kappa)$ at a given radial position for the higher Reynolds numbers which was expected.

It is extremely important for any turbulent heat transfer analysis to know the ratio ϵ_H/ϵ_M, which is the key link between momentum and heat transfer. As previously mentioned, the information on the ratio must be known if the analytical results are to be reliable, and the matter has received considerable attention for the fully developed flow through a circular tube.

Using the results of the present experimental data, an attempt was made to obtain an empirical correlation of the ratio by plotting the results of ϵ_H/ϵ_M versus the dimensionless distance, y_j^+. This is shown in Figs. 5.59 (a) and (b). The hatched areas indicate the approximate limits of 95% of the present experimental data.

Since only air is used in the present experiments, the effect of Prandtl number could not be correlated in Eq. (5.5). However, according to Mizushina et al.[89], the effect of Prandtl number could not be detected from their experimental study for the Prandtl number range of 6 ~ 40. It is extremely difficult to develop an accurate correlation of ϵ_H/ϵ_M from experimental studies due to the inherent difficulties associated with it but one concluded from the present experimental results together with those of Mizushina et al.[89] and others[7, 87, 88] that the ratio ϵ_H/ϵ_M is little affected by the order of Prandtl number for Pr > 0.5 and is greater than unity in the range of Reynolds numbers and radius ratios investigated.

The present experimental results on the ratio in the entrance regions of the annuli also indicated that the axial variation of the ratio is negligibly small and this is in accord with the finding of Abberch and Churchill[40] from their work in the thermal entrance region of a circular duct. Therefore, it can be concluded that the use of Eq. (5.5) in the analysis of heat transfer, especially for the fluid flow of Prandtl number greater than 0.5 in the entrance region of a concentric annulus, is justified. For very low Prandtl number flow, a correlation for the ratio proposed by Dwyer[105] given as:

$$\sigma(y_j^+) = 1.0 - \frac{0.2/Pr - 2.0}{(\epsilon_M/\nu)^{0.9}} \qquad (6.4)$$

was used along with Eq. (5.5).

6.2.2 Heat Transfer Coefficient

The predicted Nusselt number in the entrance region of a concentric annulus as shown in Figs. 3.29 to 3.41 clearly indicates that the value of Nusselt number for the heating boundary condition (A), Nu_i, is always greater than that of the boundary condition (B), Nu_o. This trend was obvious from the fact that the predicted bulk temperature $T^+_{b,x,1}$ was always smaller than $T^+_{b,x,2}$ for a given flow condition as mentioned in the previous section. This greater Nu_i compared with the smaller Nu_o for a given flow condition can also be deduced from other aspects of the turbulent flow in a concentric annulus. It can be shown by a force balance that the shear stress on the inner core wall, $\tau_{w,1}$ is always greater than the shear stress on the outer wall, $\tau_{w,2}$ in a concentric annulus. This greater shear stress on the inner core wall may be the result of the greater k_1 as predicted by the present analysis (see Table 3.1). The large value of k_1 in Eq. (3.21) means a larger value of ε_M which involves a greater energy loss which results in a large shear. At the same time, the larger value of k_1 means vigorous thermal diffusion and brings about a higher rate of heat transfer. Therefore, it is not surprising to see from Figs. 3.29 to 3.41 that $Nu_{x,i} > Nu_{x,o}$.

Nusselt numbers close to the entrance are, as expected, very large in comparison with the fully developed values as seen in Figs. 3.29 to 3.31. At x = 0, the thickness of the thermal boundary layer is zero and consequently, in theory, the heat transfer coefficient becomes infinite at the cross section. Fig. 3.32 indicates that the values of (Nu_x/Nu_d) for a given (x/De) and Reynolds number decrease as the radius ratio α increases. The same trend is observed in Fig. 3.33, i.e., the values of (Nu_x/Nu_d) decrease as the Pr increases.

The effect of the velocity distribution at x = 0 is compared in Figs. 3.34 and 3.35. It is evident that the values of (Nu_x/Nu_d) for a uniform initial velocity distribution are larger than those for a fully developed initial velocity distribution for the fluid flows of Pr = 0.7 and 0.001. The same trends were found[75] in the circular tube flow. These results might be expected because of the higher friction in the case of the uniform initial velocity profiles.

The choice of the ratio of eddy diffusivities, $\varepsilon_H/\varepsilon_M$, seems to have a rather small effect on the calculation of the theoretical Nusselt numbers as shown in Figs. 3.36 and 3.37. For example, the fully developed Nusselt number calculated with $\epsilon_H/\epsilon_M = 1.0$ was less than 10 per cent smaller than that calculated with the present correlation for the radius ratio 1.61 and Reynolds number 77,000. For the case of very low Prandtl number flow, both the correlations given by Eq. (5.5) and Eq. (6.4) for the ratio ϵ_H/ϵ_M were used in the analysis and the results, as shown in Fig. 3.37, indicate that the use of Eq. (5.5) resulted in high Nusselt numbers.

To approach experimentally one of the idealized conditions used in the heat transfer analysis, i.e., constant fluid properties, the heat transfer results were extrapolated to zero heating rate condition in a manner described in Section 4.4.4. Typical results obtained by such an experimental procedure for heat transfer measurement are plotted in Figs. 5.60 and 5.61. It can be seen that the effect of the heat flux on the heat transfer coefficient is not negligible as assumed by many investigators in the field of convective heat transfer with a moderate heat flux. It seems that even the moderate heat fluxes used in the present experiment still affected the transport properties which resulted in changes in the temperature profiles, yielding different heat transfer coefficients than would be obtained if properties were constant. This may explain why many experimental heat transfer results for a given flow condition available in the literature differ greatly from each other. No attempt was made here to correlate the effect of the magnitude of heat flux on heat transfer coefficient at this time and it is recommeded that a further study on this matter be made.

The extrapolated points are more in agreement with the predicted as seen from Fig. 5.60. All the experimental heat transfer coefficients in terms of Nusselt number shown in Figs. 5.62 to 5.64 and in Fig. 5.67 are the extrapolated values at the zero heating condition. Uncorrected experimental data together with corrected for the heating condition are also compared in Figs. 5.62 and 5.67 for reference.

The effect of radius ratio on the variation of $(Nu_x/Nu_d)_i$ seems to be greater than that of Reynolds number as seen from Figs. 5.65 and 5.66, in which the agreement between the analytical predictions and the experimental results are excellent. When the experimental data are plotted in the form of $(Nu_x/Nu_d)_i$, no correction of the data is needed for the heat flux.

For smaller radius ratios, the values of (Nu_x/Nu_d) are higher than those for larger radius ratios. The experimental results of Robert and Barrow[77] for the simultaneously developing heat transfer in a concentric annulus of $a = 4$ are also compared with those of the present study in Fig. 5.64. Their work is the only experimental work available in the literature comparable with the work presented here as far as the author is aware. The agreement between their experimental work and that of the present study is reasonable. The heat flux condition used by Robert and Barrow was not known. Their analytical correlation in the form of Eq. (2.7) was not compared in the figure because the values calculated from Eq. (2.7) did not result in an asymptotic condition. This could be the result of some typographical error in Eq. (2.7).

Corrected experimental Nusselt numbers for fully developed heat transfer are plotted against Reynolds number in Fig. 5.67 in which a comparison is made with the correlations or predictions of previous workers for the radius ratio of 2.31. Uncorrected data agree with the analysis of Kays and Leung[34] whereas the extrapolated data are more in agreement with the predictions of Lee[33] and the present study. The difference among the analytical results is due to difference in the premise on the expression of eddy diffusivity in each respective analysis. The curves of Davis[101] and Walger[102] are all empirical correlations and they are much higher than those of the present results or analyses. A possible explanation could be the different experimental conditions and data deduction procedures adopted by the investigators.

6.2.3 Thermal Entrance Length

For evaluating problems of the simultaneously developing region in a duct, it is essential to know the momentum boundary layer thickness as well as the thermal boundary layer thickness at a given value of (x/De). This is due to the effect of Prandtl number. At Pr = 1, the boundary layers should have the same thickness if the turbulent Prandtl number is also unity, and the boundary condition is symmetric. When the free-stream velocity is constant, the hydrodynamic boundary layer would be thicker at high Prandtl number.

However, for an assymmetric heating condition such as in the entrance region of an annulus where the two heating boundary conditions are not identical, the relationship between the boundary layer thickness and Prandtl number becomes complex. A typical development for momentum and thermal boundary layers is given in Figs. 3.12 and 3.42 for the radius ratio 2.31 and Reynolds number 44,000. It can be seen from Fig. 3.42 that the effect of Prandtl number on the thermal boundary layer thickness is considerable.

For the case of Pr = 0.001, the edge of the thermal boundary layer reached the opposite wall well before the momentum boundary layers met each other, for the case where the inner core wall heated uniformly while the outer wall insulated. However, for a moderate range of Prandtl numbers, 0.71 $\sim$ 30.0, the effect of Pr on the thermal boundary layer thickness is rather small. Therefore, for practical purposes it can be assumed that the thickness of the thermal and momentum boundary layers are to be identical for the fluids having the Prandtl number in this range. To test this assumption, a calculation was made for the Nusselt number at a point, (x/De) = 2.34, of the annulus with α = 2.31 at Re = 43980. A value of 136.5 was obtained with the thermal boundary layer thickness calculated strictly following the method of solutions given in Section 3.5.5, steps (i) to (vi), whereas a value of 137.7 was obtained when it is assumed that $\delta_t = \delta$.

The thermal entrance length in a simultaneously developing flow is defined in the present study in terms of the length of duct needed from the entrance to a cross section in the flow direction where both the generalized velocity and temperature profiles are invariant in the axial direction, when the fluid properties are assumed to be constant.

This definition can be stated as:

$$\frac{\partial}{\partial x}\left(\frac{T_w - T}{T_w - T_b}\right) = 0 \qquad (6.5)$$

For the case of constant heat flux, as in the present study, the differentiation of Eq. (6.5) with definition of heat transfer coefficient, h, Eq. (3.68) yields the following expression:

$$\frac{\partial T}{\partial x} = \frac{d\,T_w}{dx} = \frac{d\,T_b}{dx} \tag{6.6}$$

Therefore, the linear temperature gradient indicates that the fully developed region has been reached.

For the purely thermal entrance case where the velocity profile is already fully developed at the entrance, the thermal entrance length is usually defined[33] as the distance from the entrance to the cross section where the temperature profile has no straight line portion perpendicular to the fluid flow axis. This thermal entrance length of the purely thermal entrance case is denoted here as $(x/De)_{d,T,p}$. If the Prandtl number of a fluid is above a certain value, then $(x/De)_{d,T,p} = (x/De)_{d,T}$ for the simultaneously developing flow. However, for very low Prandtl number flow, this is not necessarily so. For example, if Prandtl number of the fluid is 0.001, the edge of the thermal boundary layer reaches the outer wall boundary well before the hydrodynamic boundary layer is fully developed as illustrated in Fig. 3.42. The temperature profile at that cross section has no straight line portion perpendicular to the fluid flow axis.

Accordingly this thermal entrance length, $(x/De)_{d,T,p}$, is termed here as "the pseudo thermal entrance length" to distinguish it from the thermal entrance length, $(x/De)_{d,T}$. This is because, even though the thermal boundary layer has extended itself across the flow duct, the generalized temperature profile continues to change until the flow is hydrodynamically fully developed. In this case, $(x/De)_{d,M} = (x/De)_{d,T}$. However, comparison of the non-dimensional temperature profiles at $(x/De)_{d,M}$ and at $(x/De)_{d,T,p}$ made in Fig. 3.28 shows that the effect of the developing flow is very small.

If the developing flow and heat transfer were to be solved by "the exact solution" utilizing characteristic function, value, etc., the entrance length must be redefined because parameters such as f, h, Nu approach their fully developed values asymptotically. The direct comparison of the present study with other studies using characteristics function is not applicable because of its difference of calculation method and definition. Lee[33] also drew a similar conclusion when he found that the effect of Prandtl number on $(x/De)_{d,T}$ can be completely reversed depending on the definition used; with a definition based on $(Nu_x/Nu_d) = 1.0$, the thermal entrance length increases as the Prandtl number increases, however, if the definition of thermal entrance length based on $(Nu_x/Nu_d) = 1.05$ (which is one of the definitions used for the solution using characteristics functions) is taken, the values of $(x/De)_{d,T}$ decreases markedly with increasing Prandtl number. This was in accord with the findings of Sparrow et al.[39].

The predicted effect of Prandtl number on the thermal entrance length, $(x/De)_{d,T}$ showed the same trend that Lee[33] observed in his work on the purely thermal entrance problem, as illustrated in Figs. 3.43 and 3.44. Also shown in the figures is the result of entrance length calculated using Dwyer's expression[105] for the ratio of eddy diffusivities in the case of Pr = 0.01 The result which used Eq. (5.5) is less than the result calculated using Dwyer's correlation. The difference in the results might be that, while the effect of Prandtl number in the ratio, $\varepsilon_H/\varepsilon_M$, is considered in Dwyer's correlation, Eq. (6.4), it is not in Eq. (5.5). Effect of Prandtl number on the ratio, $\varepsilon_H/\varepsilon_M$, for Pr > 0.5 has been discussed previously. There is also appreciable effect of radius ratio and Reynolds number. These effects are shown in

Fig. 3. 45. The direct comparison of entrance length for the boundary conditions (A) and (B) are also included in Fig. 3. 45 for the Prandtl number of 0. 71. The entrance length is longer for the boundary condition (A) than that of the condition (B).

The experimental thermal entrance lengths are compared with the predicted values in Fig. 5. 68. Considering the uncertainties in the experimental results, the agreement between the experiment and prediction is good, and the trend is also observable.

The experimental results for the purely thermal entrance case of the condition (A) reported by Quarmby[57] for a = 2. 88 are also plotted in the figure for a comparison with the present study. The agreement is reasonably good and this confirms that the past history of the fluid flow has little effect on the thermal entrance length for high Prandtl number flow.

CHAPTER 7

CONCLUSIONS

The following conclusions were drawn from both the analytical and experimental studies of the turbulent flow and heat transfer in concentric annuli under simultaneous development of boundary layers with one wall at a constant heat flux, the other insulated:

(1) The value of the "mixing length constant" k_1 was very sensitive to the radius ratio, Reynolds number and axial distance from the entrance, and differed greatly from that of k_2. Therefore, unlike a turbulent flow in a circular pipe, the velocity profiles for the concentric annuli expressed in $u_j^+ = \varphi(y_j^+)$ showed a complex relationship. The effects of Reynolds number, radius ratio and distance from the entrance were significant, especially for the inner region. This confirmed the concept of universal velocity profile for concentric annuli was incorrect.

(2) The hydrodynamic entrance length based on $f_x/f_d = 1.00$ was obtained for about 6 to 12 equivalent diameters from the present experimental results and this value was in good agreement with the present prediction. However, the experimental values based on the fully developed velocity profile were between about 20 and 42 equivalent diameters. The hydrodynamic entrance lengths evaluated from the axial turbulence intensity measurements were somewhere between those based on the friction factor and velocity profile.

(3) Agreement between the proposed model of the eddy diffusivity for momentum and the experimental results was good.

(4) In general, a substantial agreement was obtained between the analysis and experimental results for the turbulent heat transfer in the simultaneously developing region for the range of radius ratios and Reynolds numbers considered. The value of (Nu_x/Nu_d) for a given Reynolds number and (x/De) decreased as the radius ratio increased, and the predicted values of (Nu_x/Nu_d) also decreased as the Prandtl number increased.

(5) The past history of the fluid flow had some effects on the Nusselt numbers, i.e., the effect of the uniform velocity distribution at the entrance was to result in a Nusselt number that was always higher than if the velocity were developed at the entrance. The value of Nusselt number for the case of inner wall alone heated was always larger than that of the outer wall alone heated condition in the analysis.

(6) The fully developed heat transfer was attained from both the analytical and experimental studies generally in an entrance length of less than 40 equivalent diameters for the air flow. The analysis showed that the effect of increasing the radius ratio resulted in a decrease of $(x/De)_{d,T,j}$ for a given Prandtl number and Reynolds number. However, the effect of increasing the Reynolds number was to increase the value of $(x/De)_{d,T,j}$ for a given Prandtl number and radius ratio.

(7) For the very small Prandtl number a "pseudo thermal entrance length" was observed. This indicated that, even though the thermal boundary layer had extended itself across the flow duct, the generalized temperature profile continued to change until the flow was hydrodynamically fully developed.

(8) The extrapolated values of Nusselt number to the zero heating condition were more in agreement with the present prediction.

APPENDIX 1

THE INTEGRATION OF THE VELOCITY PROFILE, Eq. (3.35)

The equation (3.35) in Section 3.4.1 is:

$$\frac{\delta_j - y_j}{\delta_j} = \left\{1 + \frac{k_j}{6} \cdot \delta_j^+ \cdot (1 - \eta_j^2)(1 + 2\,\eta_j^2)\right\} \left(\frac{du^+}{dy^+}\right)_j \tag{3.35}$$

where $\eta_j = \dfrac{R_j^+ - r^+}{R_j^+ - r_j^+} = \dfrac{\delta_j^+ - y_j^+}{\delta_j^+}$, and

$$\delta_j^+ = | \; R_j^+ - r_j^+ \; |$$

Integrating, Eq. (3.35) becomes, as:

$$u_j^+ = \int \frac{\eta_j \, dy_j^+}{1 + \frac{k_j}{6} \; \delta_j^+ \; (1 - \eta_j^2)(1 + 2\eta_j^2)} + C_j \tag{A.1.1}$$

Let $\eta_j = x$, then $dy_j^+ = - \delta_j^+ \, dx$ and Eq. (4.1.1) becomes:

$$u_j^+ = - \int \frac{\delta_j^+ \; x \; dx}{1 + \frac{k_j}{6} \; \delta_j^+ \; (1 - x^2)(1 + 2x^2)} + C_j \tag{A.1.2}$$

Again, let $x^2 = z$ in Eq. (4.1.2), we have:

$$u_j^+ = - 3\delta_j^+ \int \frac{dz}{-2\,k_j \, \delta_j \, z^2 + k_j \, \delta_j^+ \, z + (k_j \, \delta_j^+ + 6)} + C_j \tag{A.1.3}$$

From the tables of integrals[106], it gives:

$$\int \frac{dx}{a\,x^2 + bx + c} = \frac{1}{\sqrt{b^2 - 4ac}} \ln \left| \frac{2ax + b - \sqrt{b^2 - 4ac}}{2ax + b + \sqrt{b^2 - 4ac}} \right| ,$$

$$\text{for } b^2 > 4ac \qquad \text{(A.1. 4)}$$

From Eq. (A.1.4), Eq. (A.1.3) is now found to be:

$$u_j^+ = -\frac{3}{\psi}\,\delta_j^+ \ln \left| \frac{k_j\,\delta_j^+ - 4k_j\,\delta_j^+\,\eta_j^2 - \psi}{k_j\,\delta_j^+ - 4k_j\,\delta_j^+\,\eta_j^2 + \psi} \right| + C_j \qquad \text{(A.1. 5)}$$

where $\psi = \left(9\,k_j^2\,\delta_j^{+2} + 48\,k_j\,\delta_j^+\right)^{\frac{1}{2}}$

As mentioned in Section 3.4.4, the value of constant C_j is obtained by forcing the two equations of Eq. (A.1.5) for j = 1 and 2 to pass through $u_j^+ = 12.8$ and $y_j^+ = 26$, which were found by the experimental work.

Now the value of constant C_j is:

$$C_j = 12.8 + \frac{3}{\psi}\,\delta_j^+ \ln \left| \frac{k_j\,\delta_j^+ - 4k_j\,\delta_j^+\,\eta_j^2 - \psi}{k_j\,\delta_j^+ - 4k_j\,\delta_j^+\,\eta_j^2 + \psi} \right| \qquad \text{(A.1. 6)}$$

where

$$\eta_j = \frac{\delta_j^+ - 26.0}{\delta_j^+}$$

APPENDIX 2

THE INTEGRATION OF THE MOMENTUM EQUATION

In Section 3.4.2, we derived the momentum integral equation in dimensionless form as:

$$\left(\frac{x}{De}\right)_{M,j} = \int_{u_e^+}^{u_{\delta j}^+} \frac{\delta_j^+ (R_j^+ + r_j^+)}{2\, r_j^+ (De^+)_j} u_{\delta j}^+ \, du_{\delta j}^+$$

$$- \int_o^{A^+} \frac{dA^+}{r_j^+ (De^+)_j} - \int_o^{B^+} \frac{u_{\delta j}^+ \, d\, B^+}{r_j^+ (De^+)_j} \qquad (3.39)$$

where

$$A^+ = \int_o^{\delta_j^+} u_j^{+2}\, r^+ \, dy_j^+ \; ,$$

$$B^+ = \int_o^{\delta_j^+} u_j^+ \, r^+ \, dy_j^+ \; ,$$

$$(De^+)_j = 2\, r_1^+ (\alpha - 1), \quad \text{or} \quad 2\, r_2^+ (1 - \alpha^{-1}),$$

and

$$Re = (u_e^+)_j \; (De^+)_j \qquad (3.40.b)$$

Now combining Eq. (3.40.b) and Eq. (3.39), we have:

$$\left(\frac{x}{De}\right)_{M,j} = \int_{\frac{Re}{2}}^{E^+} \frac{\delta_j^+ (R_j^+ + r_j^+)}{r_j^+ (De^+)_j^2} u_{\delta j}^+ \, dE^+$$

$$- \int_{o}^{A^+} \frac{dA^+}{r_j^+ (De^+)_j} + \int_{o}^{B^+} \frac{u_{\delta j}^+ \, dB^+}{r_j^+ (De^+)_j} \qquad (A. 2. 1)$$

where

$$E^+ = \tfrac{1}{2} u_{\delta j}^+ (De^+)_j$$

From the differential of a product, we can write:

$$\left[\tfrac{1}{2} u_{\delta j}^+ (De^+)_j\right] d \left[\int_{o}^{\delta_j^+} u_j^+ r_j^+ dy_j^+\right] \equiv d \left\{\left[\tfrac{1}{2} u_{\delta j}^+ (De^+)_j\right] \cdot \int_{o}^{\delta_j^+} u_j^+ r^+ dy_j^+\right\} - d\left[\tfrac{1}{2} u_{\delta j}^+ (De^+)_j\right] \int_{o}^{\delta_j^+} u_j^+ r^+ dy_j^+ \qquad (A. 2. 2)$$

If we devide Eq. (A. 2. 2) by $\left[r_j^+ (De^+)_j^2\right]$ and integrate both parts, then:

$$\int_{o}^{B^+} \frac{\left[u_{\delta j}^+ (De^+)_j\right] dB^+}{r_j^+ (De^+)_j^2} = \int_{o}^{F^+} \frac{dF^+}{r_j^+ (De^+)_j^2} - 2 \int_{\frac{Re}{2}}^{E^+} \frac{\left(\int_{o}^{\delta_j^+} u_j^+ r^+ dy_j^+\right) dE^+}{r_j^+ (De^+)_j^2} \qquad (A. 2. 3)$$

where

$$F^+ = \left[u_{\delta j}^+ (De^+)_j\right] \int_{o}^{\delta_j^+} u_j^+ r^+ dy_j^+$$

Rearranging Eq. (A. 2. 3), we have:

$$\int_{o}^{B^+} \frac{u^+_{\delta j}\, dB^+}{r^+_j\, (De^+)_j} = \int_{o}^{G^+} \frac{dG^+}{r^+_j\, (De^+)_j} - 2\int_{\frac{Re}{2}}^{E^+} \frac{\left(\int_o^{\delta^+_j} u^+_j\, r^+\, dy^+_j\right) dE^+}{r^+_j\, (De^+)^2_j} \qquad (A.\,2.\,4)$$

where

$$G^+ = u^+_{\delta j} \int_o^{\delta^+_j} u^+_j\, r^+\, dy^+_j$$

When the last term of Eq. (A. 2. 1) is replaced with Eq. (A. 2. 4), we have

$$\left(\frac{x}{De}\right)_{M,j} = \int_{\frac{Re}{2}}^{E^+} \left[\frac{\delta^+_j\,(R^+_j + r^+_j)}{r^+_j\,(De^+)^2_j}\, u^+_{\delta j} - \frac{2}{r^+_j\,(De^+)^2_j} \int_o^{\delta^+_j} u^+_j\, r^+\, dy^+_j\right] dE^+ + \int_o^{D^+} \frac{dD^+}{r^+_j\,(De^+)_j} \qquad (A.\,2.\,5)$$

where

$$D^+ = \int_o^{\delta^+_j} (u^+_{\delta j} - u^+_j)\, u^+_j\, r^+\, dy^+_j$$

Eq. (A. 2. 5) is Eq. (3. 41) in Section 3. 4. 2.

APPENDIX 3

EFFECT OF CHANGES IN MOMENTUM FLUX ON THE FRICTION FACTORS

If the flow is fully developed in a concentric annulus, the integration of Eq. (3.15) gives

$$\tau_{w1} = \frac{r_m^2 - r_1^2}{2 r_1} \left(- \frac{dp}{dx}\right) \qquad \text{(A. 3. 1)}$$

and

$$\tau_{w2} = \frac{r_2^2 - r_m^2}{2 r_2} \left(- \frac{dp}{dx}\right) \qquad \text{(A. 3. 2)}$$

Therefore, the wall shear stress is a function of the pressure gradient, and the radius of maximum velocity only. However, for the developing boundary layer in an annulus, the local wall shear stress is dependent not only on the local pressure gradient, but also on the changes in momentum flux.

Now the momentum integral equation for the developing region is

$$- d\left(\int_{r_1}^{r_{\delta 1}} 2\pi r \rho u^2 \, dr + \int_{r_{\delta 2}}^{r_2} 2\pi r \rho u^2 \, dr\right) +$$

$$u_{\delta 1} \, d\left(\int_{r_1}^{r_{\delta 1}} 2\pi r \rho u \, dr + \int_{r_{\delta 2}}^{r_2} 2\pi r \rho u \, dr\right)$$

$$= 2 \bar{\tau} \pi (r_2 + r_1) \, dx + \tfrac{1}{2} \, dp \, (r_2^2 - r_1^2) \pi \qquad \text{(A. 3. 3)}$$

Rearranging, Eq. (A. 3. 3) becomes

$$\bar{\tau} = \frac{u_{\delta 1}}{(r_2+r_1)} \cdot \frac{d\left(\int_{r_1}^{r_{\delta 1}} \rho u r\, dr + \int_{r_{\delta 2}}^{r_2} \rho u r\, dr\right)}{dx}$$

$$- \frac{1}{(r_2+r_1)} \cdot \frac{d\left(\int_{r_1}^{r_{\delta 1}} \rho u^2 r\, dr + \int_{r_{\delta 2}}^{r_2} \rho u^2 r\, dr\right)}{dx}$$

$$- \frac{(r_2-r_1)}{2} \cdot \frac{dp}{dx} \qquad \text{(A. 3. 4)}$$

Dimensionless mass and momentum fluxes parameters are defined for the present geometry, respectively, as:

$$M_1 = \int_{1/a}^{1} \frac{\rho}{\rho_e} \left(\frac{u}{u_b}\right) \frac{r}{r_2}\, d\left(\frac{r}{r_2}\right) \qquad \text{(A. 3. 5)}$$

and

$$M_2 = \int_{1/a}^{1} \frac{\rho}{\rho_e} \left(\frac{u}{u_b}\right)^2 \left(\frac{r}{r_2}\right) d\left(\frac{r}{r_2}\right) \qquad \text{(A. 3. 6)}$$

Then, with Eqs. (A. 3. 4), (A. 3. 5) and (A. 3. 6), the friction factor, f, defined by Eq. (3. 42) Section 3. 4. 3, becomes

$$f = \frac{2\rho_e r_2^2}{\rho (r_2+r_1)} \left(\frac{u_{\delta 1}}{u_b} \cdot \frac{dM_1}{dx} - \frac{dM_2}{dx}\right) - \frac{(r_2-r_1)}{\rho u_b^2} \cdot \frac{dp}{dx} \qquad \text{(A. 3. 7)}$$

If the momentum flux is negligible, Eqs. (A. 3. 4) and (A. 3. 7) are simplified, as:

$$\bar{\tau} = - \tfrac{1}{2} (r_2 - r_1) \frac{dp}{dx} \qquad \text{(A. 3. 8)}$$

and

$$f = - \frac{(r_2 - r_1)}{\rho u_b^2} \cdot \frac{dp}{dx} \qquad \text{(A. 3. 9)}$$

Eq. (A. 3. 8) and (A. 3. 9) are identical to those for the fully developed region.

In Fig. A. 3. 1, the mass terms for M_1, M_2, and static pressure are plotted against the axial distance from the entrance, (x/De). The momentum fluxes are approximately constant except very near the entrance, therefore, the static pressure term alone is sufficient to determine the wall shear stress or the friction factor except for the region very near the entrance. Barbin and Jones[23], and Okiishi and Serovy[28] reported that changes in momentum flux were negligible for the flow development in a pipe for (x/De) > 1. 5, and in an annulus for (x/De) > 3. 81 (α = 2. 91) and for (x/De) > 5. 33 (α = 1. 88), respectively.

In the present experimental study, for a Reynolds number of 44,000 and a radius ratio of 3. 83, the analysis by Eq. (A. 3. 7) showed that the error introduced by neglecting the variation of momentum flux in the developing region of the flow was 0. 018% at (x/De) = 5.

APPENDIX 4

DISTRIBUTION OF HEAT FLUX ACROSS THE BOUNDARY LAYER

In the steady state, the energy equation for the thermal boundary layer in an annulus can be obtained from the idealized model of Figs. 3.1(b) and (c). An energy balance made on annular fluid elements between r and (r + dr) gives:

$$- 2\pi r\,dr\,\rho u\,c_p \frac{\partial T}{\partial x}\,dx = 2\pi\,dx\left[(r+dr)\left(q + \frac{\partial q}{\partial r}\,dr\right) - qr\right] \qquad (A.4.1)$$

By rearranging, we have:

$$\frac{\partial}{\partial r}(r \cdot q) = - r\rho u\,c_p \frac{\partial T}{\partial x} \qquad (A.4.2)$$

Integrating from $r_{\delta t1}$ to r:

$$q = \frac{1}{r}\int_{r_{\delta t1}}^{r} r\rho u\,c_p \frac{dT}{dx}\,dr \qquad (A.4.3)$$

The overall energy balance gives:

$$2r_1 q_i = \rho u_b c_p (r_{\delta t1}^2 - r_1^2) \frac{dT_b}{dx} \qquad (A.4.4)$$

To simplify the problem, we now assume $\frac{dT_b}{dx} = \frac{dT}{dx} = \frac{\partial T}{\partial x}$ and $u = u_b$; this relation is only applicable for the established flow,

i. e., fully developed region. However, since the heat fluxes are already very small in the outer region of the annulus, the assumption concerning the velocity field is not critical to the evaluation of q(r) in the region of greatest importance. This matter has been studied in detail by Barrow[92].

Now from Eqs. (A. 4. 3) and (A. 4. 4), we have

$$q(r) \simeq \frac{2 r_1 q_i}{r (r_{\delta t1}^2 - r_1^2)} \int_{r_2}^{r} r\, dr$$

$$= \frac{r_1 q_i (r_{\delta t1}^2 - r^2)}{r (r_{\delta t1}^2 - r_1^2)} \qquad \text{(A. 4. 5)}$$

Introducing non-dimensional parameters:

$$(q_i^+)_x = \left(\frac{q}{q_i}\right)_x = \frac{r_1^+}{r^+} \left(\frac{r_{\delta t1}^{+2} - r^{+2}}{r_{\delta t1}^{+2} - r_1^{+2}}\right) \qquad \text{(A. 4. 6)}$$

where

$$r^+ = r_1^+ + y_1^+ \quad \text{or} \quad r_2^+ - y_2^+$$

and

$$r_{\delta t1}^+ = r_1^+ + \delta_{t1}^+$$

The corresponding equation for outer wall heated can be derived with the same methods as:

$$(q_o^+)_x = \left(\frac{q}{q_o}\right)_x = \frac{r_2^+}{r^+} \left(\frac{r^{+2} - r_{\delta t 2}^{+2}}{r_2^{+2} - r_{\delta t 2}^{+2}}\right)$$

where

$$r^+ = r_1^+ + y_1^+ \quad \text{or} \quad r_2^+ - y_2^+$$

and

$$r_{\delta t 2}^+ = r_2^+ - \delta_{t 2}^+$$

Eq. (A. 4. 6) is identical to that Lee[33] used successfully in his work on the purely thermal entrance problem.

APPENDIX 5

CORRECTION OF EXPERIMENTAL DATA

a. Thermocouple Probe

For computing the true temperature of a gas from the reading of a thermocouple probe placed in a gas stream of an annulus passage with a given heat flux at wall(s), the following corrections must be made for:

(1) the convection heat transfer between fluid and the hot junction,

(2) the radiation heat transfer between the hot junction and wall(s),

and

(3) the conduction heat transfer along the thermocouple wires.

If the conduction heat loss along the thermocouple wires is negligible compared with the convection and radiation heat transfer, then the following energy balance can be made for the hot junction:

$$hA\,(t_{gas} - t_{junction}) = \sigma\, A\, F_{\varepsilon}\, F_{g}\, (T_{w}^{4} - T_{junction}^{4}) \qquad \text{(A. 5. 1)}$$

where

h = convection heat transfer coefficient from the gas to the hot junction

A = surface area of the hot junction

F_{ε} = surface emissivity of the hot junction

F_g = radiation geometry factor

The value of $h_{junction}$ can be calculated from a simplified equation for heat transfer to a small cylinder transverse to a flow[107]:

$$h = 0.11 \; c_p \; G^{0.6} / D^{0.4} \tag{A. 5. 2}$$

where

G = mass flow rate of air

D = diameter of hot junction

For the experiment of $\alpha = 2.31$, Re = 43,000, where the velocity was 40.5 ft/sec at y = 0.14 inches, the temperature reading was 88°F and the wall temperature 127°F. The heat transfer coefficient, $h_{junction}$, calculated from Eq. (A. 5. 2) was 173 Btu/hr.°F. ft^2. Assuming the emissivity F_ϵ of the oxidized thermocouple junction 0.5 and the factor F_g = 1, the thermocouple error for the above example is:

$$(t_{gas} - t_{junction}) = 0.5 \times (0.1714 \times 10^{-8}) \; (587^4 - 548^4)/173.0$$

$$= 0.14°F$$

Although the thermocouple error in the present study will vary at different radial positions and at different Reynolds numbers, the order of the error is about the same as that given for an example above. Hence, it can be ignored.

The error due to the conduction along the thermocouple wires has been studied by Schneider[108]. Lee[58] reported that the errors at y_1 = 0.008 and 0.020 inches were about 0.8 and 0.3°F, respectively for his experiment of $\alpha = 1.632$, and Re = 40,000. To reduce the conduction heat loss along the thermocouple wires in the present study, the hot junction was mounted across the gap of a fork made of **epoxy** resin. The error from the conduction loss was assumed to be negligibly small.

b. Correction for Heat Losses

The heat flux from the core tube wall was corrected for the radiation heat loss and heat leak through the insulation of the outer tube and through the lead electric wires.

The radiation heat flux q between the hot core surface and the outer tube wall can be estimated by the following equation:

$$q = \frac{\sigma}{(1/\varepsilon_1) + (A_1/A_2)(1/\varepsilon_2 - 1)} (T_1^4 - T_2^4) \qquad (A.5.3)$$

For the experiment of $\alpha = 2.31$, Re = 43,000 where $t_1 = 110°F$, $t_2 = 79°F$ and $\varepsilon_1 = 0.07$ (for light silvery stainless steel after polished) and $\varepsilon_2 = 0.05$ (for commercial shiny copper[107]), the radiation heat flux q calculated from the above equation is about 16 Btu/hr. ft.^{2} Since the heat flux by the electric power of the heater core was about 462 Btu/hr. ft.^{2}, the heat loss due to the radiation effect was about 3%.

The heat leak through the insulation of the outer tube was determined by measuring the conduction heat transfer through the fibre glass insulation. Two thermocouples whose hot junctions were set one inch apart were used to obtain the radial temperature gradient across the 2 inches thick insulation. Three such pairs were used at known positions along the insulation and the average radial temperature gradient was obtained.

The conduction heat flow rate, q, through a hollow cylinder is:

$$q = \frac{2\pi k L}{\ln (r_2/r_1)} (T_1 - T_2) \tag{A. 5. 4}$$

For the above experiment, the heat loss calculated was approximately 4.2 Btu/hr; and the electric power to the test section was about 3400 Btu/hr. The loss due to conduction through the fibre glass insulation was, therefore, about 0.12%. The heat leak through the electric lead wire was calculated from the measured temperature gradient. Two thermocouples were placed 2 feet apart into the lead wire surface. The heat loss calculated from the simple heat conduction equation was usually less than 0.9 Btu/hr.

The heat fluxes used to calculate the heat transfer coefficient were corrected for these heat losses: radiation, conduction through the insulation, and conduction through the lead cable.

c. Pitot Tube

It is a well known fact that, when a pitot tube is used to measure fluid velocities in a boundary layer of a duct, there are certain errors which arise because the effective center of the tube does not coincide with the geometric center. These displacement effects are due to the shear and presence of the wall. A study of the displacement effects on circular pitot tubes has been made by MacMillan[109], and rectangular mouthed pitot tubes by Quarmby and Das[110]. The results of Quarbmy and Das for the displacement effects on a set of five rectangular mouthed pitot tubes of a constant thickness ratio 0.6 show that the displacement due to shear only, Δ, is given by:

$$\frac{\Delta}{b} = 0.19 \pm 0.01 \qquad (A.5.5)$$

where

Δ = displacement towards the region of higher velocity

b = outside thickness of pitot tube

When this relation was applied to the pitot tube used for the velocity measurements, the effective displacement was about 0.0044 inches.

Additional error affecting the pitot tube measurement is due to turbulence effects. As seen in Figs. 5.40 to 5.43 the turbulence intensity term $\overline{u'^2}$ is generally negligibly small except in the region very close to the wall. Calculation of the maximum error based on the method described by Lee[58] in the present experiment was less than 1%.

APPENDIX 6

NUMERICAL COMPUTATION AND SAMPLE CALCULATION

For the numerical calculations in the present study, IBM 360/65 computer at the computing center of the University of Ottawa was used. Using FORTRAN language, a number of computer programs were prepared for the numerical evaluation of the theoretical expressions for the various parameters in Chapters 3 and 5. Sample flow diagrams of numerical computation for velocity profile [Eq. (3.36)] and Nusselt number and entrance length [Eq. (3.65) and (3.70)] are shown in Fig. A.6.1 and Fig. A.6.2 as examples.

Most of the theoretical calculation requires numerical integration where accuracy of the computation is very important. In most cases, Simpson's rule was used for the numerical integration with double precision. The accuracy of numerical integration has been checked by repeating the integration process with varying mesh sizes, and satisfactory interval sizes were chosen from the comparison of the results. A typical example is given in Fig. A.6.3.

The detailed calculation procedures of the numerical evaluation are also given in Chapter 3. For the calculation of Nusselt number in the simultaneously developing region, the thicknesses of the hydrodynamic and thermal boundary layers should be known for the various (x/De).

In order to clarify the procedure used in computation of the experimental results presented in Chapter 5, a typical experiment with an annulus having the radius ratio 3.83 has been chosen as an illustration.

a. Adiabatic turbulent flow, $\alpha = 3.83$

(1) Initial Conditions:

$r_1 = 0.5$ in.
$r_2 = 1.917$ in.
$De = 2.834$ in.
$t_e = 77°F.$
$p_e = 14.62$ psia.
$y = 0.319$ in.
$x/De = 5.65$

(2) Local velocity

$$u = \left\{ \left[\left(\rho_{water} - \rho_{air} \right) \times 2.0 \times 32.174 \times \text{constant} \times \text{manometer reading} \right] / \rho_{air} \right\}^{0.5} = 17.39 \text{ ft/sec.}$$

(3) Wall shear stress and friction velocity

$$\tau_{wl} = \left[(r_1^2 - \delta_1^2)/2\, r_1 \right] \times \frac{dp}{dx} = 0.159 \times 10^{-4} \text{ psi}$$

$$u_1^* = \left[(\tau_{wl} \times 144.0)/\rho_{air} \right]^{0.5} = 1.06 \text{ ft/sec.}$$

(4) Dimensionless velocity and distance

$$u_1^+ = u/u_1^* = 16.41$$
$$y_1^+ = (y \times u_1^*)/\nu = 168.1$$

(5) Bulk velocity

$$u_b = 8 \sum_{i=1}^{20} [u_i \times (y_i + 0.5) \times 0.07085] / (3.834^2 - 1^2)$$

$$= 16.45 \text{ ft/sec.}$$

(6) Reynolds number

$$Re = \frac{u_b \cdot De}{\nu} = 23170$$

(7) Mean friction factor

$$f = [De/(2 \times \rho_{air} \times u_b^2] \times \frac{dp}{dx} \times 144.0 = 0.0078$$

(8) Eddy diffusivity for momentum

$$\frac{\varepsilon_M}{\nu} = \frac{\tau_{wl}}{\rho_{air}} / \left(\frac{du}{dy}\right) \cdot \nu - 1.0 = 21.1$$

b. <u>Heat transfer calculation, $a = 3.83$</u>

(1) Initial condition:

$r_1 = 0.5$ in.
$r_2 = 1.917$ in.
$p_e = 14.24$ psia.
$x = 56$ in.

(2) Mean velocity

$$u_b = \text{const.} \left\{\left[\left(\rho_{water} - \rho_{air}\right) \times 2.0 \times 32.174 \times \text{manometer reading}\right] / \rho_{air}\right\}^{0.5} = 16.63 \text{ ft/sec}$$

(3) Reynolds number

$$Re = \frac{u_b \cdot De}{\nu}$$

$$\doteq \frac{16.63 \times 2.834 \times \rho_{air}}{12.0 \times 0.128 \times 10^{-5}} = 23,100$$

(4) Heat flux

$$q_x = (I \times E \times 3.413)/\Delta x - q_{loss} = 128.9 \text{ Btu/hr. ft.}$$

(5) Bulk temperature

$$t_b = q_x / [\pi (r_2^2 - r_1^2) \times u_b \times c_p \times \rho_{air} \times 3600.0] + t_e$$

$$= 84.5 \text{ °F}$$

(6) Heat transfer coefficient

$$h_x = q_x / [2\pi r_1 (t_w - t_b)] = 4.17 \text{ Btu/hr. ft.}^2 \text{ °F}$$

(7) Nusselt number

$$Nu_x = (h_x \cdot De)/k = \frac{4.17 \times De}{12.0 \times 0.0157} = 62.7$$

(8) Eddy diffusivity for heat at $(r - r_1)/(r_2 - r_1) = 0.15$

$$\frac{\epsilon_H}{Pr \cdot \kappa} = (q^+)_x / (3600.0 \times 2\pi r_1 \times c_p \times \mu \times \frac{dt}{dy}) - Pr^{-1}$$

$$= (0.648 \times 128.9)/(3600.0 \times 2\pi r_1 \times 0.24 \times 0.128 \times 10^{-4}$$

$$\times dt/dy) - 1.0/0.71 = 41.4$$

In the course of calculation for these parameters the physical properties of air corresponding to the measured bulk temperature were used. The physical properties were calculated from the following equations which were formulated by a least square method based on the data of Sigwart[111] for the temperature range of 70 to 400 degrees Faranheit:

$$\mu = 0.11005 \times 10^{-4} + 0.18071 t \times 10^{-7} - 0.51587 t^2 \times 10^{-11} \quad \text{(A. 6. 1)}$$

$$c_p = 0.23980 + 0.29458 t \times 10^{-5} + 0.24471 t^2 \times 10^{-7} \quad \text{(A. 6. 2)}$$

$$k = 0.13168 \times 10^{-1} + 0.25432 t \times 10^{-4} - 0.52249 t^2 \times 10^{-8} \quad \text{(A. 6. 3)}$$

REFERENCES

1. H. Reichardt, "Vollständige Darstellung der turbulenten Geschwindigkeitsverteilung in glatten Leitungen", Zeitschrift für angewandte Mathematik und Mechanik, 31, 208-219 (1951).

2. R. G. Deissler, "Analytical Investigation of Turbulent Flow in Smooth Tubes with Heat Transfer with Variable Fluid Properties for Prandtle Number of 1". NACA TN 2242, (1950).

3. J. Laufer, "The Structure of Turbulence in Fully Developed Pipe Flow", NACA Rept. 1174, (1954).

4. C. J. Cremers and E. R. G. Eckert, "Hot-Wire Measurements of Turbulence Correlations in a Triangular Duct", J. of Applied Mech., 609-14, (1962).

5. J. A. Clark, "A Study of Incompressible Turbulent Boundary Layers in Channel Flow", J. of Basic Eng., Trans. ASME, 90, 455-68, Dec. (1968).

6. H. Barrow, "Fluid Flow and Heat Transfer in an Annulus with a Heated Core Tube", Proc. Inst. Mech. Eng., 56, 1113, (1955).

7. Y. Lee and H. Barrow, "Turbulent Flow and Heat Transfer in Concentric and Eccentric Annuli", Proceedings, I. Mech. E., 178, 1-16, (1964).

8. J. A. Brighton and J. B. Jones, "Fully Developed Turbulent Flow in Annuli", J. of Basic Eng., Trans. ASME, Sec. D, 86, 835-44, (1964).

9. R. R. Rothfus, W. K. Sartory and R. I. Kermode, "Flow in Concentric Annuli at High Reynolds Numbers", A. I. Ch. E. Journal, 12, 1086-91, Nov. (1966).

10. S. Levy, "Turbulent Flow in an Annulus", J. of Heat Transfer, ASME, 89, 25-31, Feb. (1967).

11. A. Quarmby, "An Experimental Study of Turbulent Flow Through Concentric Annuli", Int. J. Mech. Sci., 9, 205-21, (1967).

12. A. Quarmby, "An Analysis of Turbulent Flow in Concentric Annuli", Appli. Sci. Res., 19, 250-73, (1968).

13. I. Michiyoshi and T. Nakajima, "Fully Developed Turbulent Flow in a Concentric Annulus", J. of Nuclear Sci. and Tech. 5, 354-59, July, (1968).

14. N. W. Wilson and J. O. Medwell, "An Analysis of Heat Transfer for fully Developed Turbulent Flow in Concentric Annuli", J. of Heat Transfer, Trans. ASME, 90, 43-50, (1968).

15. S. S. Randhava, "An Analysis of Turbulent Flow in Concentric Annuli", A. I. Ch. E. Jour., 15, 132-33, (1969).

16. B. Kjellström and S. Hedberg, "On Shear Stress Distributions for Flow in Smooth or Partially Rough Annuli", AE-243, Aktiebolaget Atomenergi, Stockholm, Sweden, (1966).

17. J. M. Robertson, J. D. Martin, and T. H. Burkhart, "Turbulent Flow in Rough Pipes", I/EC Fundamentals, 7, 253-65, May, (1968).

18. R. G. Deissler, "Analytical and Experimental Investigation of Adiabatic Turbulent Flow in Smooth Tubes", NACA TN 2138, (1950).

19. J. S. Holdhusen, "The Turbulent Boundary Layer in the Inlet Region of Smooth Pipes", Ph. D. Thesis, Univ. of Minesota, (1952).

20. D. Ross, "Turbulent Flow in the Entrance Region of a Pipe", Trans. ASME, 78, 915, (1956).

21. A. H. Shapiro and R. D. Smith, "Friction Coefficients in the Inlet Length of Smooth Rounded Tubes", NACA, TN 1785, (1948).

22. D. A. Bowlus and J. A. Brighton, "Incompressible Turbulent Flow in the Inlet Region of a Pipe", J. of Basic Eng., Trans. ASME, 90, 431-33, Sept. (1968).

23. A. R. Barbin and J. B. Jones, "Turbulent Flow in the Inlet Region of a Smooth Pipe", J. of Basic Eng., Trans. ASME, 29-34, March, (1963).

24. J. G. Knudsen and D. L. Katz, "Fluid Dynamics and Heat Transfer", McGraw-Hill, (1958).

25. Y. L. Wang and P. A. Longwell, "Laminar Flow in the Inlet Section of Parallel Plates", A. I. Ch. E. Jour., 10, 323-29, May, (1964).

26. R. R. Rothfus, C. C. Monrad, K. G. Sikchi and W. J. Keideger, "Isothermal Skin Friction in Flow through Annular Sections", Indus. and Eng. Chem., 47, 913 (1955).

27. R. M. Olson and E. M. Sparrow, "Measurements of Turbulent Flow Development in Tubes and Annuli with Square or Rounded Entrances", A. I. Ch. E. Jour., 9, 766-70, Nov. (1963).

28. T. H. Okiishi and G. K. Serovy, "An Experimental Study of the Turbulent Flow Boundary-Layer Development in Smooth Annuli", J. of Basic Eng. Trans. ASME, 89, 823-36, (1967).

29. K. Sridhar, A. A. Nicol and A. V. A. Padmanabha, "Settling Length for Turbulent Flow of Air in Smooth Annuli with Square-Edged or Bellmouth Entrances", J. of Applied Mech., Trans. ASME, 25-28, Mar., (1970).

30. W. C. Reynolds, R. E. Lundberg and P. A. McCuen, "Heat Transfer in Annular Passages. General Formulation of Problem for Arbitrarily Prescribed Wall Temperatures or Heat Fluxes", Int. Jour. Heat Mass. Transfer, 6, 483-93, (1963).

31. A. Quarmby, "An Improved Application of Von Karman Similarity Hypothesis to Turbulent Flow in Ducts", J. of Mech. Eng. Sci., 11, 14-21, (1969).

32. H. Barrow and Y. Lee, "Heat Transfer with Unsymmetrical Thermal Boundary Conditions", Int. Jour. Heat Mass Transfer, 7, 580, (1964).

33. Y. Lee, "Turbulent Heat Transfer from the Core Tube in Thermal Entrance Regions of Concentric Annuli", Int. Jour. Heat Mass Transfer, 11, 509-22, (1968).

34. W.M. Kays and E.Y. Leung, "Heat Transfer in Annular Passager Hydrodynamically Developed Turbulent Flow with Arbitrarily Prescribed Heat Flux", Int. Jour. Heat Mass Transfer, 6, 537-57, (1963).

35. L.M.K. Boelter, D. Young and H. W. Iversen, "An Investigation of Aircraft Heaters, XXVII. Distribution of Heat Transfer Rate in the Entrance Section of a Circular Tube", NACA TN 14Sl, July (1948).

36. H. F. Poppendiek and L. D. Palmer, "Forced Convection Heat Transfer in Thermal Entrance Regions. Part II", ORNL 914 U. S. Atomic Energy Commission, Oak Redge National Lab. June, (1952).

37. J. P. Hartnett, "Experimental Determination of the Thermal Entrance Length for the Flow of Water and of Oil in Circular Pipes", Trans. ASME, 77, 1211-20, (1955).

38. H. F. Poppendiek, "Forced Convection Heat Transfer in Thermal Entrance Regions. Part I", ORNL, Oak Ridge, Tenn., (1951).

39. E.M. Sparrow, T.M. Hallman and R. Siegel, "Turbulent Heat Transfer in the Thermal Entrance Region of Pipe with Uniform Heat Flux", Appl. Res. Sect. A, 7, 37-52, (1957).

40. P.H. Abberch and S.W. Churchill, "The Thermal Entrance Region in Fully Developed Turbulent Flow", A. I. Ch. E. Jour., 6, 268-73, (1960).

41. W.B. Hall and S.A. Khan, "Experimental Investigation into the Effect of the Thermal Boundary Condition of Heat Transfer in the Entrance Region of a Pipe", J. Mech. Eng. Sci., 6, 250-55, (1964).

42. J.A. Malina and E.M. Sparrow, "Variable Property, Constant Property, and Entrance Region Heat Transfer Results for Turbulent Flow of Water and Oil in a Circular Tube", Chem. Eng. Science, 19, 953-62, Dec., (1964).

43. H. Wolf, "Heating and Cooling Air and Carbon Dioxide in the Thermal Entrance Region of a Circular Duct with Large Gas-to-wall Temperature Difference", Trans. ASME, 81, Series C, (1959).

44. A. F. Mills, "Experimental Investigation of Turbulent Heat Transfer in the Entrance Region of a Circular Conduit", J. Mech. Eng. Sci., 4, 63-77, (1962).

45. D. L. Ulrichson and R. A. Schmitch, "Laminar-Flow Heat Transfer in the Entrance Region of Circular Tubes", Int. J. Heat Mass Transfer, 8, 253-58, (1965).

46. R. Manohar, "Analysis of Laminar-Flow Heat Transfer In the Entrance Region of Circular Tubes", Int. J. Heat Mass Transfer, 12, 15-22, (1969).

47. D. M. McEligot, L. W. Ormand and H. C. Perkins, "Internal Low Reynolds Number Turbulent and Transitional Gas Flow with Heat Transfer", J. of Heat Transfer, Trans. ASME, 88, 239, May, (1966).

48. H. C. Reynolds, T. B. Swearingen, D. M. McEligot and D. M. McEligot, "Thermal Entry for Low Reynolds Number Turbulent Flow", J. Basic Eng. Trans. ASME, Paper 68-WA/FE-11, (1969).

49. L. H. Back, R. F. Cuffel and P. F. Massier, "Laminar, Transition, and Turbulent Boundary-Layer Heat Transfer Measurements with Wall Cooling in Turbulent Air Flow Through a Tube", J. of Heat Transfer, Trans. ASME, 477-87, Nov., (1969).

50. W. G. Schlinger, V. J. Berry, J. L. Mason and B. H. Sage, "Prediction of Temperature Gradients in Turbulent Streams", Gen. Discussion on Heat Transfer, Inst. Mech. Eng., and ASME, 150, (1951).

51. H. Barrow and Y. Lee, "Thermal Entry Region in Turbulent Gas Flow", Engineers, London, 215, 169, (1963).

52. A. P. Hatton and A. Quarmby, "The Effect of Axially Varing and Unsymmetrical Boundary Conditions on Heat Transfer with Turbulent Flow Between Parallel Plates", Int. J. Heat Mass Transfer, 6, 903-13, (1963).

53. A. Quarmby and R. K. Anand, "Turbulent Heat Transfer in the Thermal Entrance Region of Concentric Annuli with Uniform Wall Heat Flux", Int. J. Heat Mass Transfer, 13, 395-411, (1970).

54. A. Quarmby and R. K. Anand, "Turbulent Heat Transfer in Concentric Annuli With Constant Wall Temperatures", J. of Heat Transfer, Trans. ASME, 33-45, Feb., (1970).

55. J. C. Chen and W. S. Yu, "Entrance Region and Variable Heat Flux Effects in Turbulent Heat Transfer to Liquid Metals Flowing in Concentric Annuli", Int. J. Heat Mass Transfer, 13, 667-80, (1970).

56. R. F. Farman and R. B. Beckmann, "Entrance Region Heat Transfer in An Annulus", American Inst. Chemical Eng. Heat Trans. with Phase Change. Chem. Eng. Progress Symposium Ser., 63, (1967).

57. A. Quarmby, "Some Measurements of Turbulent Heat Transfer in the Thermal Entrance Region of Concentric Annuli", Int. J. Heat Mass Transfer, 10, 267-76, (1967).

58. Y. Lee, "Turbulent Flow and Heat Transfer in Concentric and Eccentric Annuli", Ph. D. Thesis, Univ. of Liverpool, (1964).

59. R. Jenkins, "Variation of the Eddy Conductivity with Prandtl Modulus and It's Use in Prediction of Turbulent Heat Transfer Coefficients", Heat Transfer and Fluid Mechanics Inst., 147, Stanford Univ. Press, Stanford, California, (1951).

60. B. N. Furber, W. J. Green and W. R. Vivian, "Heat Transfer in the Entrance Region of An Annulus", Int. J. Heat Mass Transfer, Fourth Int. Heat Transfer Conference, FC 3. 3, (1970).

61. R. G. Deissler, "Investigation of Turbulent Flow and Heat Transfer in Smooth Tubes, Including the Effects of Variable Fluid Properties", Trans. ASME, 73, 101-107, (1951).

62. W. H. Corcoran, F. Page, Jr., W. G. Shlinger and B. H. Sage, "Temperature Gradients in Turbulent Gas Streams", Industrial and Eng. Chem., 44, (1952).

63. R. D. Haberstroh and L. V. Baldwin, "Application of a Simplified Velocity Profile to the Prediction of Pipe-Flow Heat Transfer", Paper No. 67-HT-25, Trans. ASME, Sept., (1967).

64. C. J. Lawn, "Turbulent Heat Transfer at Low Reynolds Numbers", J. of Heat Transfer, Trans. ASME, 532-36, Nov., (1969).

65. R. A. Gowen and J. W. Smith, "Turbulent Heat Transfer from Smooth and Rough Surfaces", Int. J. of Heat Mass Transfer, 11, 1657-74, Nov., (1969).

66. A. R. Pickering, "Forced Convective Heat Transfer to Water in an Annulus", United Kingdom Atomic Energy Authority, AEEW-R 295, (1964).

67. W. A. Sutherland and W. M. Kays, "Heat Transfer in an Annulus with Variable Circumferential Heat Flux", Int. J. Heat Mass Transfer, 7, 1187-94, (1964).

68. A. J. Ziegenhagen, "Approximate Eigenvalues for Heat Transfer to Laminar or Turbulent Flow in an Annulus", Int. J. Heat Mass Transfer, 8, 499-505, (1965).

69. I. Michiyoshi and T. Nakajima, "Heat Transfer in Turbulent Flow with Internal Heat Generation in Concentric Annulus, (I) Fully Developed Thermal Situation", J. of Nuclear Sci. and Tech., 5, 476-84, Sept., (1968).

70. A. Quarmby and R. K. Anand, "Fully Developed Turbulent Heat Transfer in Concentric Annuli with Uniform Wall Heat Fluxes", Chem. Eng. Sci., 24, 171-87, (1969).

71. W. M. Kays, "Numerical Solutions for Laminar-Flow Heat Transfer in Circular Tubes", Trans. ASME, 77, 1265-74, (1955).

72. H. L. Langhaar, "Steady Flow in the Transition Length of a Straight Tube", J. Appl. Mech., 9, A55-58, (1942).

73. E. M. Sparrow, "Analysis of Laminar Forced-Convection Heat Transfer in Entrance Region of Flat Rectangular Ducts", NACA TN 3331, (1955).

74. H. S. Heaton, W. C. Reynolds and W. M. Kays, "Heat Transfer in Annular Passages; Simultaneous Development of Velocity and Temperature Fields in Laminar Flow", Int. J. Heat Mass Trans., 7, 763-81, (1964).

75. R. G. Deissler, "Turbulent Heat Transfer and Friction in the Entrance Regions of Smooth Passages", Trans. ASME, 88, 1221-23, (1955).

76. H. Barrow, "Heat Transfer in the Entry Region of a Pipe", The Engineer, 220, 139-43, (1968).

77. A. Roberts and H. Barrow, "Turbulent Heat Transfer to Air in the Vicinity of the Entry of an Internally Heated Annulus", Proceedings, Thermodynamics and Fluid Mechanics Conv., Bristol, (1968).

78. N. W. Wilson and J. O. Medwell, "An Analysis of the Developing Turbulent Hydrodynamic and Thermal Boundary Layers in an Internally Heated Annulus", Paper No. 70-HT-9, Trans. ASME, 1-7, (1970).

79. Y. Lee and S. D. Park, "Developing Turbulent Flow in Concentric Annuli; An Analytical and Experimental Study", to be published in Wärme-und Stoffübertragung.

80. S. D. Park and Y. Lee, "Diabatic Turbulent Flow in the Entrance Region of Concentric Annuli", Paper No. 70-CSME-9, 84th Annual Meeting, The Eng. Inst. Canada, (1970).

81. H. Barrow, Y. Lee and A. Roberts, "The Similarity Hypothesis Applied to Turbulent Flow in an Annulus", Int. Jour. Heat Mass Transfer, 8, 1499, (1965).

82. H. Schlichting, "Boundary Layer Theory", Pergamon Press, Ltd., New York, 6th Edition, (1968).

83. J.O. Hinze, "Turbulence", McGraw-Hill, Chapter I, (1959).

84. W.M. Kays, "Convective Heat and Mass Transfer", McGraw-Hill, (1966).

85. E. R. G. Eckert, "Introduction to the Transfer of Heat and Mass", McGraw-Hill Book Company, Inc., New York, N. Y., first edition, 74, (1950).

86. A. Roberts, "A Comment on the Turbulent Flow Velocity Profile In a Concentric Annulus", Int. J. Heat Mass Transfer, 10, 709-12, (1967).

87. F. Page, W. G. Schlinger, D.K. Breaux, and B. H. Sage, "Point Values of Eddy Conductivity and Viscosity in Uniform Flow Between Parallel Plates", Ind. Eng. Chem., 44, 424-30, (1952).

88. C. Sleicher and M. Tribus, "Heat Transfer to a Pipe with Turbulent Flow and Arbitrary Wall Temperature Distribution", Trans. ASME, 79, 789, (1957).

89. T. Mizushina, R. Ito, and F. Ogino, "Eddy Diffusivity Distribution Near the Wall", 4th Int. Heat Transfer Conference, 2, FC 218, (1970).

90. E. Y. Leung, W. M. Kays and W. C. Reynolds, "Heat Transfer with Turbulent Flow in Concentric and Eccentric Annuli with Constant and Variable Heat Flux", Report AHT4, Sanford Univ. (1962).

91. T. J. Hanratty, "Development of Temperature Profile for Turbulent Heat Exchange in a Pipe", Tech. Report No. 10, Univ. of Ill., (1961).

92. H. Barrow, "Semi-Theoretical Solution of Asymmetric Heat Transfer in Annular Flow", Journal Mech. Eng. Sci., 2, 331-36, (1960).

93. British Standard Code, "Orifice Plate with Corner Tappings", B. S. 1042: Part 1, 107, (1964).

94. A. D. Young and J. N. Maas, "The Behaviour of a Pitot Tube in a Traverse Pressure Gradient", A. R. C., R & M 1770, (1937).

95. F. Homann, "The Effect of High Viscosity on the Flow Around a Cylinder and a Sphere", NACA TM 1344, (1952).

96. B. Kjellström and S. Hedberg, "Calibration of a DISA Hot-wire Anemometer and Measurements in a Circular Channel for Confirmation of the Calibration", DISA Information No. 9, (1970).

97. DISA Elecktronik A/S, Herlev, Denmark, "Instruction Manual for Type 55D 41/42 Calibration Equipment", (1970).

98. C. A. Bankston, "The Transition from Turbulent to Laminar Gas Flow in a Heated Pipe", ASME paper 69-HT-54, (1969) and J. of Heat Transfer, Trans. ASME, 92, 569-79, Nov., (1970).

99. IBM Application Program, "System 360 Sci. Subroutine Package", 360A-CM-03X, Version III, 1968.

100. F. B. Hildebrand, "Introduction ot Numerical Analysis", McGraw-Hill, New York, 64-68, (1956).

101. E. S. Davis, "Heat Transfer and Pressure Drop in Annuli", ASME Trans. 65, 755, (1943).

102. O. Walger, "Wärmeübergang in Ringförmigen Strömungs-querschnitten", Chem. Ing. Tech., 25, 474, (1953).

103. S. J. Kline and E. A. McClintock, "The Description of Uncertainties in Single Sample Experiments", Mech. Eng., 3, (1953).

104. I. G. Dalla Lana and S. E. Christiansen, "Air Flow in a Tube with a Diverging Inlet: I Development of the Turbulent Velocity Profile", The Canadian J. of Chem. Eng., 45, (1967).

105. O. E. Dwyer, "Recent Development Liquid-Metal Heat Transfer", Atomic Energy Review, 4, 3-92, (1966).

106. H. B. Dwight, "Tables of Integrals and Other Mathematical Data", The MacMillan Co., New York, 4th Edition, (1965).

107. W. H. McAdams, "Heat Transmission", McGraw-Hill, New York, (1954).

108. P. J. Schneider, "Conduction Heat Transfer", Addison-Wesley Pub. Co. Inc., (1957).

109. F. A. MacMillan, "Experiments on Pitot Tubes in Shear Flow", ARC R&M 3028, (1957).

110. A. Quarmby and M. K. Das, "Displacement Effects on Pitot Tubes with Rectangular Mouths", The Aeronautical Quarterly, (1968).

111. E. R. G. Eckert and R. M. Drake, Jr., "Heat and Mass Transfer", McGraw-Hill, New York, Appendix of Property Values, (1959).

Table 3.1 Constant k_1, Concentric Annuli, Developing Flow.

(a) $\alpha = 1.61$

δ^* \ Re	23,000	44,000	77,000	110,000
0.05		0.48981	0.46402	0.45704
0.10	0.47933	0.45803	0.45310	0.45114
0.15	0.46101	0.45310	0.44984	0.44790
0.20	0.45506	0.45179	0.44790	0.44596
0.25	0.45310	0.44984	0.44596	0.44468
0.50	0.44790	0.44468	0.44276	0.44148
0.75	0.44532	0.44276	0.44084	0.44021
1.00	0.44340	0.44148	0.44021	0.43894

(b) $\alpha = 2.31$

δ^* \ Re	23,000	44,000	77,000	110,000
0.05		0.59628	0.52378	0.50995
0.10	0.55468	0.51191	0.49840	0.49523
0.15	0.51781	0.50030	0.49272	0.48897
0.20	0.50607	0.49650	0.48897	0.48524
0.25	0.50030	0.49146	0.48524	0.48278
0.50	0.48897	0.48278	0.47910	0.47667
0.75	0.48401	0.47910	0.47546	0.47425
1.00	0.48032	0.47667	0.47304	0.47184

Table 3.1 (continued)

(c) $\alpha = 3.83$

Re / δ*	23,000	44,000	77,000	110,000
0.05		0.71751	0.62915	0.60218
0.10	0.68676	0.60596	0.57999	0.56921
0.15	0.61745	0.57999	0.56566	0.55746
0.20	0.59469	0.56921	0.55746	0.55053
0.25	0.58363	0.56213	0.55283	0.54595
0.50	0.55746	0.54595	0.53917	0.53469
0.75	0.54824	0.53917	0.53246	0.53025
1.00	0.54142	0.53469	0.53025	0.52584

(d) $\alpha = 15.32$

Re / δ*	23,000	44,000	77,000	110,000
0.05			1.09600	1.00950
0.10	1.27443	1.02342	0.93412	0.89653
0.15	1.06637	0.94268	0.88435	0.85656
0.20	0.98222	0.90475	0.85656	0.83344
0.25	0.94268	0.88032	0.83725	0.81838
0.50	0.85656	0.82212	0.79631	0.78193
0.75	0.82588	0.79631	0.77837	0.76432
1.00	0.80727	0.78193	0.76432	0.75395

Table 3.2 Theoretical Friction Factor and Entrance Length for Concentric Annulus, Entrance Region.

α	Re	δ*	x/De	$f \times 10^3$
		0.2	0.912	12.664
		0.3	1.498	11.174
		0.4	2.273	10.224
1.10	10088.	0.5	3.165	9.650
		0.6	4.156	9.298
		0.7	5.238	9.085
		0.8	6.404	8.968
		0.9	7.637	8.915
		1.0	8.926	8.907
		0.1	0.442	12.073
		0.2	1.080	9.416
		0.3	1.925	8.261
		0.4	2.895	7.667
1.10	23521.	0.5	3.958	7.322
		0.6	5.085	7.109
		0.7	6.293	6.982
		0.8	7.585	6.915
		1.0	10.356	6.893
		0.1	0.498	9.705
		0.2	1.312	7.595
		0.3	2.286	6.790
		0.4	3.349	6.370
1.10	44142.	0.5	4.507	6.125
		0.6	5.739	5.976
		0.7	7.038	5.887
		0.8	8.419	5.841
		1.0	11.405	5.838
		0.1	0.601	7.938
		0.2	1.536	6.402
		0.3	2.592	5.803
		0.4	3.758	5.439
1.10	77864.	0.5	5.003	5.304
		0.6	6.320	5.191
		0.7	7.718	5.125
		1.0	12.334	5.093

Table 3.2 (continued)

α	Re	δ^*	x/De	$f x 10^3$
		0.1	0.670	7.091
		0.2	1.664	5.816
		0.3	2.785	5.312
		0.4	3.999	5.043
1.10	110368.	0.5	5.308	4.886
		0.6	6.677	4.788
		0.7	8.127	4.732
		1.0	12.896	4.707
		0.1	0.785	5.952
		0.2	1.874	5.001
		0.3	3.090	4.614
		0.4	4.400	4.404
1.10	200736.	0.5	5.784	4.279
		0.6	7.251	4.203
		0.7	8.807	4.160
		1.0	13.834	4.142
		0.2	0.936	12.866
		0.3	1.419	11.280
		0.4	2.088	10.311
1.61	10071.	0.5	2.882	9.744
		0.6	3.763	9.391
		0.7	4.725	9.167
		0.8	5.772	9.039
		0.9	6.903	8.983
		1.0	8.114	8.978
		0.1	0.448	12.328
		0.2	0.979	9.580
		0.3	1.709	8.415
		0.4	2.546	7.808
1.61	23011.	0.5	3.477	7.454
		0.6	4.494	7.240
		0.7	5.591	7.109
		0.8	6.769	7.039
		1.0	9.358	7.014

Table 3.2 (continued)

α	Re	δ^*	x/De	$f \times 10^3$
		0.1	0.459	9.795
		0.2	1.159	7.685
		0.3	1.999	6.877
		0.4	2.941	6.457
1.61	44200.	0.5	3.973	6.212
		0.6	5.086	6.060
		0.7	6.281	5.972
		0.8	7.553	5.924
		1.0	10.332	5.919
		0.1	0.531	8.041
		0.2	1.329	6.499
		0.3	2.256	5.899
		0.4	3.281	5.581
1.61	77566.	0.5	4.394	5.395
		0.6	5.587	5.279
		0.7	6.860	5.212
		0.8	8.214	5.180
		1.0	11.150	5.180
		0.1	0.586	7.195
		0.2	1.441	5.914
		0.3	2.422	5.405
		0.4	3.501	5.134
1.61	110071.	0.5	4.667	4.975
		0.6	5.915	4.878
		0.7	7.241	4.820
		0.8	8.644	4.789
		1.0	11.684	4.789
		0.1	0.677	6.072
		0.2	1.621	5.109
		0.3	2.686	4.715
		0.4	3.848	4.503
1.61	198034.	0.5	5.097	4.377
		0.6	6.427	4.299
		0.7	7.836	4.253
		1.0	12.529	4.229

Table 3.2 (continued)

α	Re	δ^*	x/De	$f\times10^3$
		0.2	0.918	12.917
		0.3	1.326	11.295
		0.4	1.921	10.338
2.31	10005.	0.5	2.626	9.761
		0.6	3.425	9.425
		0.7	4.311	9.212
		0.8	5.283	9.088
		0.9	6.343	9.026
		1.0	7.489	9.010
		0.1	0.431	12.344
		0.2	0.883	9.571
		0.3	1.521	8.418
		0.4	2.265	7.826
2.31	22974.	0.5	3.103	7.480
		0.6	4.028	7.270
		0.7	5.040	7.142
		0.8	6.133	7.074
		1.0	8.575	7.050
		0.1	0.415	9.793
		0.2	1.019	7.706
		0.3	1.758	6.908
		0.4	2.597	6.494
2.31	43973.	0.5	3.527	6.252
		0.6	4.545	6.103
		0.7	5.645	6.016
		0.8	6.829	5.970
		1.0	9.447	5.965
		0.1	0.470	8.067
		0.2	1.165	6.539
		0.3	1.985	5.944
		0.4	2.905	5.628
2.31	77068.	0.5	3.911	5.445
		0.6	5.010	5.330
		0.7	6.191	5.264
		0.8	7.449	5.234
		1.0	10.243	5.226

Table 3.2 (continued)

α	Re	δ^*	x/De	$f x 10^3$
2.31	110076.	0.1	0.512	7.208
		0.2	1.257	5.941
		0.3	2.124	5.438
		0.4	3.088	5.170
		0.5	4.140	5.013
		0.6	5.280	4.917
		0.7	6.507	4.860
		0.8	7.820	4.830
		1.0	10.700	4.830
2.31	199888.	0.1	0.589	6.082
		0.2	1.413	5.130
		0.3	2.356	4.741
		0.4	3.398	4.529
		0.5	4.529	4.404
		0.6	5.749	4.327
		0.7	7.048	4.286
		1.0	11.491	4.262
3.83	10009.	0.2	0.891	12.739
		0.3	1.201	11.120
		0.4	1.696	10.204
		0.5	2.302	9.661
		0.6	3.001	9.333
		0.7	3.785	9.139
		0.8	4.660	9.029
		0.9	5.633	8.974
		1.0	6.689	8.971
3.83	22867.	0.1	0.411	12.200
		0.2	0.764	9.453
		0.3	1.293	8.343
		0.4	1.928	7.774
		0.5	2.651	7.448
		0.6	3.467	7.251
		0.7	4.367	7.137
		0.8	5.358	7.076
		0.9	6.443	7.054
		1.0	7.648	7.048

Table 3.2 (continued)

α	Re	δ*	x/De	fx10³
		0.1	0.359	9.601
		0.2	0.852	7.597
		0.3	1.468	6.837
		0.4	2.185	6.443
3.83	44460.	0.5	2.994	6.215
		0.6	3.888	6.080
		0.7	4.875	6.001
		0.8	5.956	5.959
		1.0	8.416	5.951
		0.1	0.388	7.954
		0.2	0.952	6.479
		0.3	1.633	5.907
		0.4	2.417	5.604
3.83	77170.	0.5	3.286	5.430
		0.6	4.248	5.326
		0.7	5.306	5.264
		1.0	9.048	5.235
		0.1	0.421	7.100
		0.2	1.032	5.882
		0.3	1.761	5.399
		0.4	2.587	5.143
3.83	111778.	0.5	3.504	4.994
		0.6	4.517	4.904
		0.7	5.629	4.851
		0.8	6.816	4.829
		1.0	9.546	4.824
		0.1	0.477	6.015
		0.2	1.151	5.094
		0.3	1.941	4.717
		0.4	2.824	4.517
3.83	202160.	0.5	3.820	4.395
		0.6	4.887	4.326
		0.7	6.071	4.284
		1.0	10.202	4.267

Table 3.2 (continued)

α	Re	δ^*	x/De	$f \times 10^3$
		0.3	1.082	10.705
		0.4	1.455	9.875
8.00	10077.	0.5	1.939	9.395
		0.6	2.513	9.113
		0.7	3.169	8.953
		0.8	3.942	8.857
		1.0	5.739	8.829
		0.1	0.373	11.642
		0.2	0.637	9.047
		0.3	1.050	8.039
		0.4	1.553	7.530
8.00	23111.	0.5	2.140	7.242
		0.6	2.812	7.075
		0.7	3.570	6.981
		1.0	6.383	6.950
		0.1	0.291	9.215
		0.2	0.642	7.358
		0.3	1.108	6.659
		0.4	1.670	6.302
8.00	44533.	0.5	2.318	6.100
		0.6	3.067	5.981
		0.7	3.909	5.916
		1.0	7.087	5.888
		0.1	0.292	7.654
		0.2	0.698	6.288
		0.3	1.216	5.760
		0.4	1.831	5.487
8.00	77708.	0.5	2.533	5.331
		0.6	3.335	5.241
		0.7	4.244	5.191
		1.0	7.602	5.178

Table 3.2 (continued)

α	Re	δ^*	x/De	$f\times10^3$
		0.1	0.306	6.877
		0.2	0.745	5.737
		0.3	1.297	5.288
		0.4	1.945	5.054
8.00	111003.	0.5	2.686	4.920
		0.6	3.531	4.842
		0.7	4.487	4.798
		1.0	7.981	4.790
		0.1	0.340	5.819
		0.2	0.829	4.959
		0.3	1.430	4.611
		0.4	2.131	4.427
8.00	204951.	0.5	2.944	4.319
		0.6	3.846	4.258
		0.7	4.858	4.225
		1.0	8.592	4.220
		0.3	1.060	10.351
		0.4	1.334	9.596
15.32	10017.	0.5	1.720	9.171
		0.6	2.197	8.926
		0.7	2.749	8.793
		1.0	4.982	8.725
		0.2	0.533	8.739
		0.3	0.828	7.814
		0.4	1.218	7.353
15.32	23153.	0.5	1.697	7.097
		0.6	2.257	6.953
		0.7	2.914	6.876
		1.0	5.493	6.855

Table 3.2 (continued)

α	Re	δ^*	x/De	$f \times 10^3$
		0.1	0.249	8.892
		0.2	0.500	7.150
		0.3	0.854	6.502
		0.4	1.298	6.176
15.32	43882.	0.5	1.834	5.994
		0.6	2.465	5.892
		0.7	3.204	5.838
		1.0	6.029	5.833
		0.1	0.227	7.398
		0.2	0.525	6.117
		0.3	0.921	5.627
		0.4	1.413	5.377
15.32	77060.	0.5	1.998	5.238
		0.6	2.692	5.159
		1.0	6.524	5.121
		0.1	0.229	6.682
		0.2	0.552	5.604
		0.3	0.975	5.184
		0.4	1.494	4.969
15.32	108790.	0.5	2.114	4.848
		0.6	2.834	4.781
		1.0	6.856	4.749
		0.1	0.245	5.672
		0.2	0.608	4.855
		0.3	1.072	4.528
		0.4	1.636	4.358
15.32	199933.	0.5	2.314	4.262
		0.6	3.083	4.209
		1.0	7.387	4.187
		0.3	1.145	9.943
		0.4	1.330	9.263
30.00	10220.	0.5	1.629	8.893
		0.6	2.014	8.688
		0.7	2.482	8.580
		1.0	4.364	8.565

Table 3.2 (continued)

α	Re	δ*	x/De	fx10³
		0.2	0.488	8.450
		0.3	0.703	7.596
		0.4	1.004	7.177
30.00	23072.	0.5	1.387	6.951
		0.6	1.844	6.829
		1.0	4.603	6.778
		0.1	0.222	8.534
		0.2	0.396	6.914
		0.3	0.662	6.317
		0.4	1.009	6.022
30.00	44124.	0.5	1.442	5.862
		0.6	1.965	5.776
		1.0	5.017	5.755
		0.1	0.180	7.141
		0.2	0.391	5.941
		0.3	0.694	5.487
		0.4	1.084	5.259
30.00	77003.	0.5	1.562	5.136
		0.6	2.132	5.071
		1.0	5.504	5.058
		0.1	0.172	6.436
		0.2	0.402	5.431
		0.3	0.727	5.044
		0.4	1.139	4.848
30.00	110090.	0.5	1.649	4.742
		0.6	2.255	4.686
		1.0	5.797	4.677
		0.1	0.198	5.507
		0.2	0.481	4.734
		0.3	0.853	4.428
		0.4	1.318	4.271
30.00	197953.	0.5	1.878	4.186
		1.0	6.251	4.141

Table 3.3 Theoretical Nusselt Number and Entrance Length for Concentric Annulus, Inner Wall Heated, Simultaneously Developing Region, Pr = 0.71

α	Re	δ*	x/De	Nu
		0.1	0.363	85.56
		0.2	1.437	56.25
1.61	10093.	0.4	4.300	42.33
		0.6	9.139	37.36
		0.8	16.552	34.34
		1.0	27.436	32.44
		0.1	0.651	123.91
		0.2	1.941	92.03
1.61	23029.	0.4	5.174	74.20
		0.6	10.741	66.40
		0.8	19.238	61.55
		1.0	31.468	58.48
		0.1	0.846	181.77
		0.2	2.296	142.06
1.61	44217.	0.4	5.798	118.97
		0.6	11.834	107.98
		0.8	21.027	100.65
		1.0	34.218	96.01
		0.1	1.000	261.41
		0.2	2.569	213.02
1.61	77582.	0.4	6.293	181.57
		0.6	12.680	166.73
		0.8	22.386	156.06
		1.0	36.354	149.31
		0.1	1.088	334.06
		0.2	2.728	277.24
1.61	110086.	0.4	6.570	239.36
		0.6	13.187	219.61
		0.8	23.188	206.05
		1.0	37.629	197.49

Table 3.3 (continued)

α	Re	δ*	x/De	Nu
1.61	198048.	0.1	1.227	512.13
		0.2	2.979	434.54
		0.4	7.018	381.04
		0.6	13.969	351.50
		0.8	24.415	331.03
		1.0	39.614	318.13
2.31	10017.	0.1	0.371	85.89
		0.2	1.860	58.04
		0.4	4.013	44.70
		0.6	8.746	39.51
		0.8	15.536	36.64
		1.0	25.620	34.86
2.31	22984.	0.1	0.631	127.00
		0.2	1.823	95.98
		0.4	4.772	78.62
		0.6	10.179	70.88
		0.8	17.879	66.22
		1.0	29.111	63.33
2.31	43982.	0.1	0.798	187.93
		0.2	2.124	149.55
		0.4	5.312	126.12
		0.6	11.149	115.38
		0.8	19.418	108.31
		1.0	31.483	103.95
2.31	77077.	0.1	0.931	273.49
		0.2	2.363	225.34
		0.4	5.720	194.94
		0.6	11.925	178.38
		0.8	20.622	168.06
		1.0	33.385	161.72

Table 3.3 (continued)

α	Re	δ^*	x/De	Nu
		0.1	1.010	350.91
		0.2	2.506	294.08
2.31	110085.	0.4	5.964	257.73
		0.6	12.368	236.62
		0.8	21.299	223.41
		1.0	34.488	215.31
		0.1	1.129	547.95
		0.2	2.720	468.88
2.31	199897.	0.4	6.360	414.52
		0.6	13.079	382.49
		0.8	22.369	362.30
		1.0	36.261	350.01
		0.1	0.387	86.55
		0.2	1.318	60.98
3.83	10116.	0.4	3.676	49.20
		0.6	8.065	44.52
		0.8	13.900	41.92
		1.0	22.907	40.36
		0.1	0.601	131.97
		0.2	1.657	102.97
3.83	22959.	0.4	4.254	86.73
		0.6	9.260	79.45
		0.8	15.760	75.26
		1.0	25.674	72.77
		0.1	0.737	199.96
		0.2	1.900	163.75
3.83	44542.	0.4	4.663	142.03
		0.6	10.072	131.11
		0.8	16.979	124.67
		1.0	27.600	120.88

Table 3.3 (continued)

α	Re	δ^*	x/De	Nu
		0.1	0.841	291.68
		0.2	2.083	246.58
3.83	77246.	0.4	4.974	217.36
		0.6	10.675	201.70
		0.8	17.857	192.32
		1.0	29.060	186.86
		0.1	0.902	385.87
		0.2	2.200	328.92
3.83	111850.	0.4	5.188	290.98
		0.6	1.084	270.85
		0.8	18.439	258.69
		1.0	30.036	251.66
		0.1	1.002	598.96
		0.2	2.386	519.33
3.83	202228.	0.4	5.486	468.05
		0.6	11.645	437.65
		0.8	19.221	419.02
		1.0	31.436	408.39
		0.1	0.410	97.05
		0.2	1.065	78.41
15.32	10059.	0.4	2.958	70.62
		0.6	5.739	67.63
		0.8	9.178	66.00
		1.0	16.476	64.88
		0.1	0.501	157.62
		0.2	1.181	136.15
15.32	23193.	0.4	3.263	124.73
		0.6	6.255	120.28
		0.8	9.815	117.76
		1.0	17.695	116.54

Table 3.3 (continued)

α	Re	δ*	x/De	Nu
		0.1	0.550	243.93
		0.2	1.271	216.80
15.32	43919.	0.4	3.479	200.59
		0.6	6.589	194.11
		0.8	10.176	190.36
		1.0	18.563	188.63
		0.1	0.592	370.04
		0.2	1.354	333.16
15.32	77096.	0.4	3.659	310.88
		0.6	6.851	301.52
		0.8	10.426	296.04
		1.0	19.300	293.60
		0.1	0.618	484.30
		0.2	1.403	438.64
15.32	108824.	0.4	3.770	409.33
		0.6	7.006	397.49
		0.8	10.562	390.48
		1.0	19.746	378.34
		0.1	0.668	777.94
		0.2	1.493	713.20
15.32	199967.	0.4	3.949	671.14
		0.6	7.245	652.90
		0.8	10.743	641.97
		1.0	20.503	637.47

Table 3.4 Theoretical Nusselt Number and Entrance Length for Concentric Annulus, Inner Wall Heated, Simultaneously Developing Region, $\alpha = 2.31$

Pr	Re	δ*	x/De	Nu
		0.1	0.089	54.62
		0.2	0.414	27.93
0.01	43982.	0.4	1.707	16.05
		0.6	3.955	12.30
		0.8	7.150	10.44
		1.0	11.334	9.45
		0.1	0.456	84.77
		0.2	1.521	56.48
0.10	43982.	0.4	4.401	42.36
		0.6	9.526	35.79
		0.8	16.789	31.88
		1.0	26.838	29.65
		0.1	0.798	187.93
		0.2	2.124	149.55
0.71	43982.	0.4	5.312	126.12
		0.6	11.149	115.38
		0.8	19.418	108.31
		1.0	31.483	103.95
		0.1	0.836	218.01
		0.2	2.177	176.69
1.00	43982.	0.4	5.382	150.68
		0.6	11.258	139.39
		0.8	19.581	131.92
		1.0	31.843	127.26
		0.1	0.929	342.63
		0.2	2.299	290.00
3.00	43982.	0.4	5.532	254.04
		0.6	11.473	241.88
		0.8	19.889	234.00
		1.0	32.716	228.91

Table 3.4 (continued)

Pr	Re	δ*	x/De	Nu
10.00	43982.	0.1	1.004	529.90
		0.2	2.390	461.65
		0.4	5.638	411.74
		0.6	11.603	400.06
		0.8	20.051	393.30
		1.0	33.595	388.83
30.00	43982.	0.1	1.070	750.81
		0.2	2.466	664.05
		0.4	5.724	597.84
		0.6	11.696	586.93
		0.8	20.154	581.86
		1.0	34.676	578.48

Table 3.5 Theoretical Nusselt Number and Entrance Length for Concentric Annulus, Fully Developed Region, Inner wall Heated.

α	Pr	Re	x/De	Nu
2.31	0.01	43982.	11.334	9.45
	0.10	43982.	26.838	29.65
	1.00	43982.	31.843	127.26
	3.00	43982.	32.716	228.91
	10.00	43982.	33.595	388.83
	30.00	43982.	34.676	578.48
1.10	0.71	10088.	29.140	30.40
		23521.	33.839	55.38
		44143.	36.861	89.07
		77864.	39.323	139.72
		110368.	40.738	183.10
		200736.	43.010	297.00
1.61	0.71	10093.	27.436	32.44
		23029.	31.468	58.48
		44217.	34.218	96.01
		77582.	36.353	149.31
		110086.	37.629	197.49
		198048.	39.614	318.13
2.31	0.71	10017.	25.620	34.86
		22984.	29.111	63.33
		43982.	31.483	103.95
		77077.	33.385	161.72
		110085.	34.488	215.31
		199897.	36.261	350.01
3.83	0.71	10116.	22.907	40.36
		22959.	25.674	72.77
		44542.	27.600	120.88
		77246.	29.060	186.86
		111850.	30.036	251.66
		202228.	31.436	408.39

Table 3.5 (continued)

α	Pr	Re	x/De	Nu
8.00	0.71	10077.	19.213	51.13
		23111.	21.025	92.60
		44533.	22.350	153.00
		77706.	23.369	237.74
		111003.	24.013	316.99
		204952.	25.063	523.80
15.32	0.71	10059.	16.476	64.88
		23193.	17.695	116.54
		43919.	18.563	188.63
		77096.	19.300	293.60
		108790.	19.746	387.34
		199967.	20.503	637.47
30.00	0.71	10221.	14.339	86.33
		23072.	15.430	147.84
		44124.	15.604	237.23
		77003.	16.091	365.08
		110090.	16.406	485.40
		197953.	16.923	782.97

Table 3.6 Theoretical Nusselt Number and Entrance Length for Concentric Annulus, Outer Wall Heated, Simultaneously Developing Region, Pr = 0.71

α	Re	δ*	x/De	Nu
		0.1	0.354	85.59
		0.2	1.404	55.09
1.61	10116.	0.4	4.337	40.81
		0.6	8.413	36.06
		0.8	15.490	33.08
		1.0	26.116	31.26
		0.1	0.652	122.06
		0.2	1.982	89.17
1.61	23048.	0.4	5.311	70.85
		0.6	9.943	63.87
		0.8	18.176	59.15
		1.0	30.130	56.22
		0.1	0.873	176.65
		0.2	2.365	136.86
1.61	44234.	0.4	5.990	113.26
		0.6	9.943	63.87
		0.8	20.018	96.58
		1.0	32.903	92.13
		0.1	1.040	252.45
		0.2	2.664	203.71
1.61	77598.	0.4	6.519	172.60
		0.6	11.844	159.68
		0.8	21.446	149.55
		1.0	35.072	143.08
		0.1	1.137	321.66
		0.2	2.839	264.63
1.61	110071.	0.4	6.835	227.30
		0.6	12.330	210.07
		0.8	22.276	197.27
		1.0	36.348	189.05

Table 3.6 (continued)

α	Re	δ*	x/Dc	Nu
		0.1	1.285	489.64
		0.2	3.110	413.93
1.61	198061.	0.4	7.326	361.48
		0.6	13.101	335.80
		0.8	23.584	316.63
		1.0	38.361	304.23
		0.1	0.365	85.79
		0.2	1.345	55.87
2.31	10057.	0.4	4.113	41.56
		0.6	7.622	36.78
		0.8	13.987	33.98
		1.0	23.494	32.31
		0.1	0.643	123.24
		0.2	1.893	90.36
2.31	23018.	0.4	5.015	72.22
		0.6	8.973	65.66
		0.8	16.368	61.22
		1.0	26.993	58.52
		0.1	0.843	177.19
		0.2	2.248	138.86
2.31	44012.	0.4	5.639	115.44
		0.6	9.910	106.51
		0.8	17.992	99.90
		1.0	29.407	95.83
		0.1	1.001	256.39
		0.2	2.525	208.13
2.31	77104.	0.4	6.133	176.98
		0.6	10.648	164.21
		0.8	19.263	154.70
		1.0	31.328	148.77

Table 3.6 (continued)

α	Re	δ*	x/De	Nu
		0.1	1.091	327.65
		0.2	2.688	270.99
2.31	110110.	0.4	6.432	233.65
		0.6	11.091	217.46
		0.8	20.018	205.38
		1.0	32.471	197.82
		0.1	1.228	503.56
		0.2	2.944	428.04
2.31	199920.	0.4	6.897	375.28
		0.6	11.791	350.63
		0.8	21.208	332.43
		1.0	34.290	320.95
		0.1	0.386	84.90
		0.2	1.267	56.94
3.83	10029.	0.4	3.817	42.41
		0.6	6.728	37.87
		0.8	12.043	35.44
		1.0	19.995	34.04
		0.1	0.639	125.37
		0.2	1.777	92.41
3.83	22895.	0.4	4.640	74.59
		0.6	7.851	68.52
		0.8	14.032	64.33
		1.0	22.775	62.07
		0.1	0.818	182.24
		0.2	2.107	144.48
3.83	44482.	0.4	5.211	121.18
		0.6	8.612	112.19
		0.8	15.405	106.31
		1.0	24.777	102.87

Table 3.6 (continued)

α	Re	δ*	x/De	Nu
3.83	77199.	0.1	0.952	261.66
		0.2	2.347	214.73
		0.4	5.636	183.80
		0.6	9.222	172.26
		0.8	16.454	163.83
		1.0	26.313	158.87
3.83	111790.	0.1	1.038	341.77
		0.2	2.504	285.59
		0.4	5.903	246.04
		0.6	9.592	231.03
		0.8	17.121	220.14
		1.0	27.302	213.75
3.83	202160.	0.1	1.156	524.06
		0.2	2.717	446.13
		0.4	6.322	393.61
		0.6	10.155	370.57
		0.8	18.124	355.86
		1.0	28.796	346.19
15.32	10040.	0.1	0.461	82.53
		0.2	0.910	59.34
		0.4	3.309	45.93
		0.6	5.516	41.23
		0.8	8.290	39.44
		1.0	12.801	38.65
15.32	23174.	0.1	0.664	129.41
		0.2	1.511	98.79
		0.4	3.833	81.61
		0.6	6.339	76.25
		0.8	9.396	72.95
		1.0	14.202	71.69

Table 3.6 (continued)

α	Re	δ*	x/De	Nu
		0.1	0.777	190.11
		0.2	1.766	154.60
15.32	43901.	0.4	4.214	131.80
		0.6	6.817	123.24
		0.8	10.159	119.57
		1.0	15.206	117.68
		0.1	0.868	279.17
		0.2	1.942	234.34
15.32	77060.	0.4	4.537	204.72
		0.6	7.260	192.87
		0.8	10.787	187.00
		1.0	16.058	184.27
		0.1	0.915	357.19
		0.2	2.053	307.15
15.32	108790.	0.4	4.701	268.64
		0.6	7.519	254.90
		0.8	11.151	247.09
		1.0	16.562	243.64
		0.1	0.996	564.56
		0.2	2.202	490.56
15.32	199934.	0.4	5.014	438.87
		0.6	7.916	416.05
		0.8	11.773	406.69
		1.0	17.433	401.40

Table 3.7 Theoretical Nusselt Number and Entrance Length for Concentric Annulus, Fully Developed Region, Outer Wall Heated, $\alpha = 2.31$

Pr	Re	x/De	Nu
0.01	10005.	3.243	6.71
	22974.	6.564	7.60
	43973.	10.603	8.85
	110076.	18.139	12.27
	199888.	23.402	16.35
0.10	10005.	14.837	12.10
	22974.	20.814	18.56
	43973.	25.095	27.57
	110076.	30.117	51.52
	199888.	32.766	79.71
0.71	10057.	23.494	32.31
	23018.	26.993	58.52
	77104.	31.328	148.77
	110110.	32.471	197.82
	199920.	34.290	320.95
1.00	10005.	24.375	38.29
	22974.	27.513	70.74
	77068.	31.545	183.20
	110076.	32.636	244.62
	199888.	34.394	399.35
3.00	10005.	26.612	64.51
	22974.	28.782	123.95
	77068.	32.057	335.18
	110076.	33.023	452.39
	199888.	34.635	750.80

Table 3.7 (continued)

Pr	Re	x/De	Nu
10.00	10005.	28.924	104.80
	22974.	30.048	206.79
	77068.	32.553	576.81
	110076.	33.396	784.83
	199888.	34.864	1319.18
30.00	10005.	31.755	152.38
	22974.	31.586	304.85
	77068.	33.152	864.43
	110076.	33.846	1181.33
	199888.	35.141	1999.52

Table 3.8 Theoretical Nusselt Number and Entrance Length for Concentric Annulus, Fully Developed Region, Outer Wall Heated, Pr = 0.71

α	Re	x/De	Nu
	10088.	28.873	30.18
	23521.	10.356	54.98
1.10	44143.	36.598	88.39
	77864.	39.066	137.61
	110368.	40.483	181.60
	200736.	42.765	294.47
	10116.	26.116	31.26
	23048.	30.130	56.22
1.61	44234.	32.903	92.13
	77598.	35.072	143.08
	11071.	36.348	189.05
	198061.	38.361	304.23
	10057.	23.494	32.31
	23018.	26.993	58.52
2.31	44012.	29.407	95.83
	77104.	31.328	148.77
	110110.	32.471	197.82
	199920.	34.290	320.95
	10029.	19.995	34.04
	22895.	22.775	62.07
3.83	44482.	24.777	102.87
	77199.	26.313	158.87
	111790.	27.302	213.75
	202160.	28.796	346.19
	10077.	15.690	36.78
	23111.	17.635	67.53
8.00	44533.	19.042	111.96
	77708.	20.172	174.07
	111003.	20.868	232.00
	204952.	22.019	382.88

Table 3.8 (continued)

α	Re	x/De	Nu
15.32	10040.	12.801	38.65
	23174.	14.202	71.69
	43901.	15.206	117.68
	77060.	16.058	184.27
	108790.	16.562	243.64
	199934.	17.433	401.40
30.00	10221.	10.688	40.78
	23072.	11.643	74.89
	44124.	12.382	124.35
	77003.	12.989	194.50
	110090.	13.378	260.28
	197953.	14.011	422.35

TABLE 4.1

Essential Dimensions

Main Annular Duct Assembly

	O.D.	I.D.	Wall Thic.	Material	α	De	x/De*
Outer Tube	4.0	3.834	0.083	Copper		3.834	43.8
Core 1	2.375	2.067	0.154	S. S.	1.61	1.459	115.2
Core 2	1.660	1.442	0.109	S. S.	2.31	2.174	77.3
Core 3	1.000	0.930	0.035	S. S.	3.83	2.834	59.3
Core 4	0.250	0.152	0.049	S. S.	15.32	3.584	46.8

*available

Table 5.1 Experimental Friction Factor of Concentric Annulus, Entrance Region.

α	Re	x/De	$(p_e-p)/u_b^2$	$f\times10^3$
		1.03	0.625	10.459
		2.06	0.645	8.949
		4.11	0.675	7.579
1.61	18319.	6.85	0.718	7.440
		15.08	0.836	7.198
		30.16	1.050	7.280
		58.26	1.488	7.291
		102.81	2.150	7.391
		1.03	0.620	6.268
		2.06	0.633	5.671
		4.11	0.653	5.683
1.61	43155.	6.85	0.689	6.225
		10.97	0.736	6.122
		38.38	1.058	6.098
		69.91	1.456	6.136
		115.15	2.037	5.903
		1.03	0.632	6.297
		2.06	0.636	5.697
		4.11	0.656	5.612
1.61	42635.	6.85	0.691	6.178
		15.08	0.791	5.926
		24.67	0.899	5.853
		69.91	1.462	6.164
		102.81	1.899	6.299
		1.03	0.607	3.330
		2.06	0.614	3.538
		4.11	0.629	4.556
1.61	75133.	6.85	0.659	5.452
		24.69	0.840	5.357
		38.38	0.984	5.467
		102.81	1.700	5.469
		115.15	1.823	5.217

Table 5.1 (continued)

α	Re	x/De	$(p_e-p)/\rho u_b^2$	$f\times10^3$
		0.69	0.630	12.916
		1.38	0.647	10.333
		2.76	0.668	7.542
2.31	21912.	9.36	0.732	7.266
		10.12	0.775	7.072
		25.76	0.988	7.193
		55.20	1.394	7.438
		69.00	1.630	7.236
		1.38	0.629	5.564
		2.76	0.644	5.937
		4.60	0.668	6.313
2.31	43193.	7.36	0.701	6.123
		20.24	0.847	5.645
		39.10	1.061	6.121
		46.92	1.160	6.103
		69.00	1.463	6.143
		1.38	0.616	2.895
		2.76	0.627	4.764
		4.60	0.648	5.556
2.31	75675.	7.36	0.677	5.450
		16.56	0.769	5.443
		20.24	0.812	5.471
		39.10	1.003	5.309
		69.00	1.365	5.482
		1.38	0.597	3.182
		2.76	0.607	4.390
		4.60	0.626	5.159
2.31	108195.	7.36	0.653	5.282
		10.12	0.683	4.980
		39.10	0.954	4.730
		46.92	1.024	4.667
		69.00	1.276	4.775

Table 5.1 (continued)

α	Re	x/De	$(p_e - p)/\rho u_b^2$	$f \times 10^3$
		0.53	0.576	25.405
		1.06	0.599	18.147
		2.12	0.622	9.222
3.83	23167.	3.53	0.642	7.311
		7.76	0.708	7.777
		19.76	0.869	7.024
		42.34	1.178	7.247
		59.28	1.432	7.131
		0.53	0.552	18.366
		2.12	0.582	6.960
		3.53	0.603	6.989
3.83	45432.	5.65	0.629	6.077
		7.76	0.655	5.875
		42.34	1.044	6.165
		59.93	1.194	6.419
		59.28	1.270	5.744
		0.53	0.551	12.030
		1.06	0.562	9.045
		2.12	0.575	6.850
3.83	79873.	5.65	0.616	5.237
		7.76	0.641	5.435
		9.88	0.662	4.941
		29.99	0.867	5.072
		59.28	1.188	5.061
		0.53	0.547	11.221
		2.12	0.568	6.482
		3.53	0.590	6.331
3.83	109330.	5.65	0.607	4.776
		7.76	0.630	5.042
		9.88	0.649	4.518
		59.28	1.147	4.352
		65.63	1.209	5.091

Table 5.1 (continued)

α	Re	x/De	$(p_e-p)/\rho u_b^2$	$f\times10^3$
15.32	30618.	0.42	0.572	33.862
		1.67	0.610	8.246
		4.46	0.649	7.619
		6.14	0.677	0.927
		10.04	0.726	6.927
		12.28	0.757	6.465
		23.72	0.912	6.553
		46.88	1.244	6.543
15.32	47304.	0.42	0.545	25.972
		2.79	0.592	6.997
		4.46	0.615	6.460
		6.14	0.635	5.963
		10.04	0.679	5.591
		15.63	0.741	5.672
		46.88	1.133	5.700
		51.90	1.191	5.833
15.32	80696.	0.42	0.538	19.312
		0.84	0.552	12.727
		2.79	0.577	6.715
		6.14	0.618	5.674
		7.81	0.636	5.198
		12.28	0.681	5.007
		23.72	0.805	5.066
		46.88	1.072	5.078
15.32	115814.	0.42	0.527	16.192
		0.84	0.538	10.897
		2.79	0.562	6.050
		6.14	0.598	5.178
		10.04	0.635	4.764
		12.28	0.657	4.626
		15.63	0.685	4.535
		46.88	1.015	4.676

Table 5.2 Experimental Nusselt Number of Concentric Annulus, Simultaneously Developing Region, $\alpha = 1.61$, $Pr = 0.71$

Re	Q	x/De	t_b	h	Nu
-	$\frac{Btu}{hr.ft}$	-	^oF	$\frac{Btu}{hr.ft^2.^oF}$	-
		1.03	78.96	14.38	115.48
		2.06	79.24	9.89	79.38
		6.85	79.90	6.22	49.87
		10.99	80.64	6.48	51.91
19833.	134.64	19.19	82.15	6.35	50.71
		30.16	84.28	6.34	50.51
		38.38	85.87	6.13	48.69
		58.26	89.73	6.19	48.91
		82.25	94.52	6.09	47.77
		115.15	101.37	6.15	47.83
		1.03	79.00	14.92	119.81
		2.06	79.36	10.15	81.48
		6.85	80.58	7.68	61.49
		10.97	81.84	7.56	60.45
24229.	268.50	19.19	84.39	7.22	57.50
		30.16	87.90	7.06	55.85
		38.38	90.52	6.83	53.86
		58.26	97.02	7.05	55.02
		82.25	105.23	6.91	53.32
		115.15	116.71	6.99	53.13
		1.03	78.98	19.08	153.19
		2.06	79.24	14.90	119.56
		6.85	80.39	12.69	101.66
		10.97	81.50	12.44	99.43
46405.	463.80	19.19	83.69	11.57	92.98
		30.16	86.73	11.49	91.14
		38.38	89.00	11.09	87.70
		58.26	94.59	11.36	89.00
		115.15	111.23	11.98	91.65
		129.54	115.78	12.23	93.00
		1.03	78.41	28.53	229.28
		2.06	78.59	22.19	178.26
		4.11	78.94	19.21	154.27
		6.85	79.45	19.06	152.93
77657.	532.74	10.97	80.23	18.41	147.52
		19.19	81.82	17.18	137.33
		30.16	83.95	16.80	133.78
		38.38	85.56	16.32	129.63
		58.26	89.58	17.05	134.58
		115.15	101.43	17.39	134.95

Table 5.3 Experimental Nusselt Number of Concentric Annulus, Simultaneously Developing Region, $\alpha = 2.31$ $Pr = 0.71$

Re	Q	x/De	t_b	h	Nu
-	$\frac{Btu}{hr.ft}$	-	^oF	$\frac{Btu}{hr.ft^2.^oF}$	-
		0.34	75.97	18.43	219.80
		1.03	76.25	14.19	158.65
		3.68	76.90	6.00	71.28
		5.98	77.62	5.71	57.70
22258.	134.92	10.12	79.14	5.65	57.01
		16.56	81.20	5.47	64.54
		23.00	82.78	5.40	63.55
		32.43	86.63	5.23	61.15
		47.15	91.33	5.10	59.16
		66.24	98.00	5.36	61.59
		0.34	76.45	28.49	338.57
		1.03	76.63	19.18	227.89
		3.68	77.20	9.71	115.19
		5.98	77.78	9.78	115.91
43340.	200.00	10.12	78.98	9.50	112.40
		16.56	80.62	9.24	109.10
		23.00	81.85	8.96	105.52
		32.43	84.82	8.54	100.19
		47.15	88.53	8.57	99.88
		82.11	95.91	8.51	98.17
		0.34	81.15	34.99	417.00
		1.03	81.29	23.36	278.34
		3.68	81.78	13.83	164.71
		5.98	82.28	13.99	166.54
75262.	303.76	10.12	83.30	13.36	158.66
		16.56	84.68	12.92	153.18
		23.00	85.70	12.34	146.09
		32.43	88.26	12.36	145.67
		66.24	95.72	12.70	147.95
		82.11	97.61	12.28	142.75
		1.03	78.88	23.20	271.24
		3.68	79.09	19.53	227.26
		5.98	79.31	18.34	213.18
		10.12	79.76	18.26	211.85
109705.	188.51	16.56	80.39	17.86	206.87
		23.00	80.82	16.15	185.81
		32.43	81.96	16.93	195.43
		47.15	83.32	16.30	187.58
		66.24	85.16	16.93	194.49
		82.11	85.97	16.48	189.09

Table 5.4 Experimental Nusselt Number of Concentric Annulus, Simultaneously Developing Region, $\alpha = 3.83$ $Pr = 0.71$

Re	Q	x/De	t_b	h	Nu
-	$\frac{Btu}{hr.ft}$	-	^{o}F	$\frac{Btu}{hr.ft^{2}.^{o}F}$	-
23091.	139.45	0.53	80.28	10.20	158.66
		1.06	80.47	6.46	100.57
		2.12	80.85	4.87	75.74
		5.65	82.20	4.29	66.60
		9.88	83.90	4.22	65.31
		15.53	86.19	4.19	64.63
		19.76	87.89	4.17	64.06
		29.99	92.22	4.08	62.33
		59.28	104.67	4.24	63.59
		66.69	108.80	4.29	64.05
44461.	210.79	0.53	75.99	15.34	240.34
		1.06	76.13	10.11	158.31
		2.12	76.45	8.25	129.22
		5.65	77.54	7.22	112.88
		9.88	78.89	6.96	108.63
		15.53	80.72	7.01	108.95
		19.76	82.11	6.92	107.36
		29.99	85.41	6.59	101.96
		59.28	95.36	6.91	105.13
		66.69	98.01	6.88	104.19
78441.	297.04	0.53	76.07	21.63	338.95
		1.06	76.19	14.94	233.98
		2.12	76.45	12.67	198.35
		5.65	77.35	11.14	174.21
		9.88	78.48	10.74	167.65
		15.53	79.99	10.62	165.39
		19.76	81.13	10.47	162.69
		29.99	83.89	10.20	157.79
		59.28	92.11	10.15	155.06
		66.69	94.14	9.75	148.58
107205.	298.98	0.53	76.14	26.05	408.16
		1.06	76.22	18.56	290.78
		2.12	76.41	16.16	253.04
		5.65	77.08	14.33	224.23
		9.88	77.91	13.68	213.66
		15.53	78.99	13.66	213.06
		19.76	79.84	13.67	212.84
		29.99	81.88	13.05	202.57
		59.28	87.73	13.20	203.03
		66.69	89.24	12.91	198.05

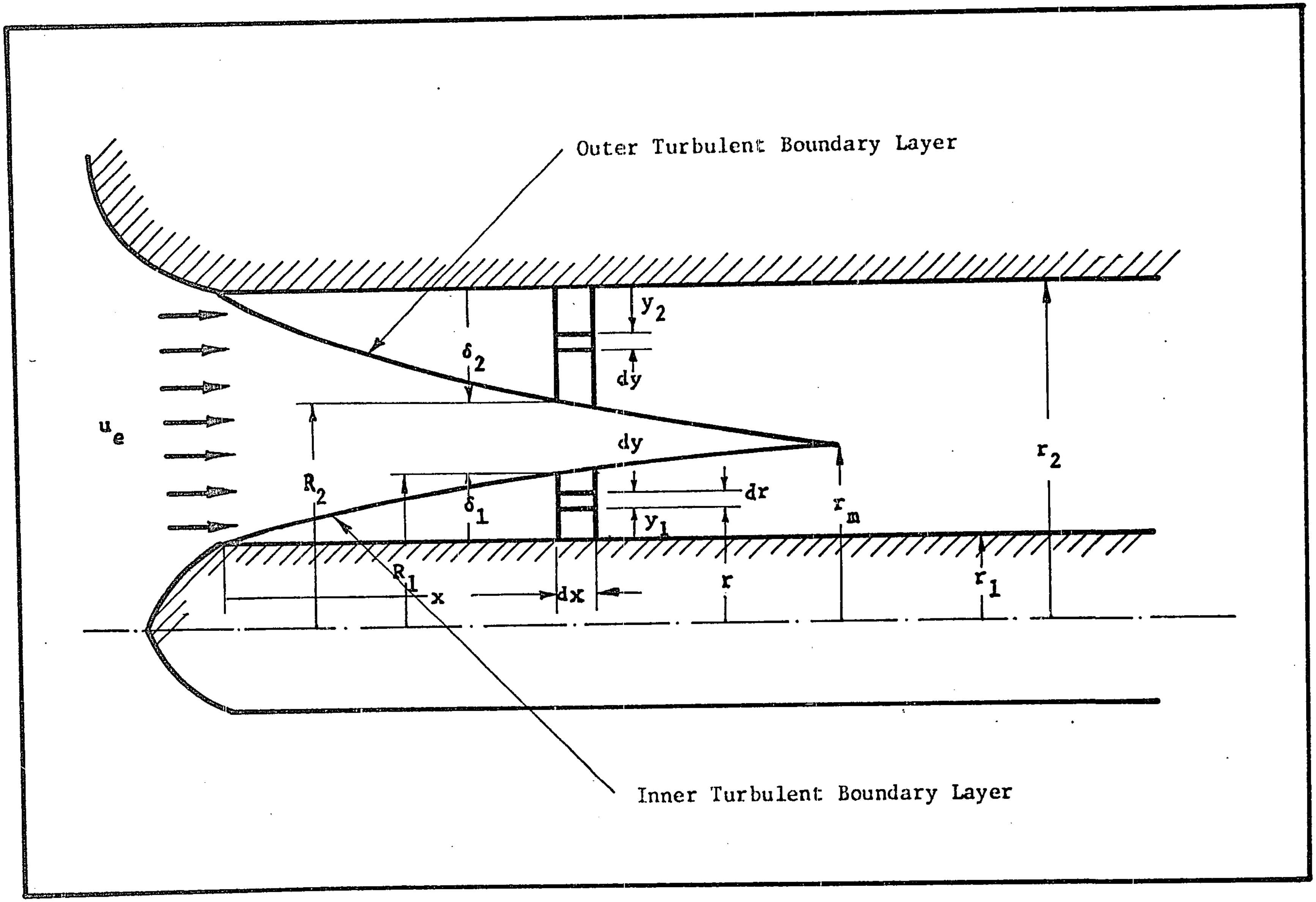

Fig. 3.1 (a) Idealized Model, Hydrodynamic Boundary Layer.

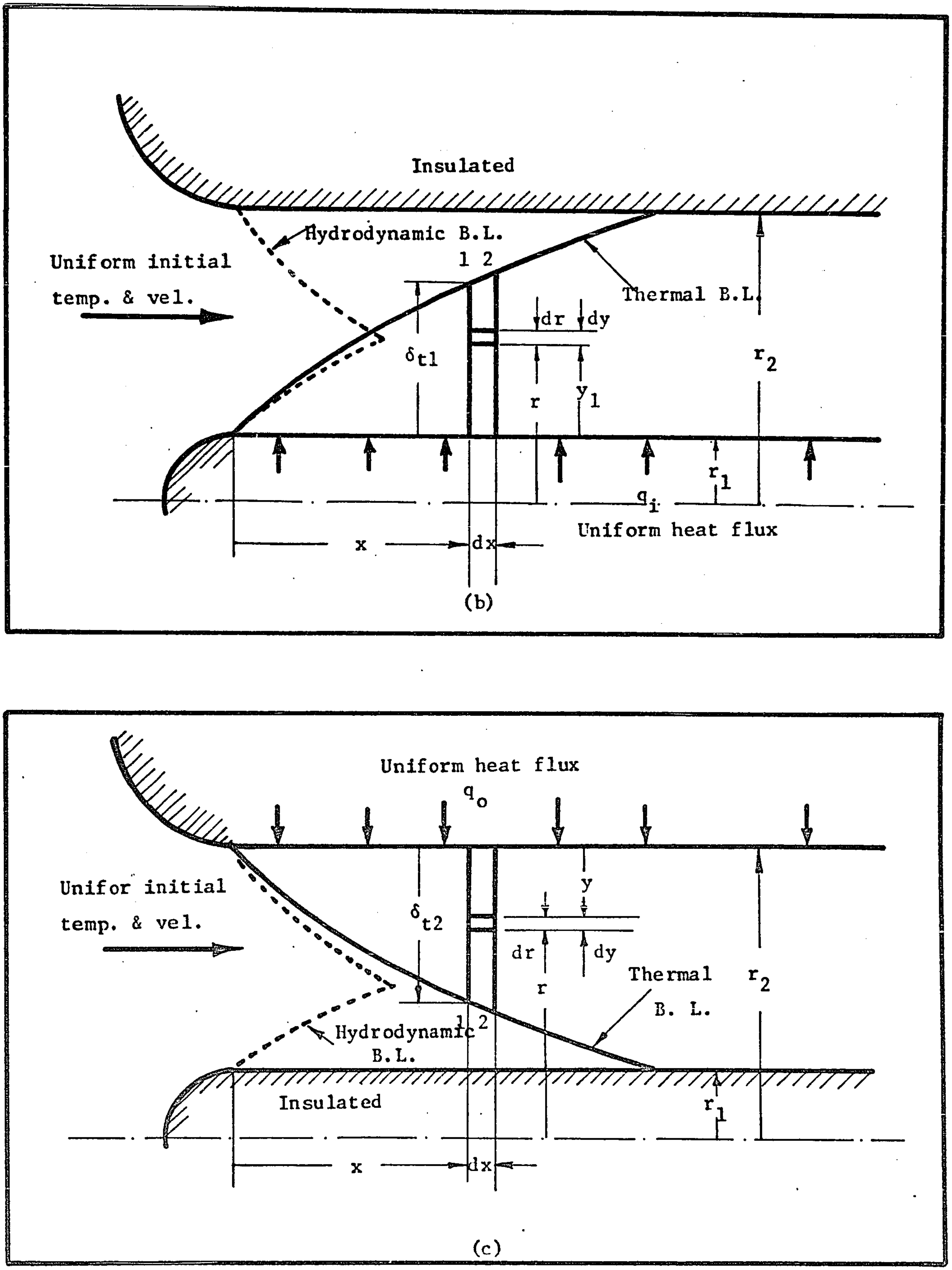

Fig. 3.1 Idealized Model, Thermal Boundary Layer.

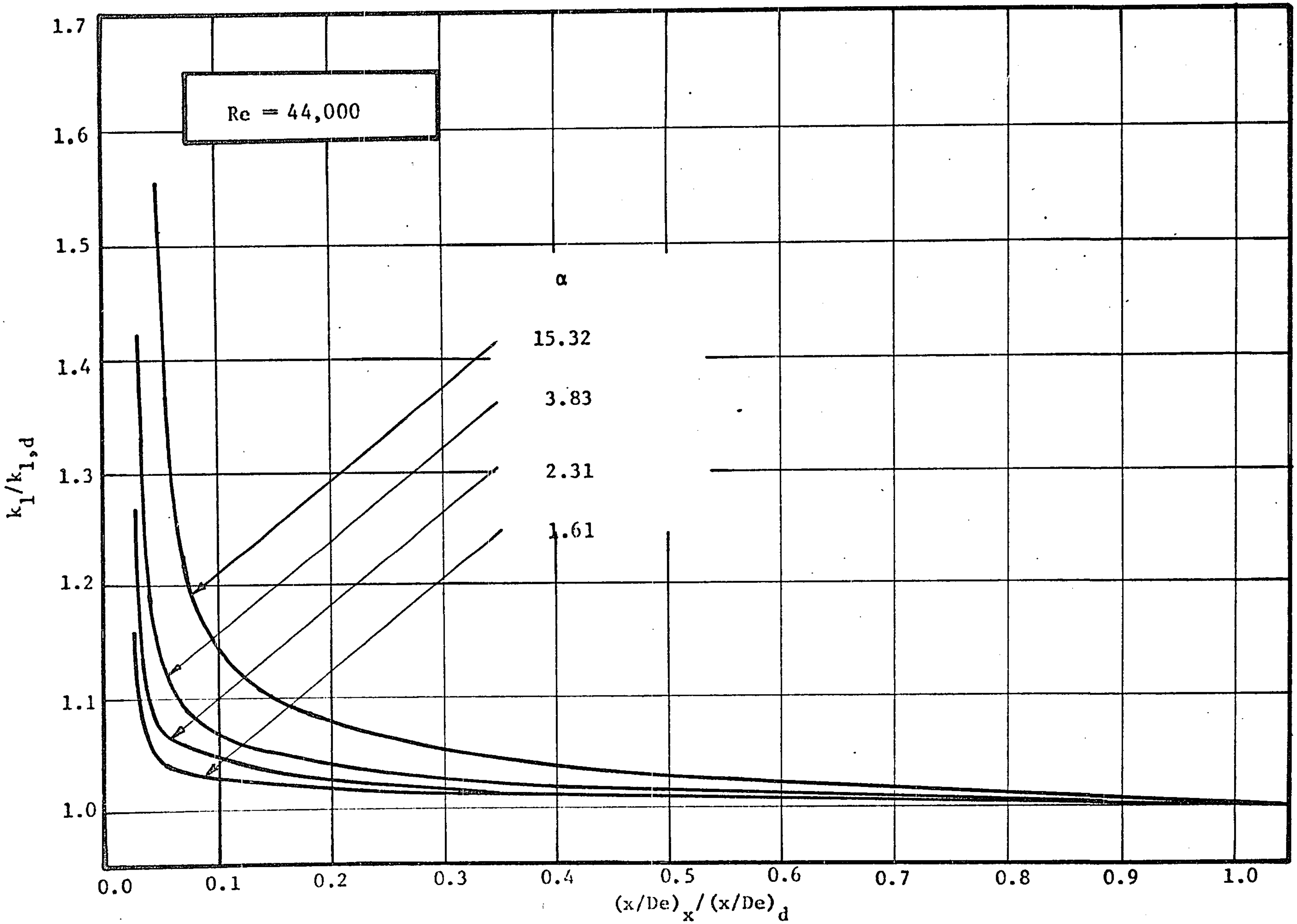

Fig. 3.2 Effect of Radius Ratio on Constant k_1, Entrance Region.

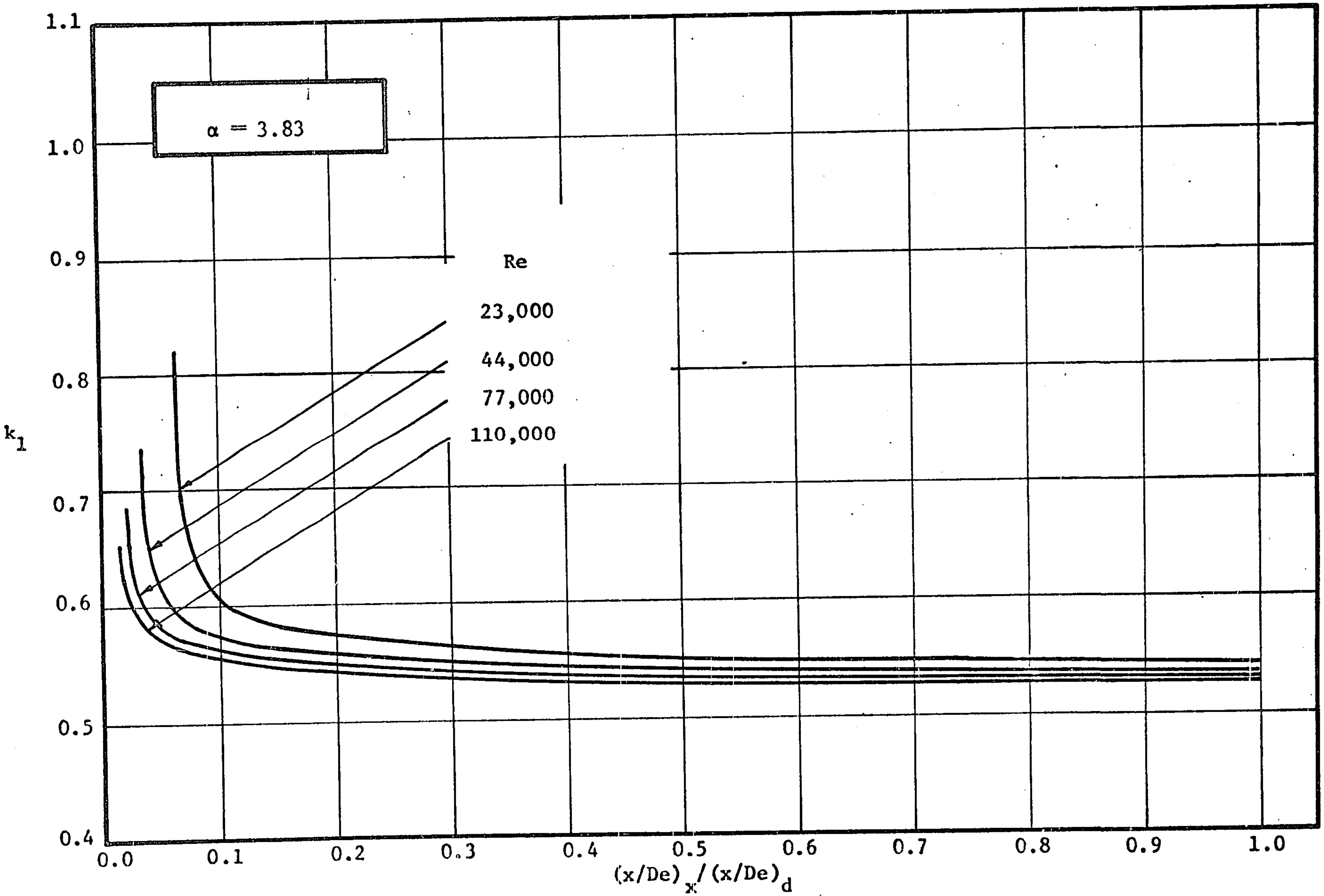

Fig. 3.3 Effect of Reynolds Number on Constant k_1, Entrance Regions.

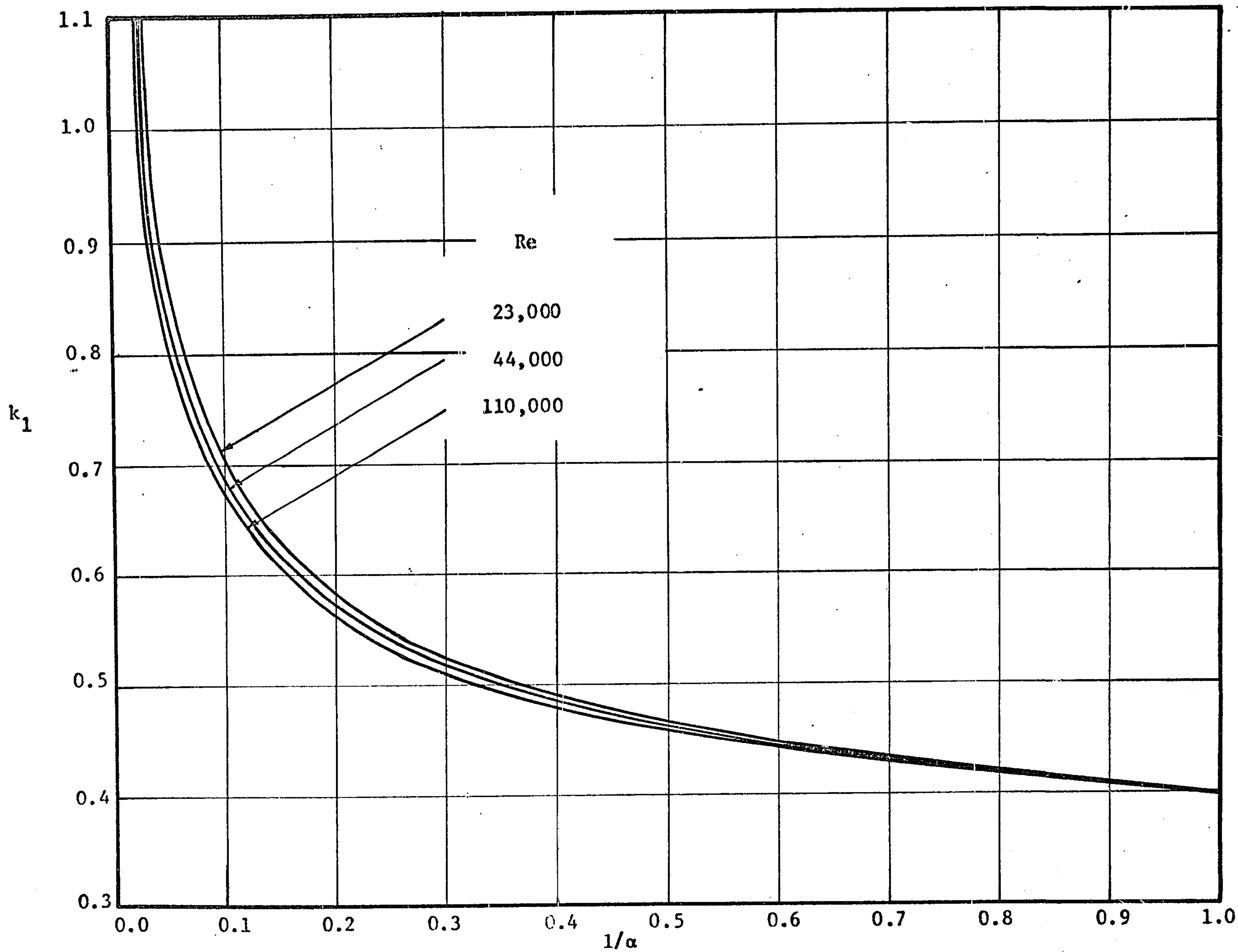

Fig. 3.4 Effects of Reynolds Number and Radius Ratio on Constant k_1, Fully Developed Regions.

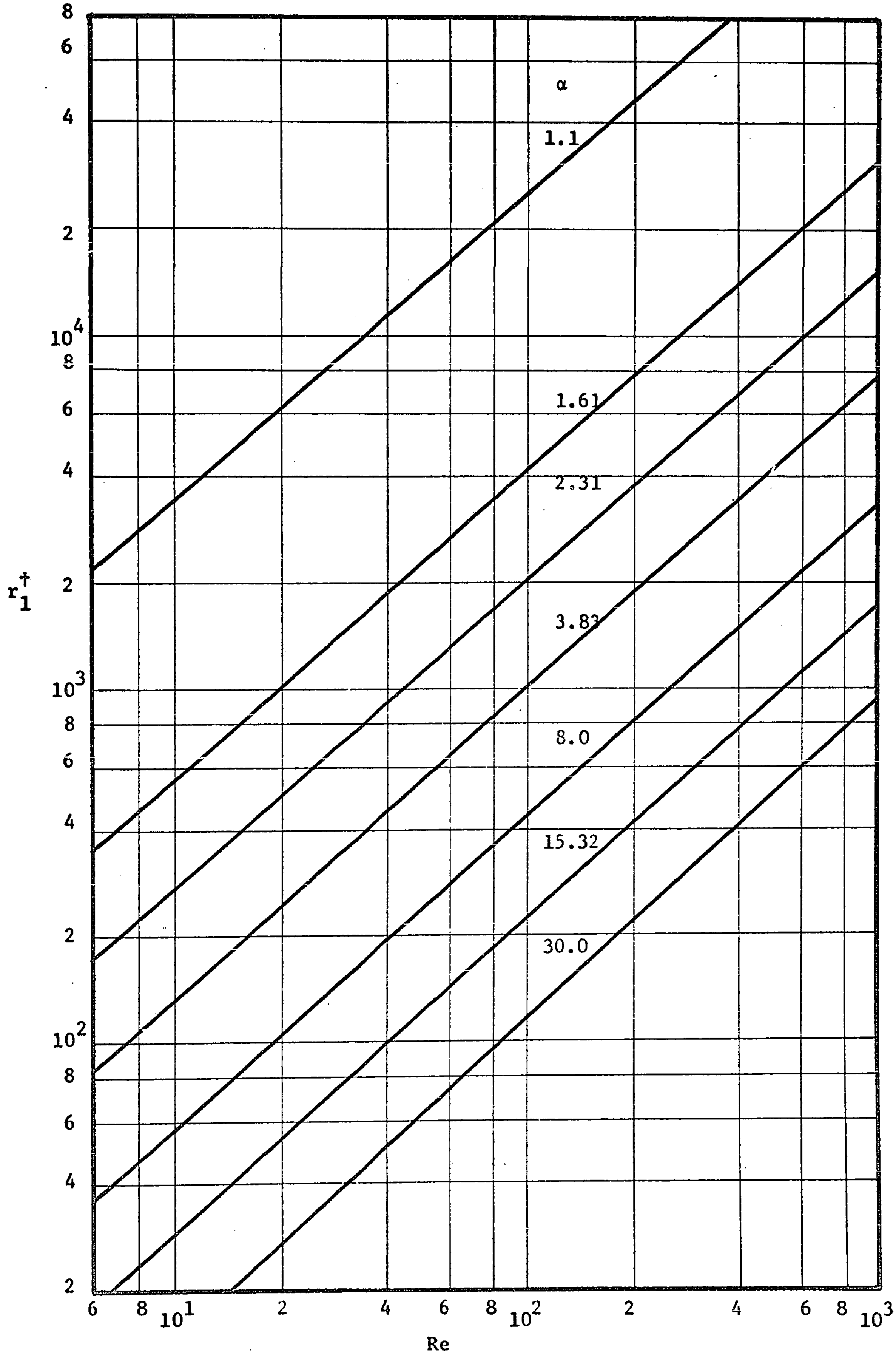

Fig. 3.5 Relationship between $r_1^{\dagger}$ and Reynolds Number.

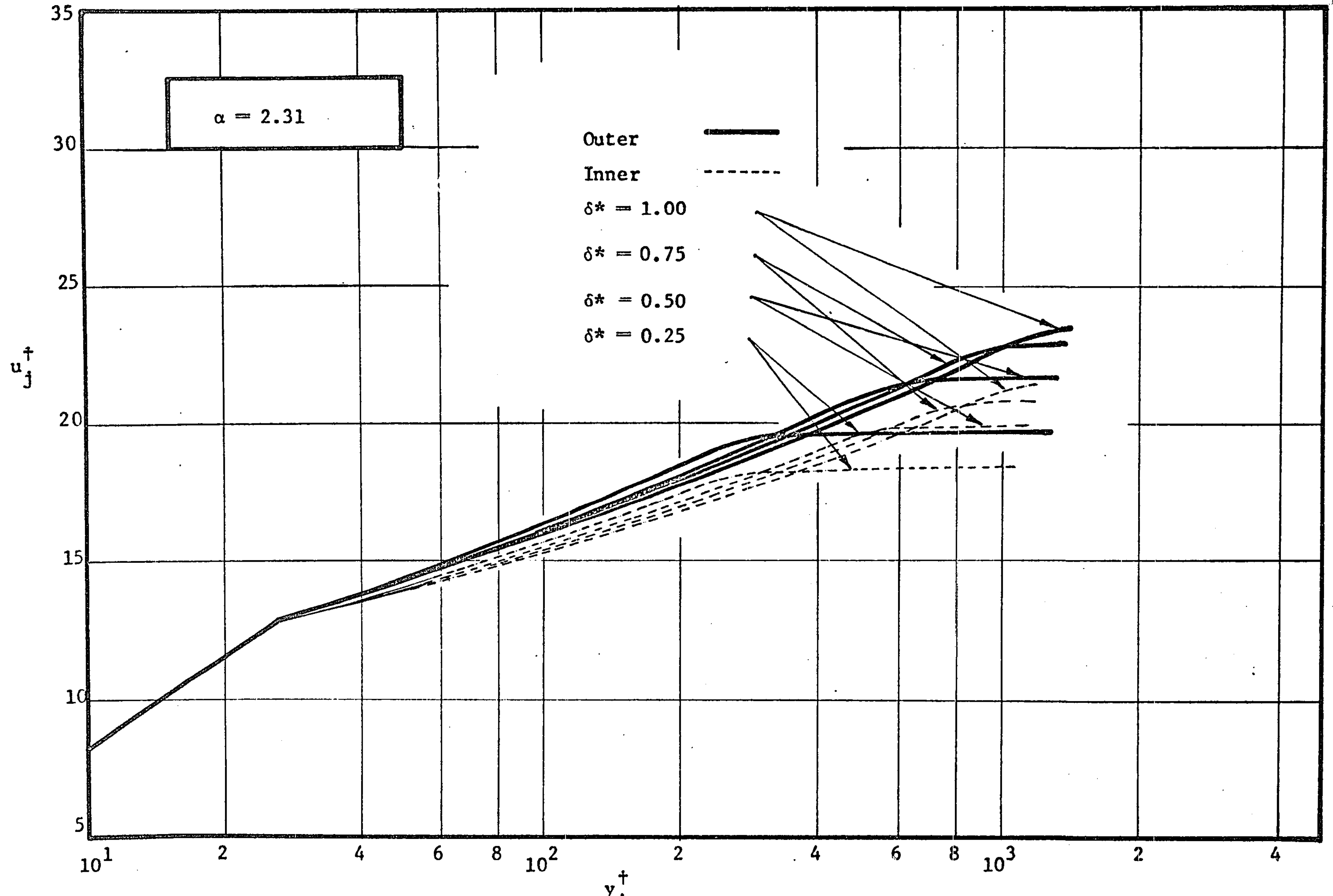

Fig. 3.6 Predicted Velocity Profiles, Entrance Regions, Re = 110,000.

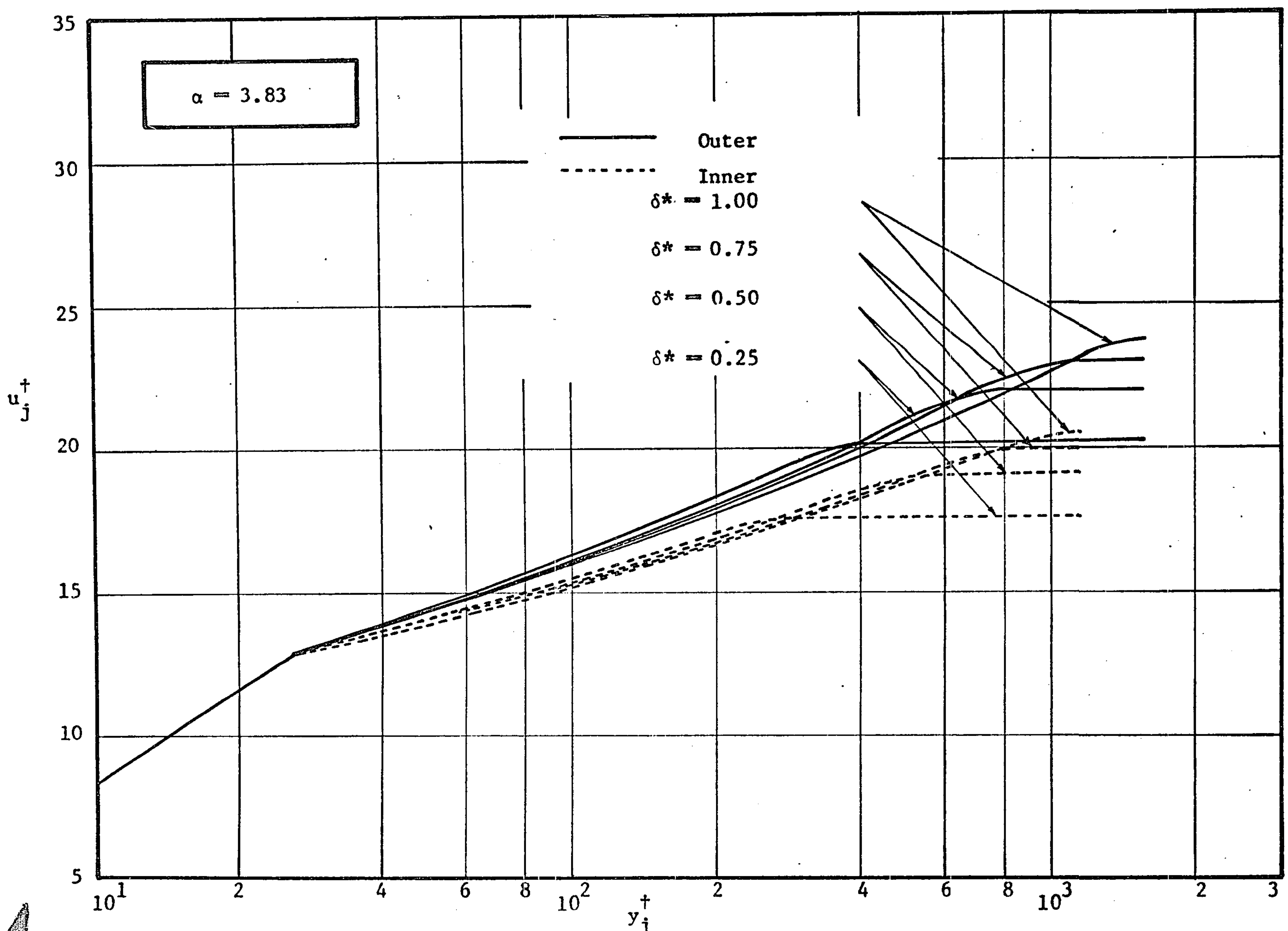

Fig. 3.7 Predicted Velocity Profiles, Entrance Regions, Re = 110,000

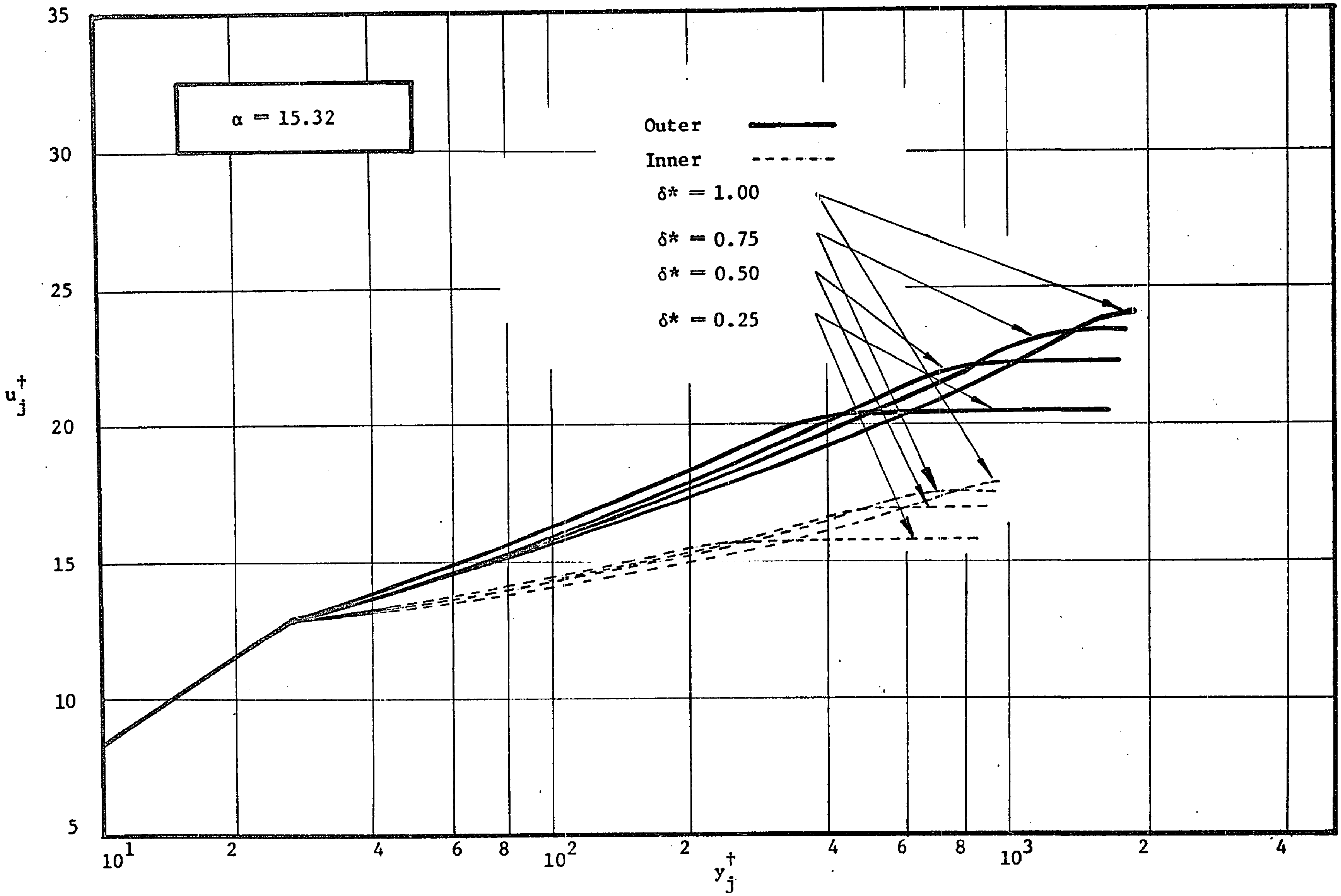

Fig. 3.8 Predicted Velocity Profiles, Entrance Regions, Re = 110,000

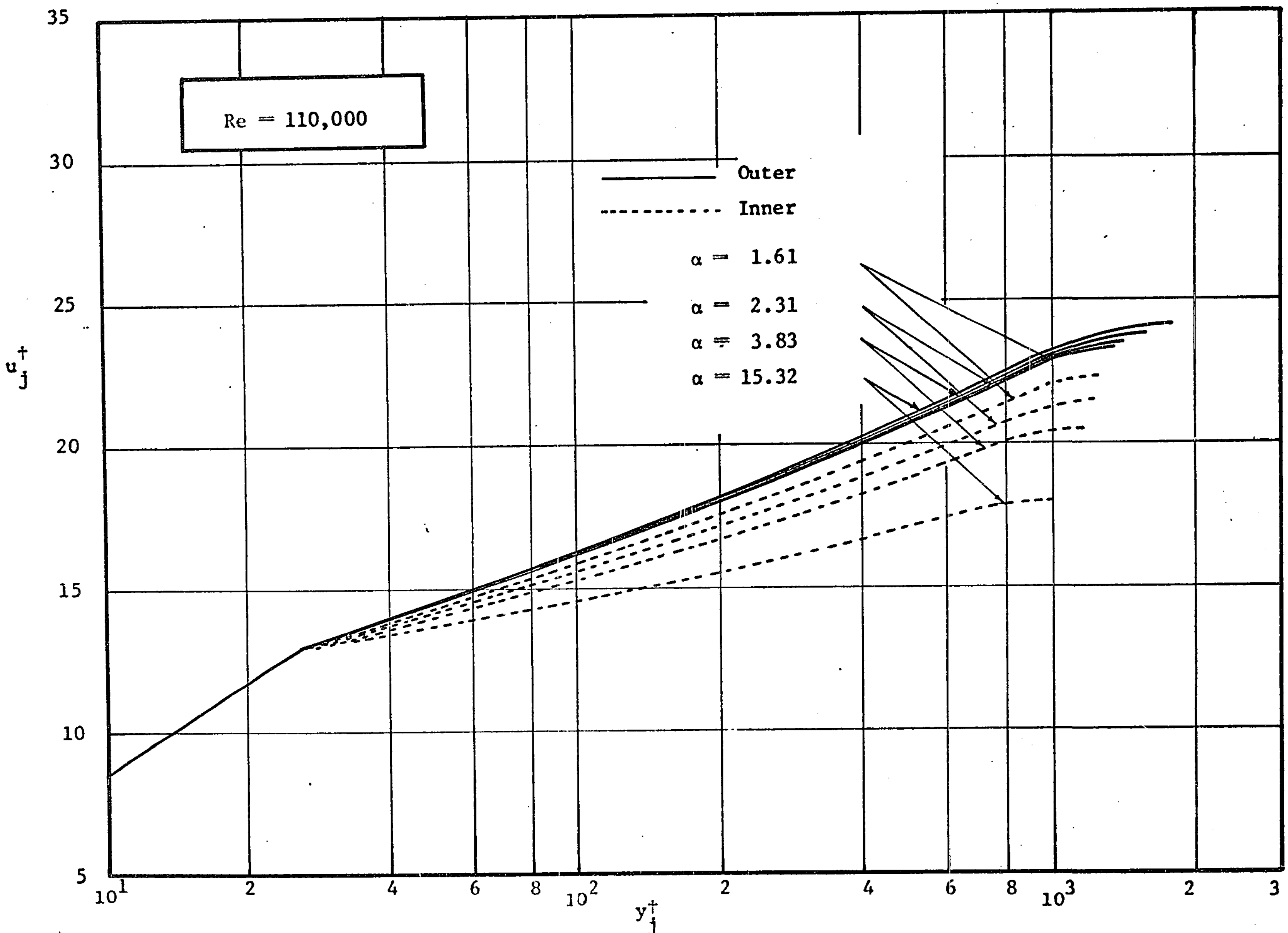

Fig. 3.9 Predicted Velocity Profiles, Fully Developed Regions, Effect of α.

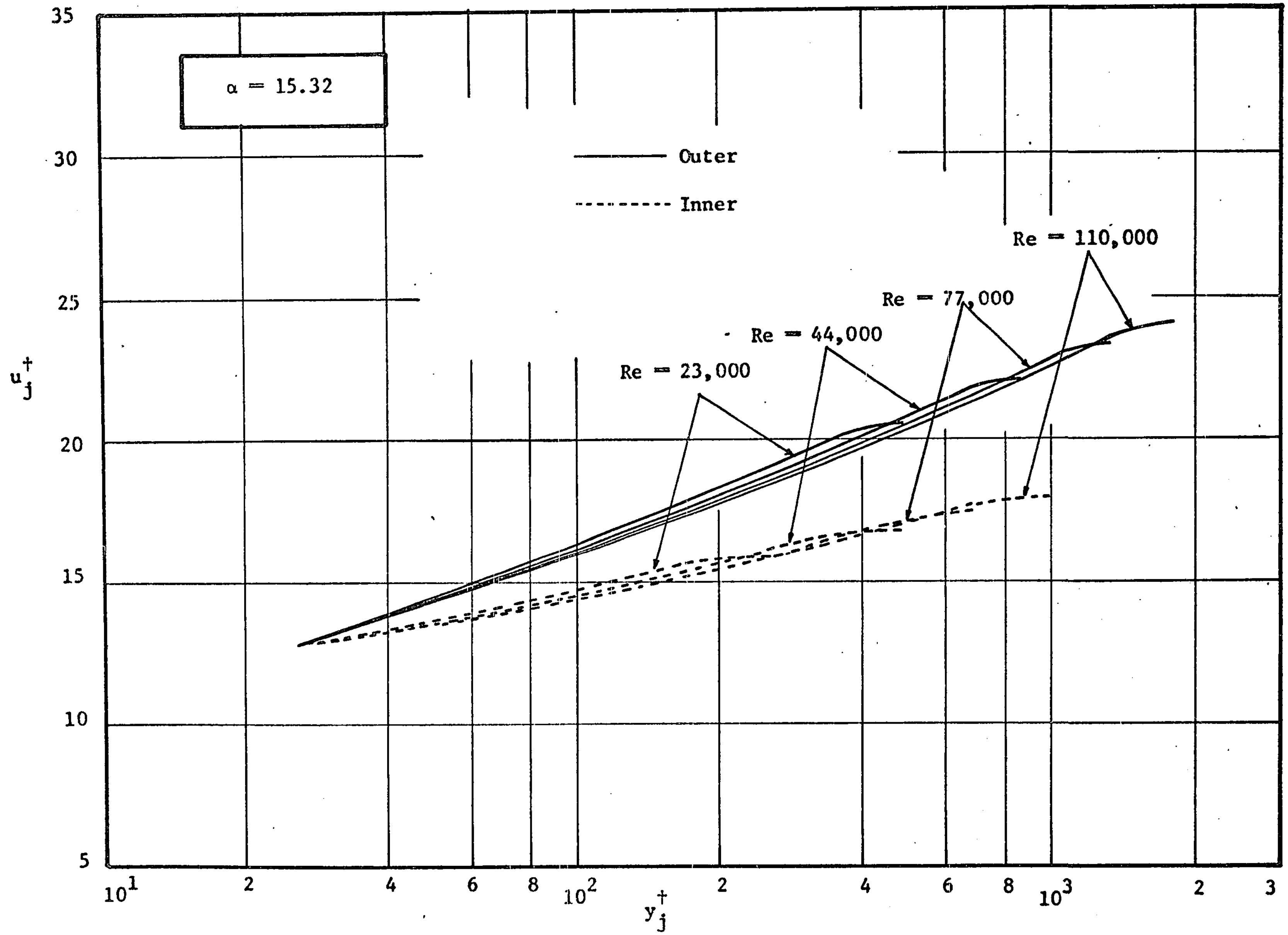

Fig. 3.10 Predicted Velocity Profile, Fully Developed Regions, Effect of Re.

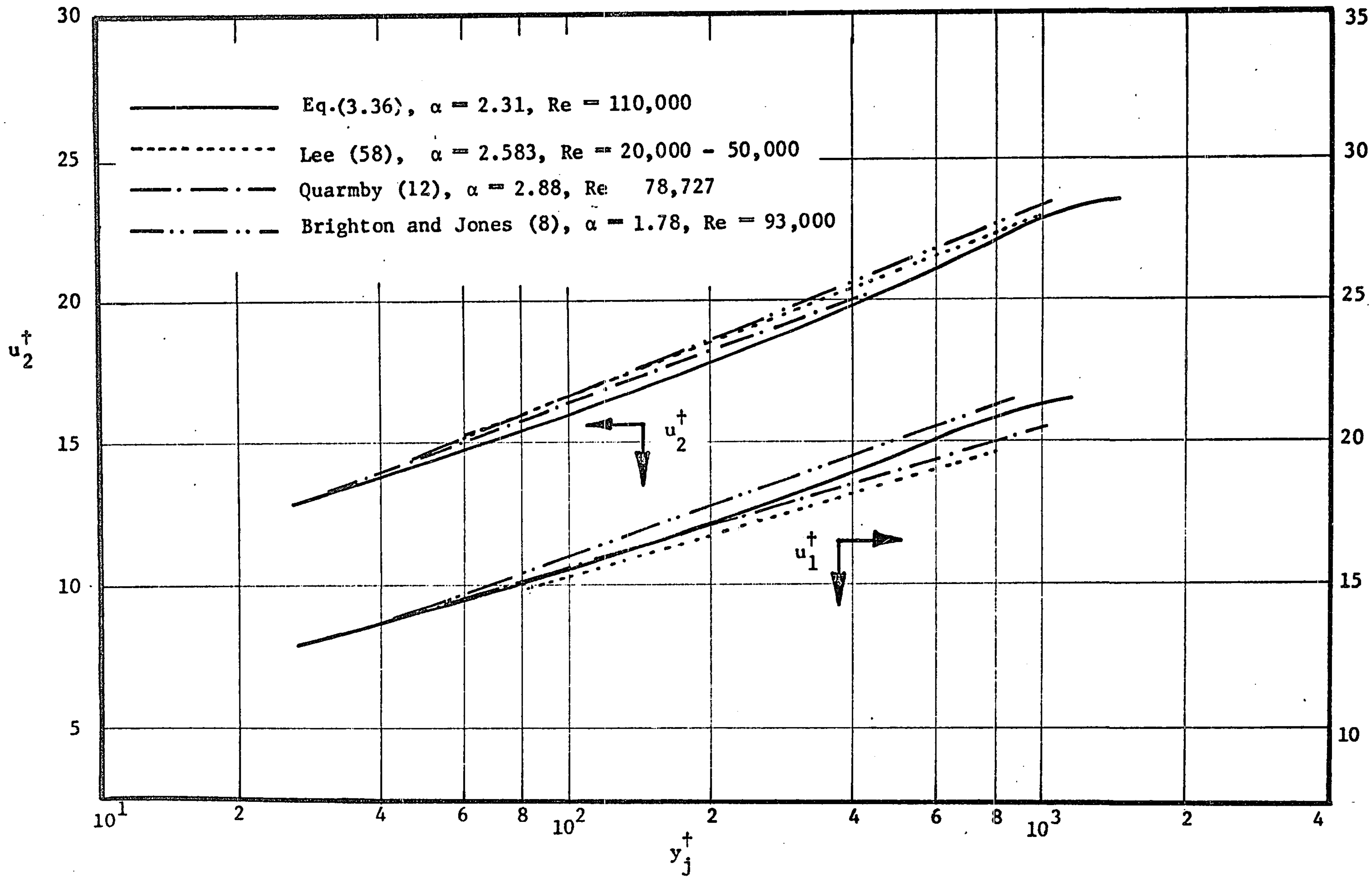

Fig. 3.11 Comparison between Present Prediction and Other Correlations for Velocity Profile, Fully Developed.

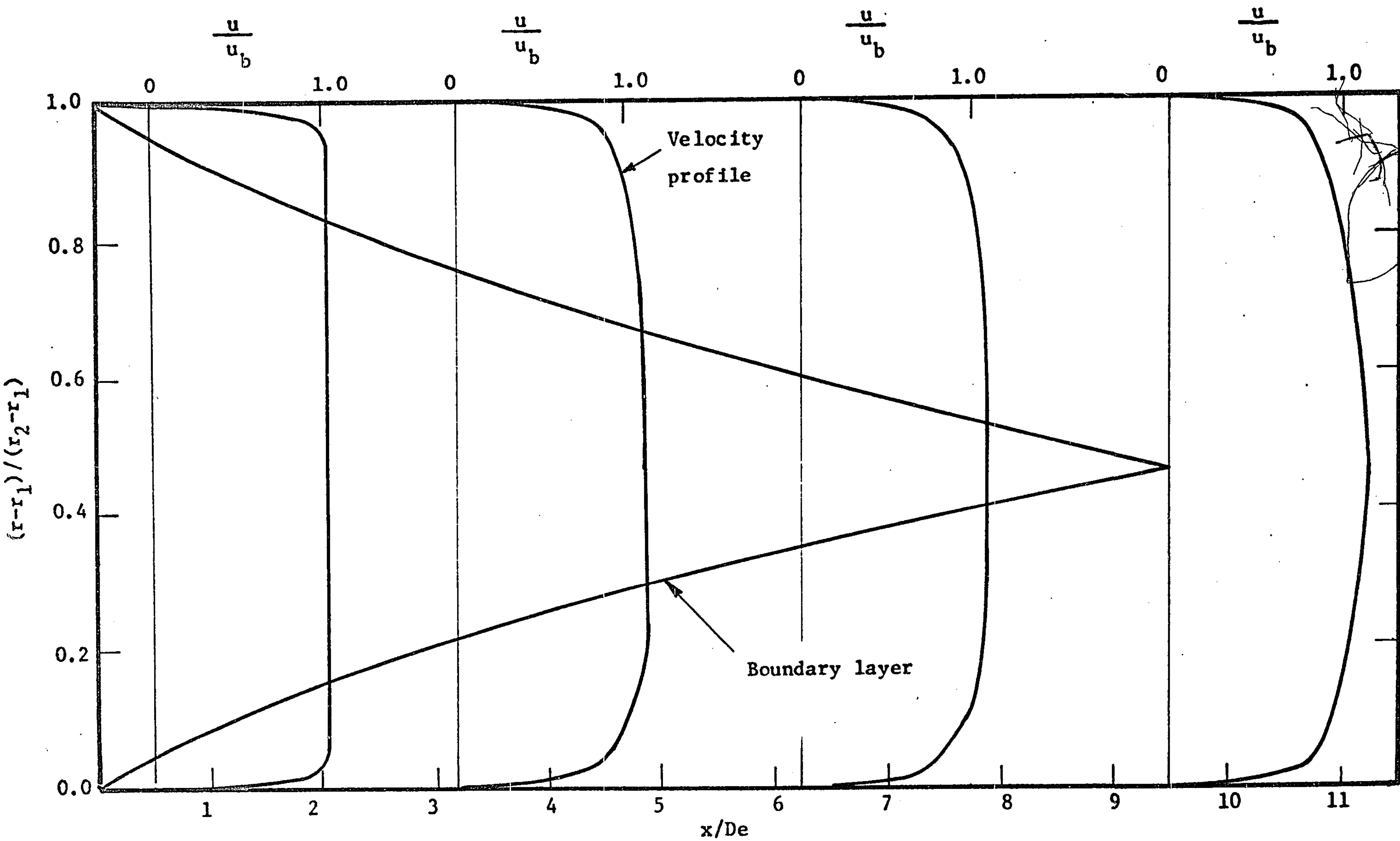

Fig. 3.12 Development of Hydrodynamic Boundary Layer, Entrance Region, $\alpha = 2.31$, Re = 44,000

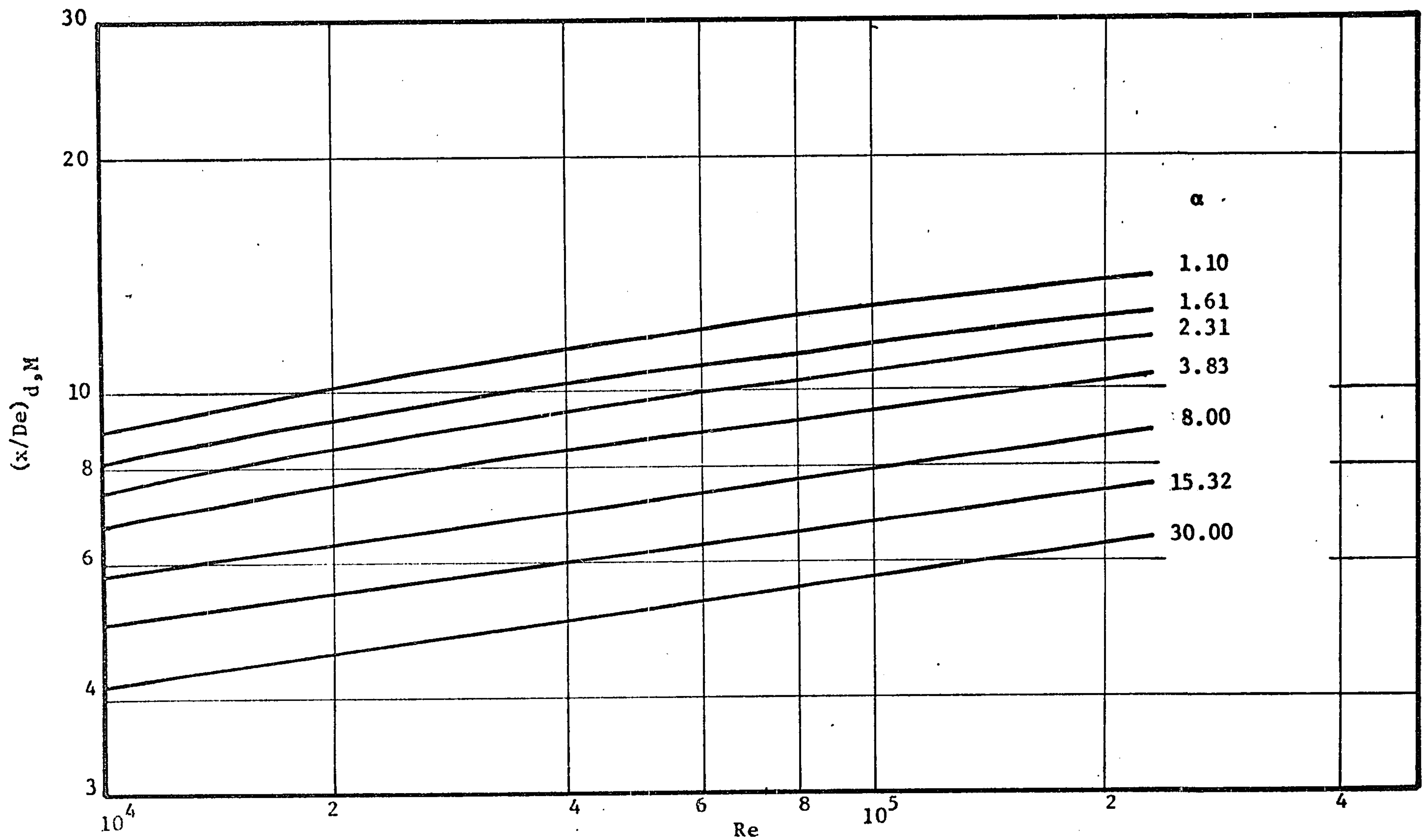

Fig. 3.13 Predicted Hydrodynamic Entrance Lengths, Concentric Annuli.

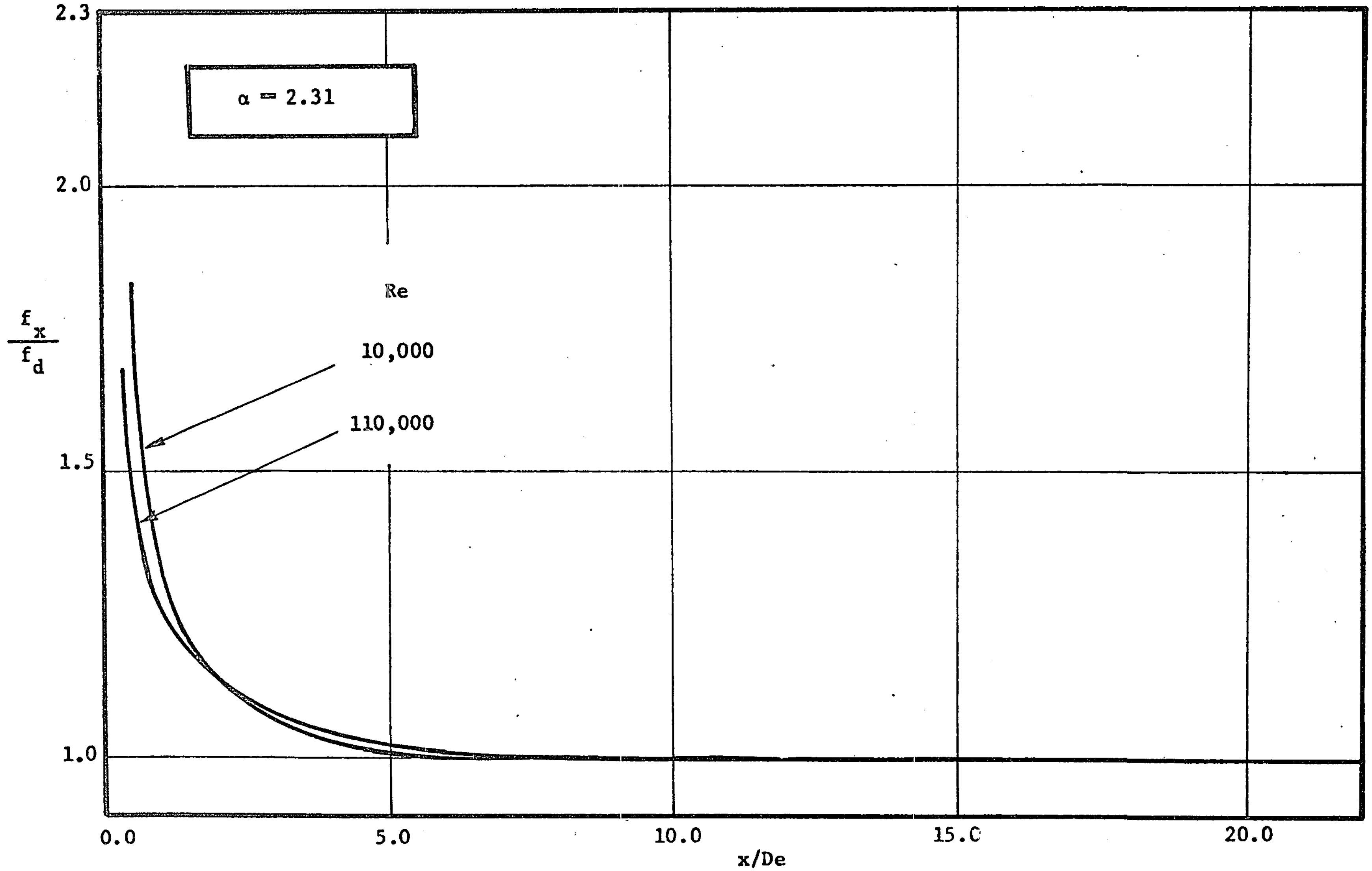

Fig. 3.14 Predicted Friction Factors, Entrance Regions, Effect of Re.

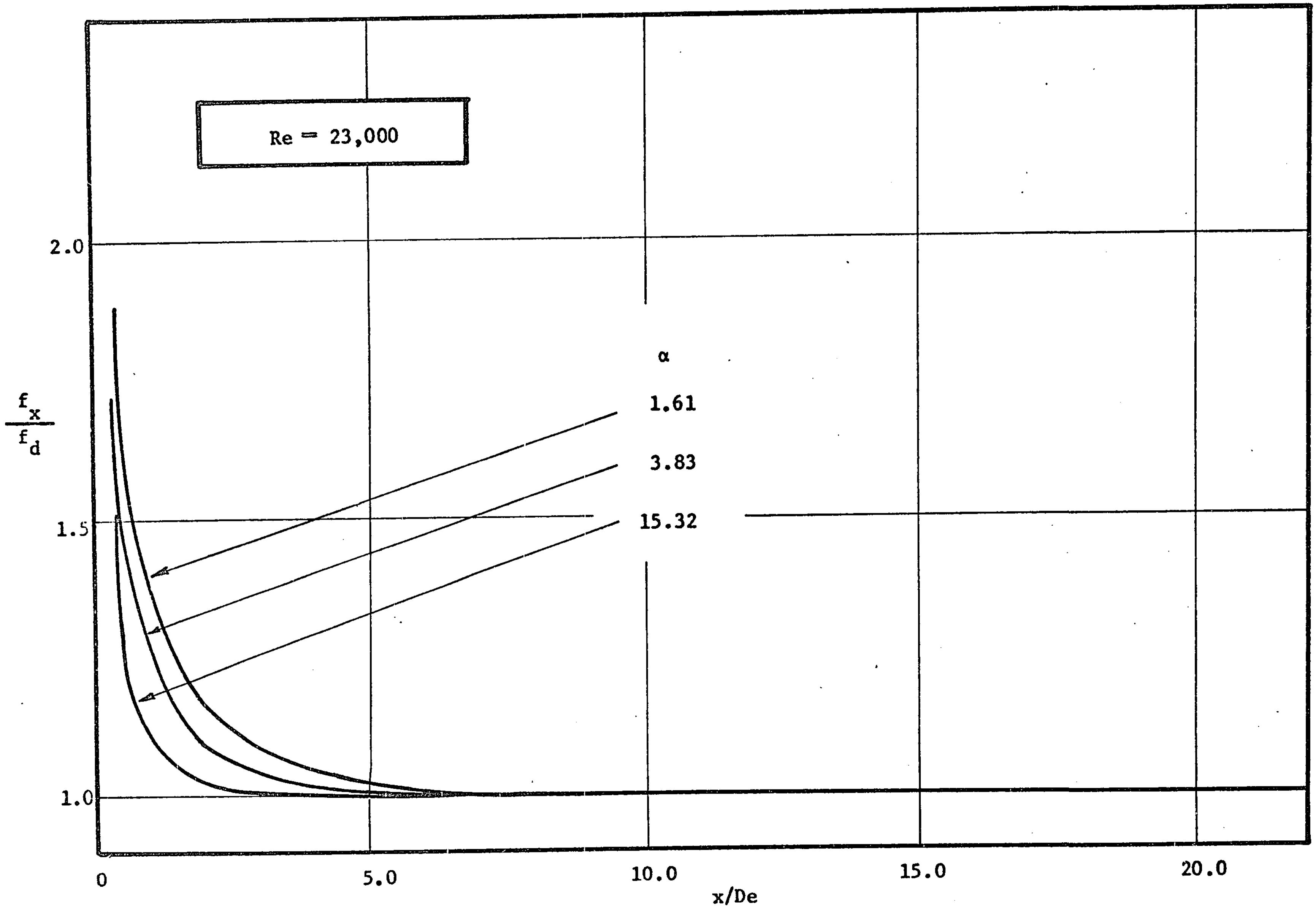

Fig. 3.15 Predicted Friction Factors, Entrance Regions, Effect of α.

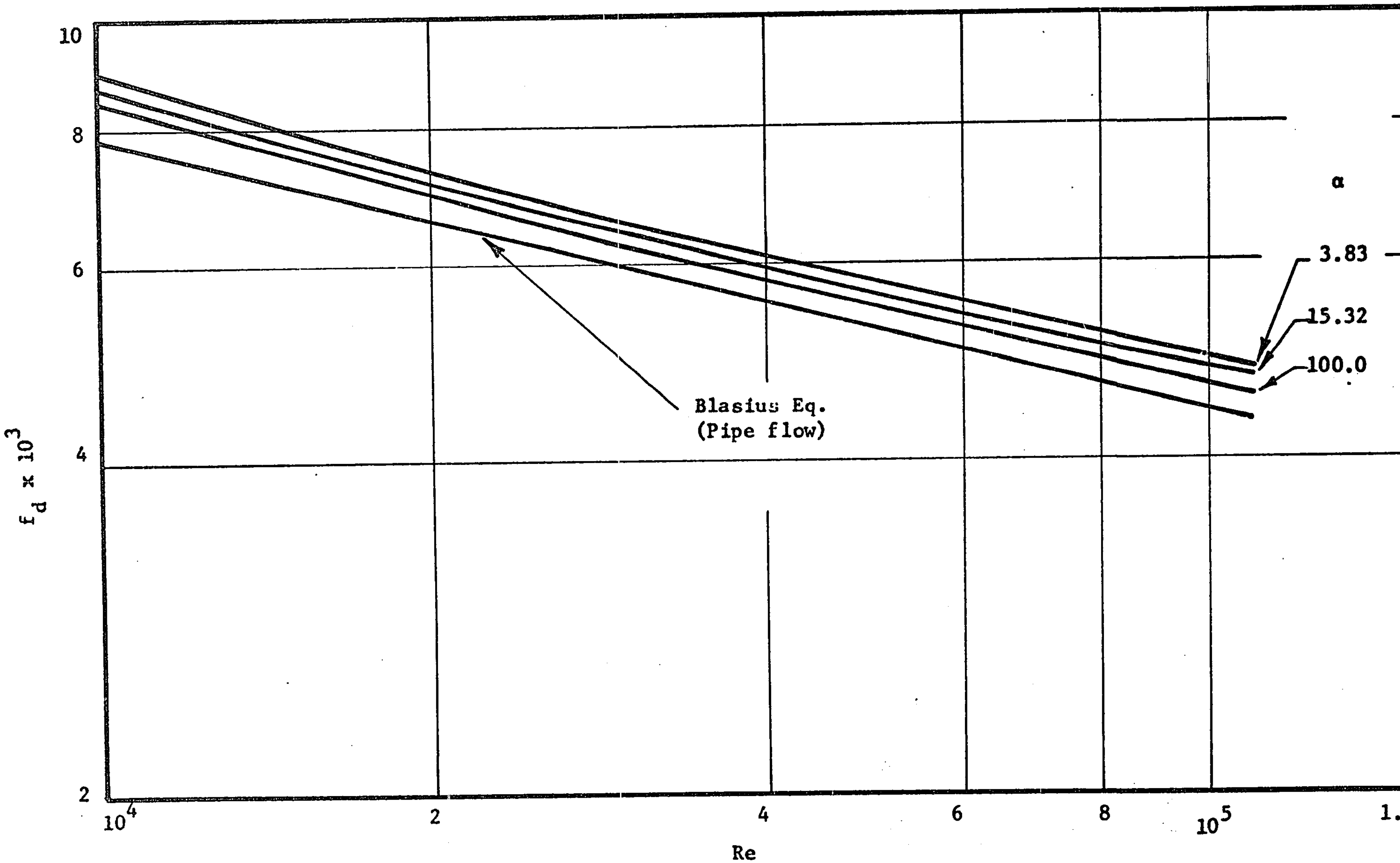

Fig. 3.16 Predicted Friction Factors of Concentric Annulus, Fully Developed.

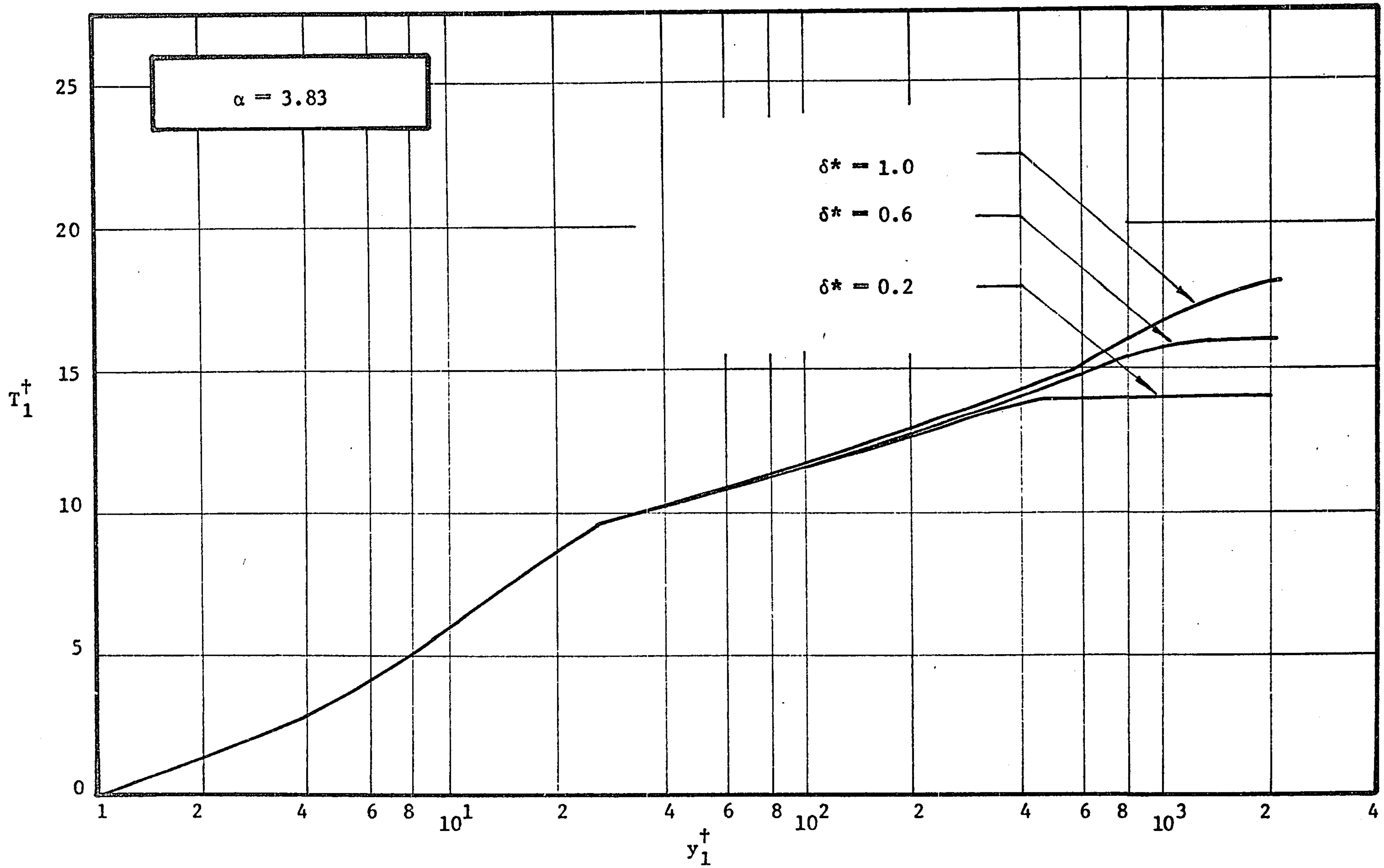

Fig. 3.17 Predicted Temperature Profiles, Entrance Regions, Inner Wall Heated, Outer Wall Insulated, Re = 77,000, Pr = 0.71

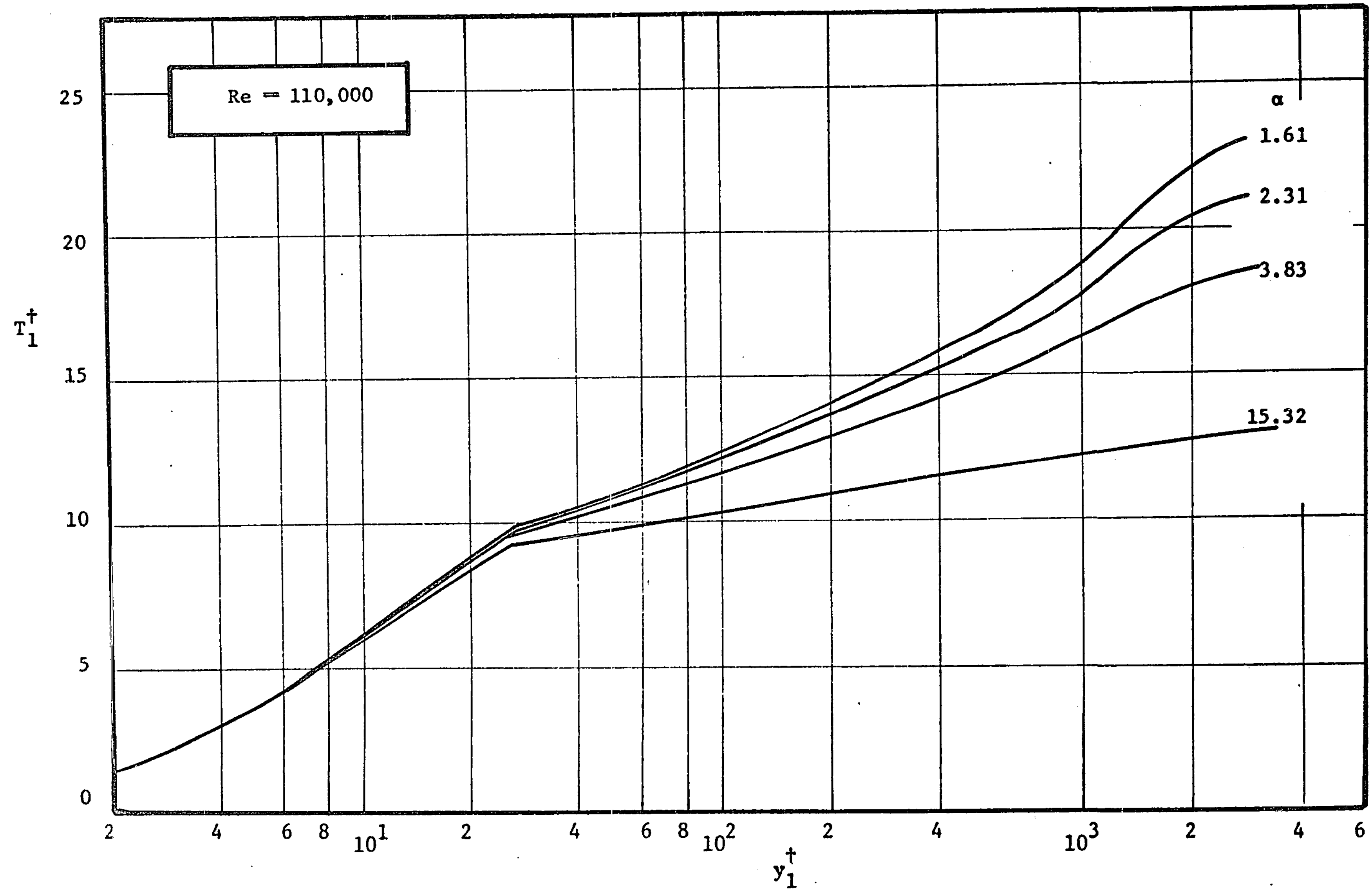

Fig. 3.18 Predicted Temperature Profiles, Fully Developed Regions, Inner Wall Heated, Outer Wall Insulated, Effect of α, $Pr = 0.71$

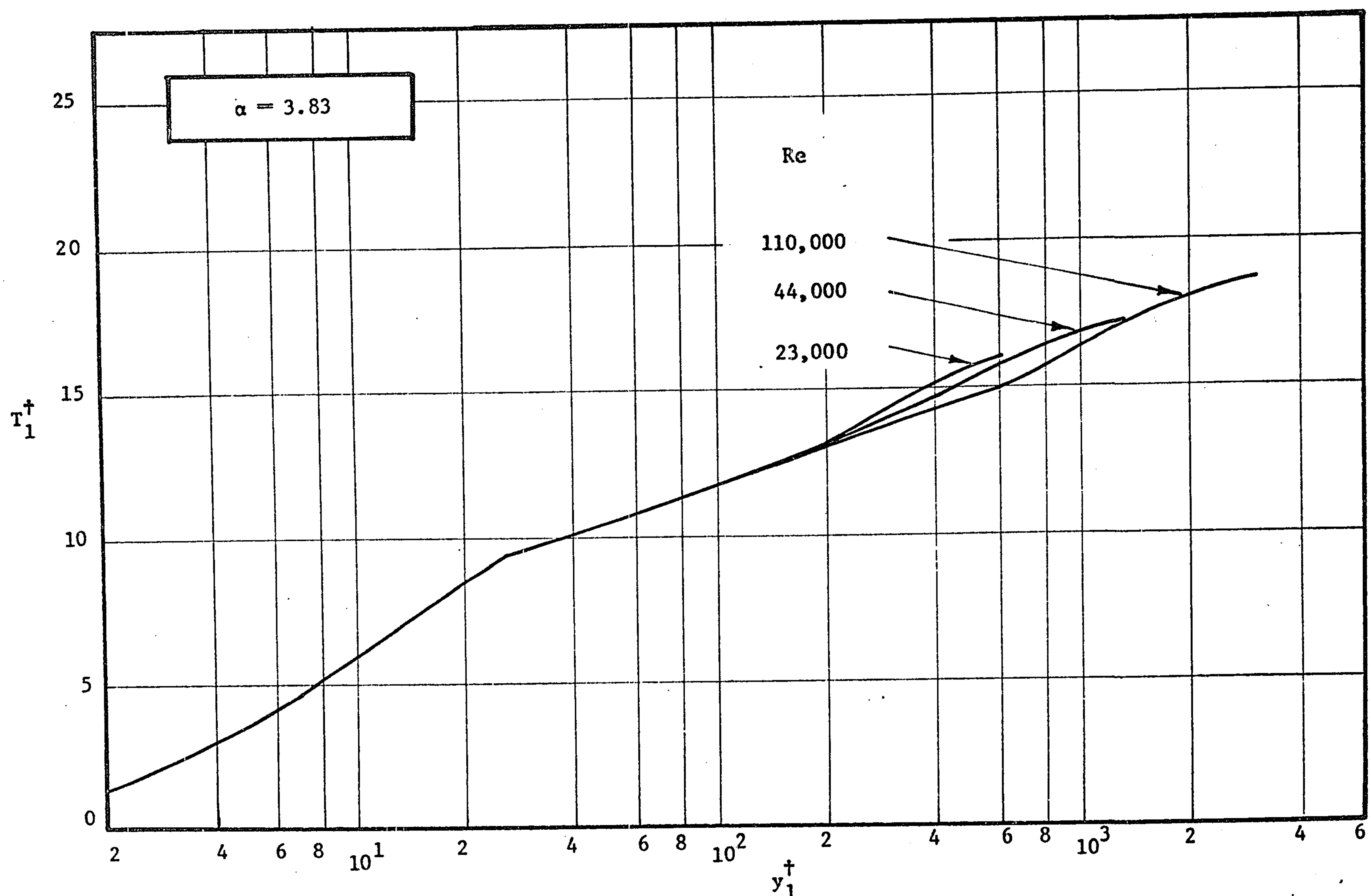

Fig. 3.19 Predicted Temperature Profiles, Fully Developed Regions, Inner Wall Heated, Outer Wall Insulated, Effect of Re, Pr = o.71

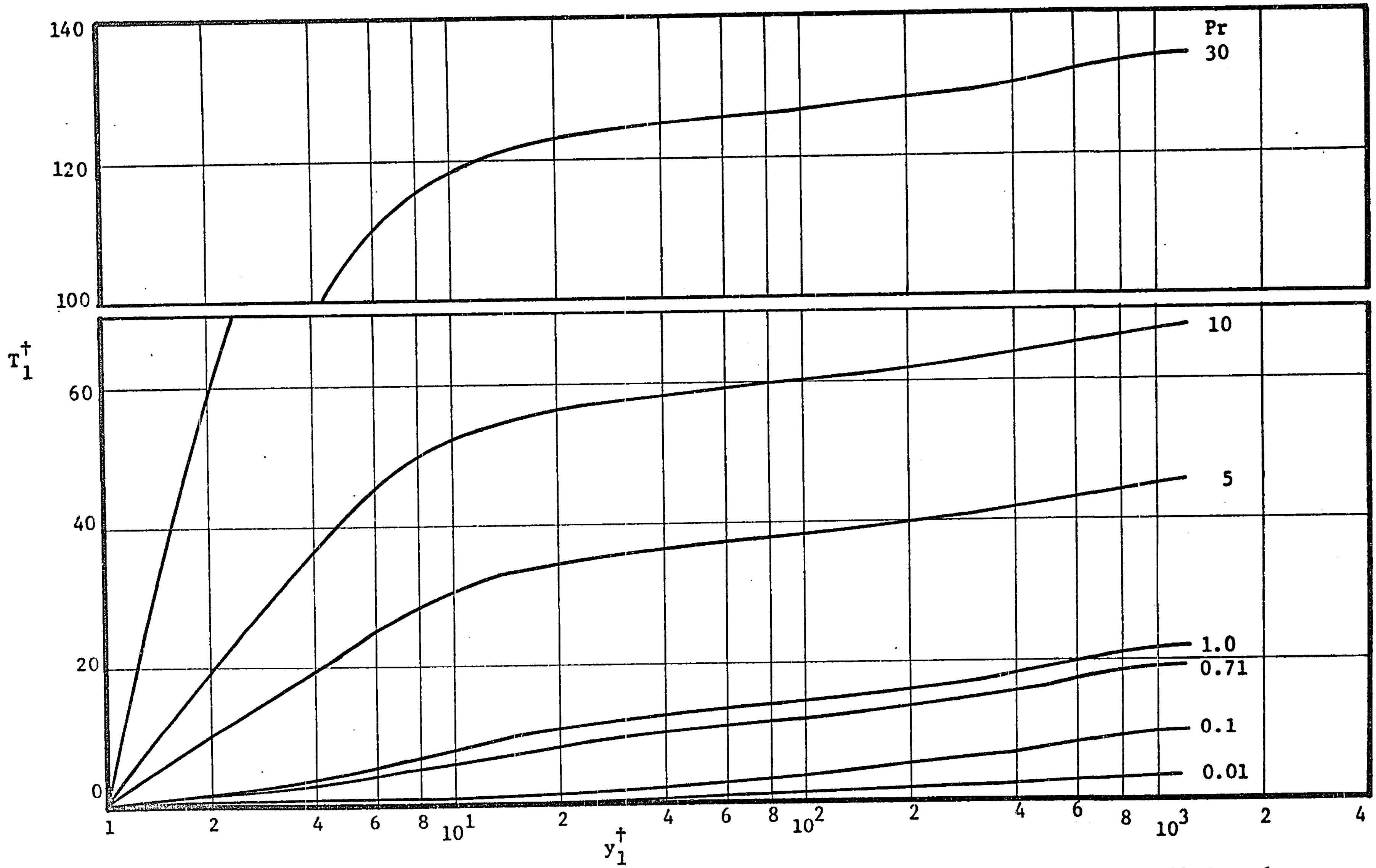

Fig. 3.20 Predicted Temperature Profiles, Fully Developed Regions, Inner Wall Heated, Outer Wall Insulated, Effect of Pr, $\alpha = 2.31$, $Re = 44,000$

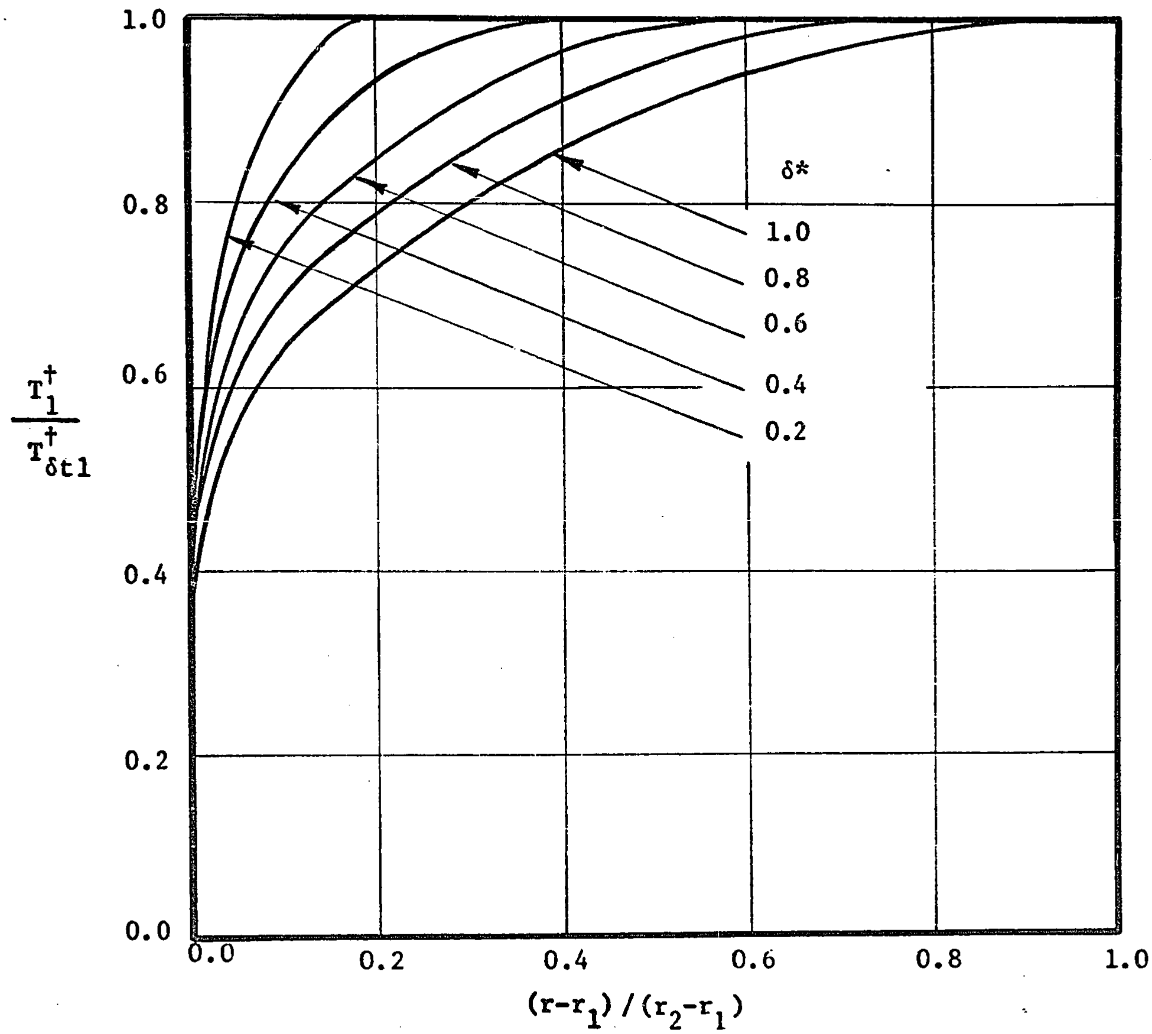

Fig. 3.21 Predicted Temperature Profiles in Entrance Regions, Inner Wall Heated, Outer Wall Insulated, Re = 23,000 $\alpha = 2.31$, Pr = 0.71.

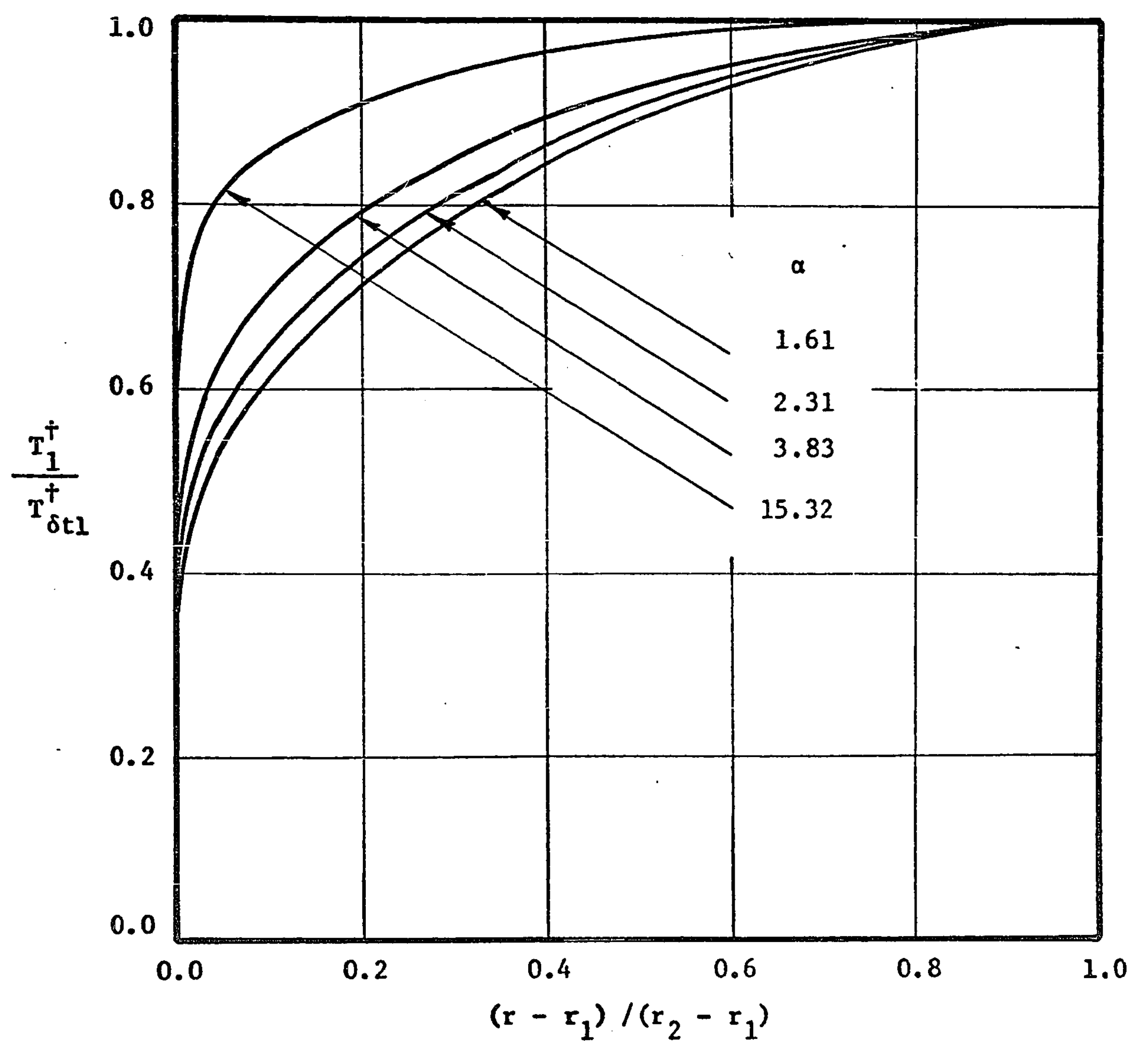

Fig. 3.22 Predicted Temperature Prefiles, Fully Developed Regions, Inner Wall Heated, Outer Wall Insulated, Effect of α

$Re = 44{,}000$, $Pr = 0.71$

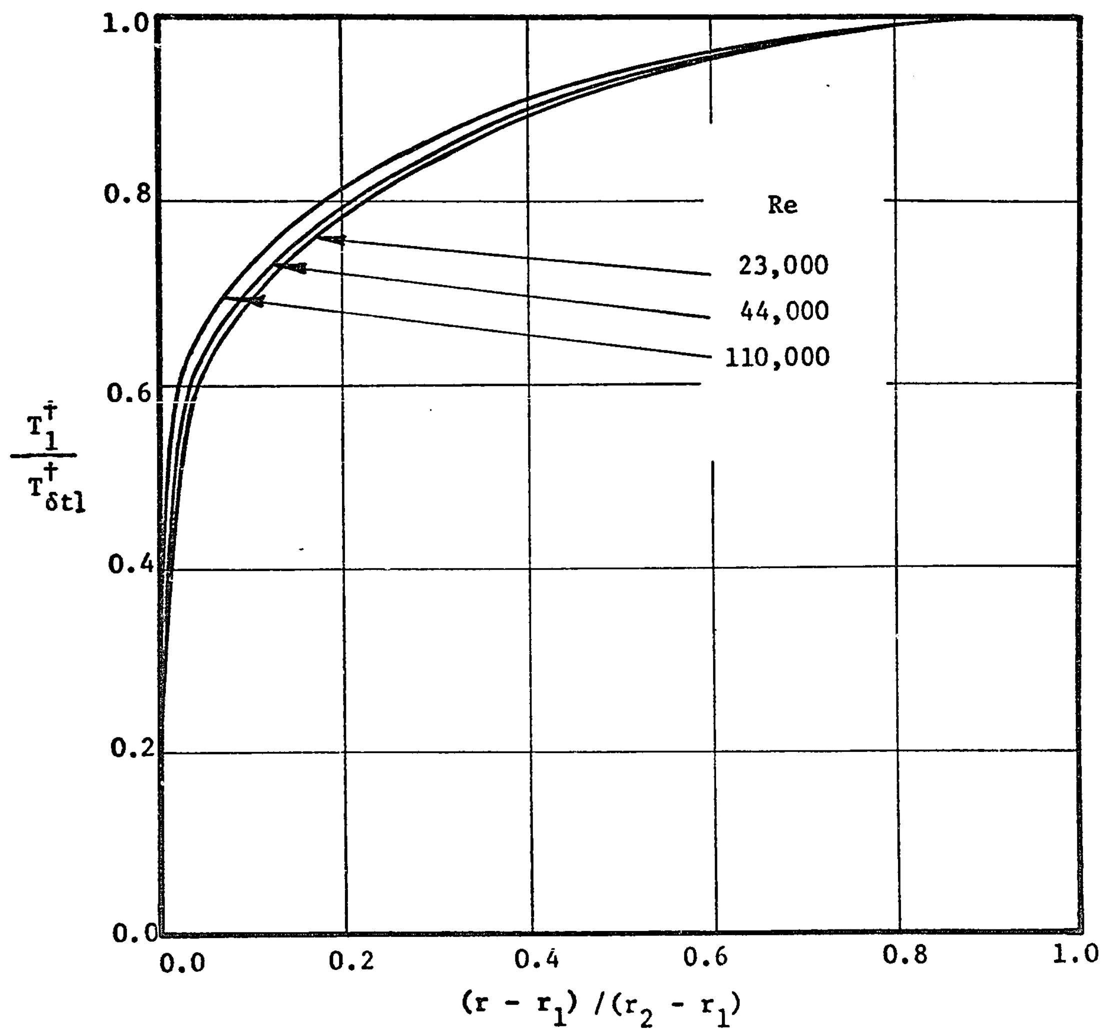

Fig. 3.23 Predicted Temperature Profiles, Fully Developed Regions, Inner Wall Heated, Outer Wall Insulated, Effect of Re, $\alpha = 3.83$, $Pr = 0.71$

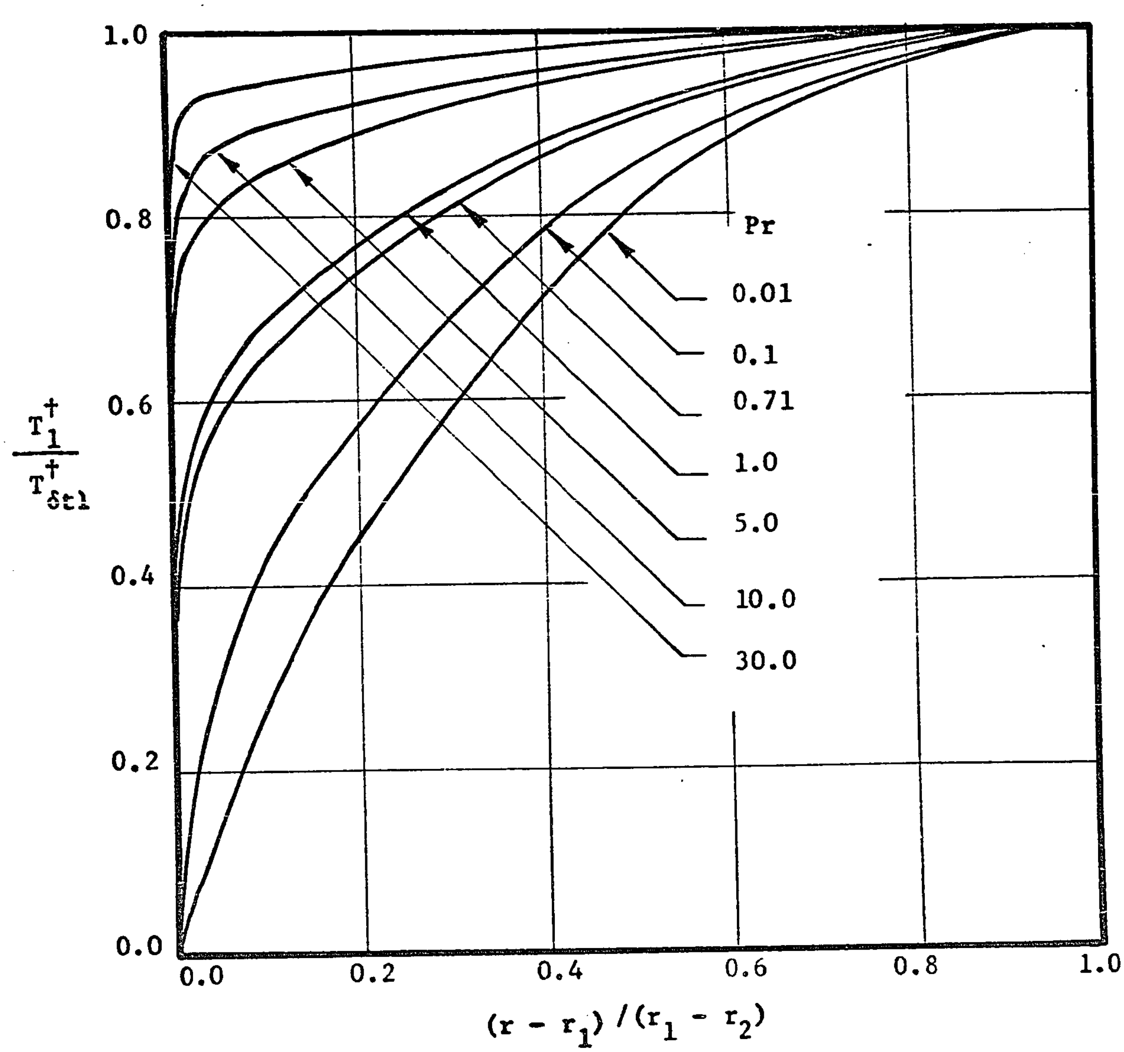

Fig. 3.24 Predicted Temperature Profiles, Fully Developed Regions, Inner Wall Heated, Outer Wall Insulated, Effect of Pr, $\alpha = 2.31$, Re = 44,000

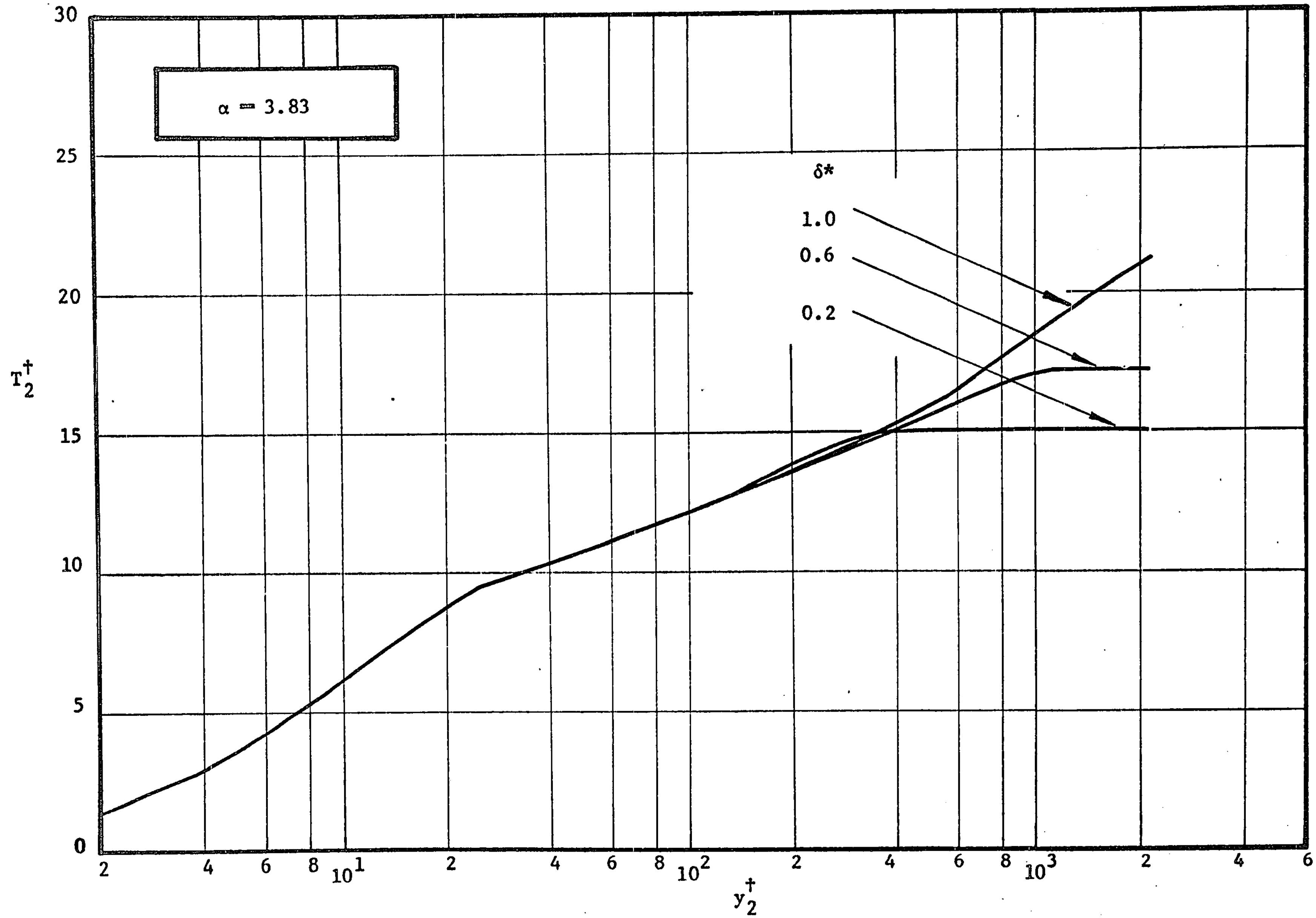

Fig. 3.25 Predicted Temperature Profiles, Entrance Regions, Outer Wall Heated, Inner Wall Insulated, Re = 77,000, Pr = 0.71

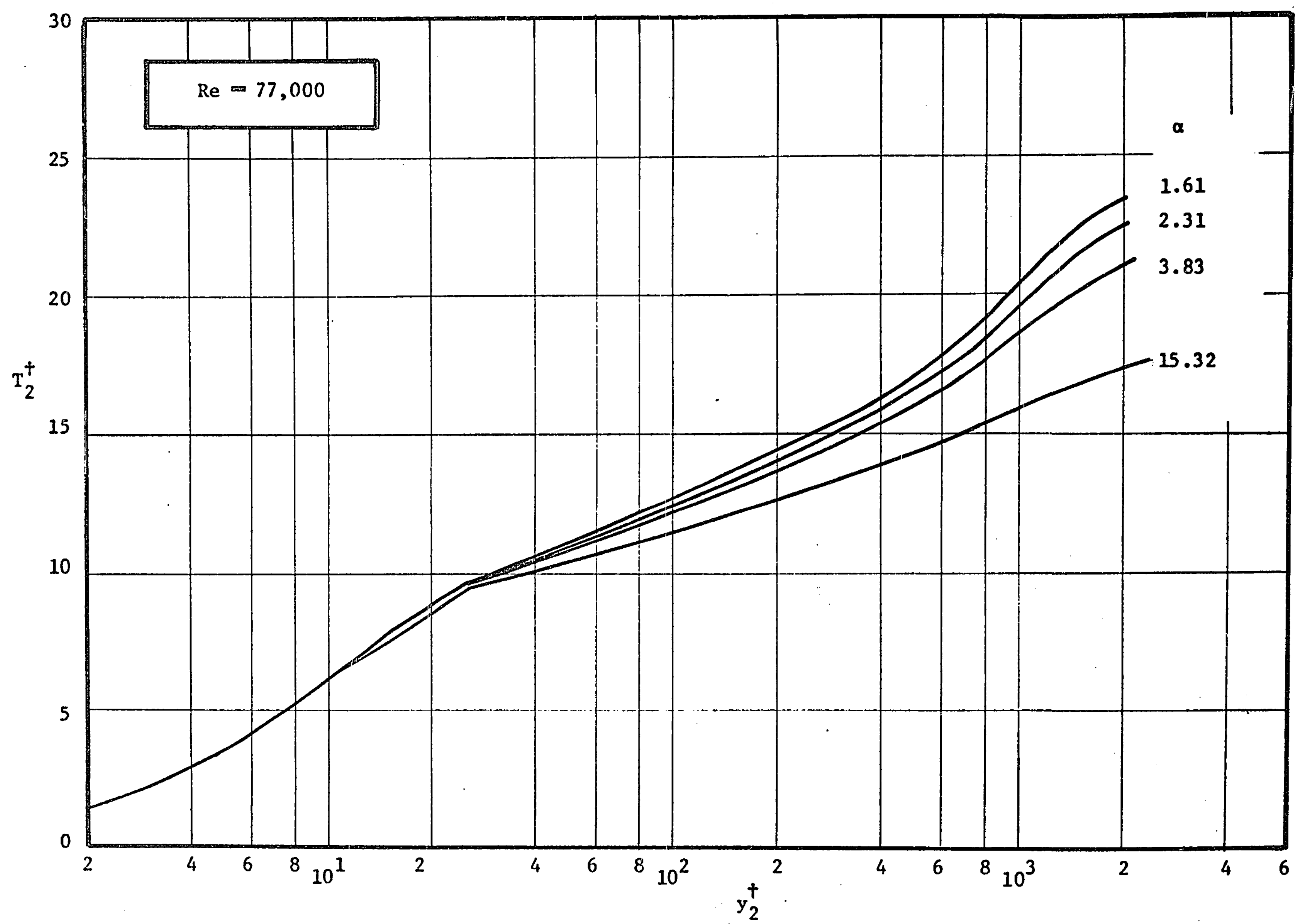

Fig. 3.26 Predicted Temperature Profiles, Fully Developed Regions, Outer Wall Heated, Inner Wall Insulated, Effect of α, Pr = 0.71

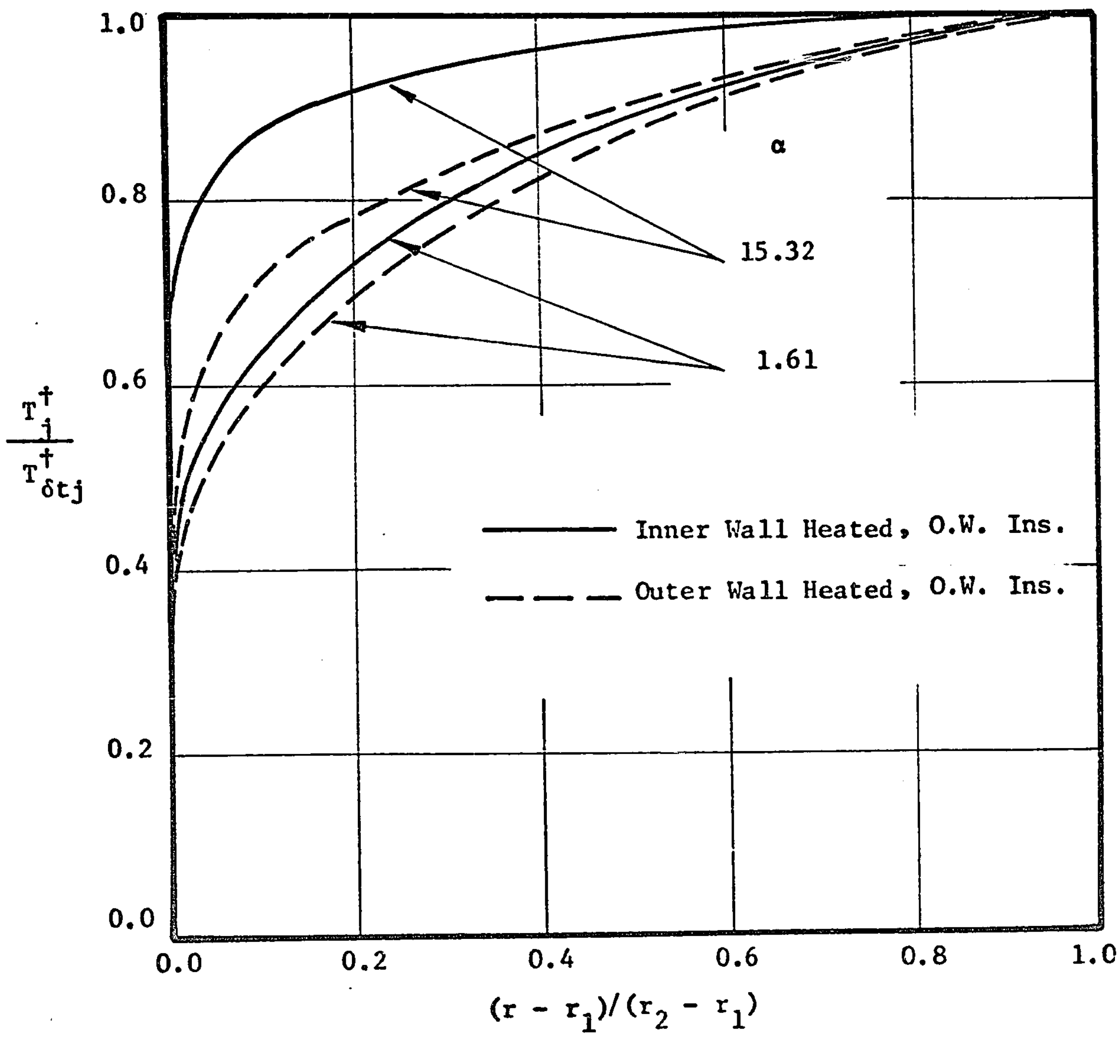

Fig. 3.27 Predicted Temperature Profiles, Fully Developed Regions, Effect of Wall Boundary Condition, Re = 77,000 Pr = 0.71

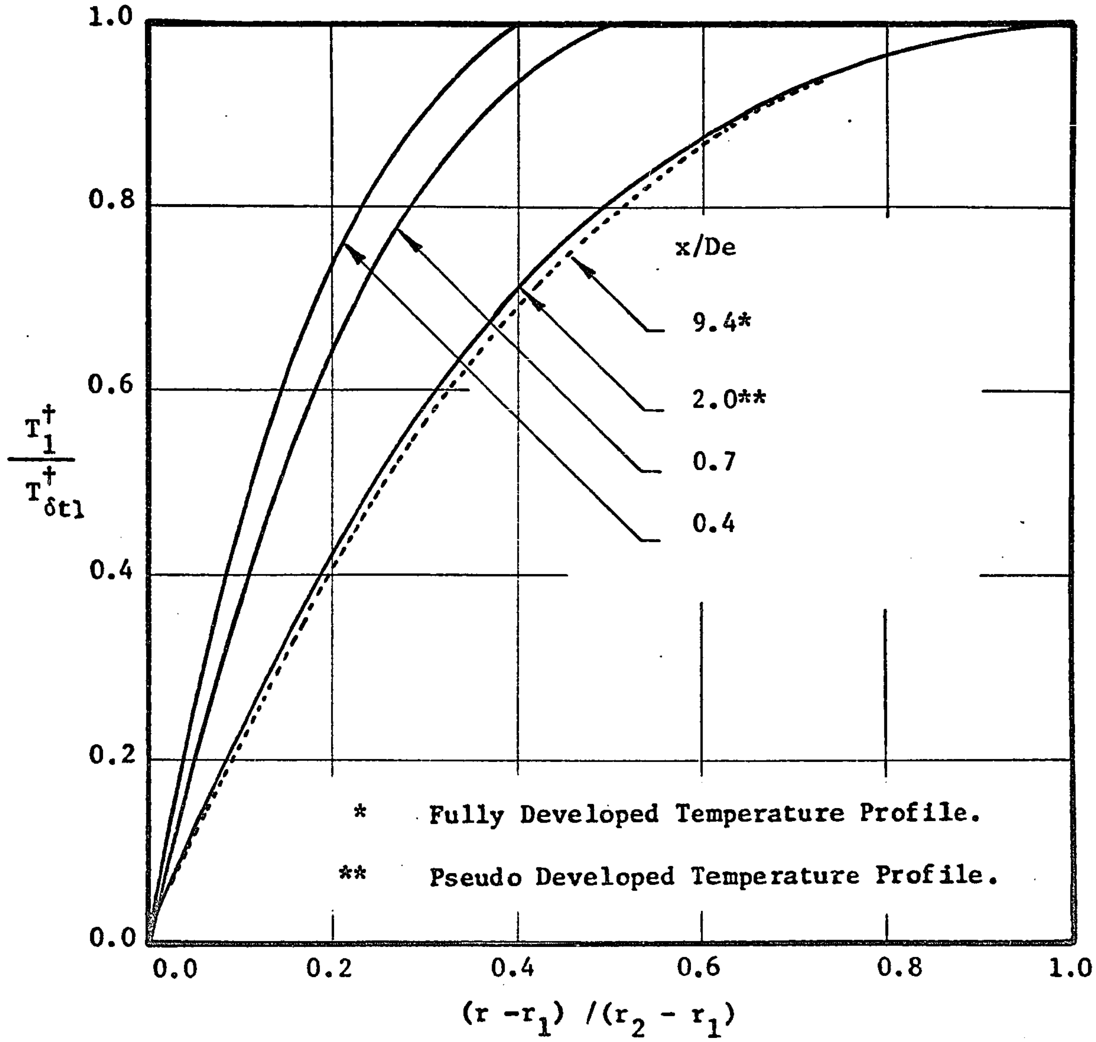

Fig. 3.28 Development of Temperature Profiles, Inner Wall Heated, Outer Wall Insulated, Effect of Very Low Pr.
$Pr = 0.001$, $\alpha = 2.31$, $Re = 44{,}000$.

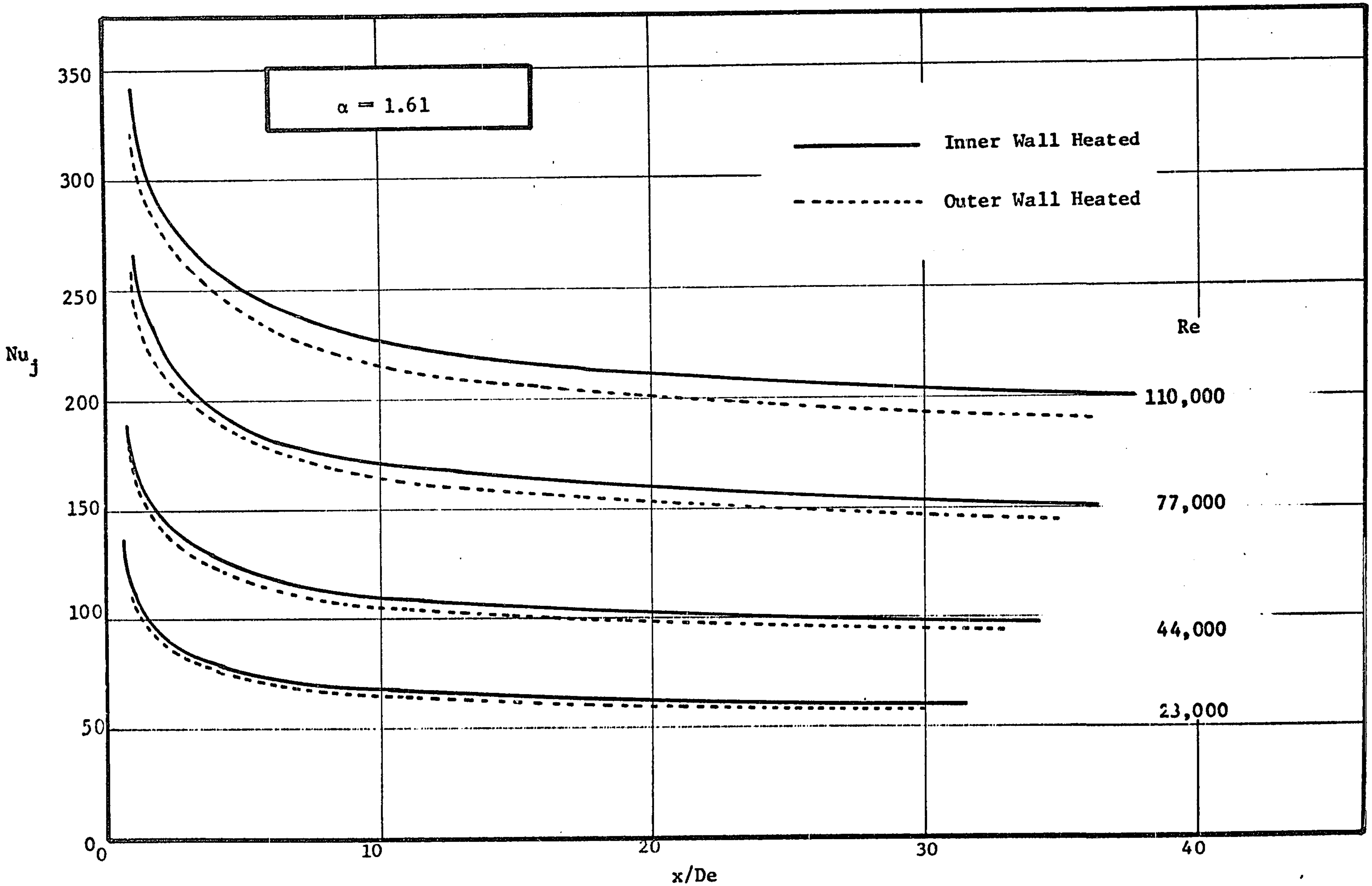

Fig. 3.29 Predicted Nusselt Numbers, Entrance Regions, Pr = 0.71

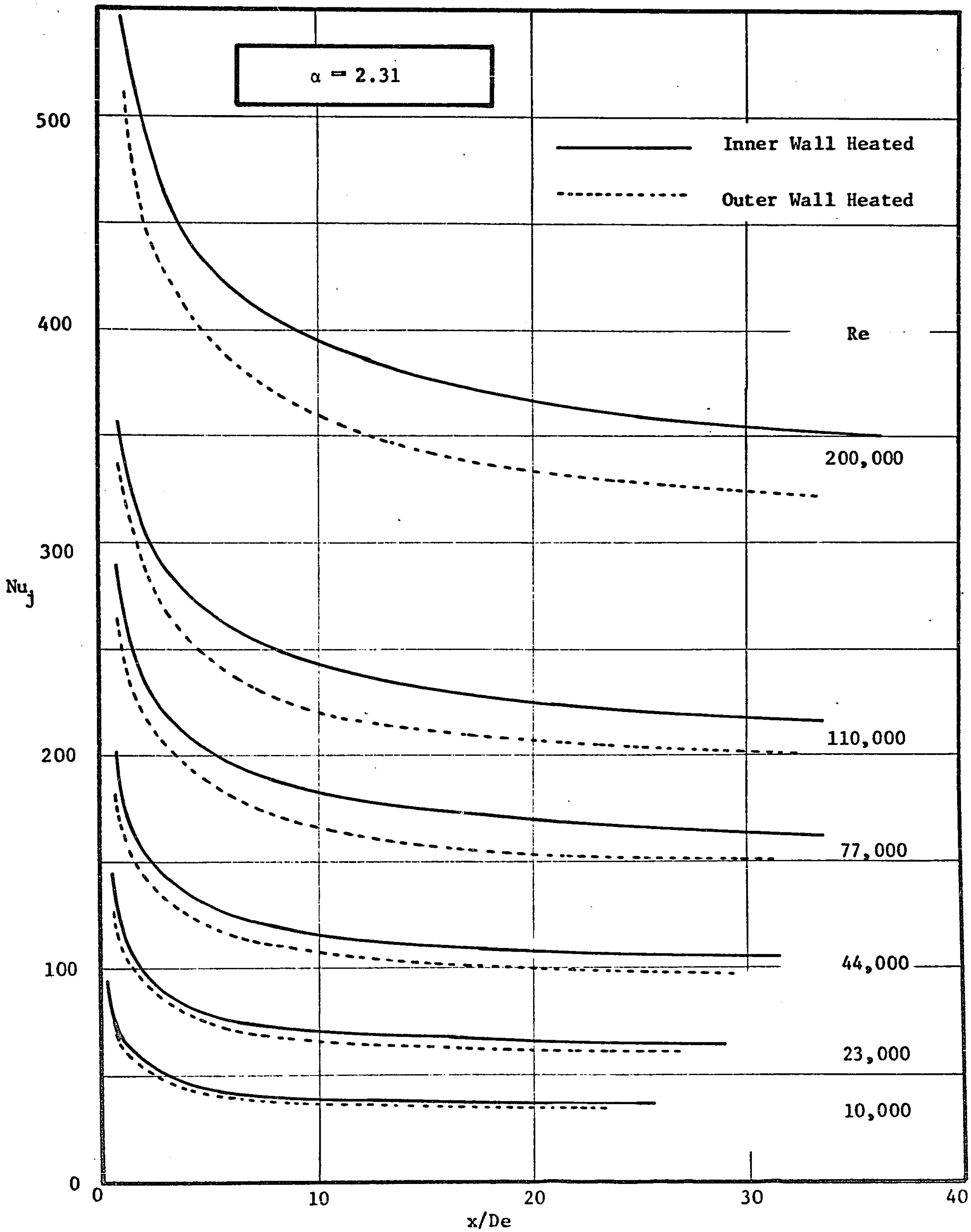

Fig. 3.30 Predicted Nusselt Numbers, Entrance Regions, Pr = 0.71

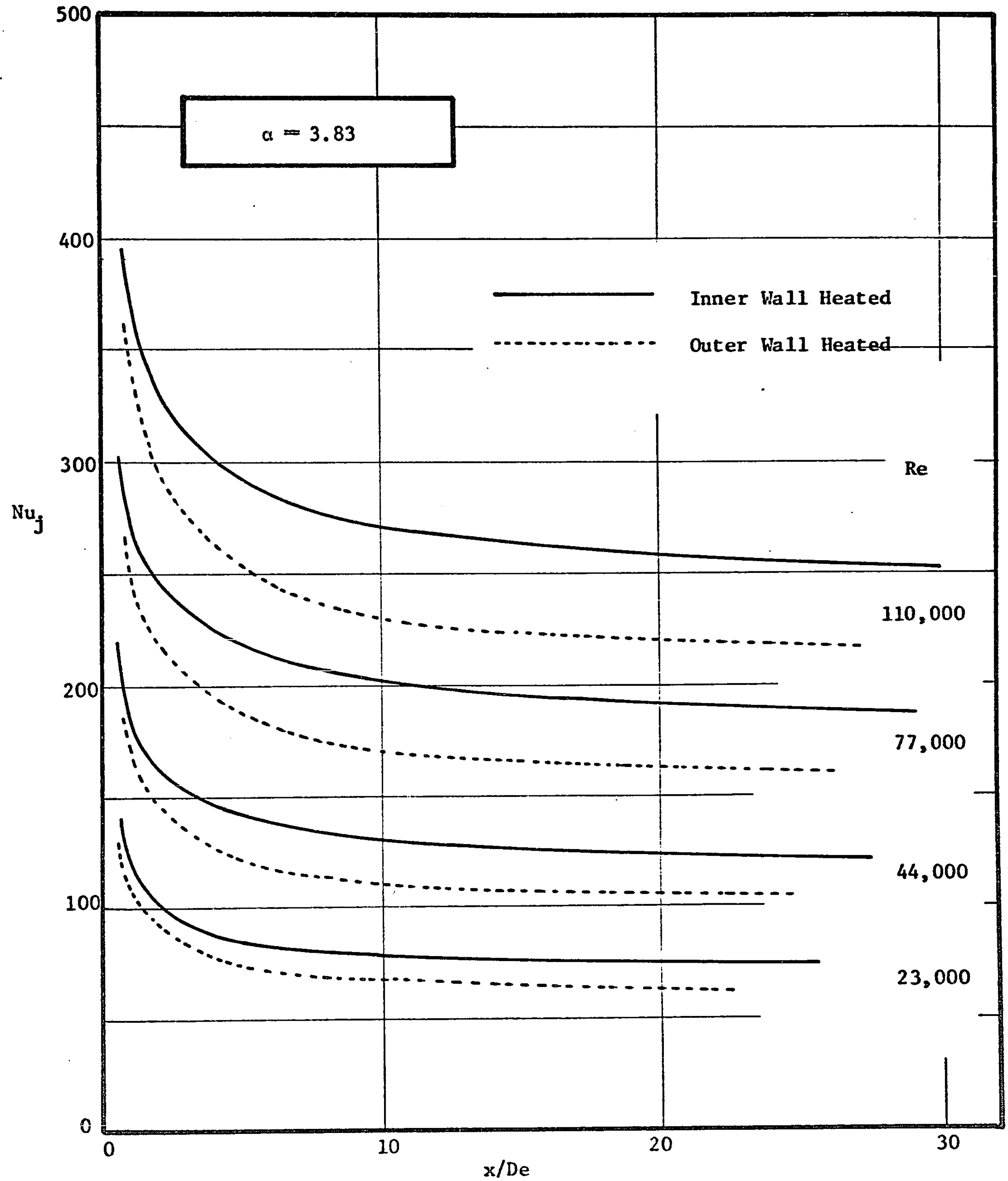

Fig. 3.31 Predicted Nusselt Numbers, Entrance Regions, Pr = 0.71

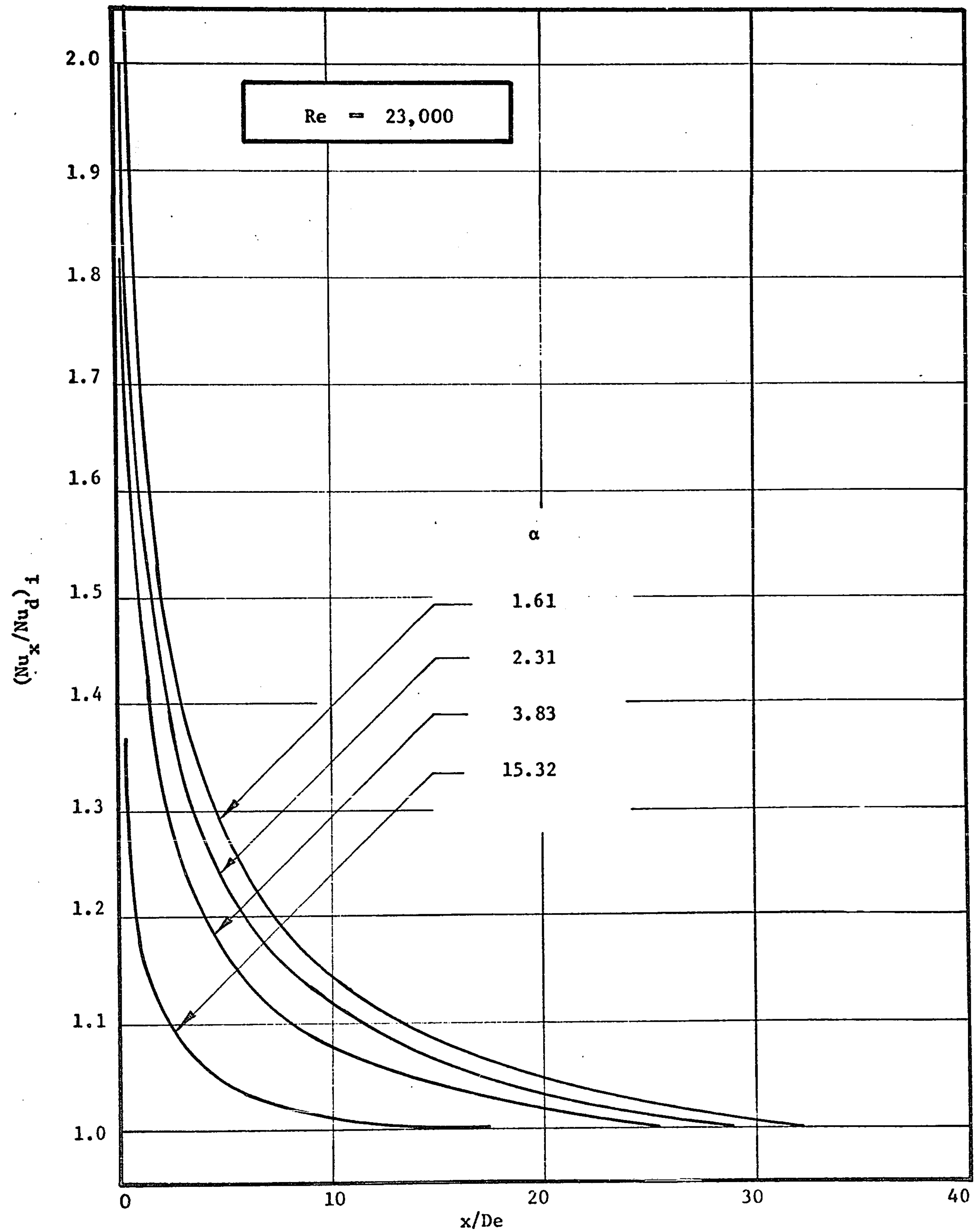

Fig. 3.32 Predicted Nusselt Numbers, Entrance Regions, Inner Wall Heated, Outer Wall Insulated, Effect of α, Pr = 0.71

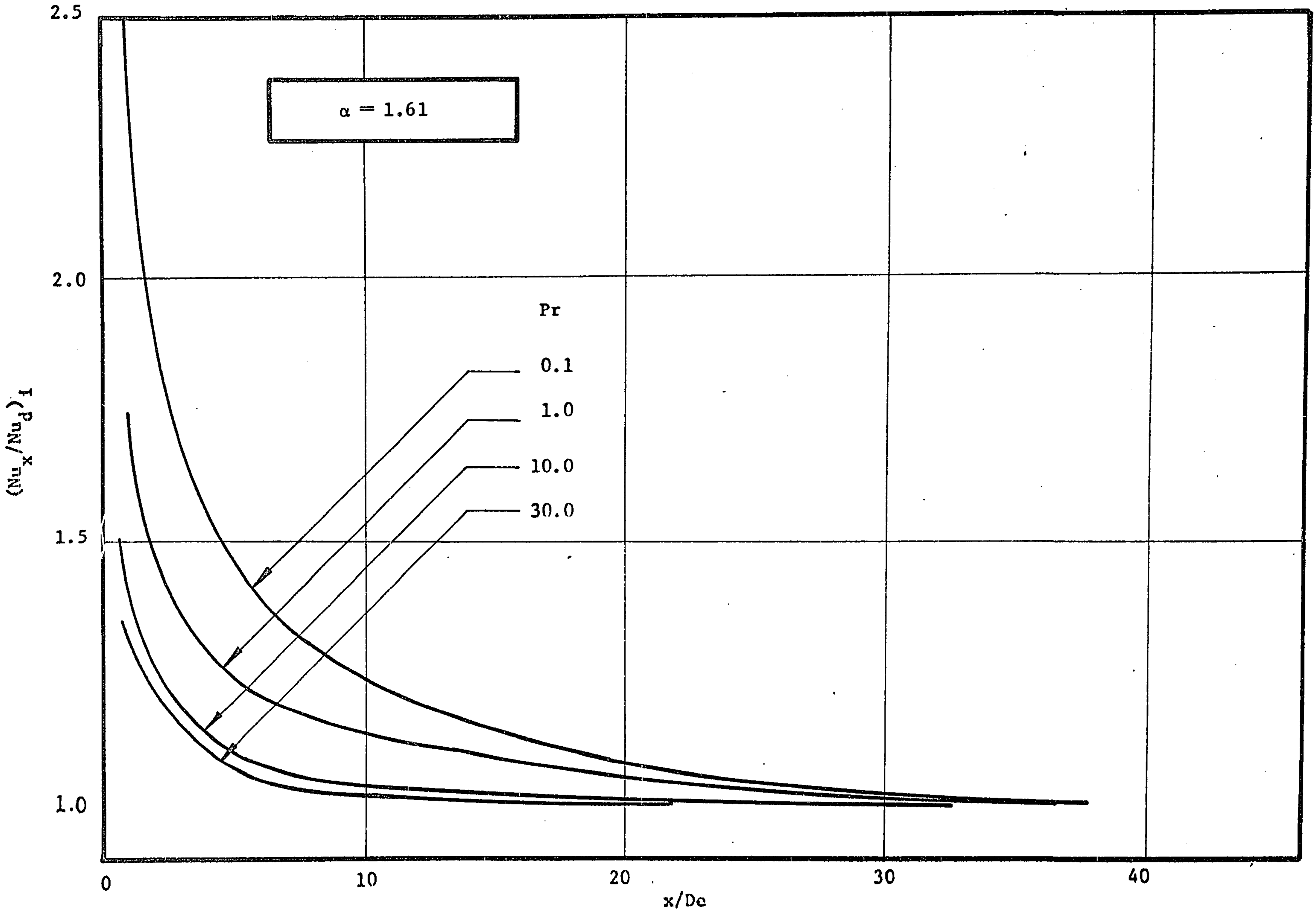

Fig. 3.33 Predicted Nusselt Numbers, Entrance Regions, Inner Wall Heated, Outer Wall Insulated, Effect of Pr, Re = 77,000

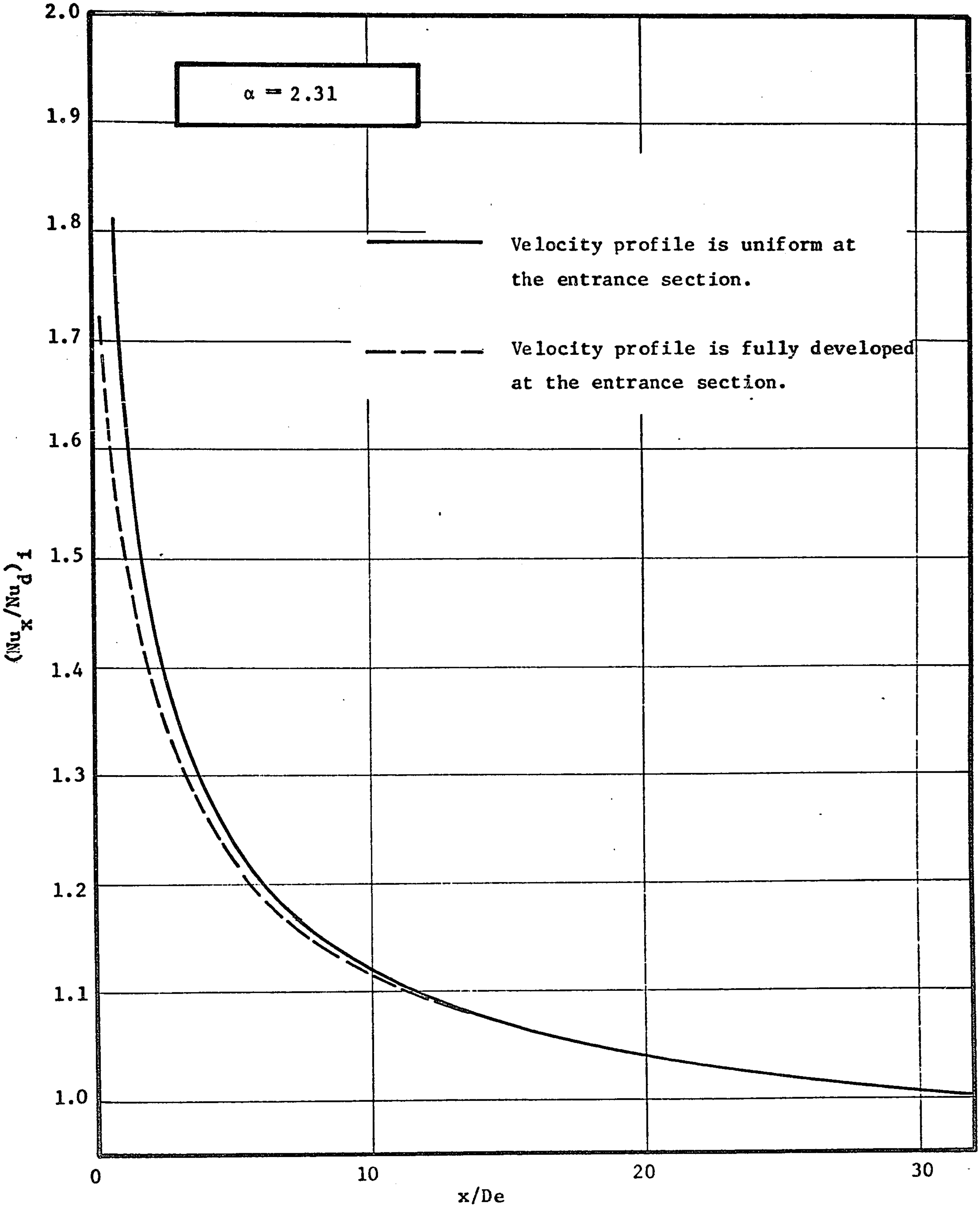

Fig. 3.34 Predicted Nusselt Numbers, Entrance Regions, Inner Wall Heated, Outer Wall Insulated, Effect of Initial Velocity Profile, Re = 44,000, Pr = 0.71

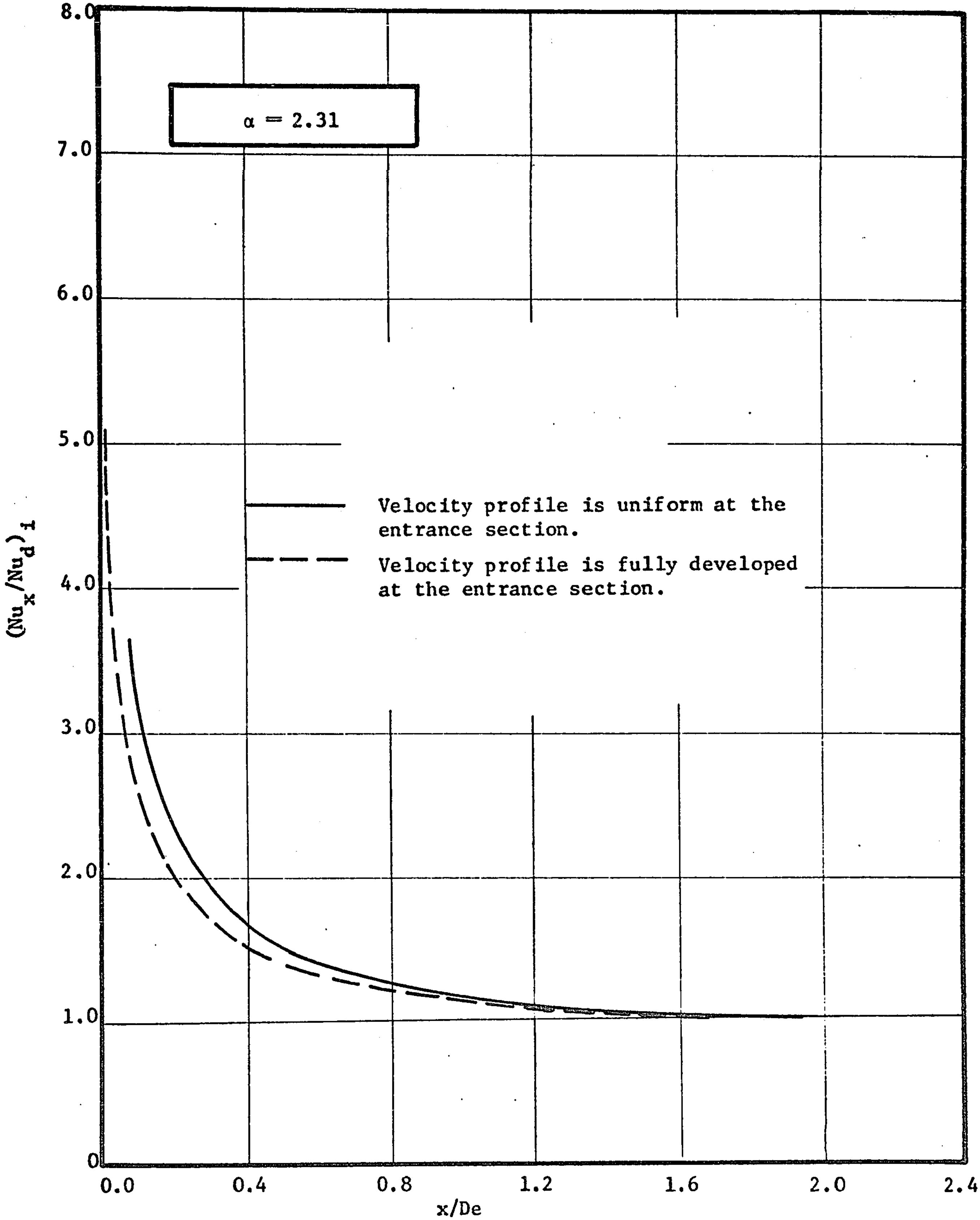

Fig. 3.35 Predicted Nusselt Numbers, Entrance Regions, Inner Wall Heated, Outer Wall Insulated, Effect of Initial Velocity Profile, Re = 44,000, Pr = 0.001

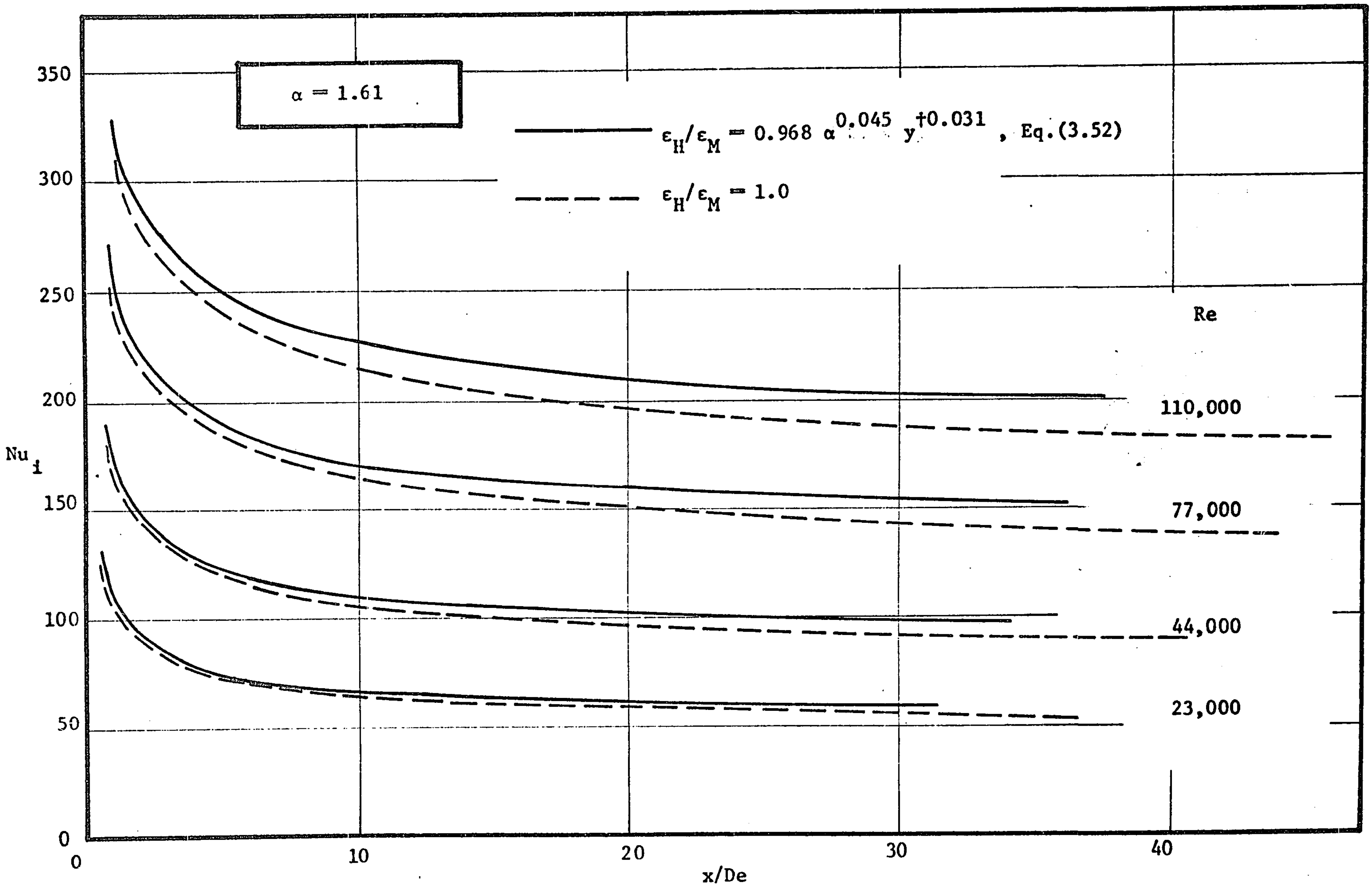

Fig. 3.36 Predicted Nusselt Numbers, Entrance Regions, Inner Wall Heated, Outer Wall Insulated, Effect of σ and Re, Pr = 0.71

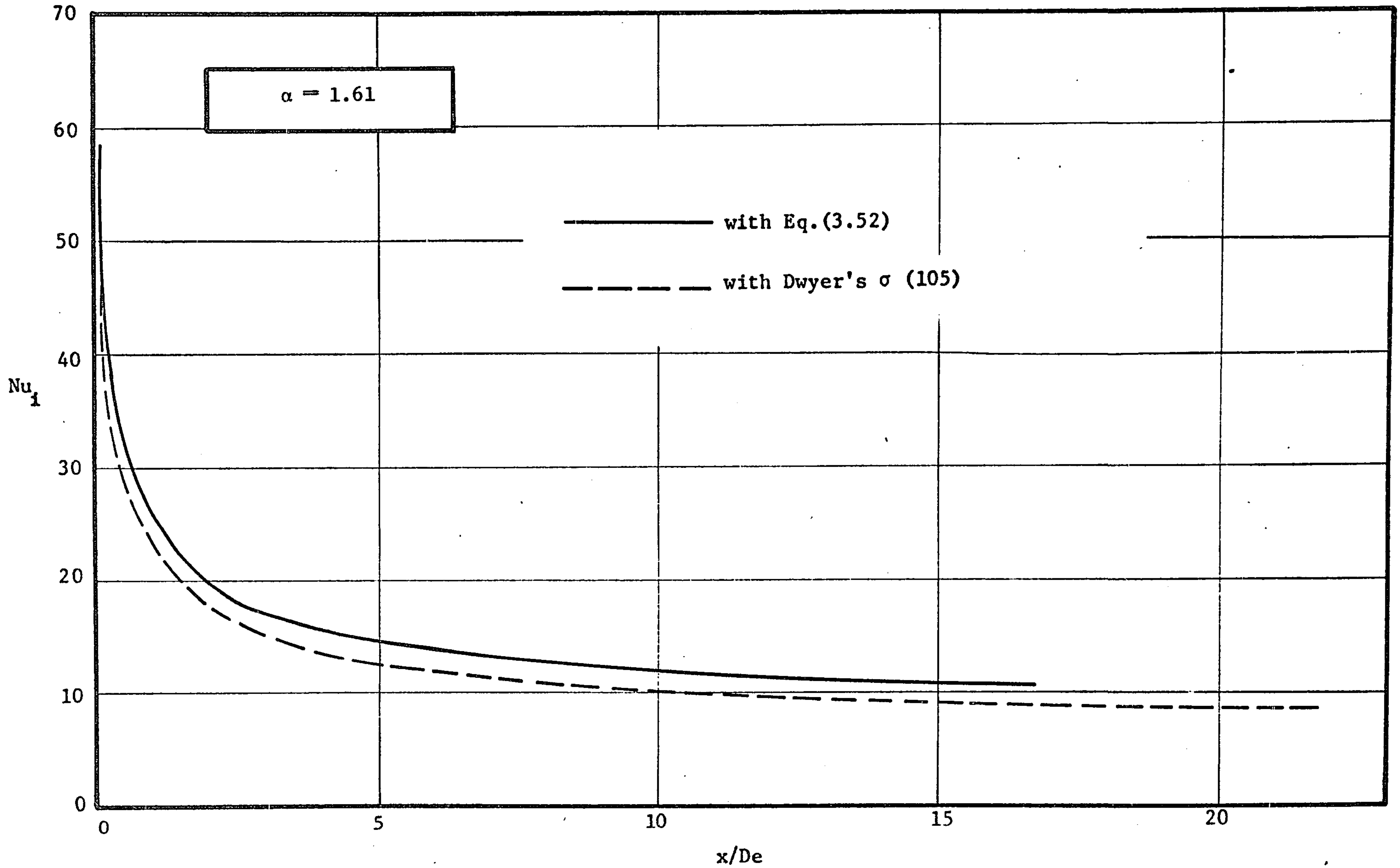

Fig. 3.37 Predicted Nusselt Numbers, Entrance Regions, Inner Wall Heated, Outer Wall Insulated, Effect of σ for Low Pr, Re = 77,000, Pr = 0.71

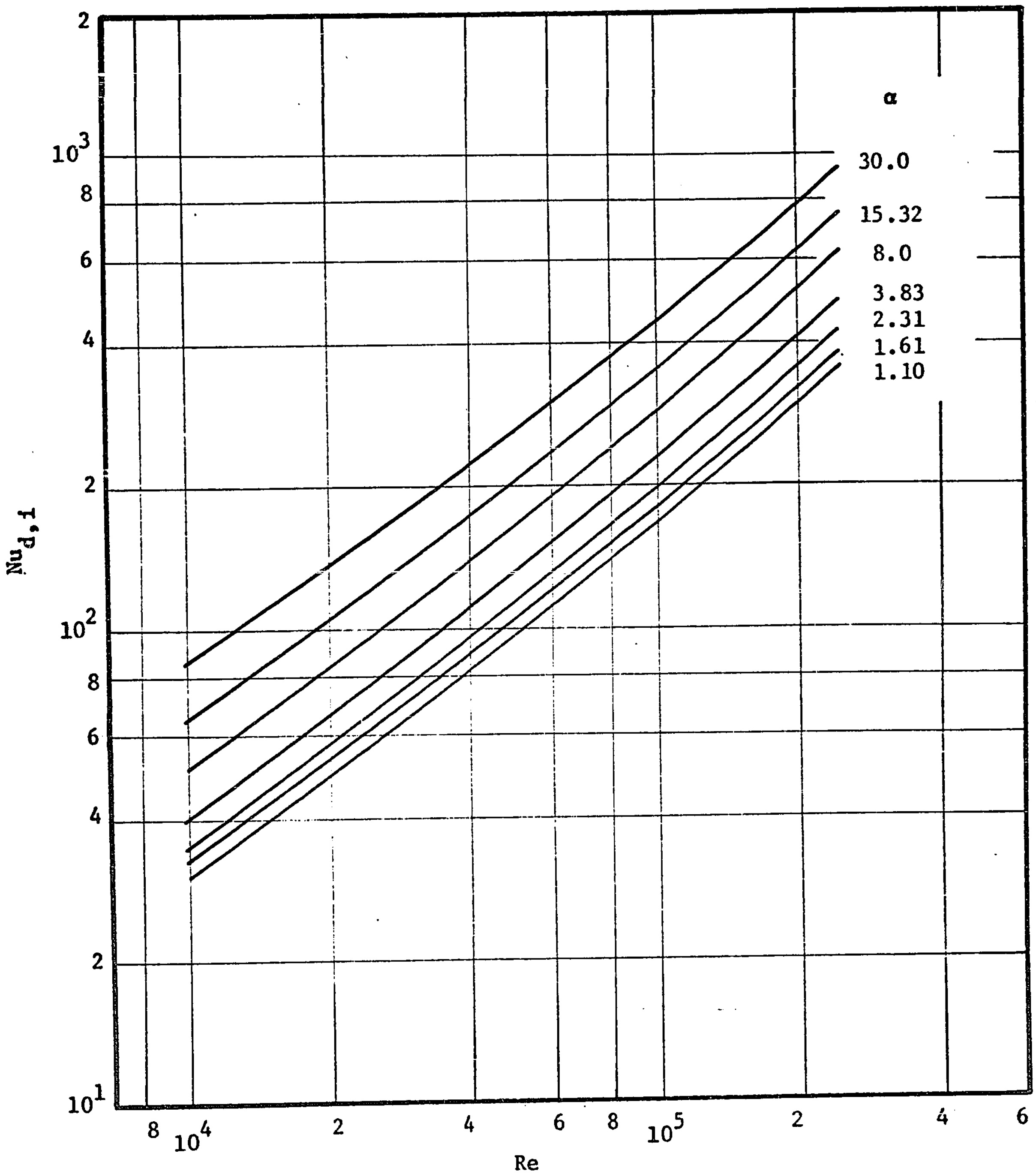

Fig. 3.38 Predicted Nusselt Numbers, Fully Developed Regions, Inner Wall Heated, Outer Wall Insulated, Effect of α, Pr = 0.71

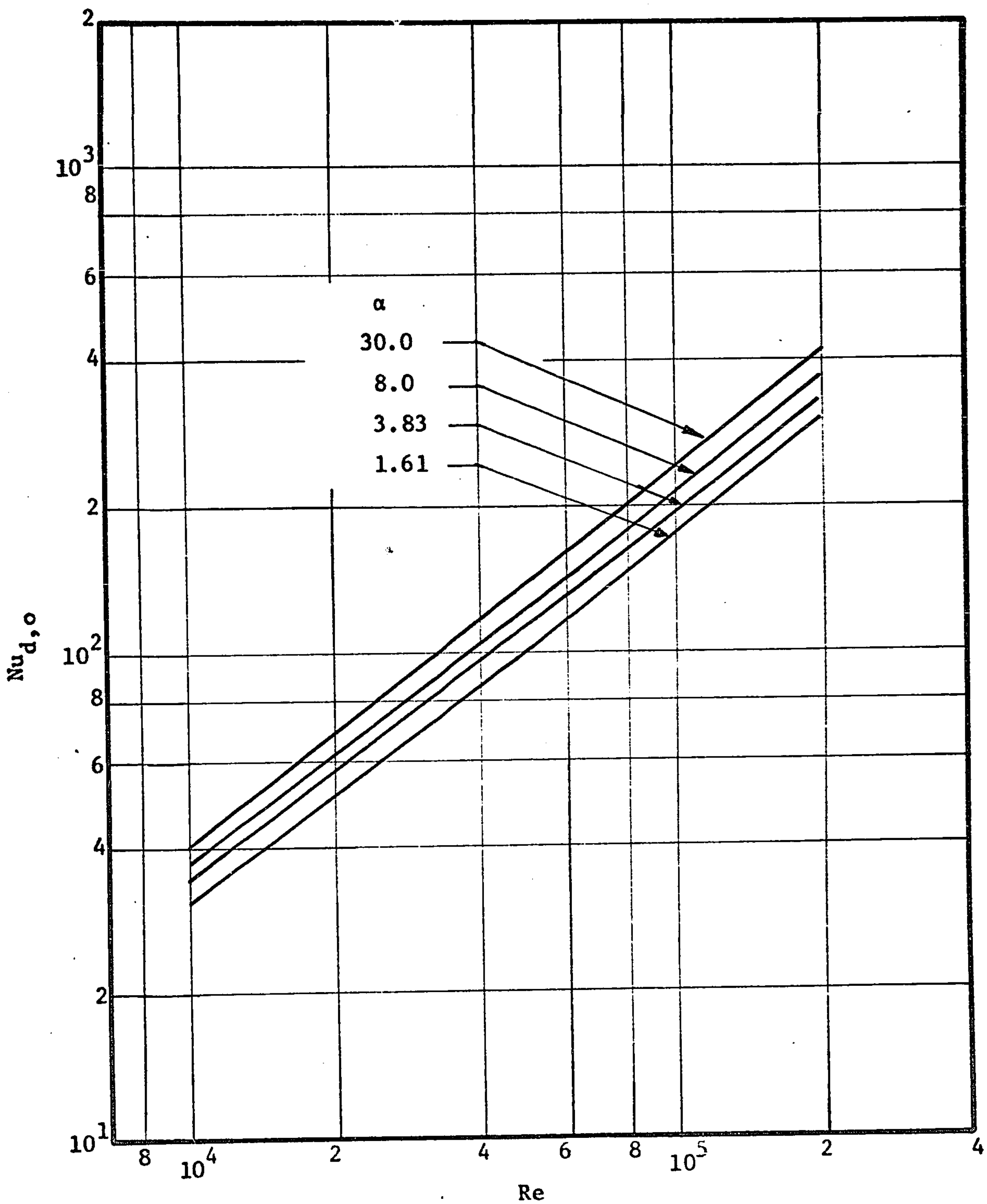

Fig. 3.39 Predicted Nusselt Numbers, Fully Developed Regions, Outer Wall Heated, Inner Wall Insulated, Effect of α, Pr = 0.71

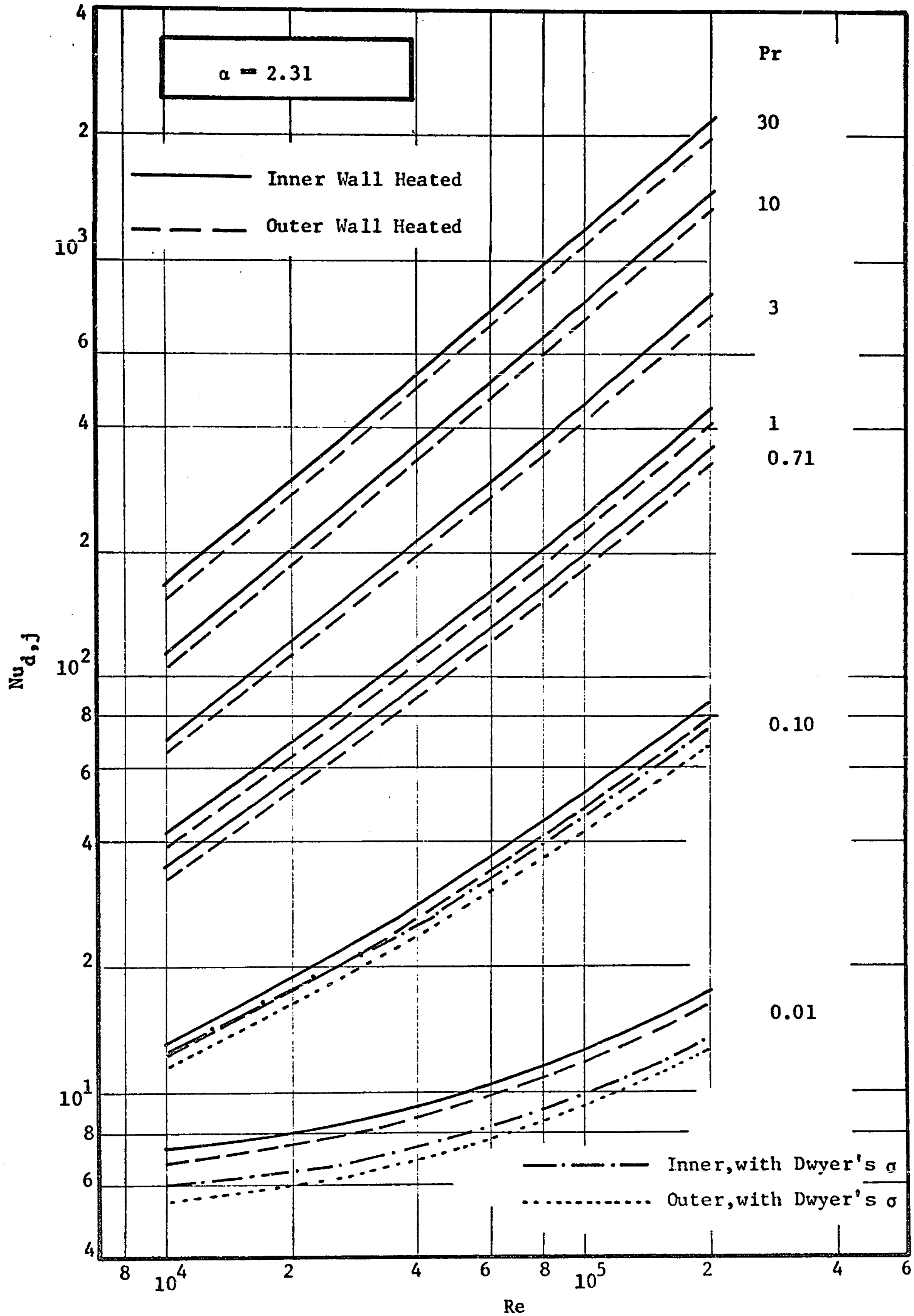

Fig. 3.40 Predicted Nusselt Numbers, Fully developed Regions, Effect of Pr.

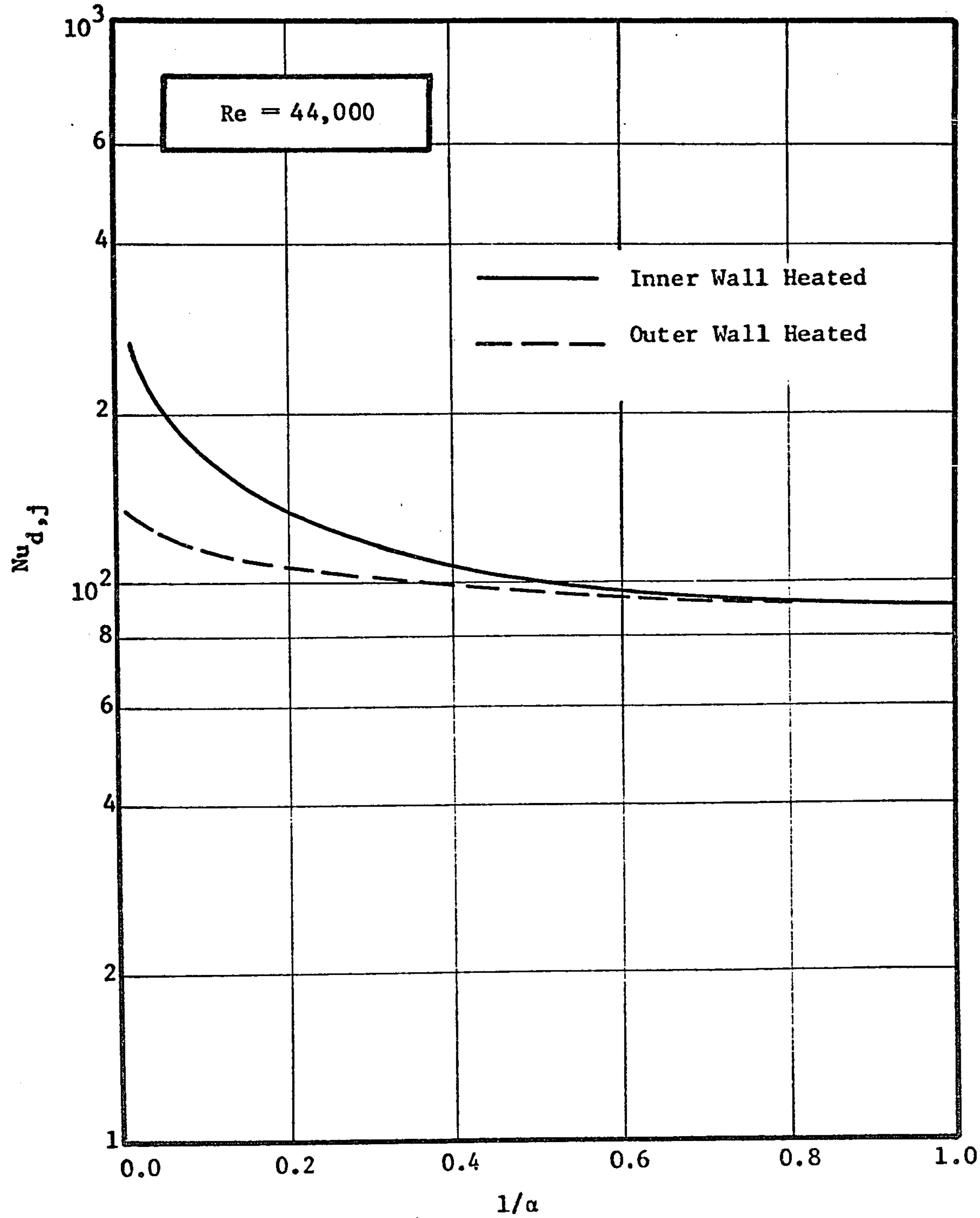

Fig. 3.41 Effect of Radius Ratio on Fully Developed Nusselt Numbers, $Pr = 0.071$

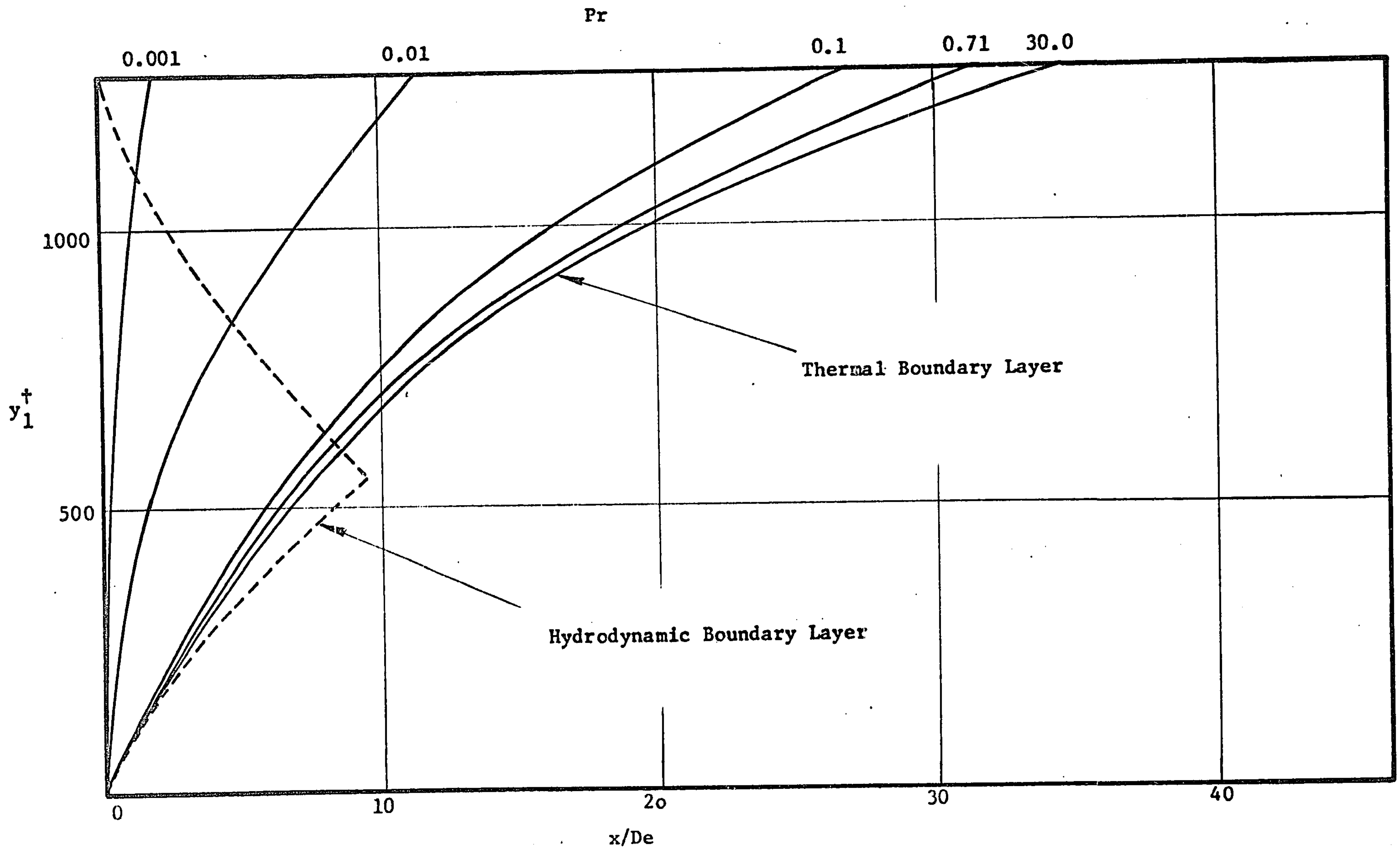

Fig. 3.42 Development of Hydrodynamic and Thermal Boundary Layers, Entrance Region, Inner Wall Heated, Outer Wall Insulated, Effect of Pr, $\alpha = 2.31$, Re = 44,000

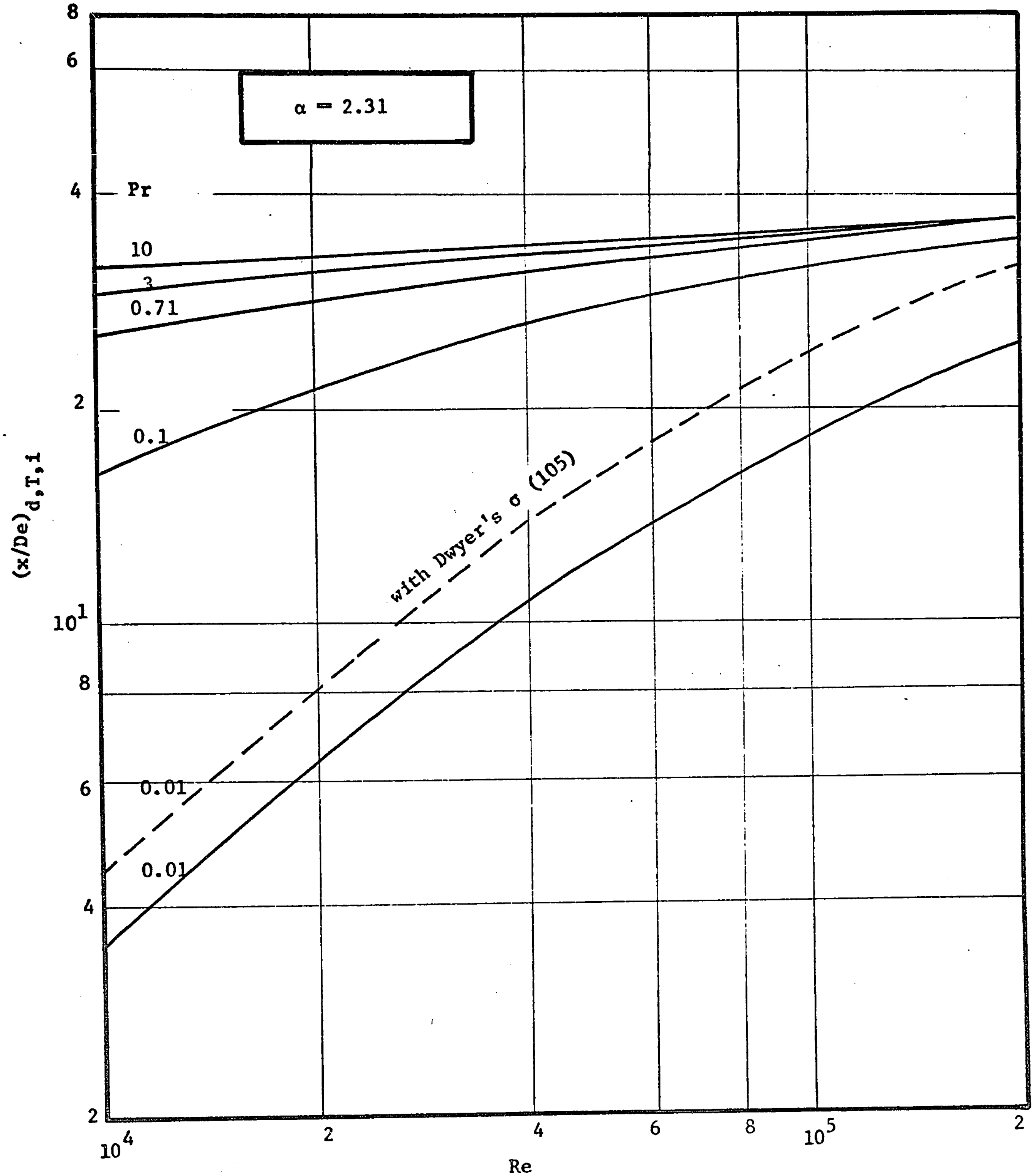

Fig. 3.43 Effect of Prandtl Number on the Entrance Length, Inner Wall Heated, Outer Wall Insulated.

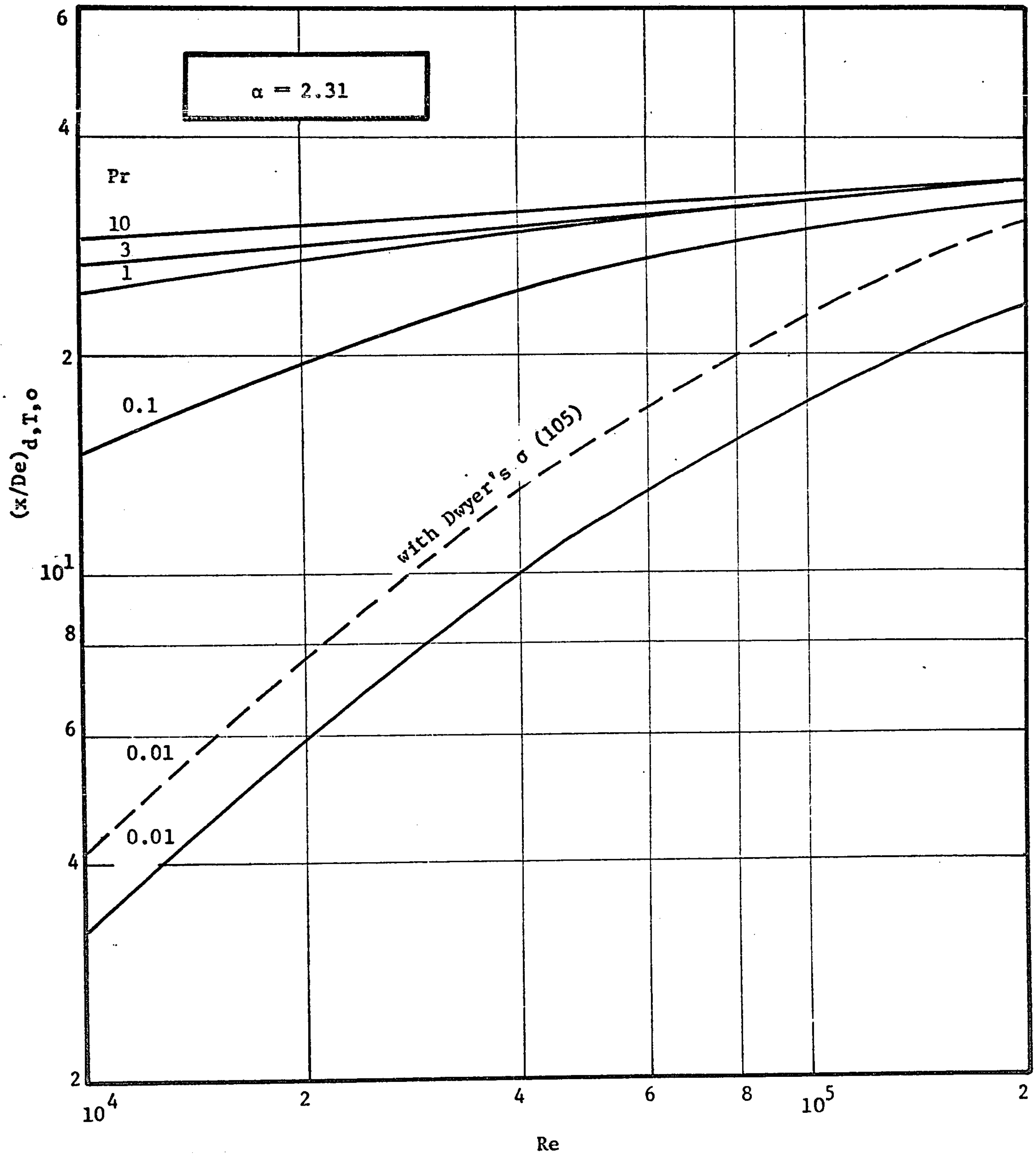

Fig. 3.44 Effect of Prandtl Number on the Entrance Length, Outer Wall Heated, Inner Wall Insulated.

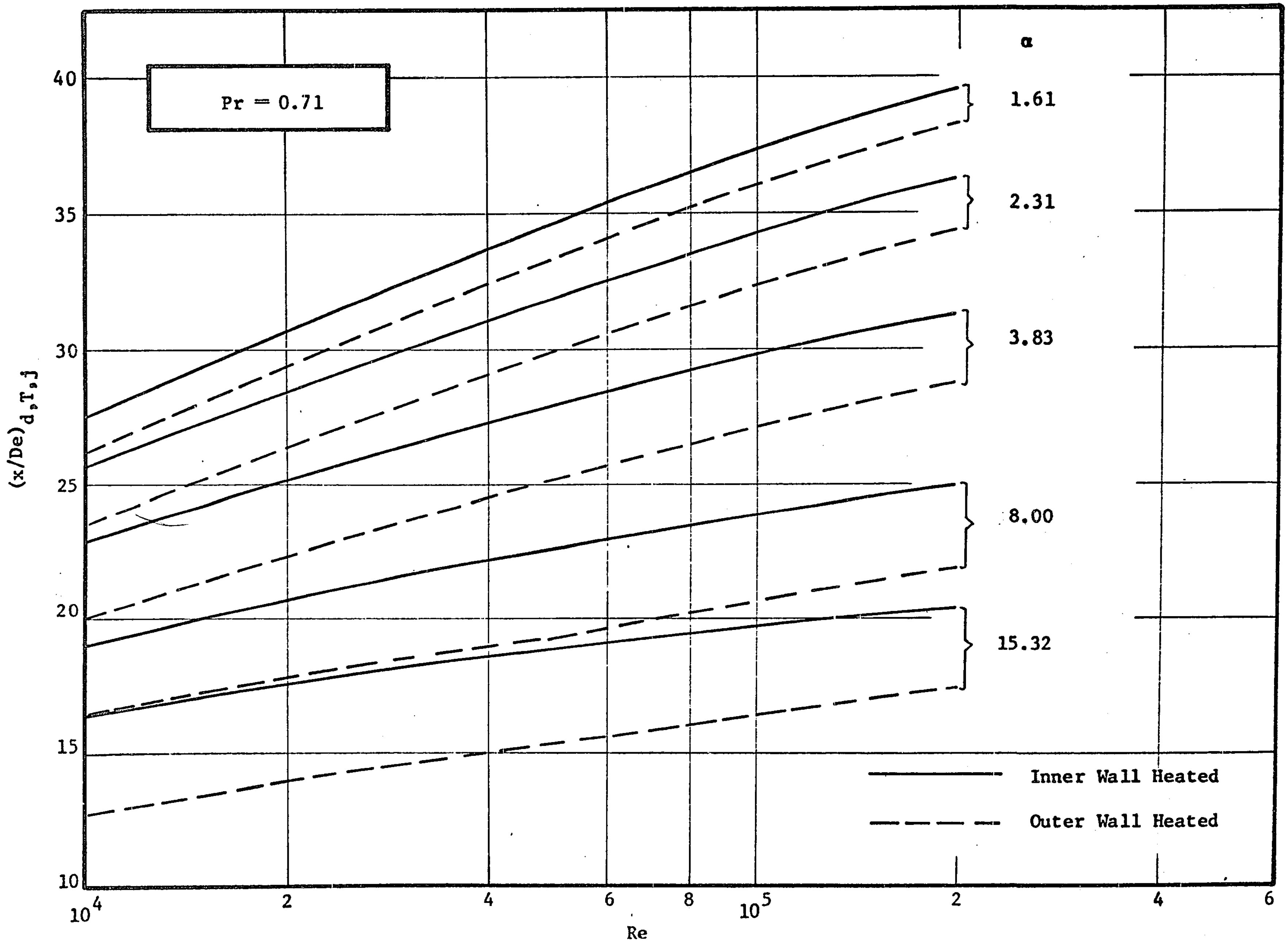

Fig. 3.45 Predicted Entrance Length, Effect of α and Boundary Condition.

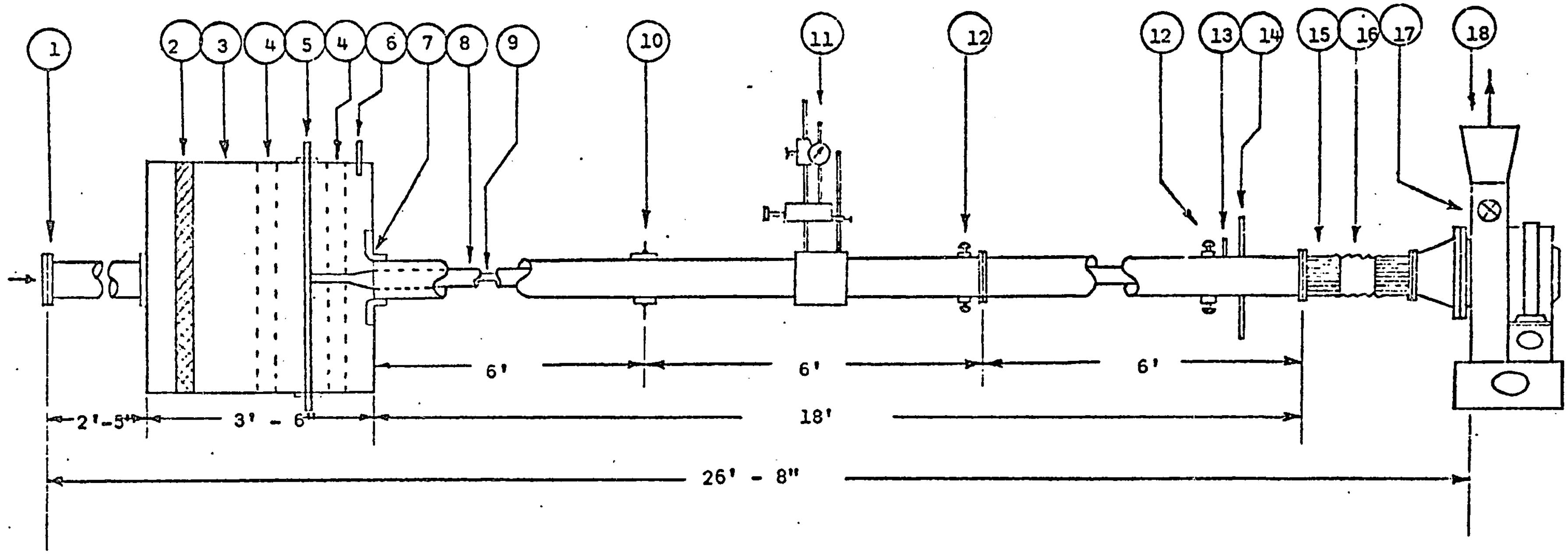

① B. S. ORIFICE

② AIR FILTER

③ SETTLING CHAMBER

④ SETTLING SCREENS

⑤ CORE SUPPORT AND POWER TERMINAL

⑥ THERMOMETER AND T.C. WELL

⑦ BELL MOUTH INLET AND TRIP WIRE

⑧ CORE TUBE

⑨ T.C. AND VOLTAGE LEADS

⑩ WIRE SUPPORT

⑪ PITOT TUBE, T.C. AND HOT WIRE PROBE TRAVERSING MECHANISM

⑫ CORE TUBE SUPPORT

⑬ VOLTAGE AND T.C. LEADS OUTLET

⑭ POWER LINE TERMINAL

⑮ HONEYCOMB

⑯ FLEXIBLE TUBE

⑰ FLOW CONTROL VALVE

⑱ BLOWER

FIG. 4.1 SCHEMATIC DIAGRAM OF HEAT EXCHANGER

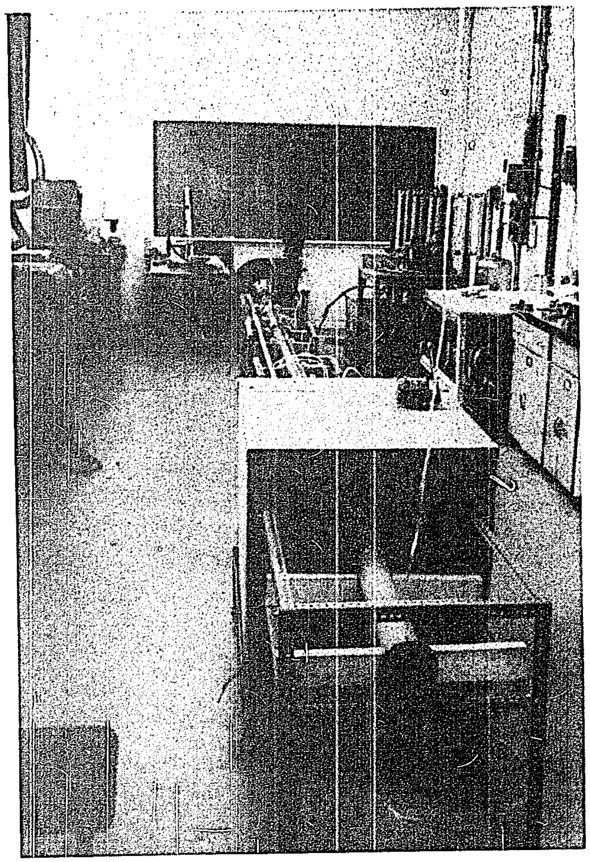

Fig.4.2.a Experimental Apparatus from Inlet End.

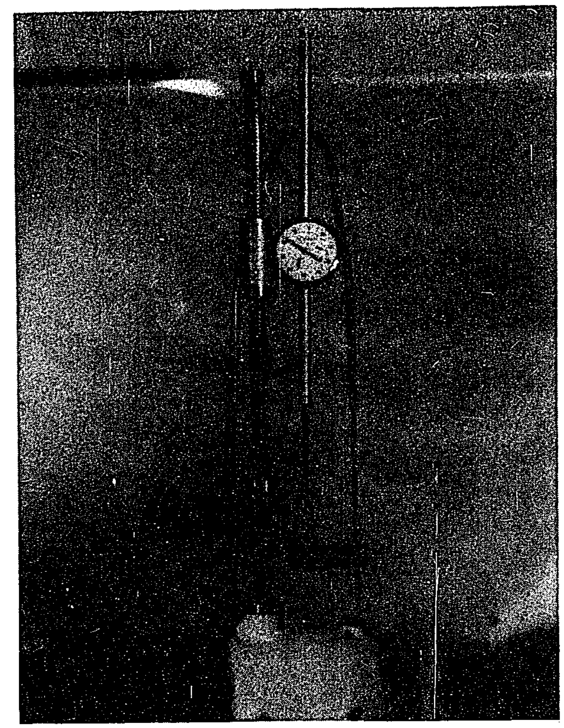

Fig.4.2.b Traversing Machanism with a Probe.

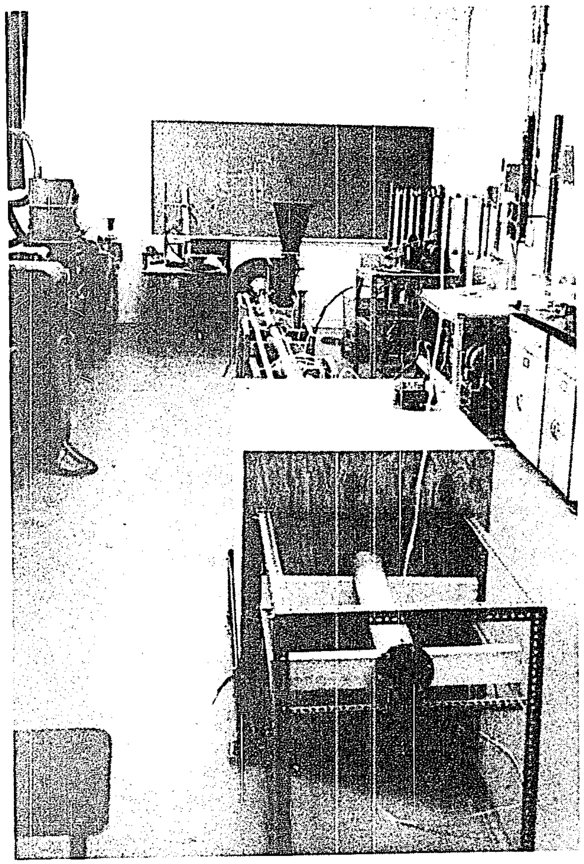

Fig.4.2.a Experimental Apparatus
from Inlet End.

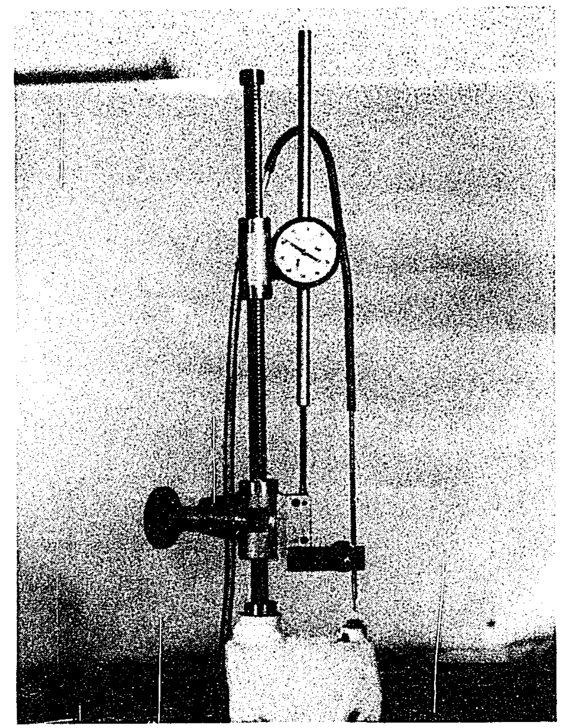

Fig.4.2.b Traversing Machanism
with a Probe.

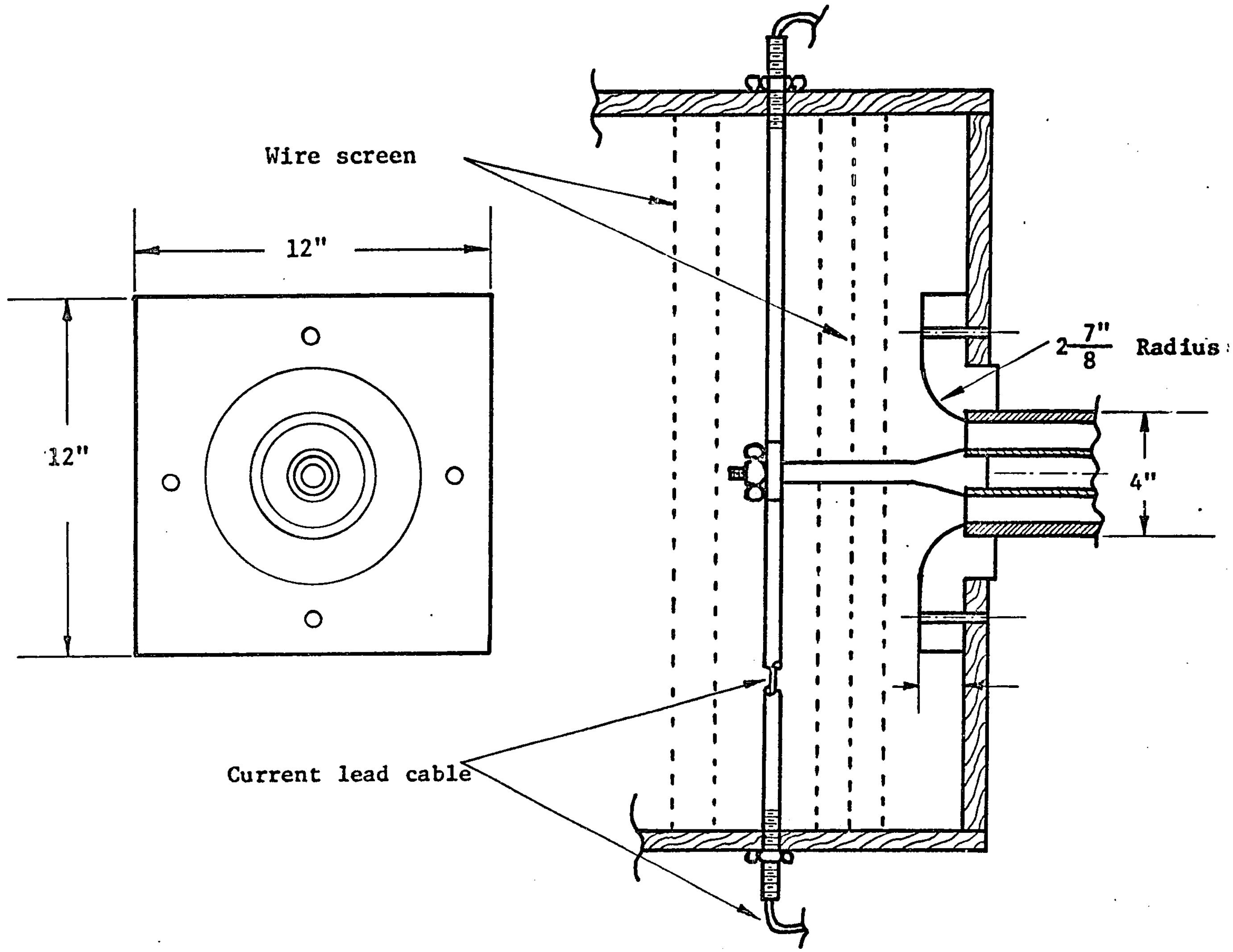

Fig. 4.3 Details of Annulus Entrance

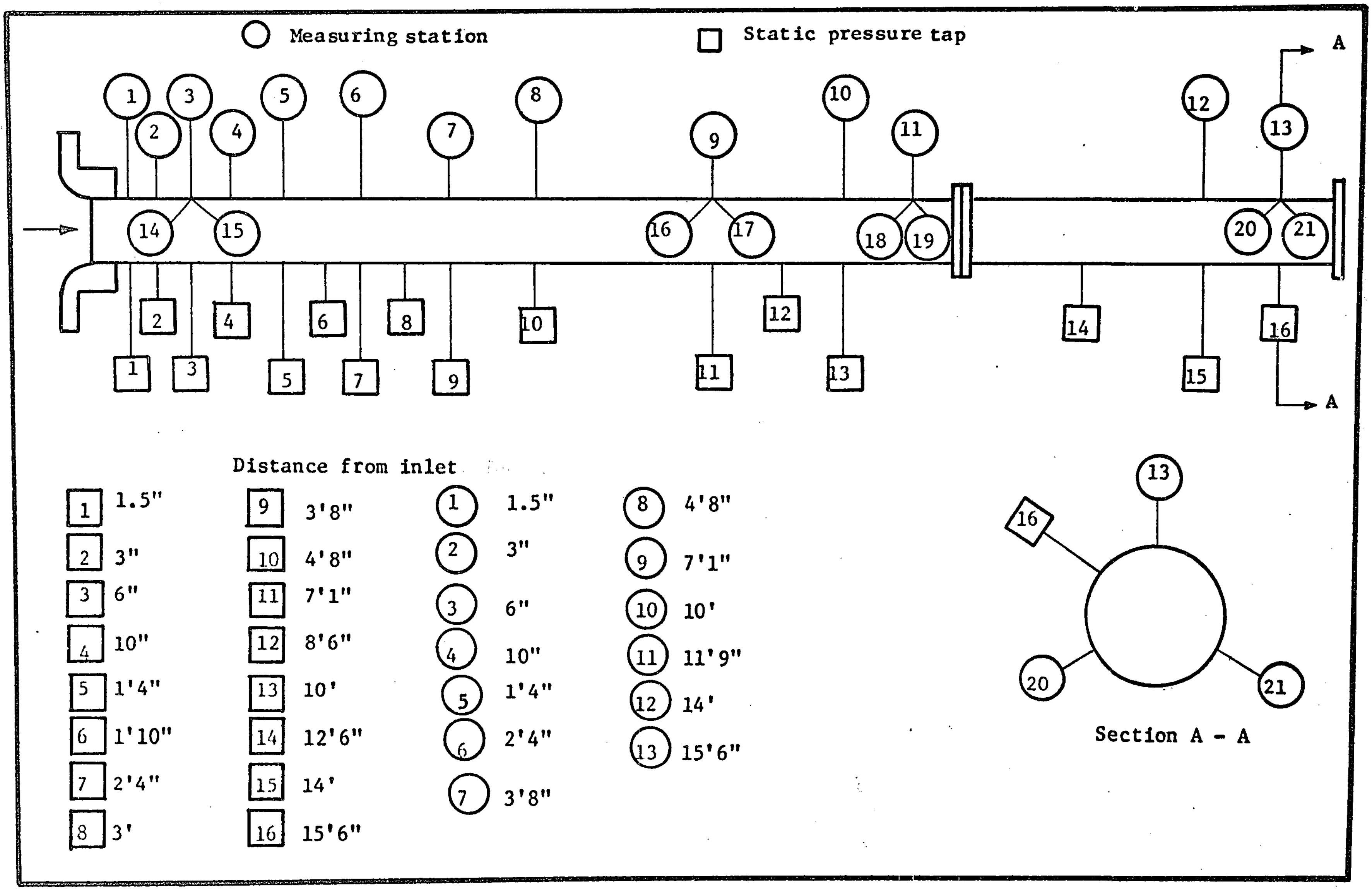

Fig. 4.4 Outer Tube Measuring Stations and Static Pressure Taps.

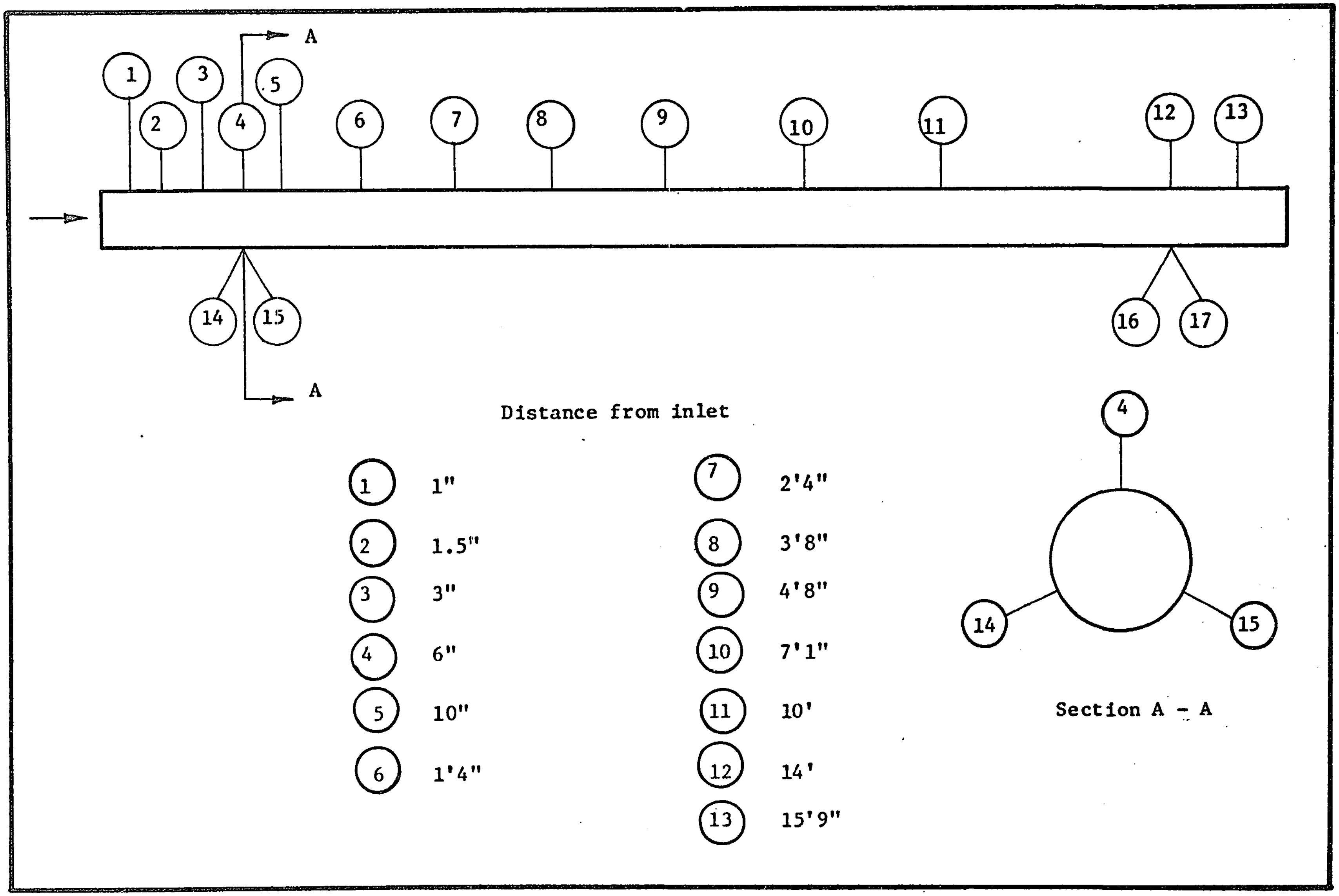

Fig. 4.5 Core Tube Thermocouple Locations. for $\alpha = 1.61$, 2.31 and 3.83

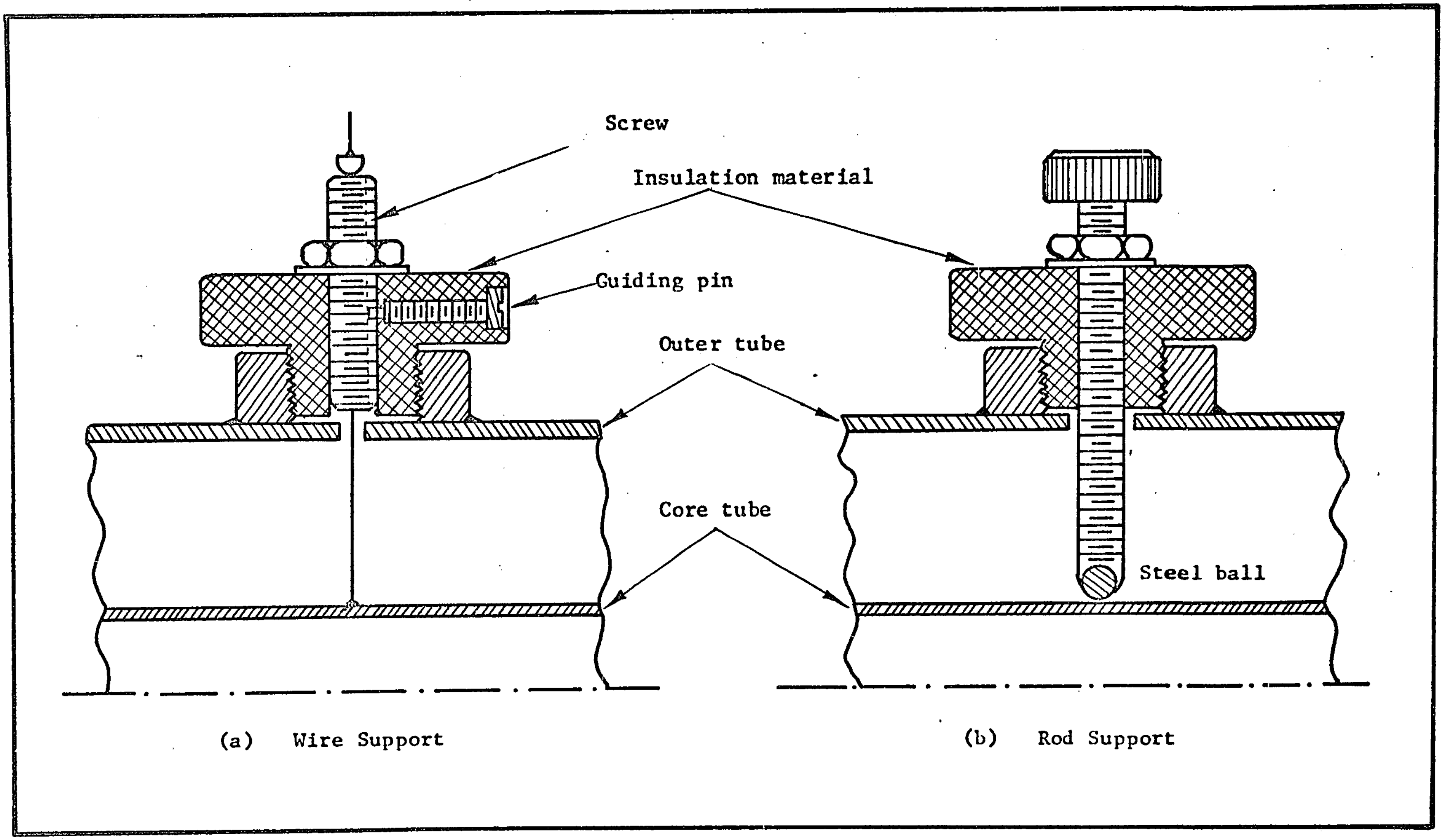

Fig. 4.6 Details of Core Tube Support.

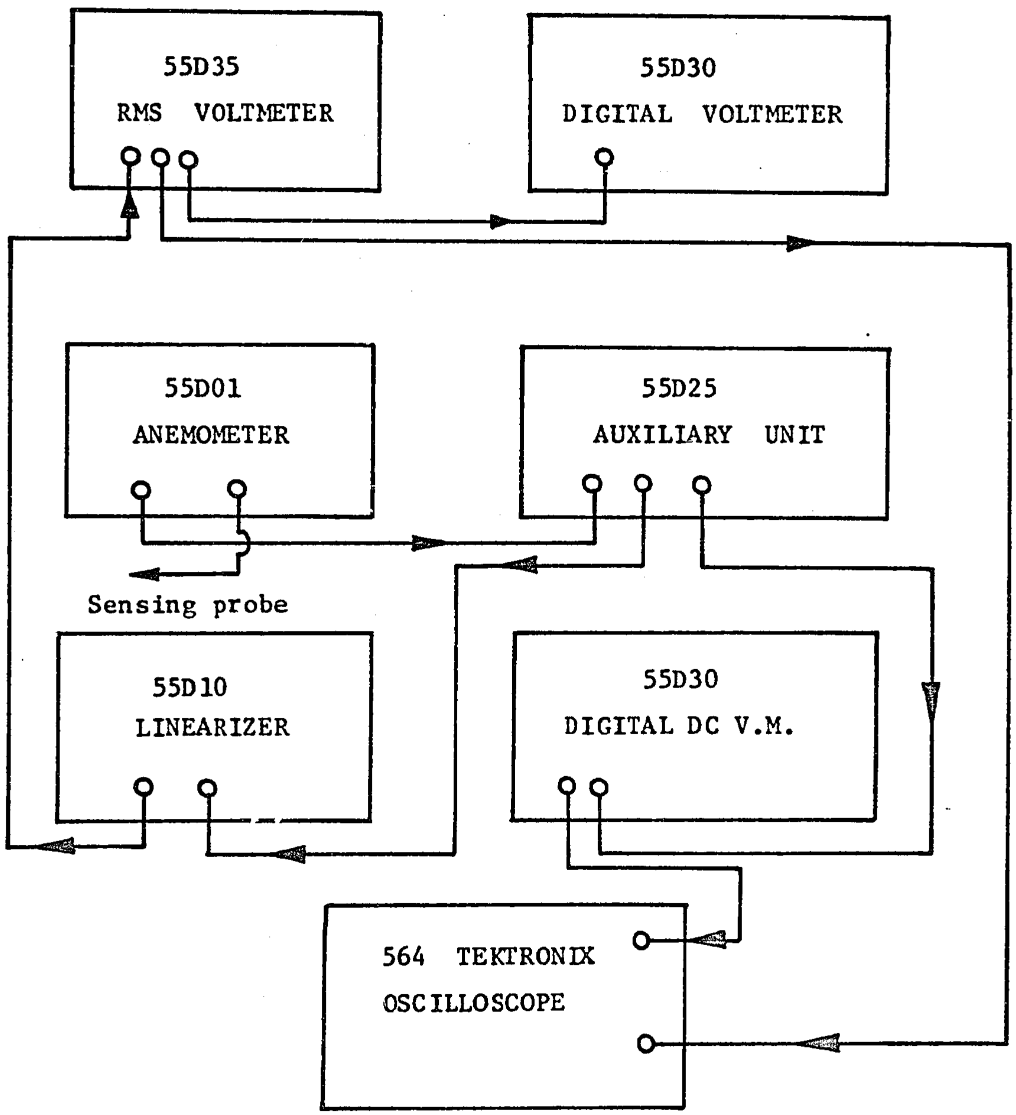

Fig. 4.7 Hot-wire Anemometry System.

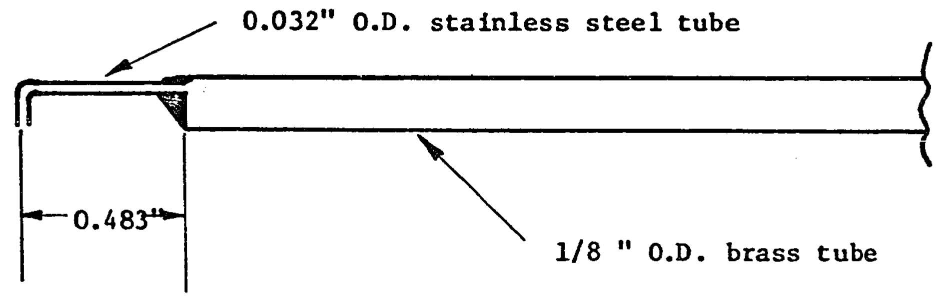

Fig. 4.8 (a) Details of Total Pressure Probe

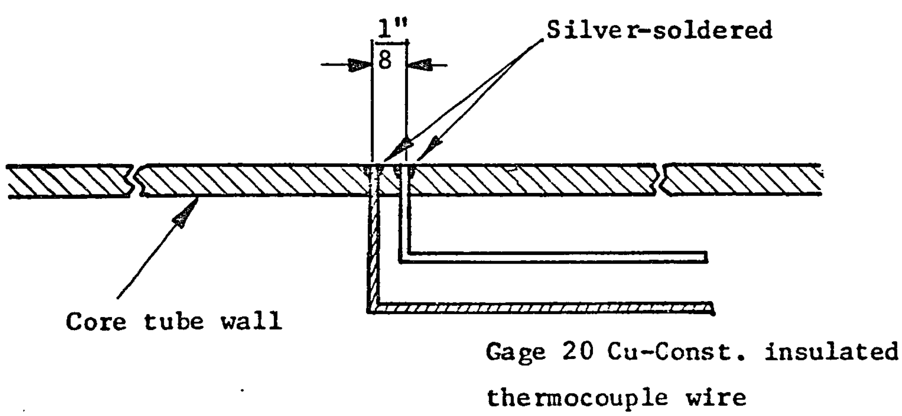

Fig. 4.8 (b) Details of Wall Thermocouple.

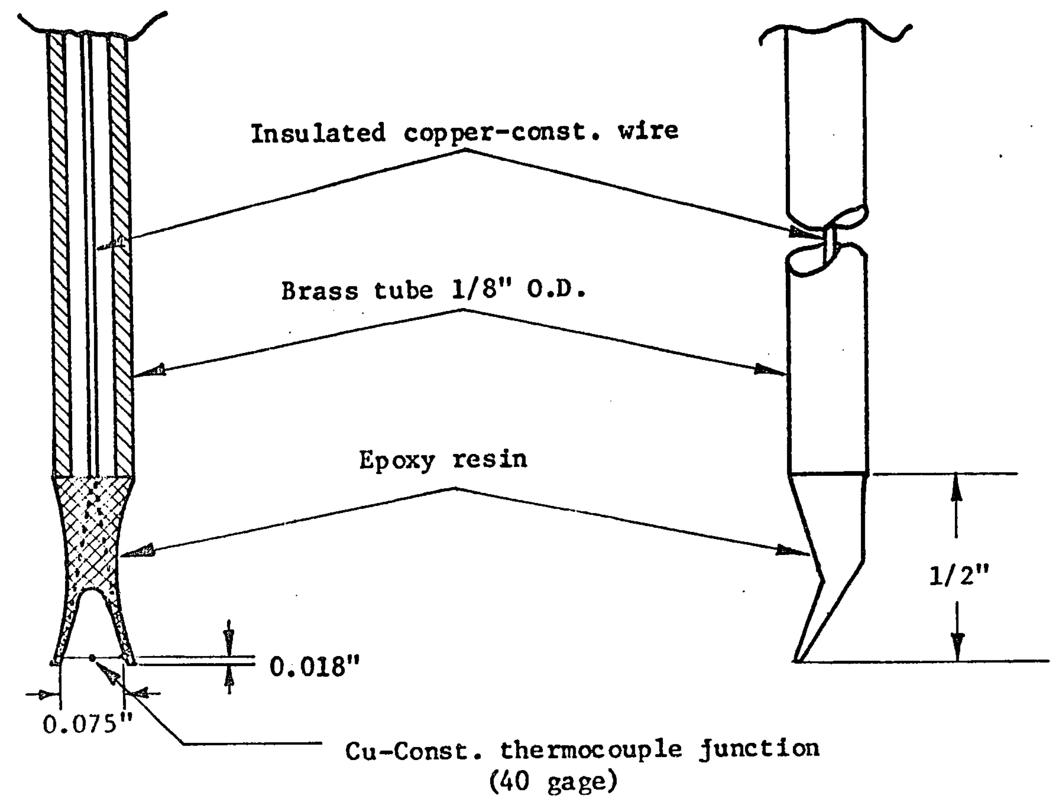

Fig. 4.9 Detailed Diagram of Traversing Thermocouple Probe.

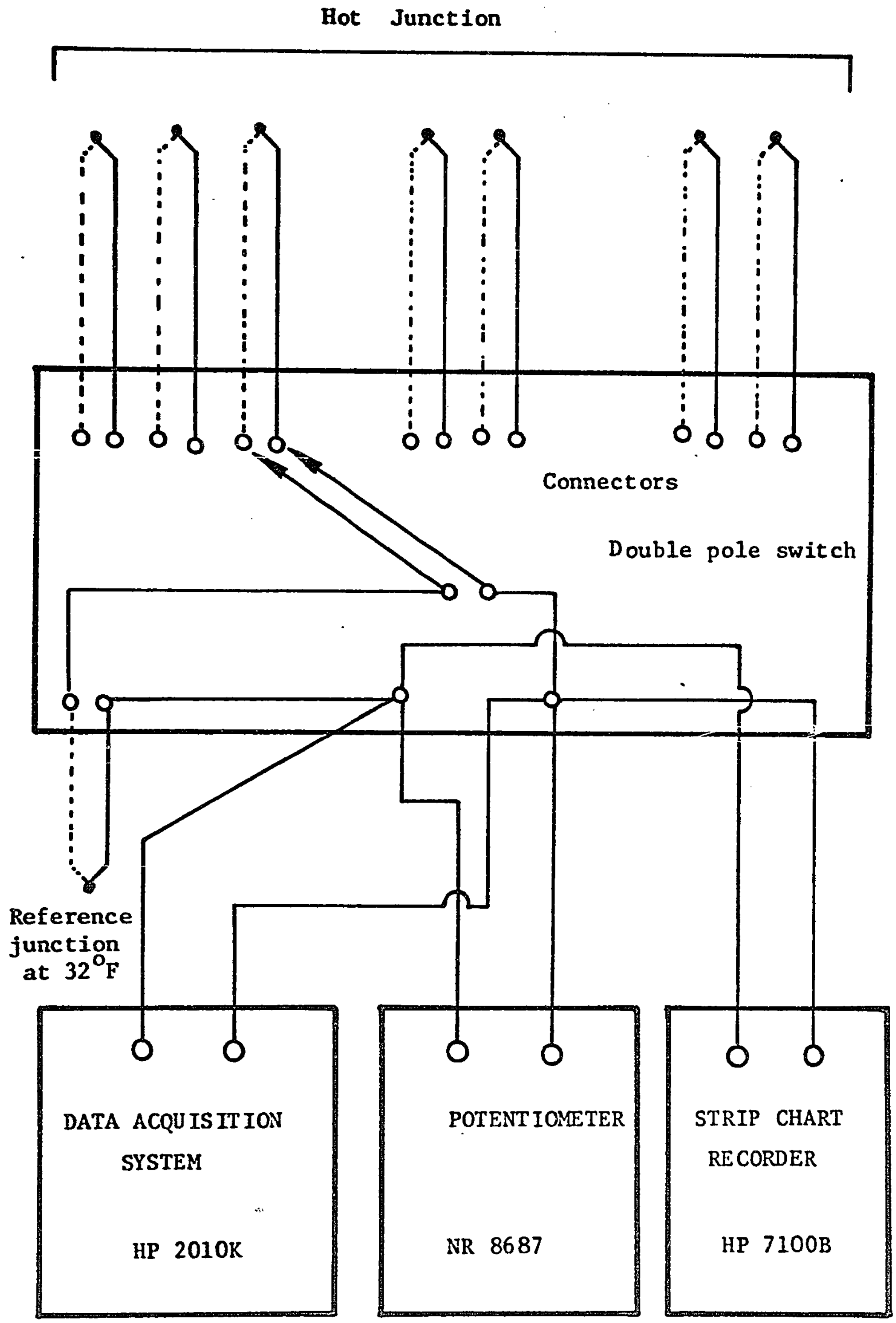

Fig. 4.10 Thermocouple Circuit.

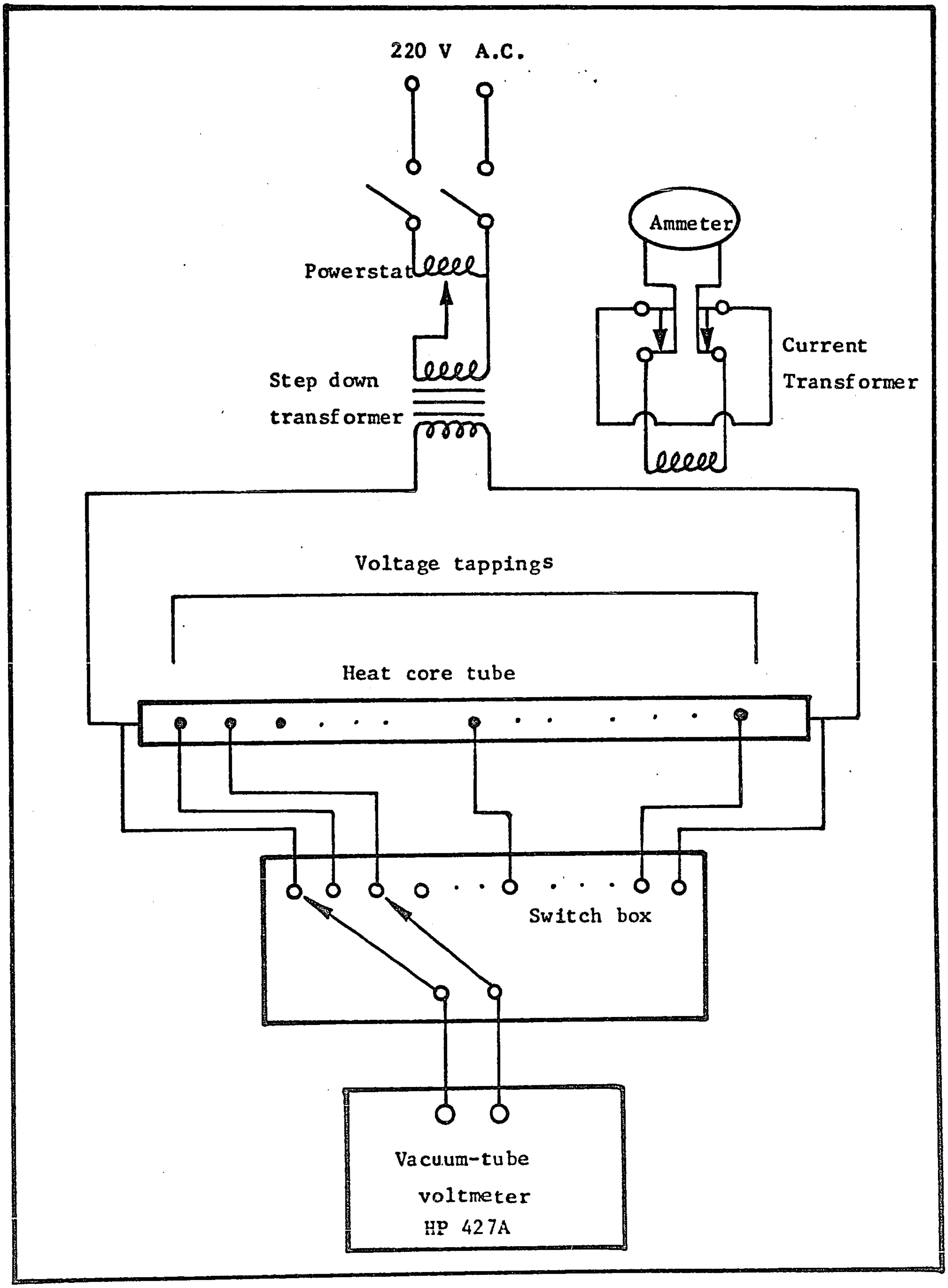

Fig. 4.11 Power Supply and Instrumentation Circuit.

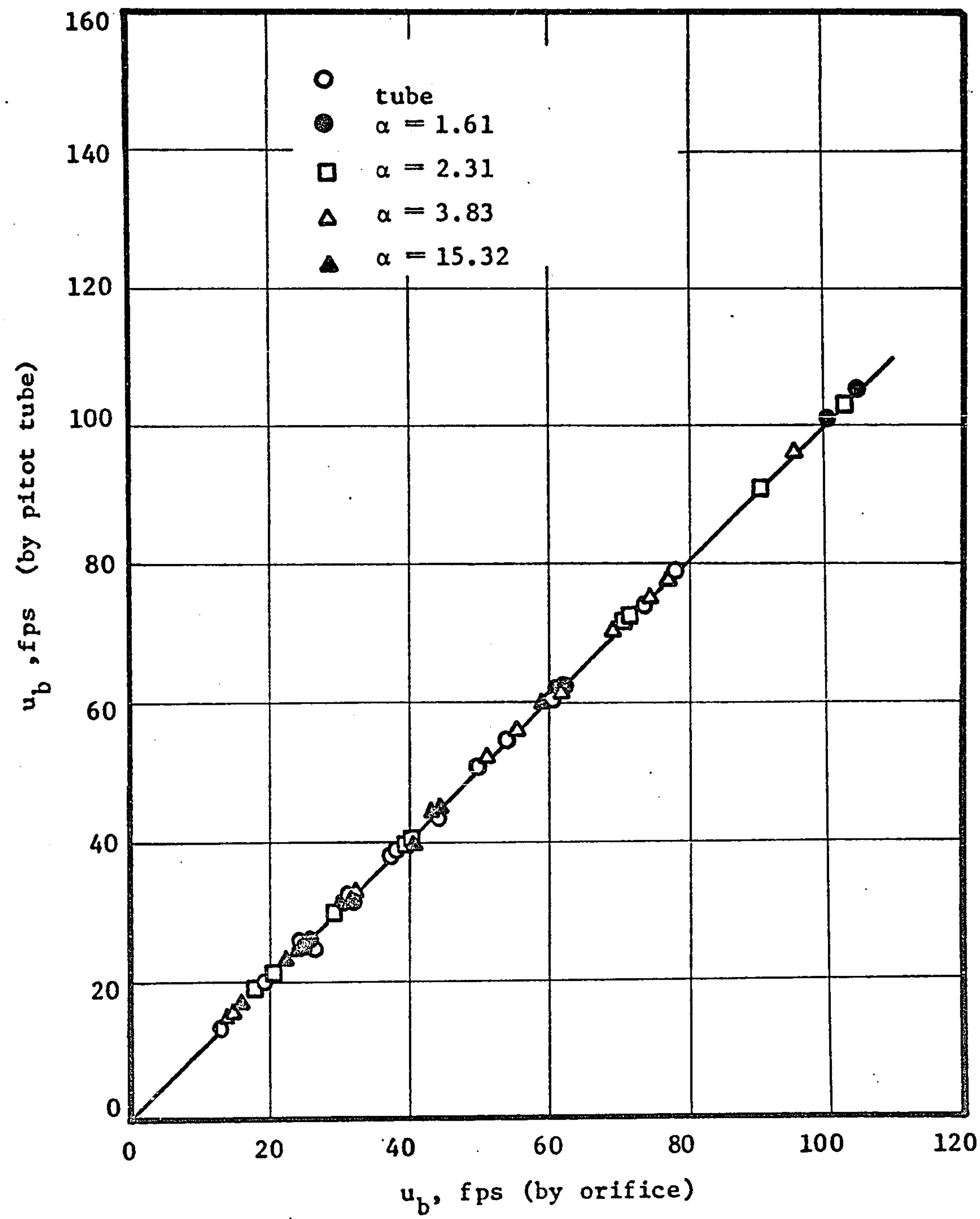

Fig. 4.12 Calibration Curve of Orifice.

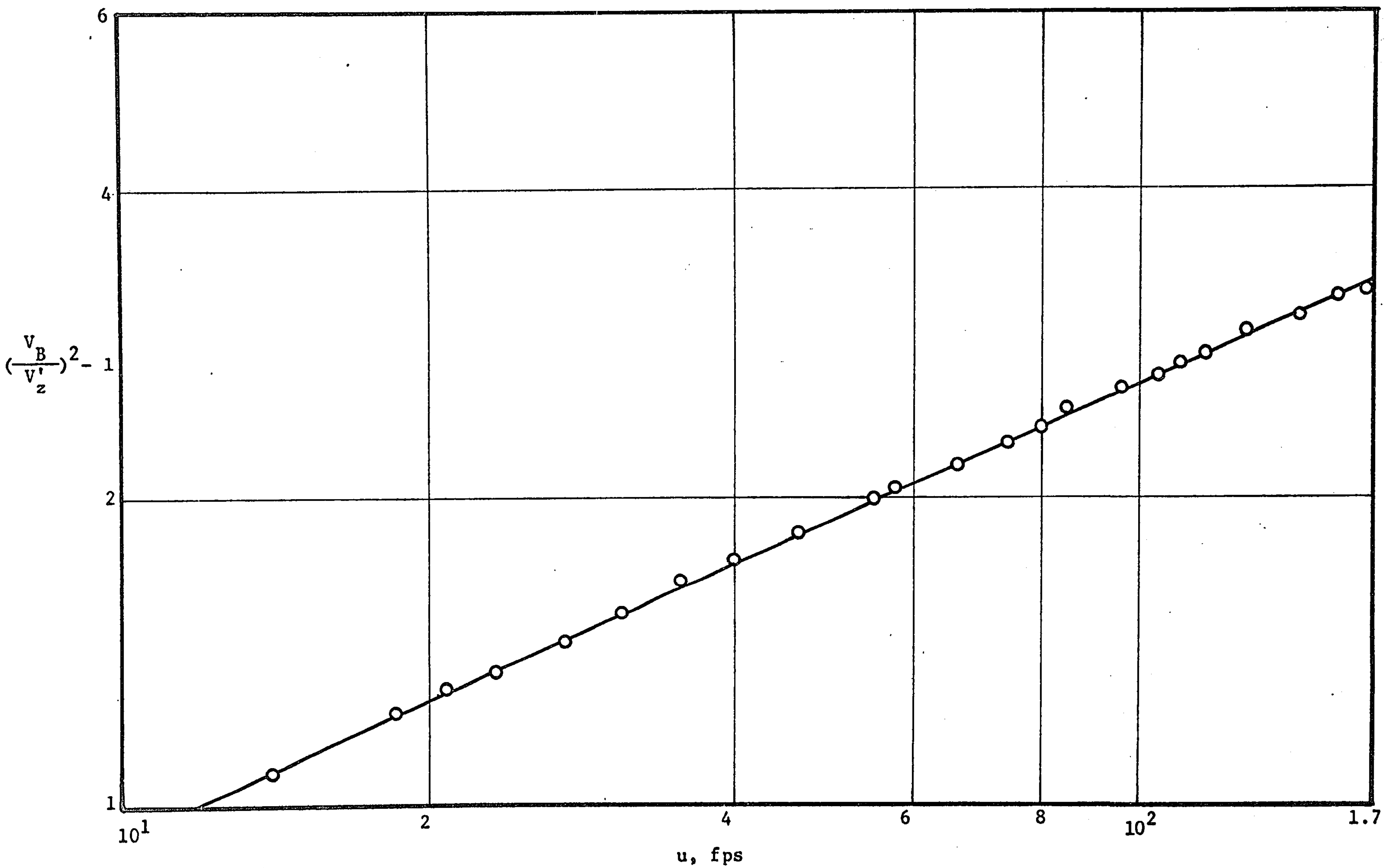

Fig. 4.13 Calibration Curve of a Hot-wire Probe (without Linearizer)

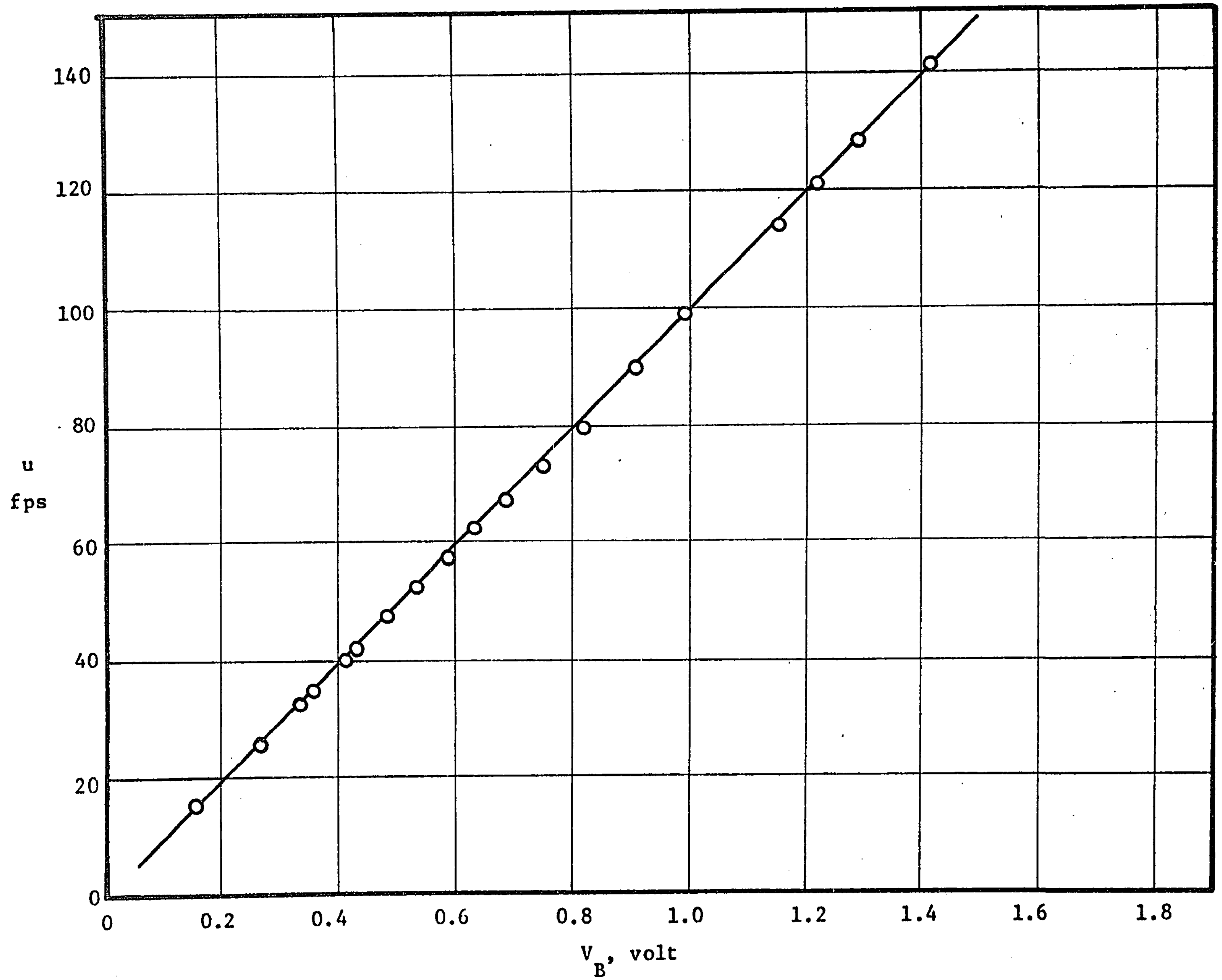

Fig. 4.14 Calibration Curve of a Hot-wire Probe (with a Linearizer)

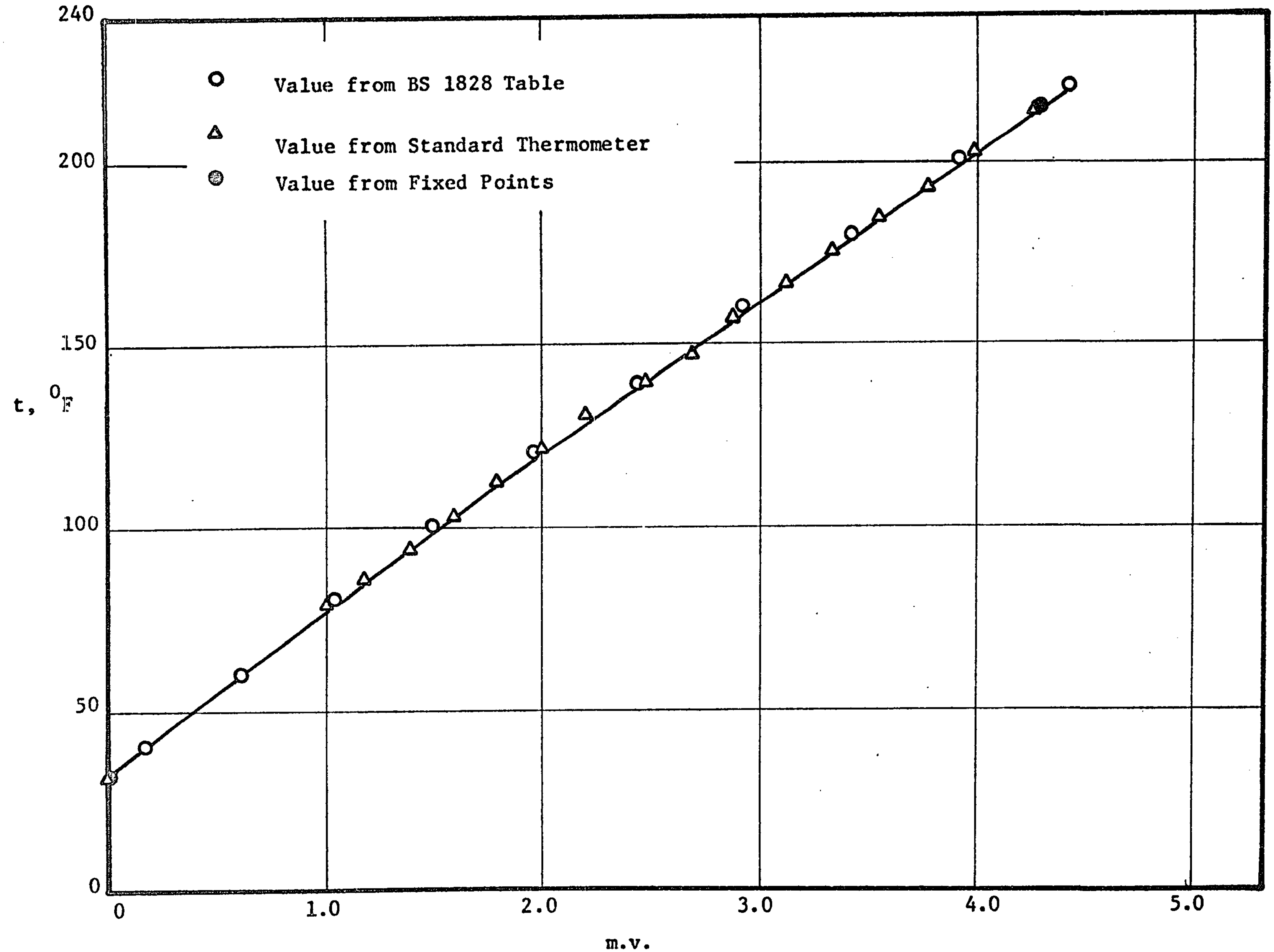

Fig. 4.15 Calibration Curve of Thermocouple.

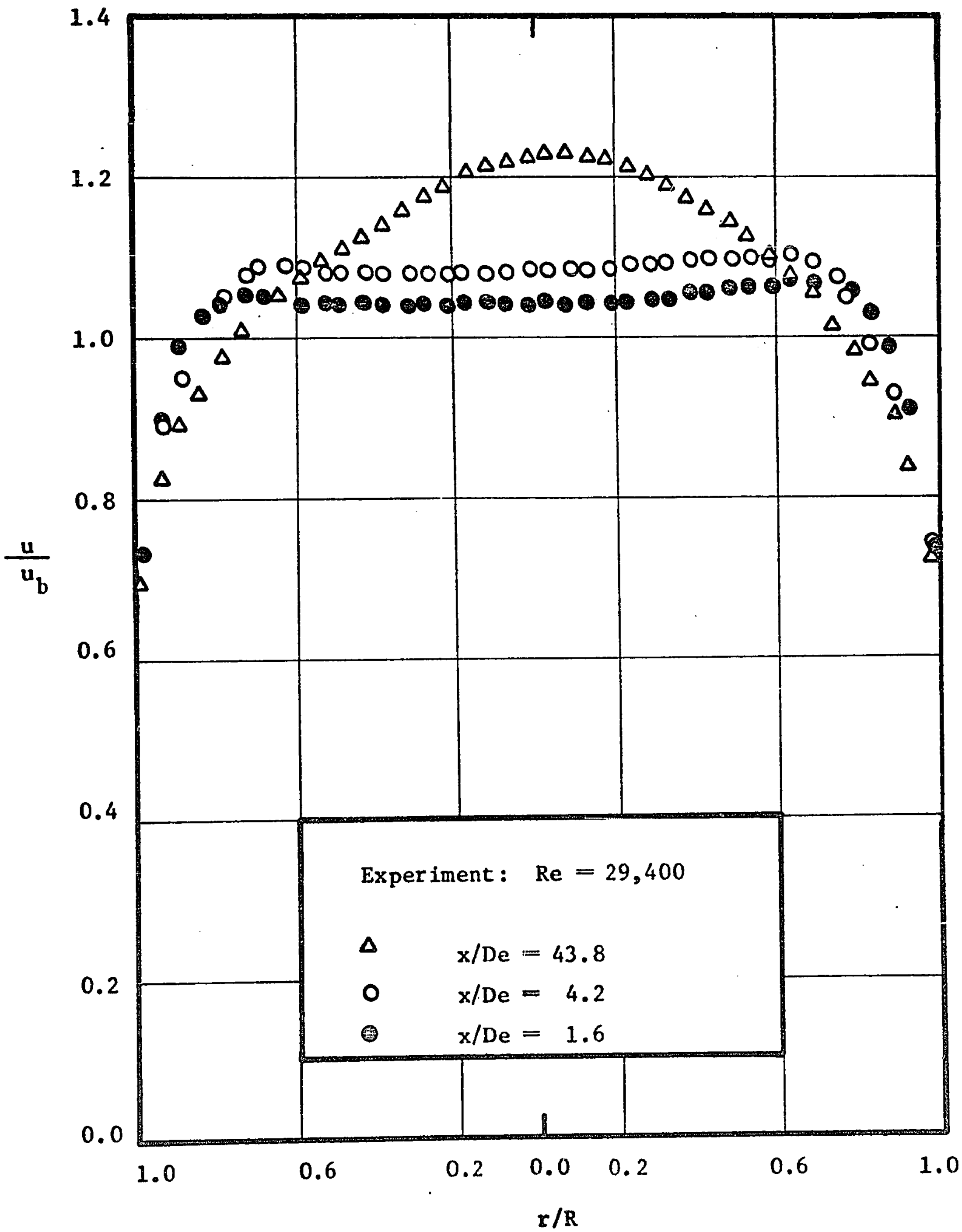

Fig. 5.1 Experimental Velocity Profiles, Circular Tube.

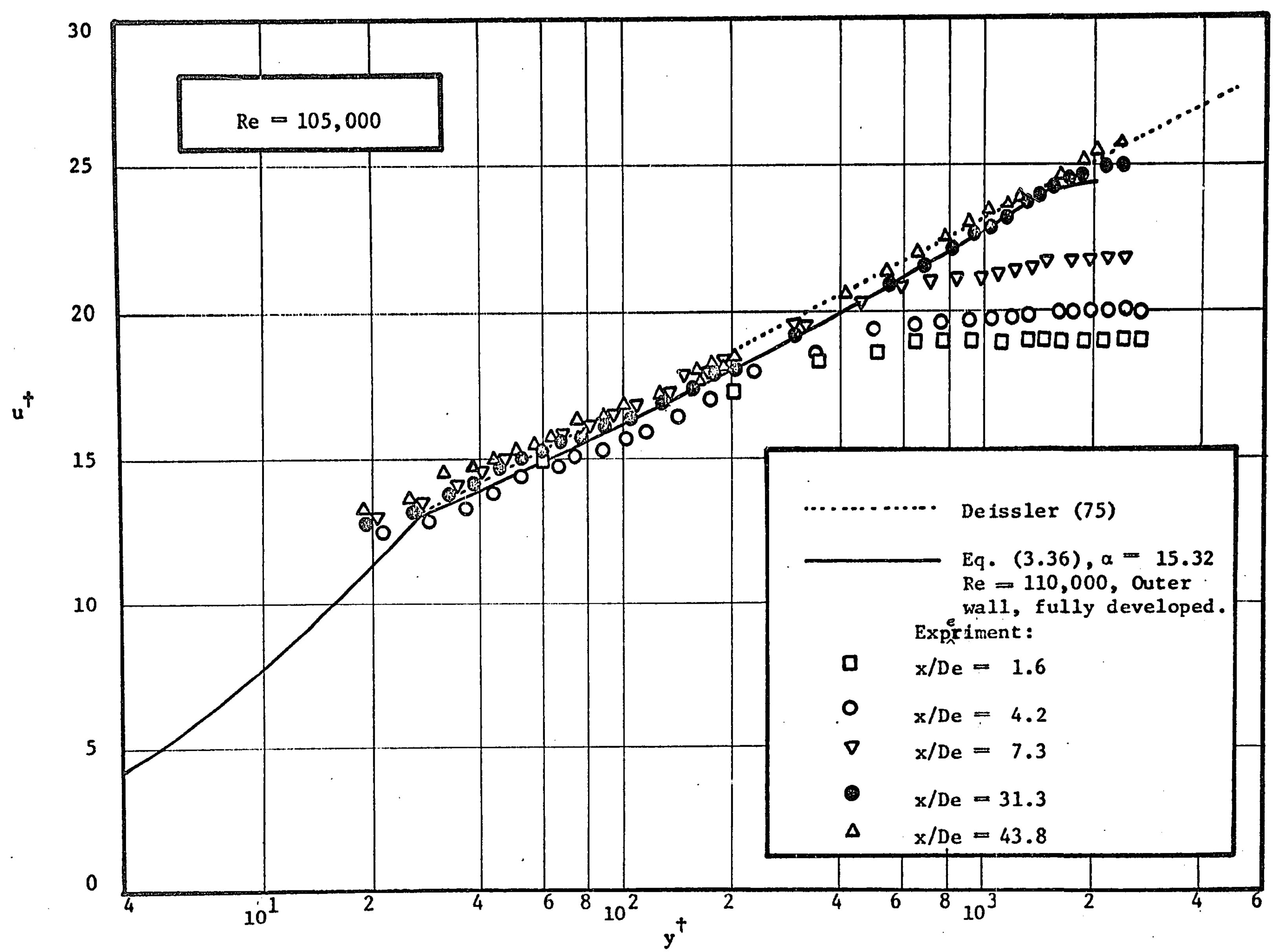

Fig. 5.2 Non-Dimensional Velocity Profiles, Entrance Region, Circular Tube.

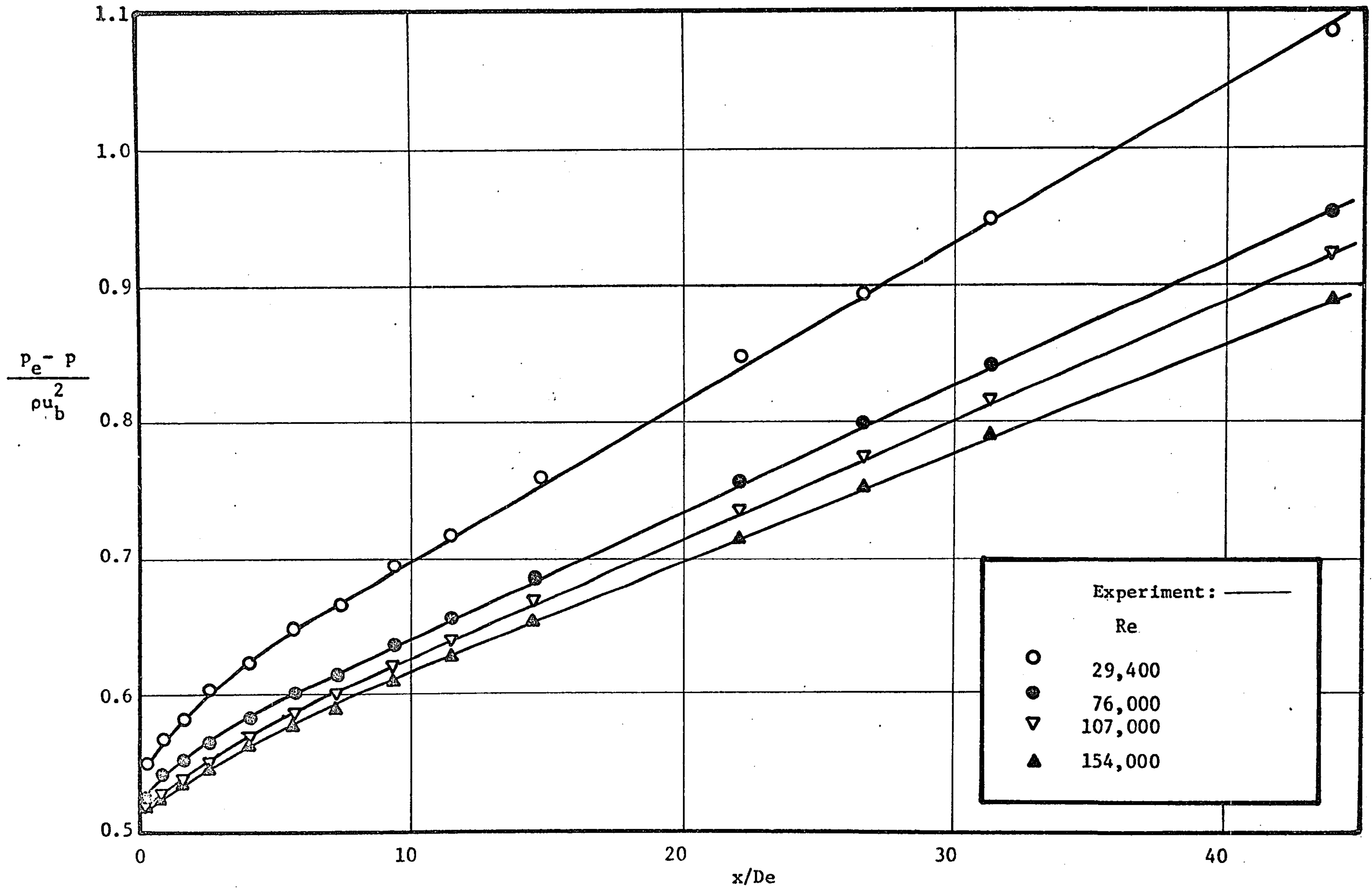

Fig. 5.3 Variation of Static Pressure along Circular Tube, Entrance Region.

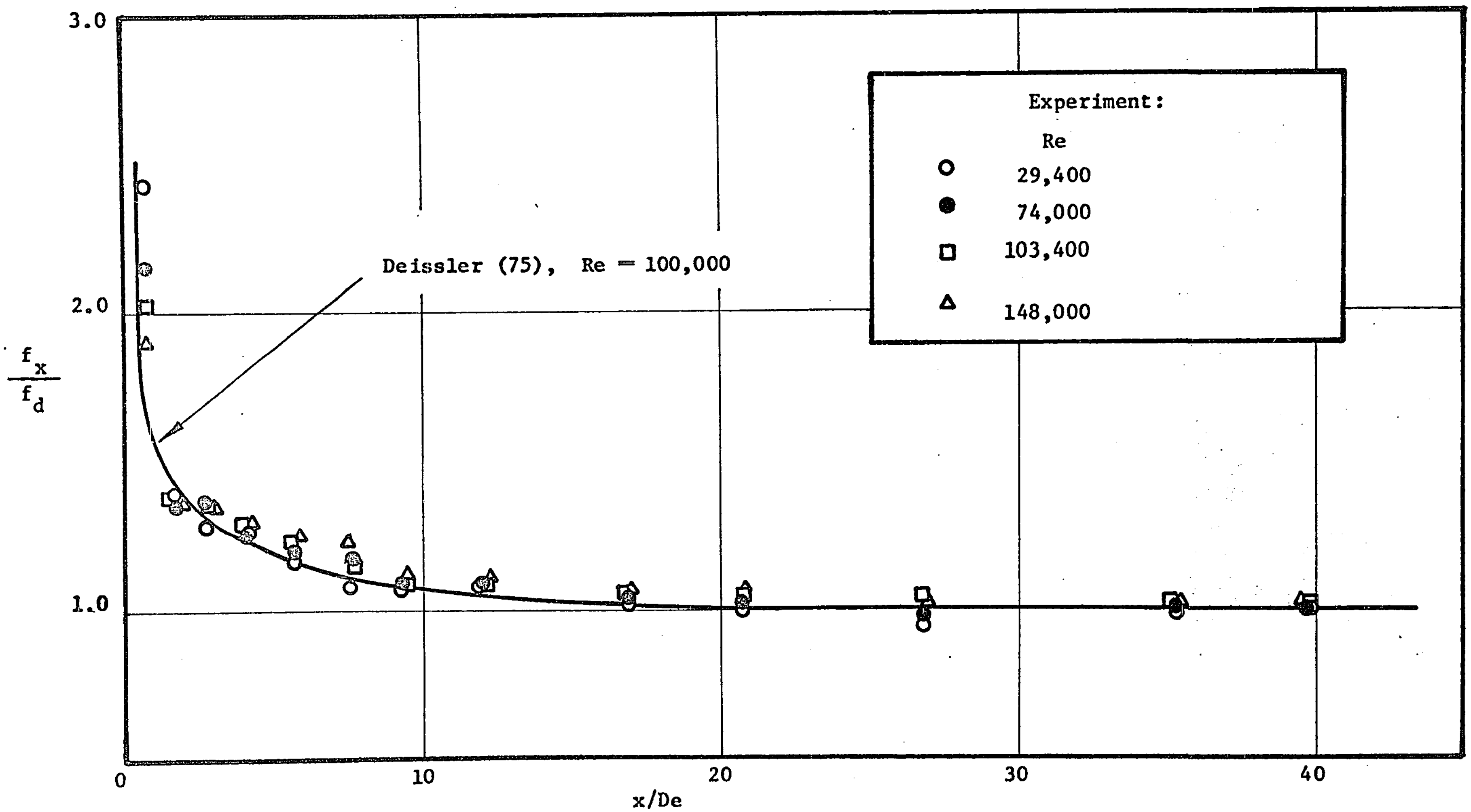

Fig. 5.4 Comparison of Experimental Friction Factors with Deissler's Prediction, Circular Tube,(with Trip Wire)

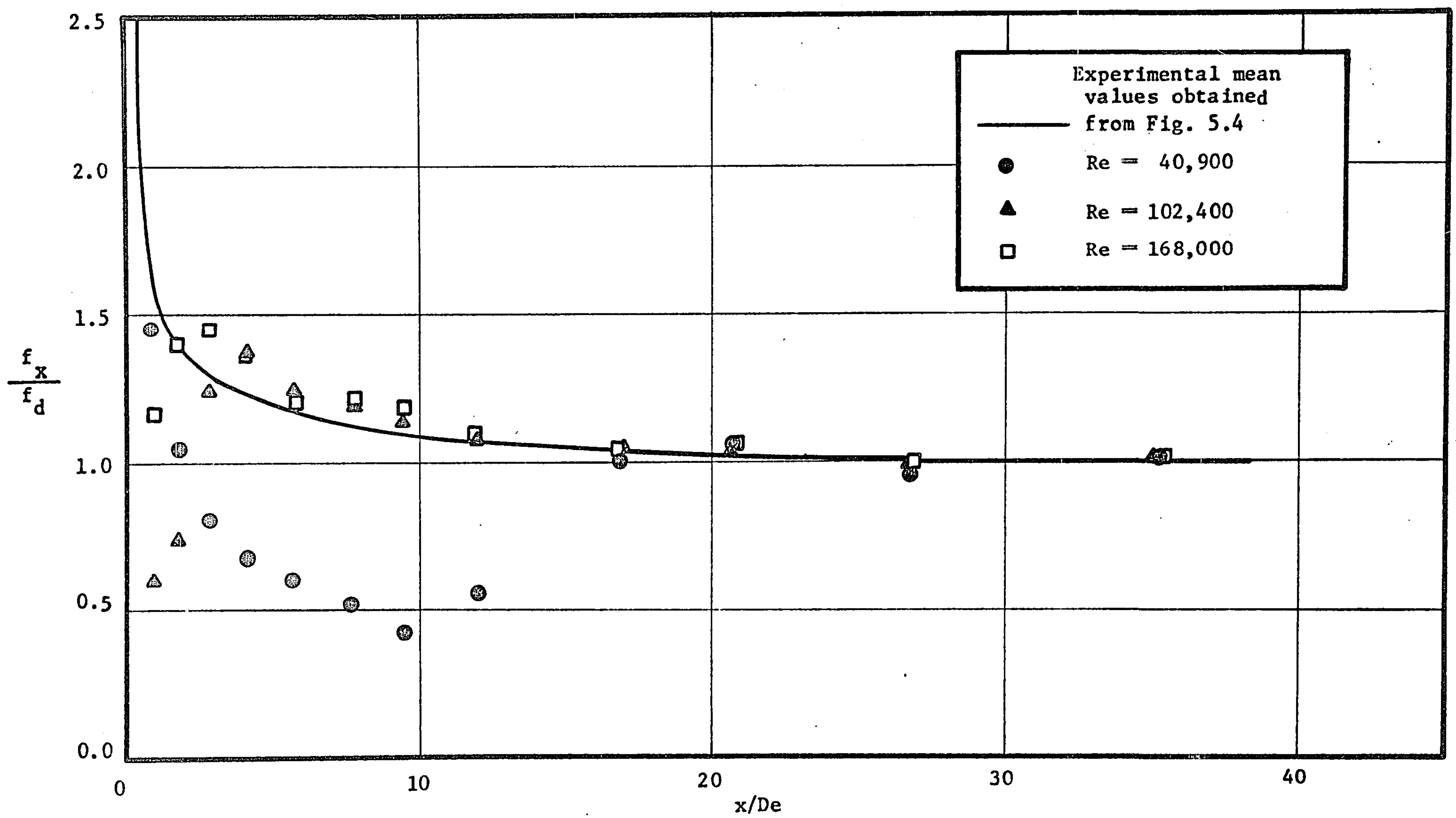

Fig. 5.5 Experimental Friction Factors, Circular Tube, (without Trip Wire)

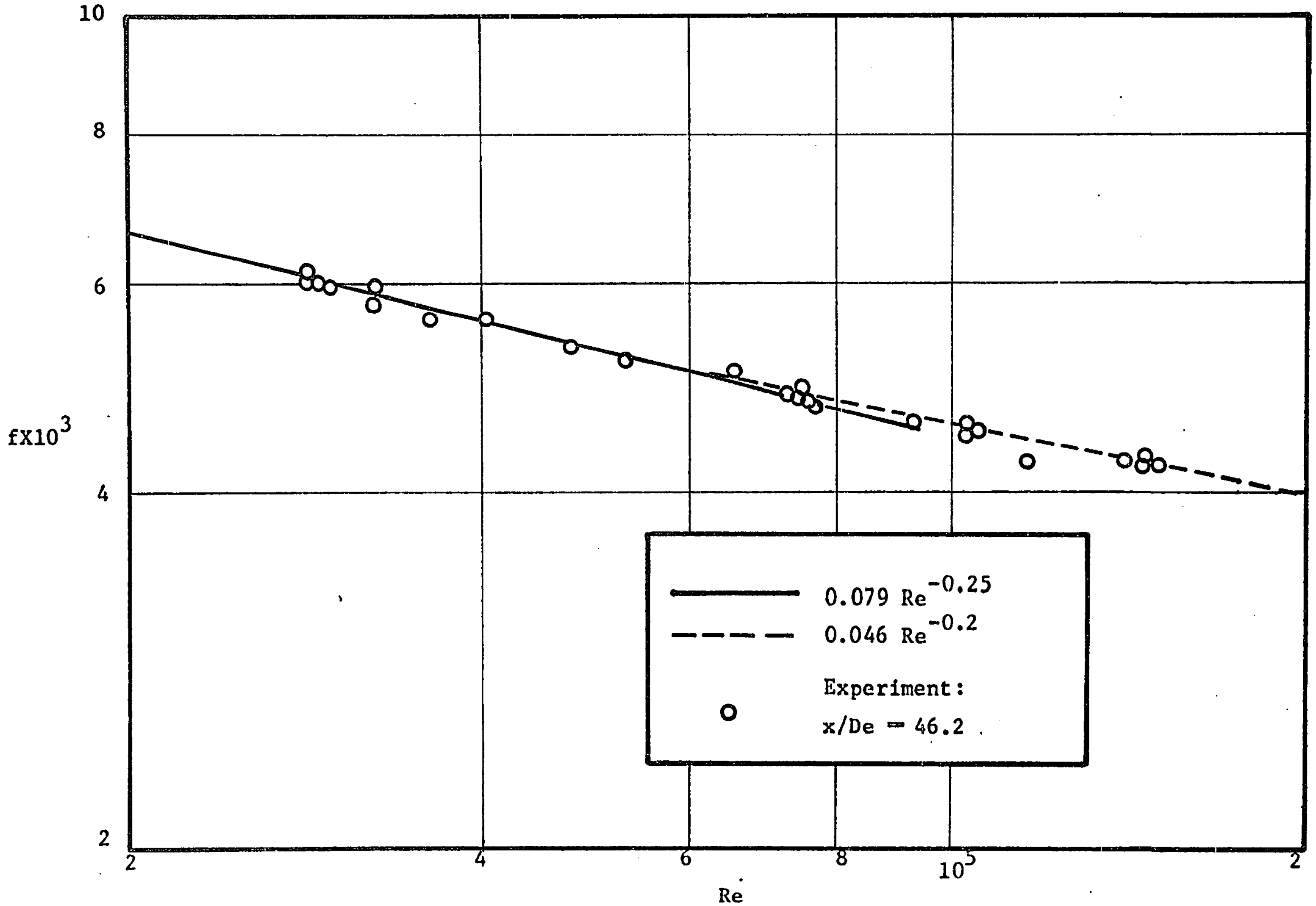

Fig. 5.6 Comparison of Experimental Friction Factors with Previous Correlations, Circular Tube, Fully Developed Flow.

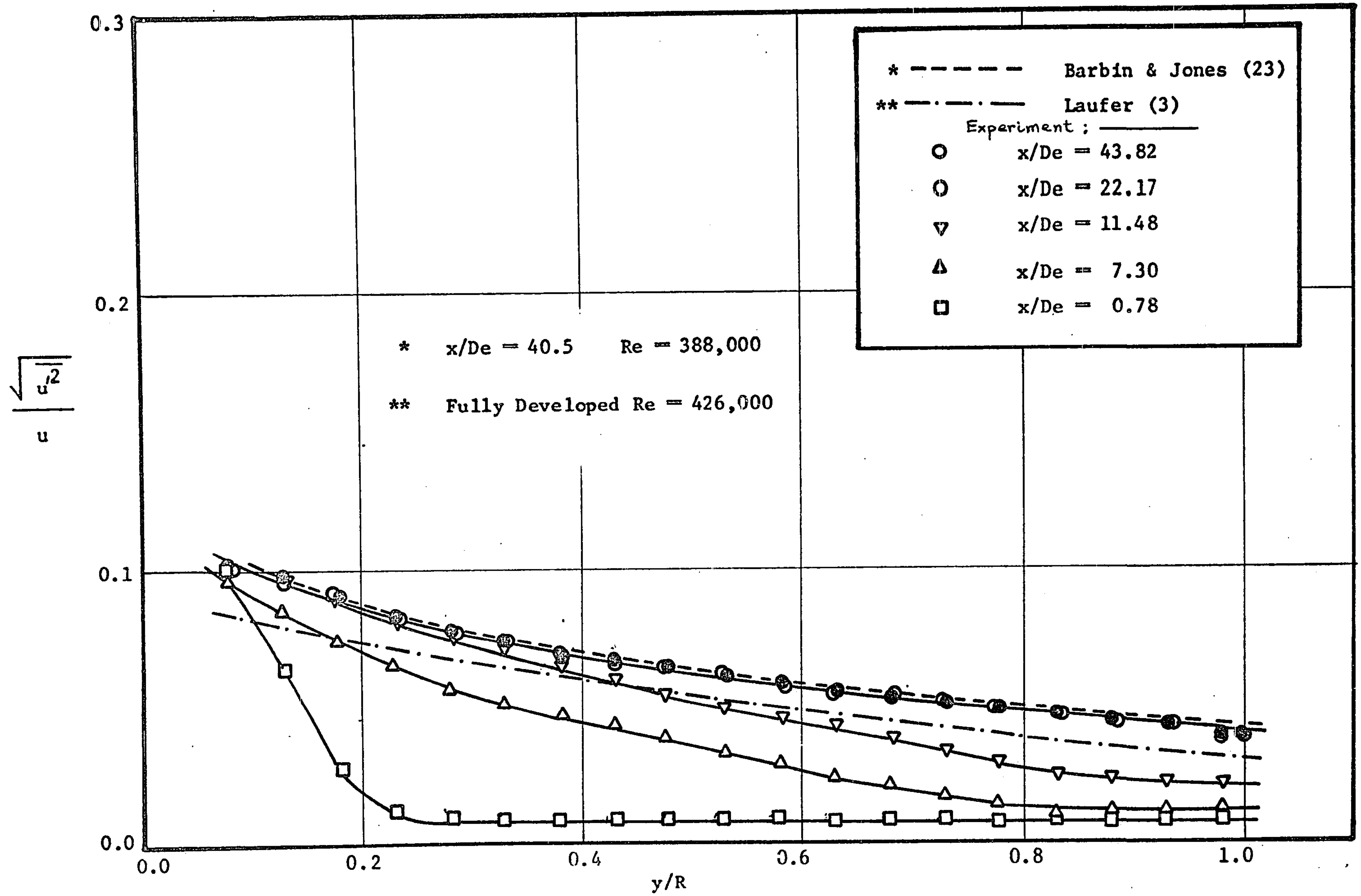

Fig. 5.7 Axial Turbulence Intensities, Circular Tube, Re = 130,000.

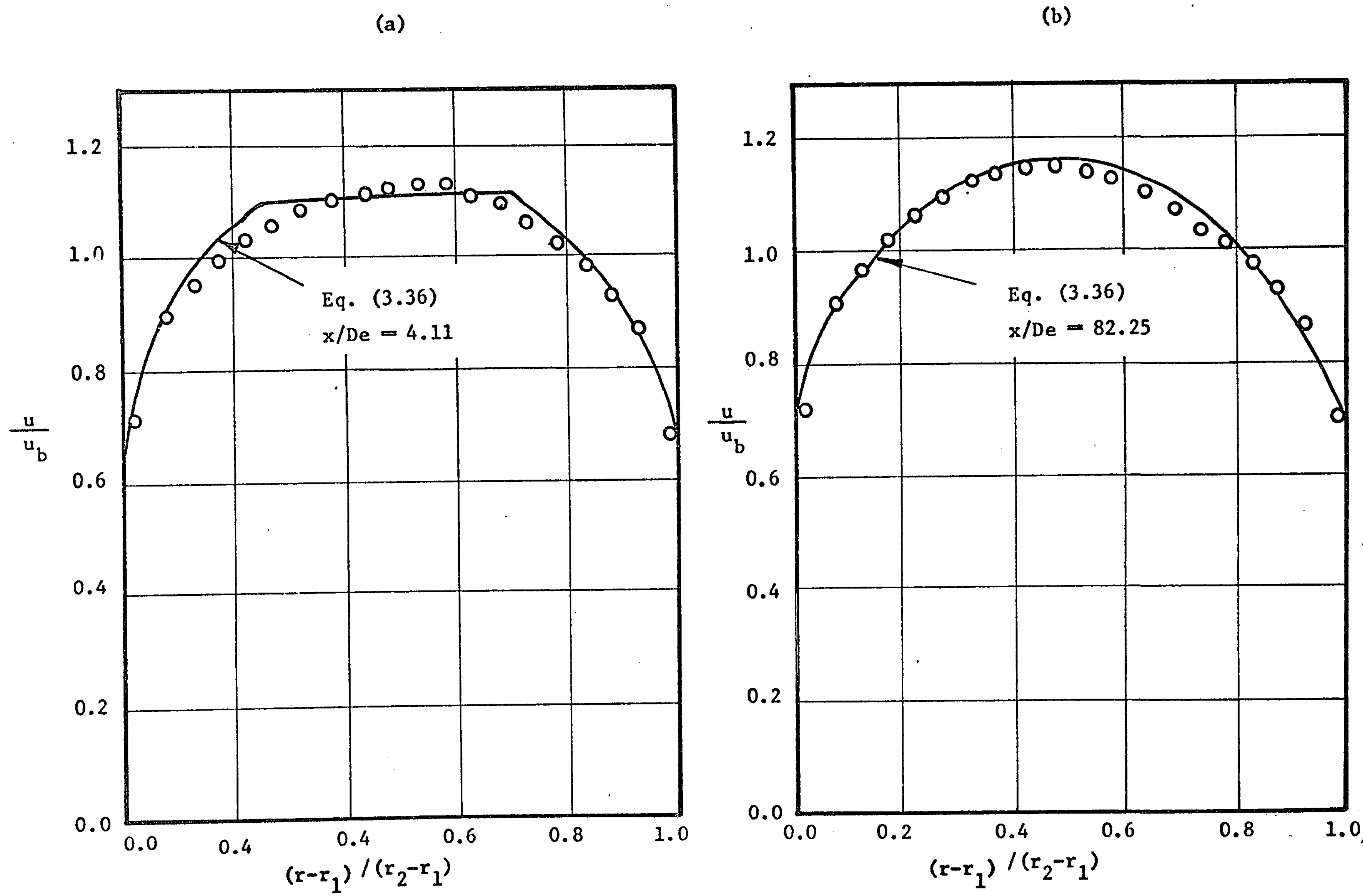

Fig, 5.8 Comparison Between Prediction and Experiment for Velocity Profile, $\alpha = 1.61$, $Re = 23,000$.

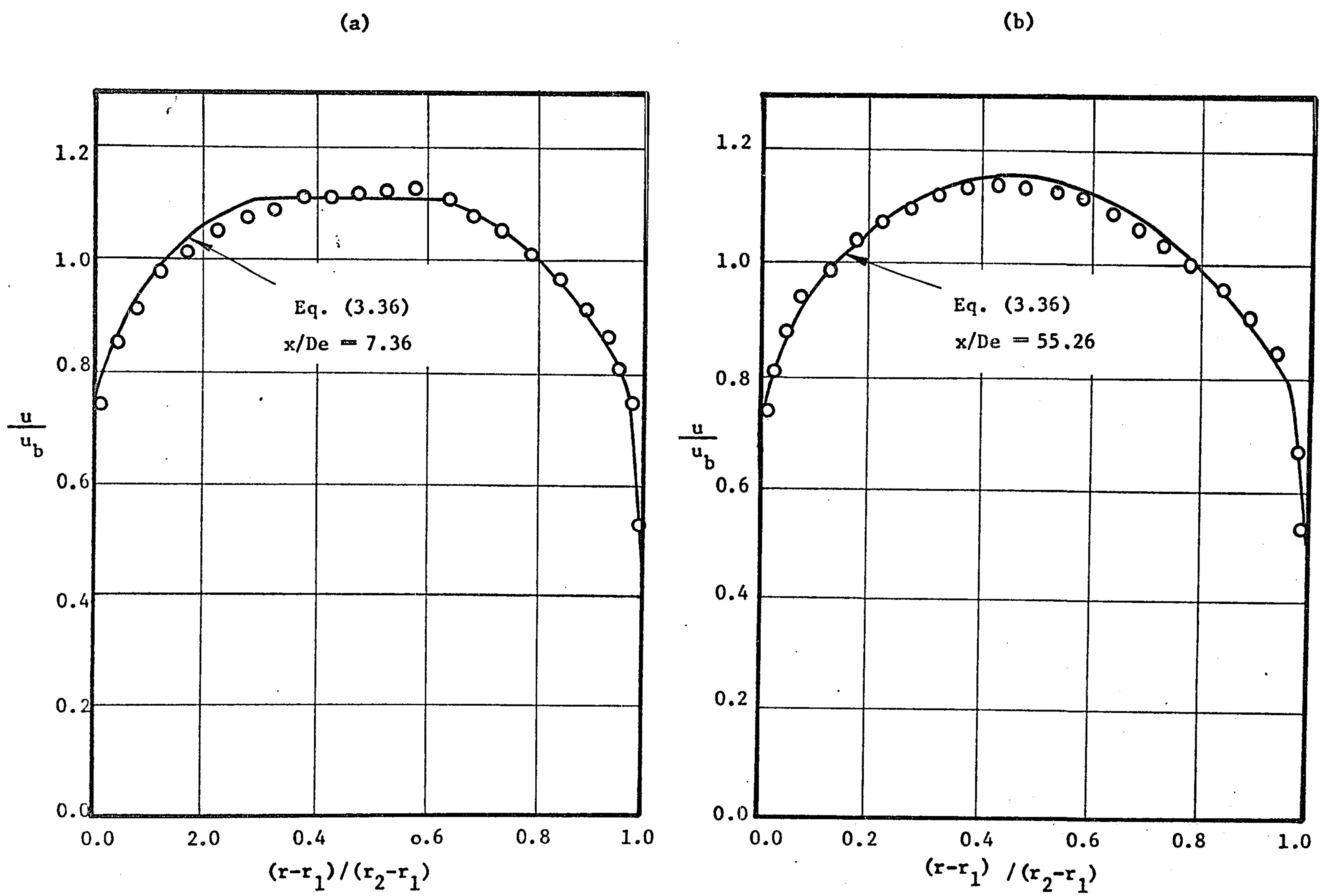

Fig. 5.9 Comparison Between Prediction and Experiment, $\alpha = 2.31$, Re = 23,000 .

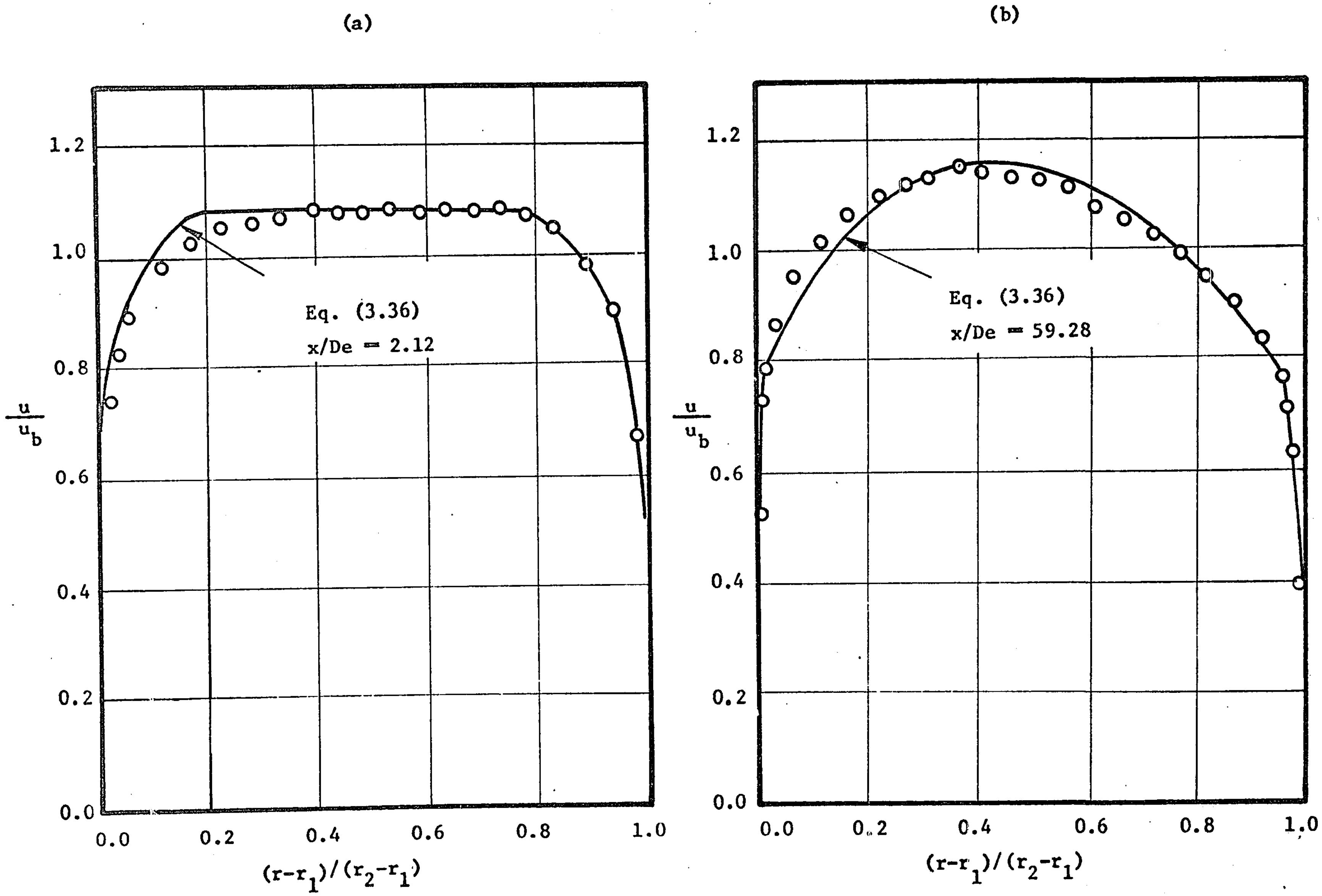

Fig. 5.10 Comparison Between Prediction and Experiment, $\alpha = 3.83$, $Re = 23{,}000$.

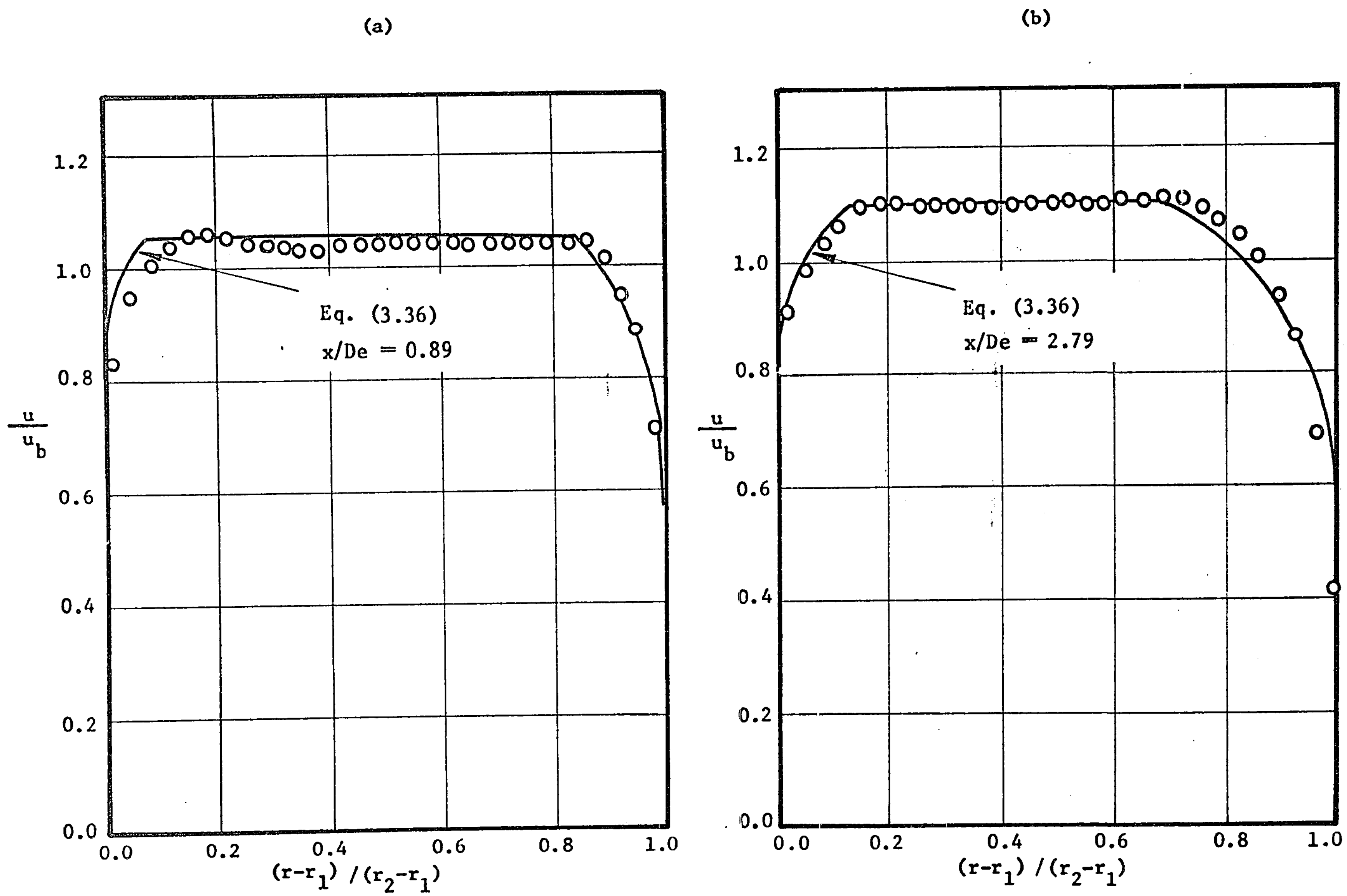

Fig. 5.11 Comparison Between Prediction and Experiment for Velocity Profile, $\alpha = 15.32$, $Re = 44{,}000$.

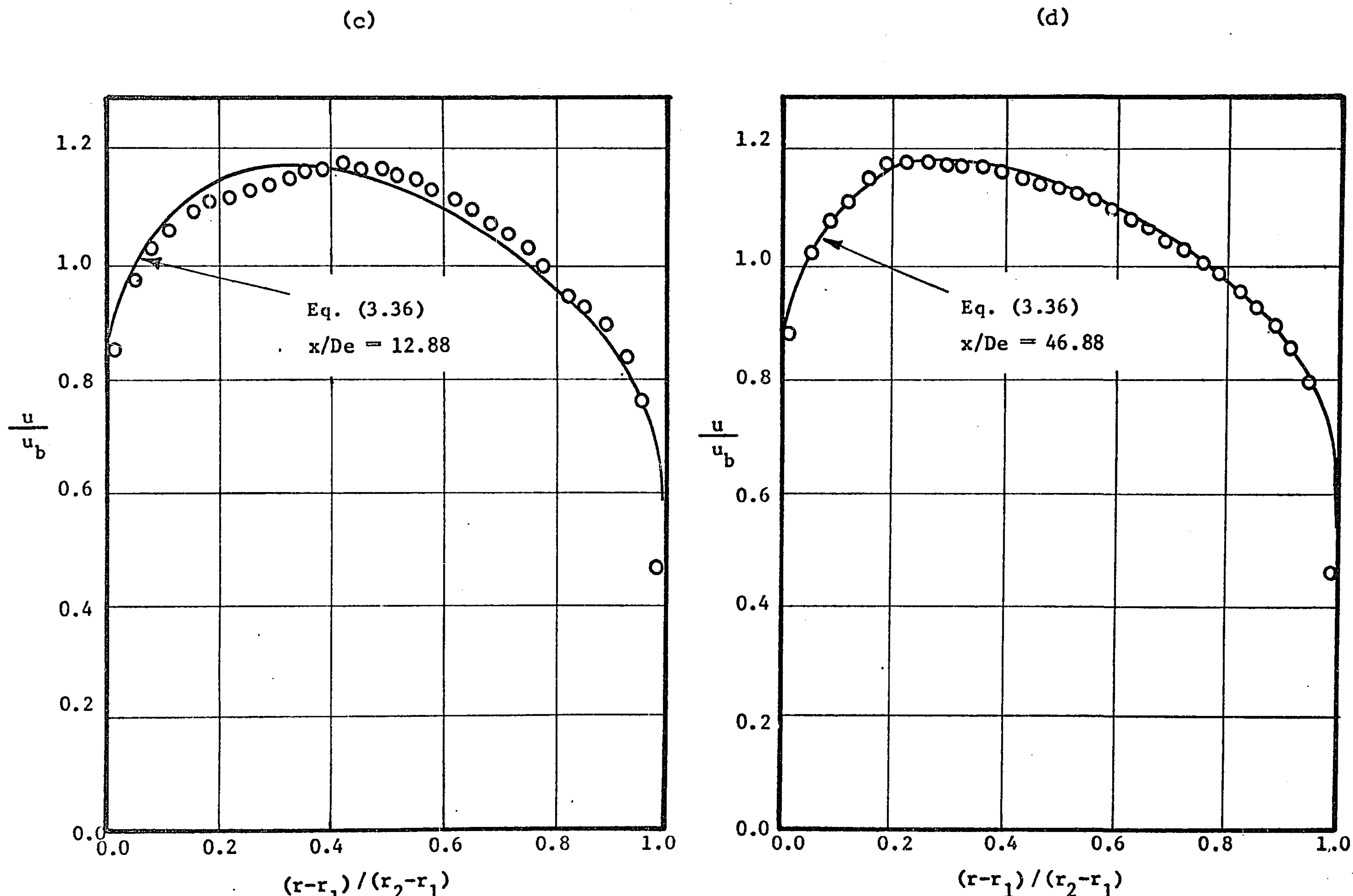

Fig. 5.11 Comparison Between Prediction & Experiment for Velocity Profile, $\alpha = 15.32$, Re = 44,000 .
(continued)

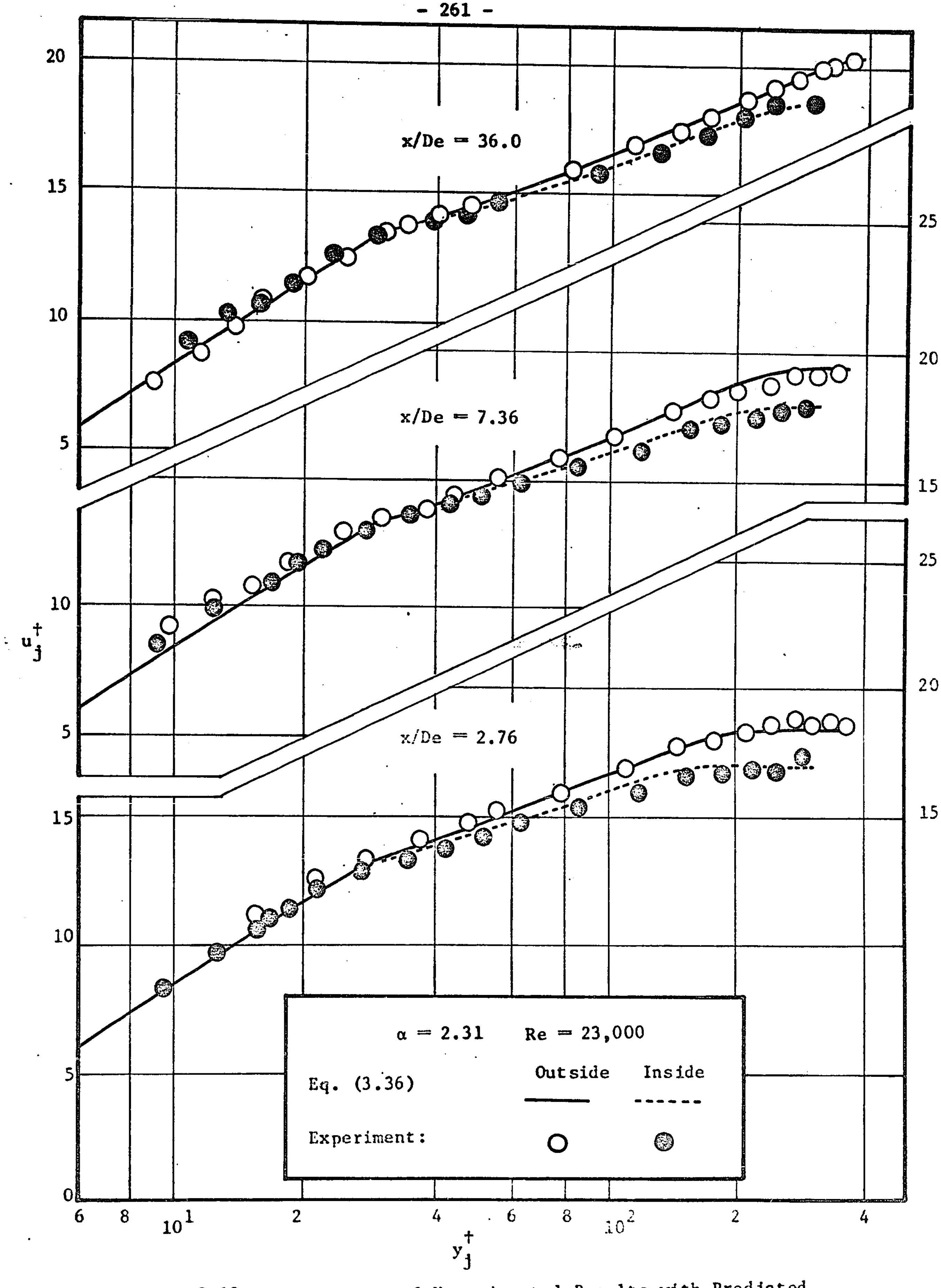

Fig. 5.12 Comparison of Experimental Results with Predicted Velocity Profiles, Entrance Region.

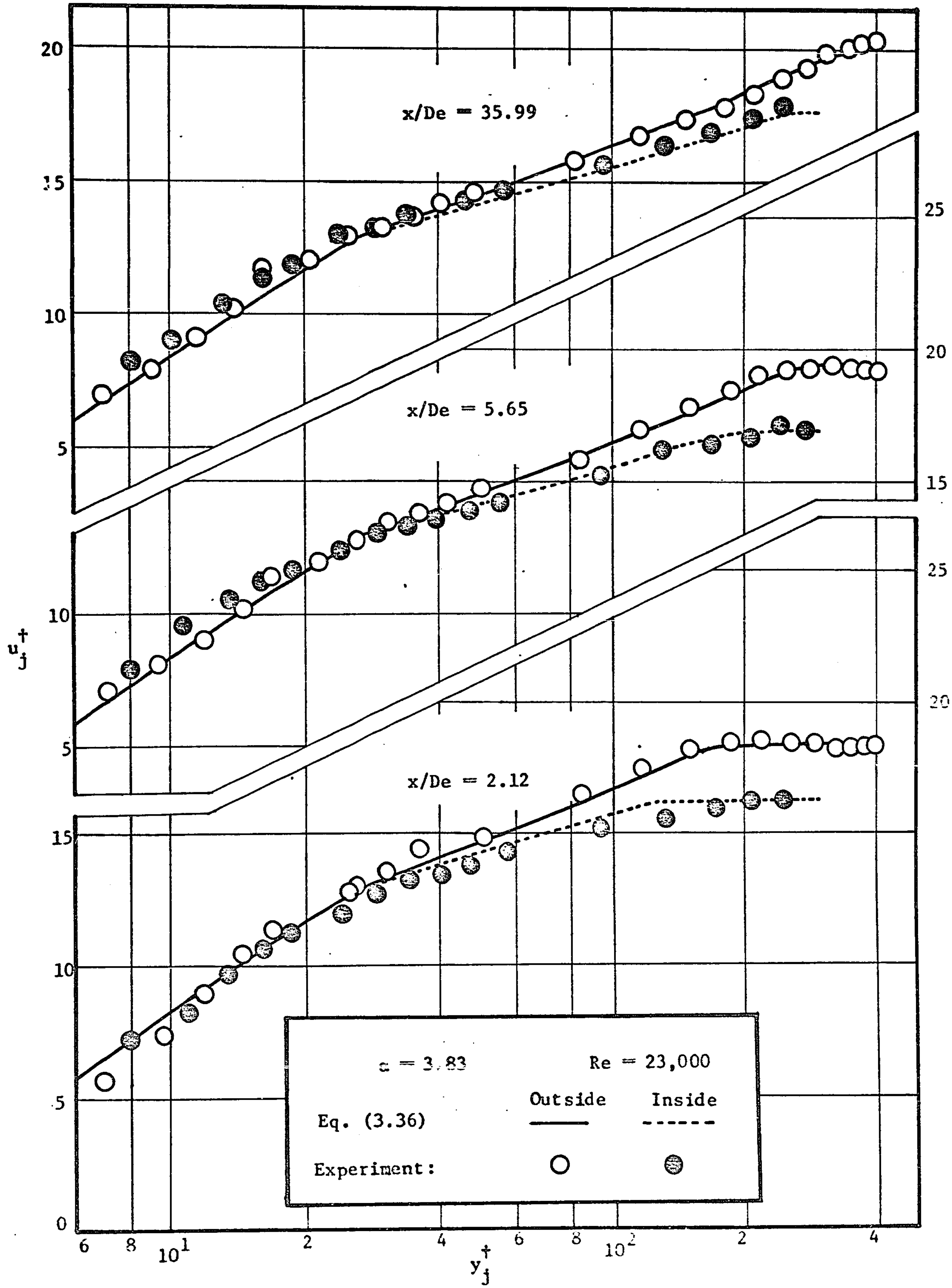

Fig. 5.13 Comparison of Experimental Results with Predicted Velocity Profiles, Entrance Region.

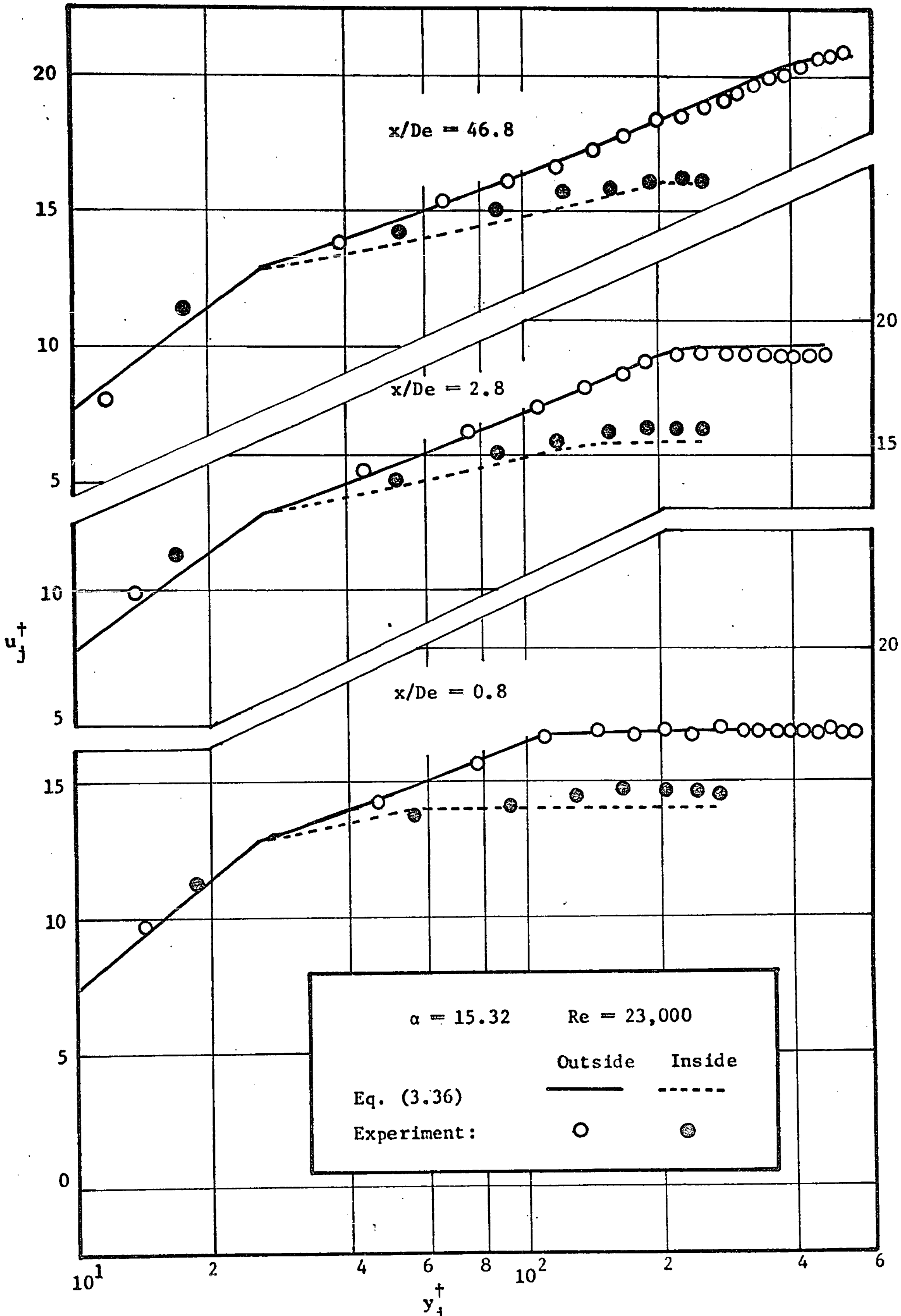

Fig. 5.14 Comparison of Experimental Results with Predicted Velocity Profiles, Entrance Region.

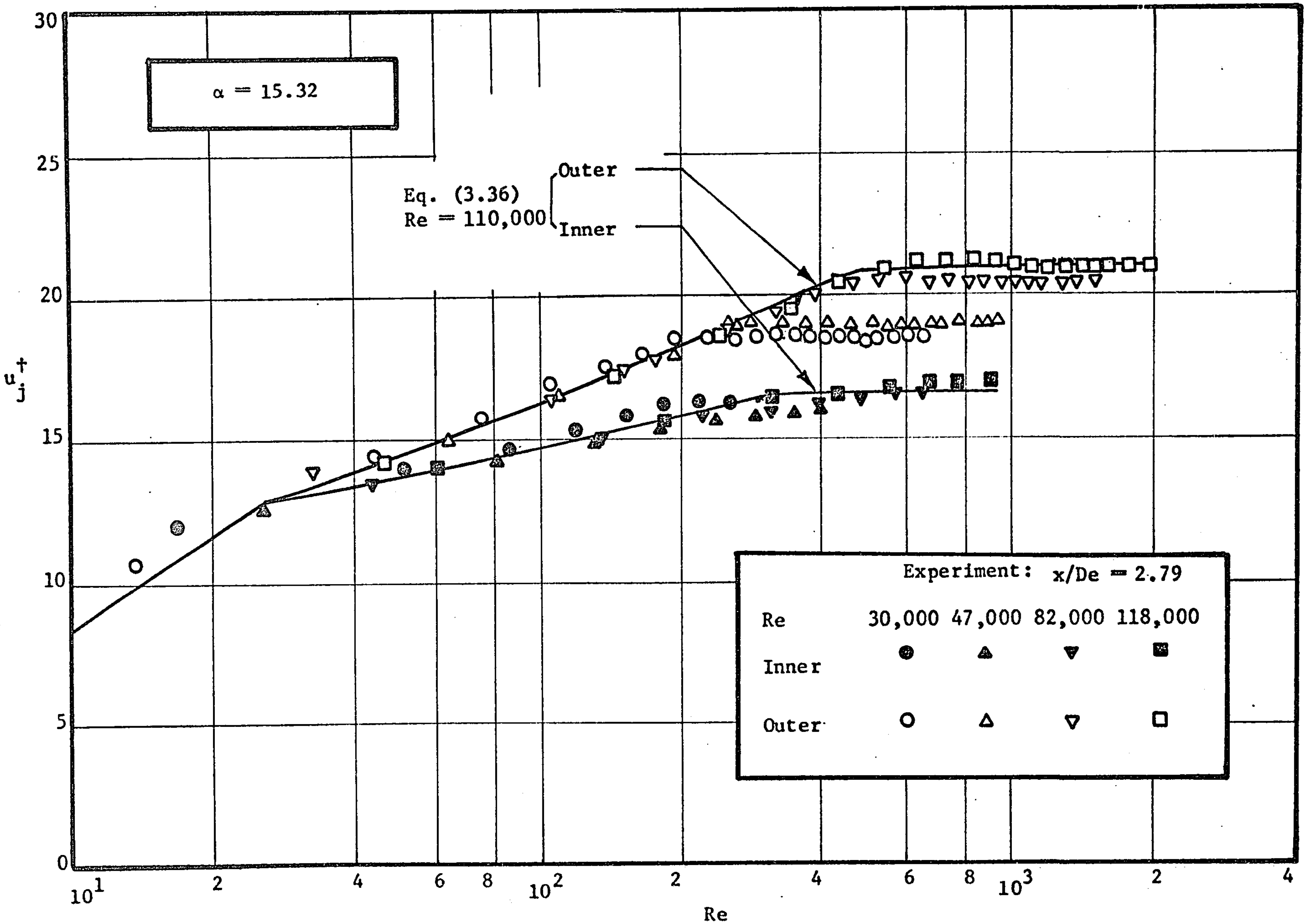

Fig. 5.15 Comparison of Experimental Results with Predicted Velocity Profiles, Entrance Region.

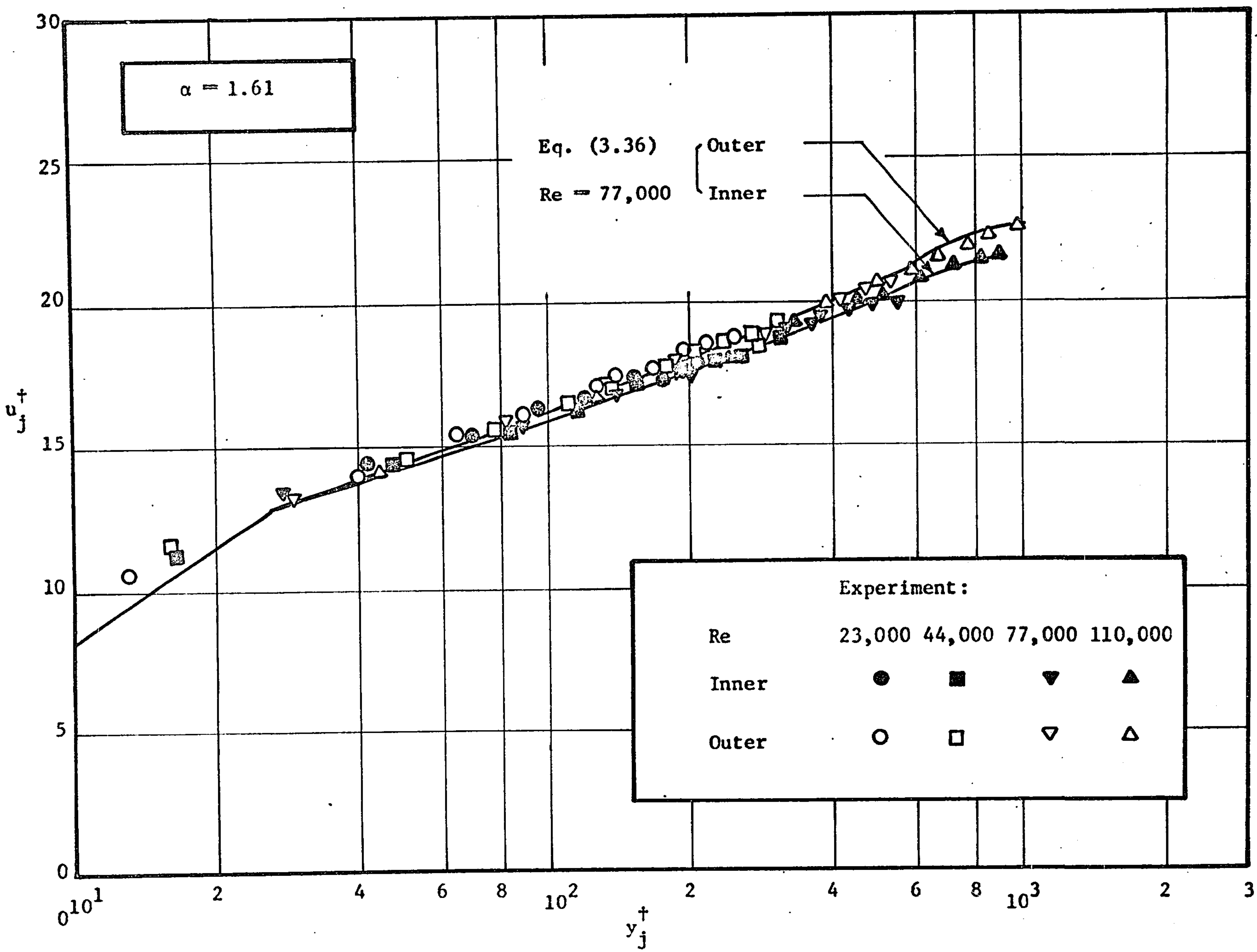

Fig. 5.16 Comparison of Experimental Results with Predicted Velocity Profiles, Fully Developed

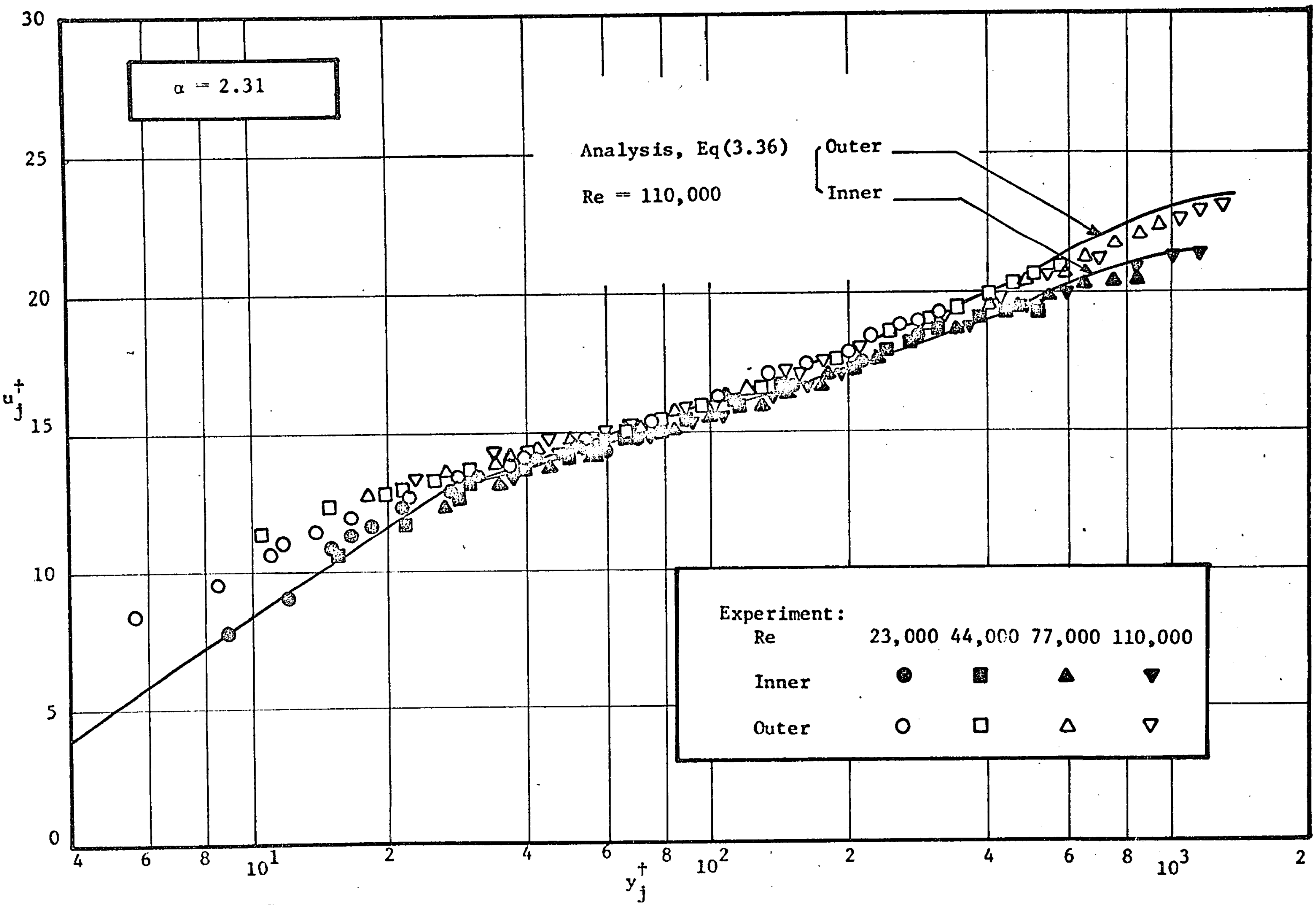

Fig. 5.17 Comparison of Experimental Results with Predicted Velocity Profiles, Fully Developed.

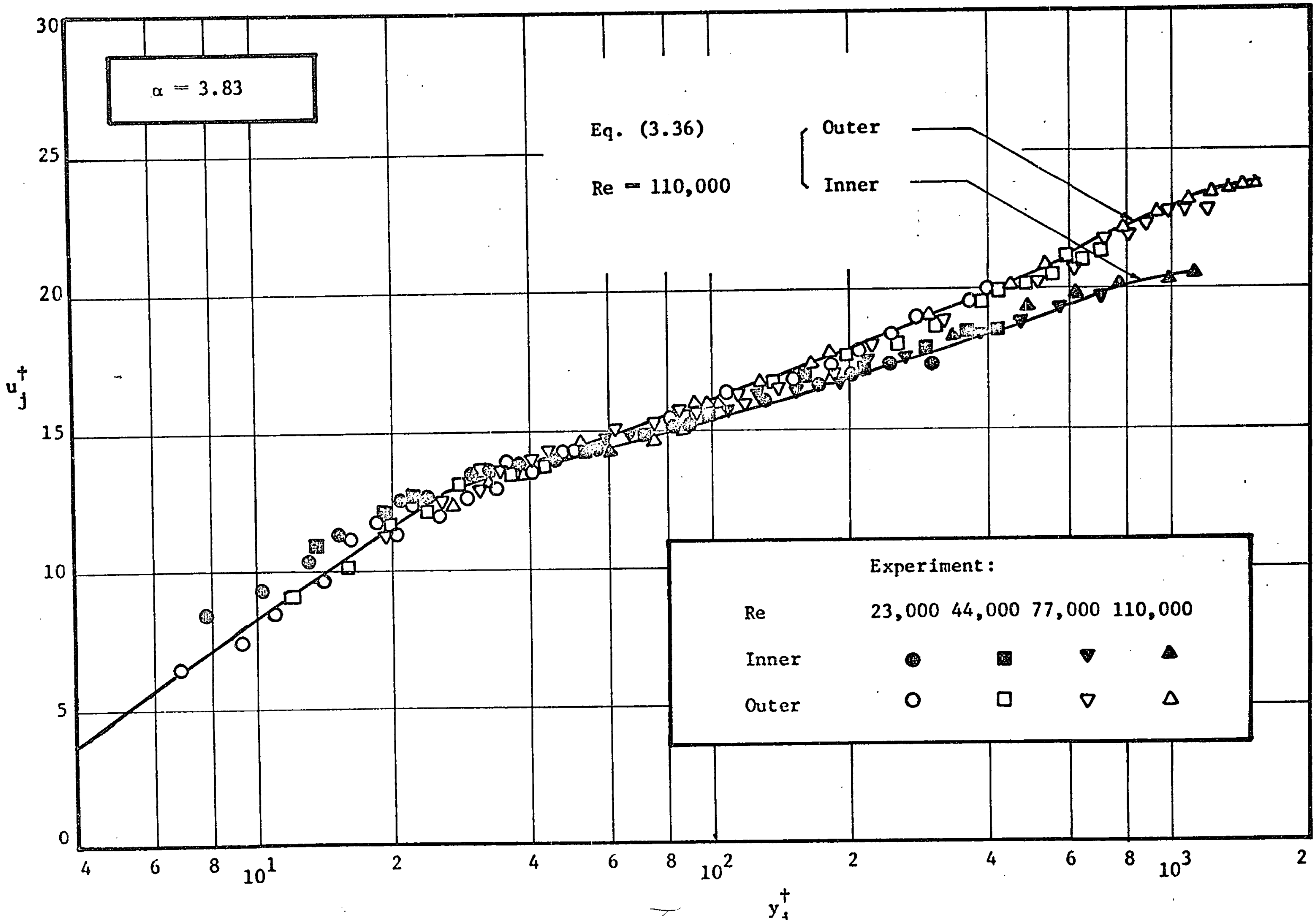

Fig. 5.18 Comparison of Experimental Results with Predicted Velocity Profiles, Fully Developed.

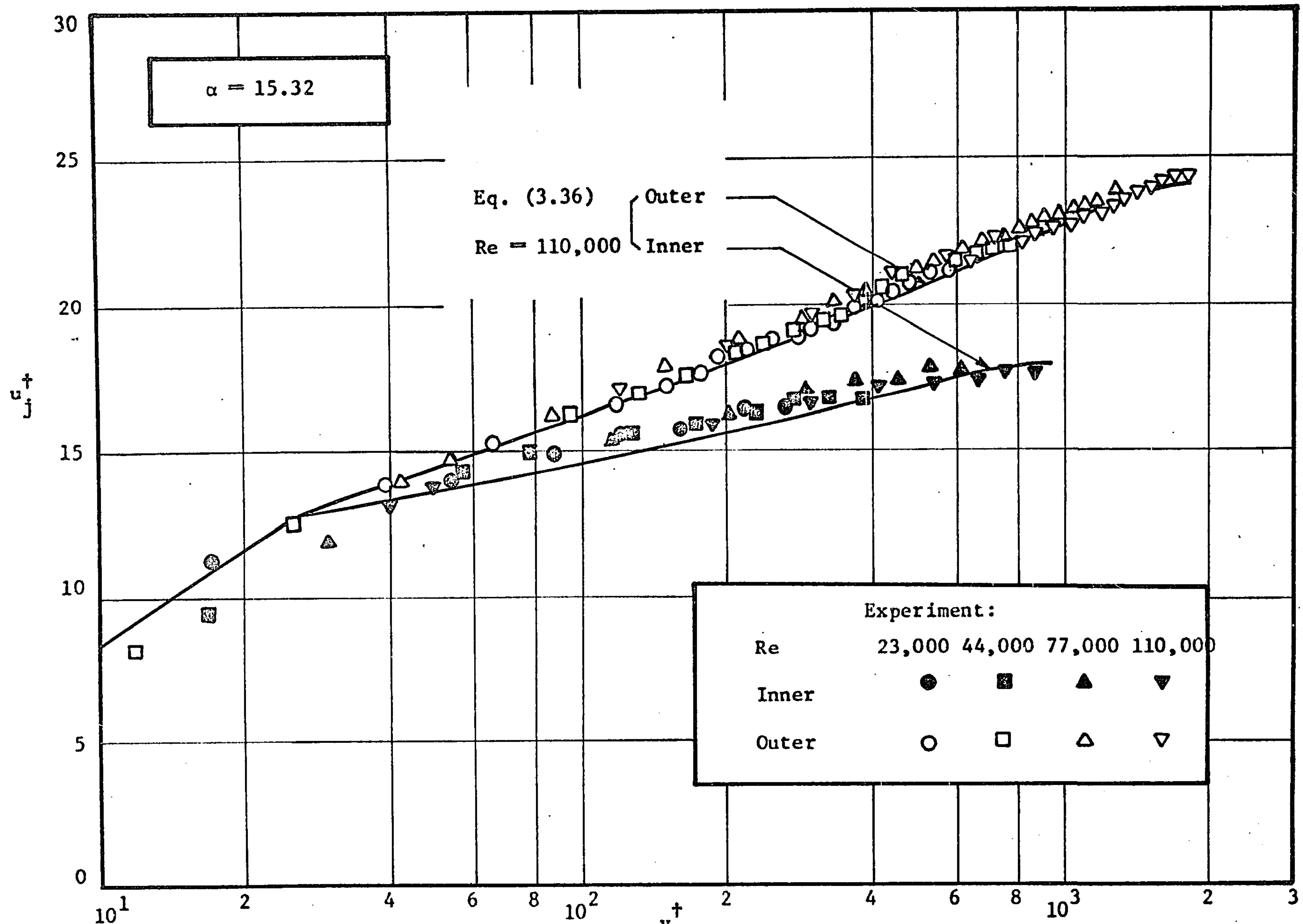

Fig. 5.19 Comparison of Experimental Results with Predicted Velocity Profiles, Fully Developed.

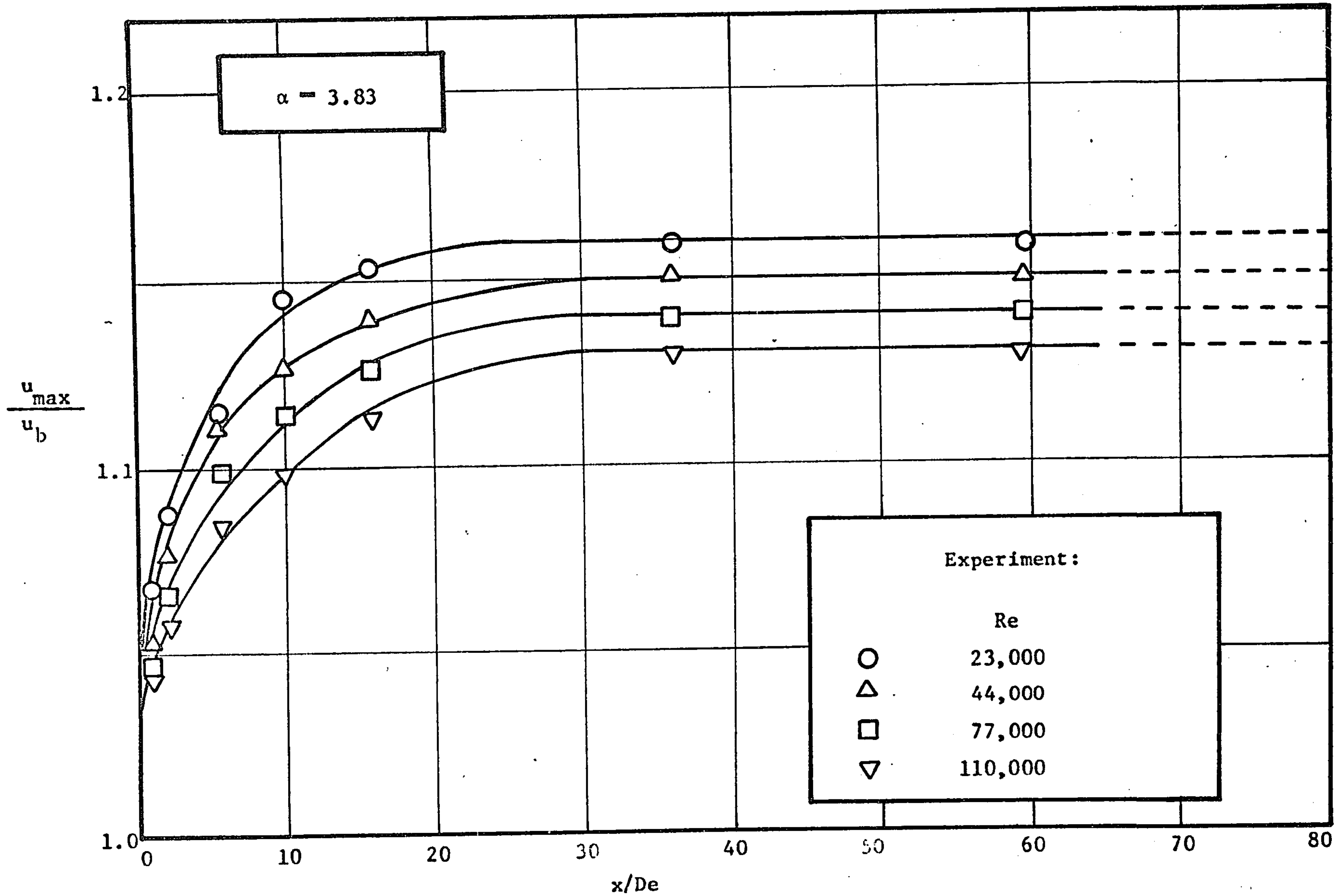

Fig. 5.20 Core Velocity Distribution, Entrance Region.

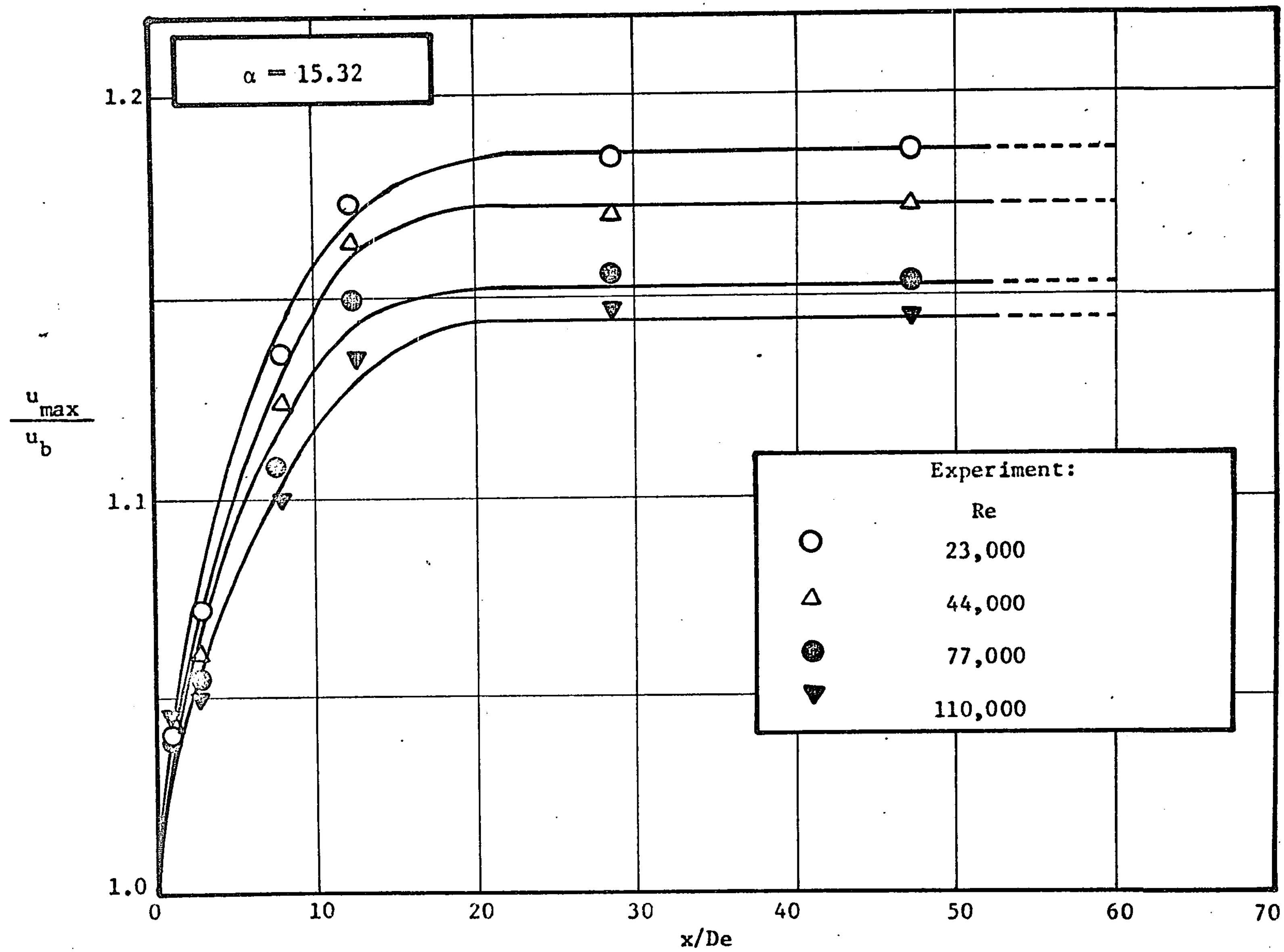

Fig. 5.21 Core Velocity Distribution, Entrance Region.

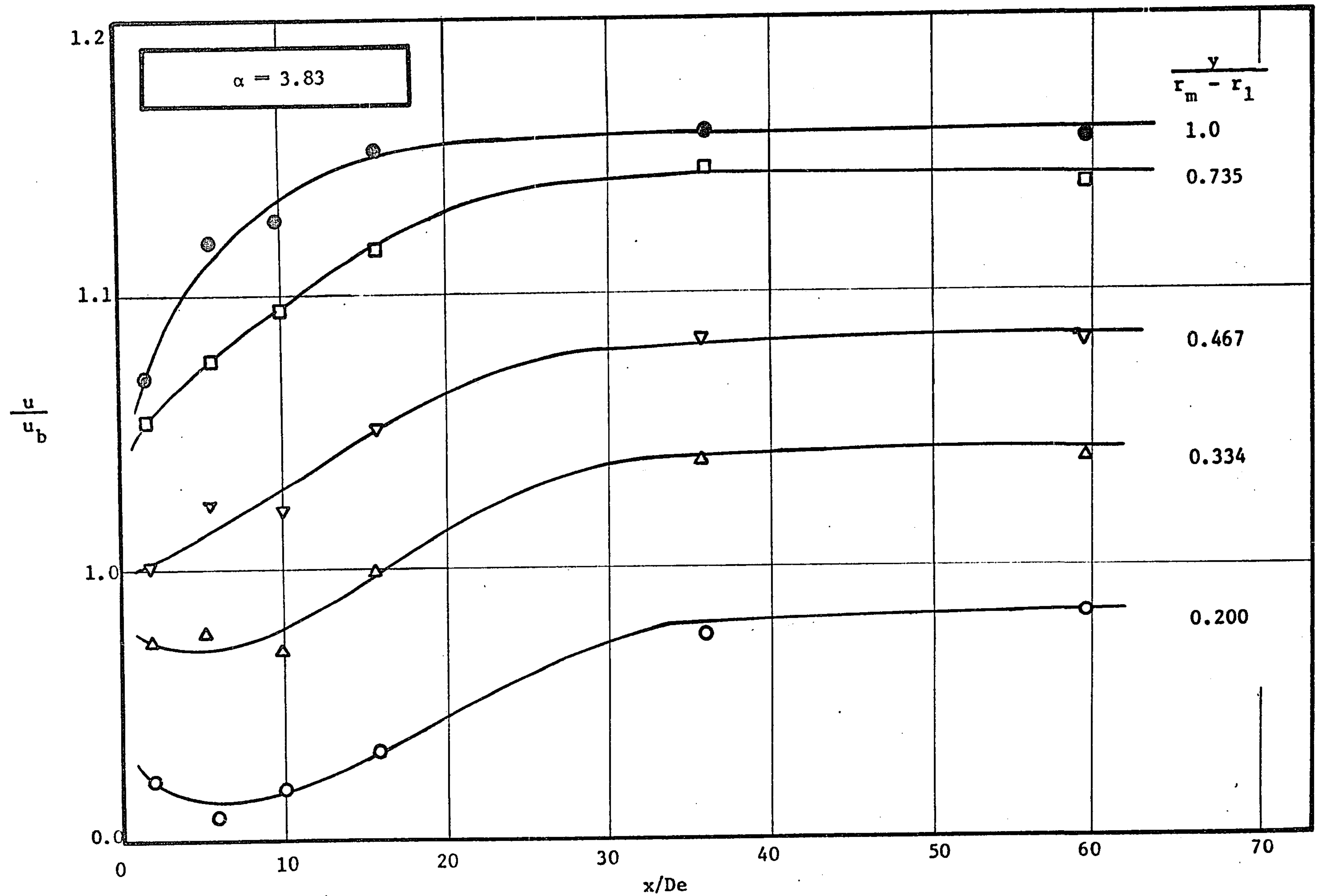

Fig. 5.22 Local Velocity Distribution, Entrance Region, Re = 23,000

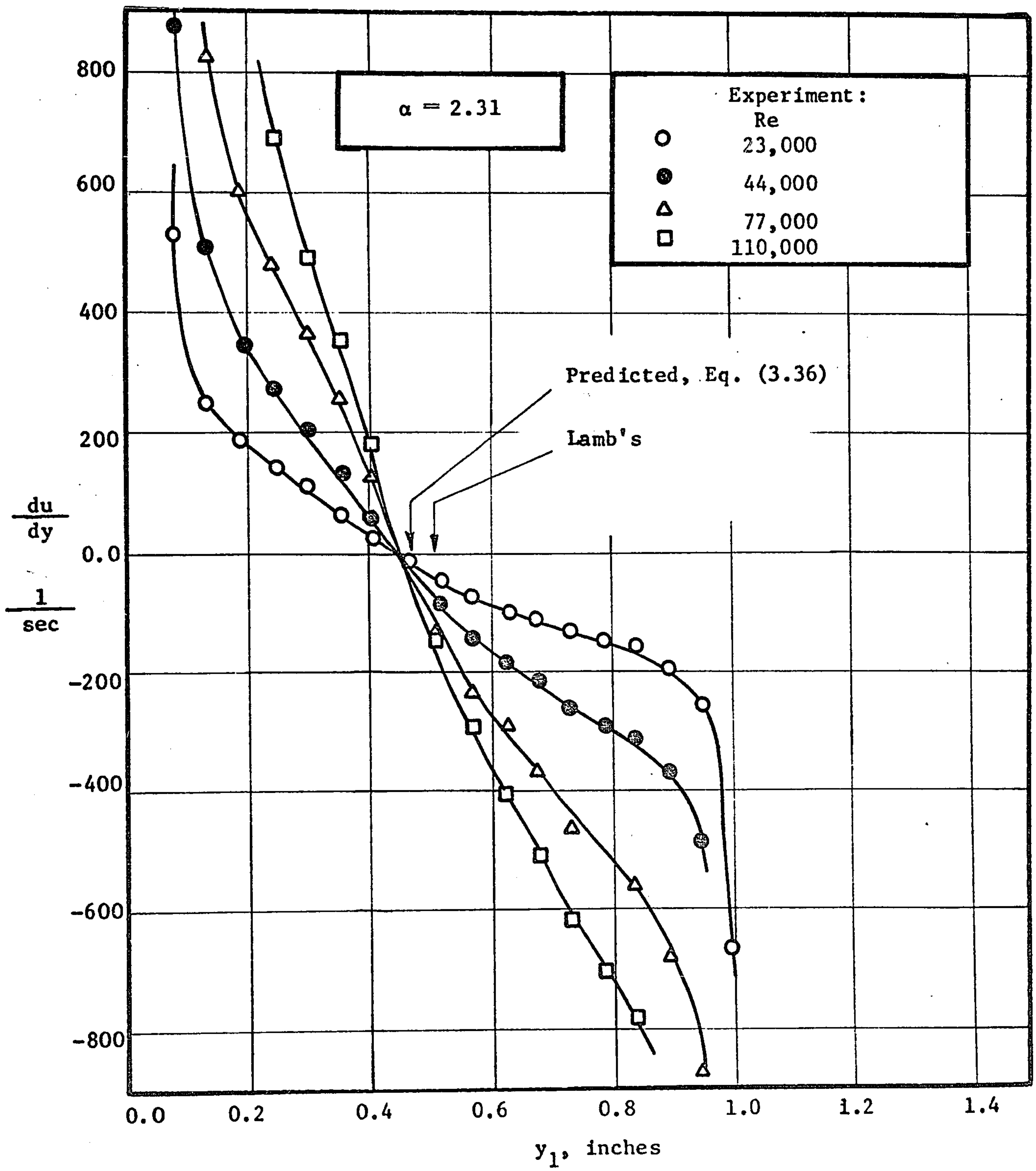

Fig 5.23 Velocity Gradient in Region of Maximum Velocity.

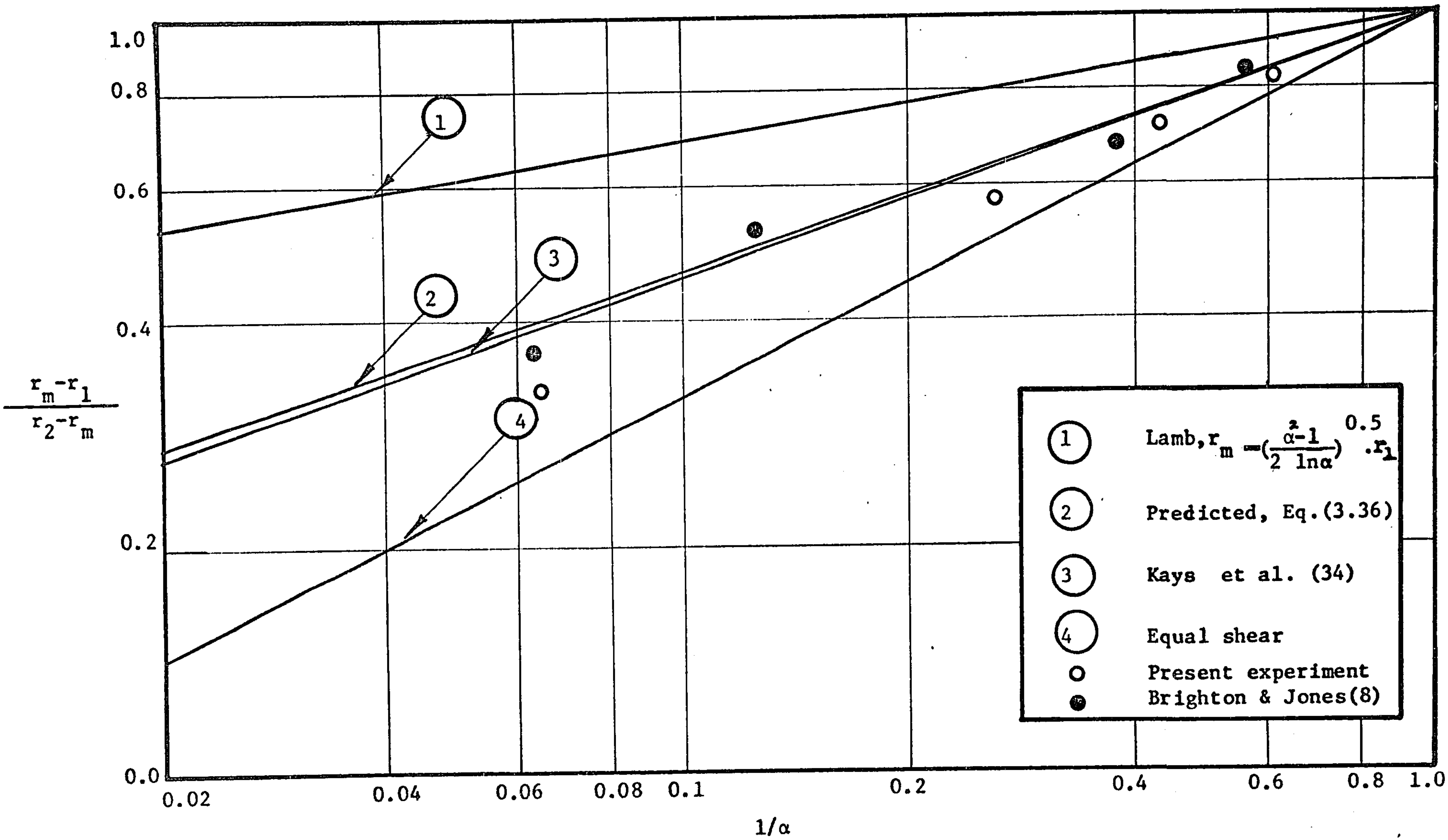

Fig. 5.24 Comparison Between Prediction and Experiment for Radius of Maximum Velocity, Concentric Annulus, Fully Developed Flow.

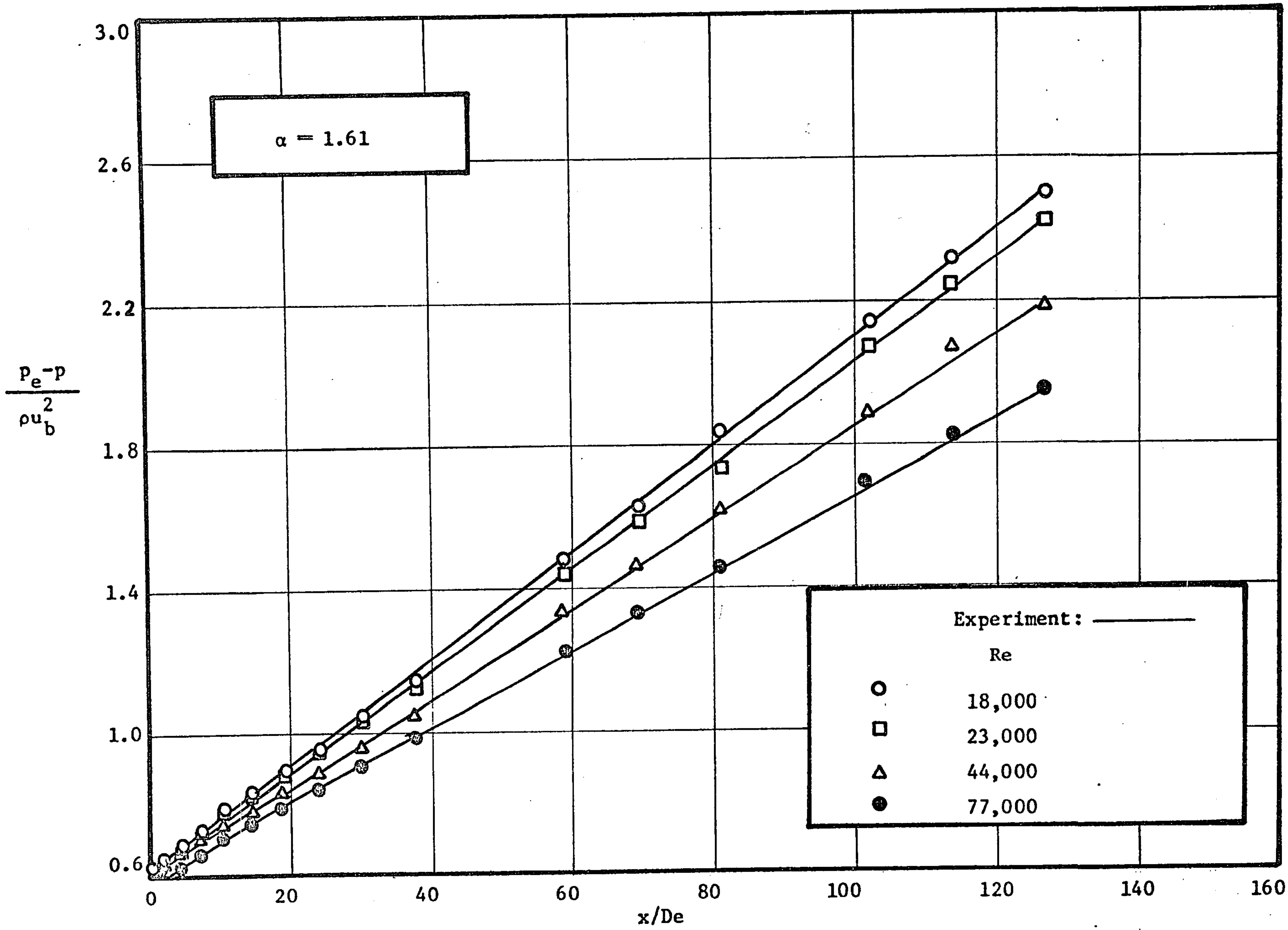

Fig. 5.25 Variation of Static Pressure, Entrance Region.

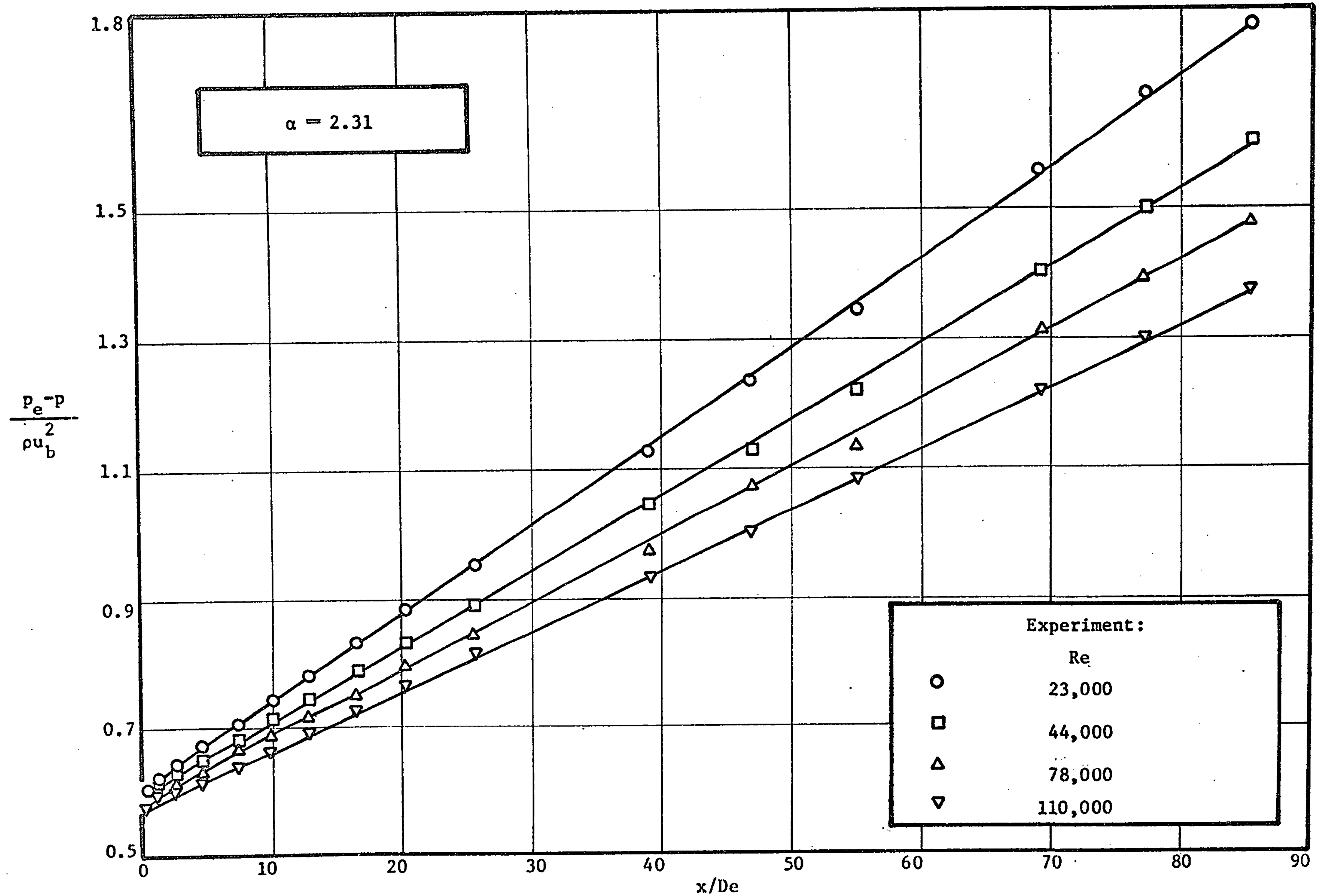

Fig. 5.26 Variation of Static Pressure, Entrance Region.

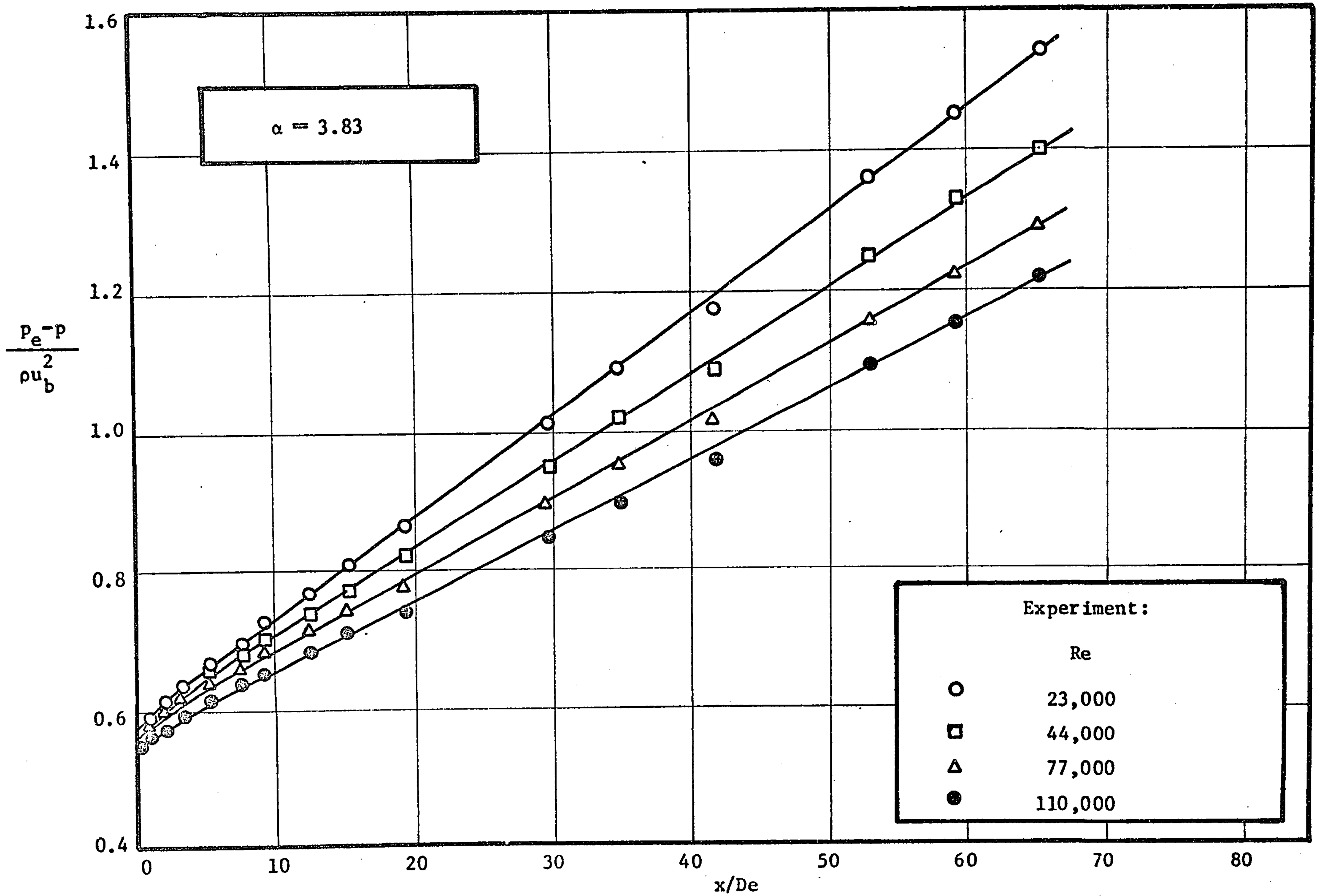

Fig. 5.27 Variation of Static Pressure, Entrance Region.

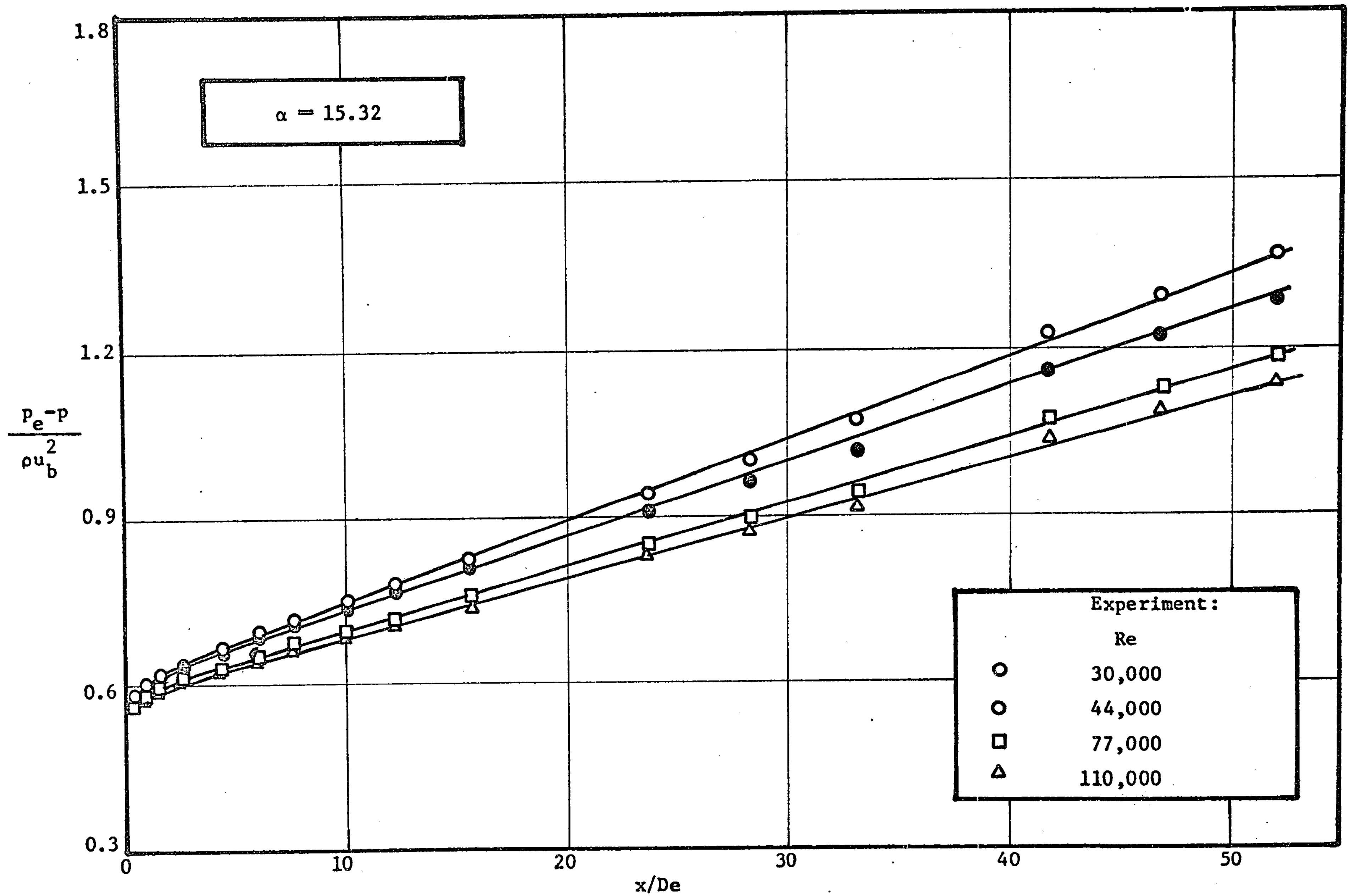

Fig. 5.28 Variation of Static Pressure, Entrance Region.

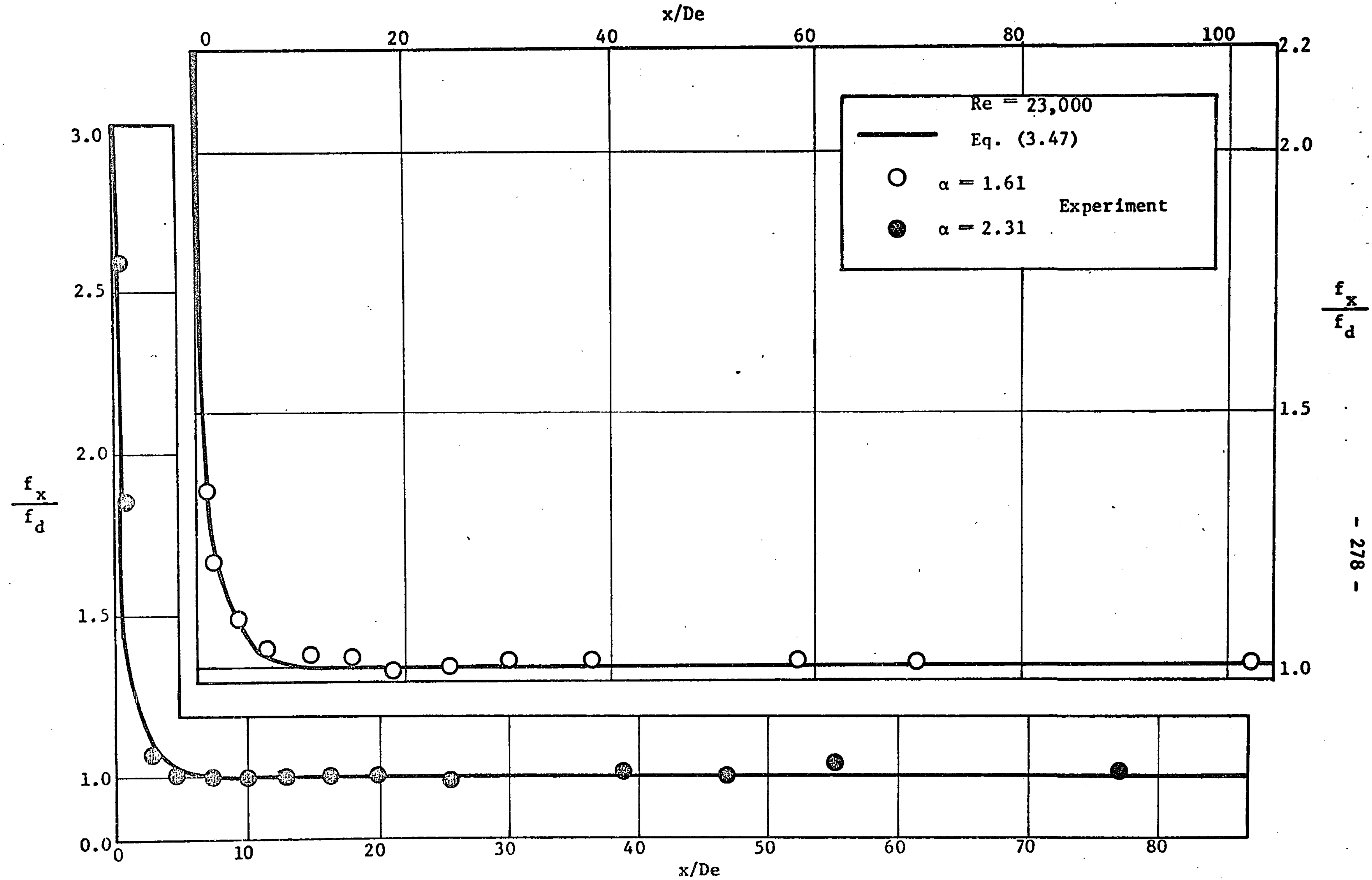

Fig. 5.29 Comparison of Experimental Results with Predicted Friction Factors, Entrance Regions. Concentric Annuli.

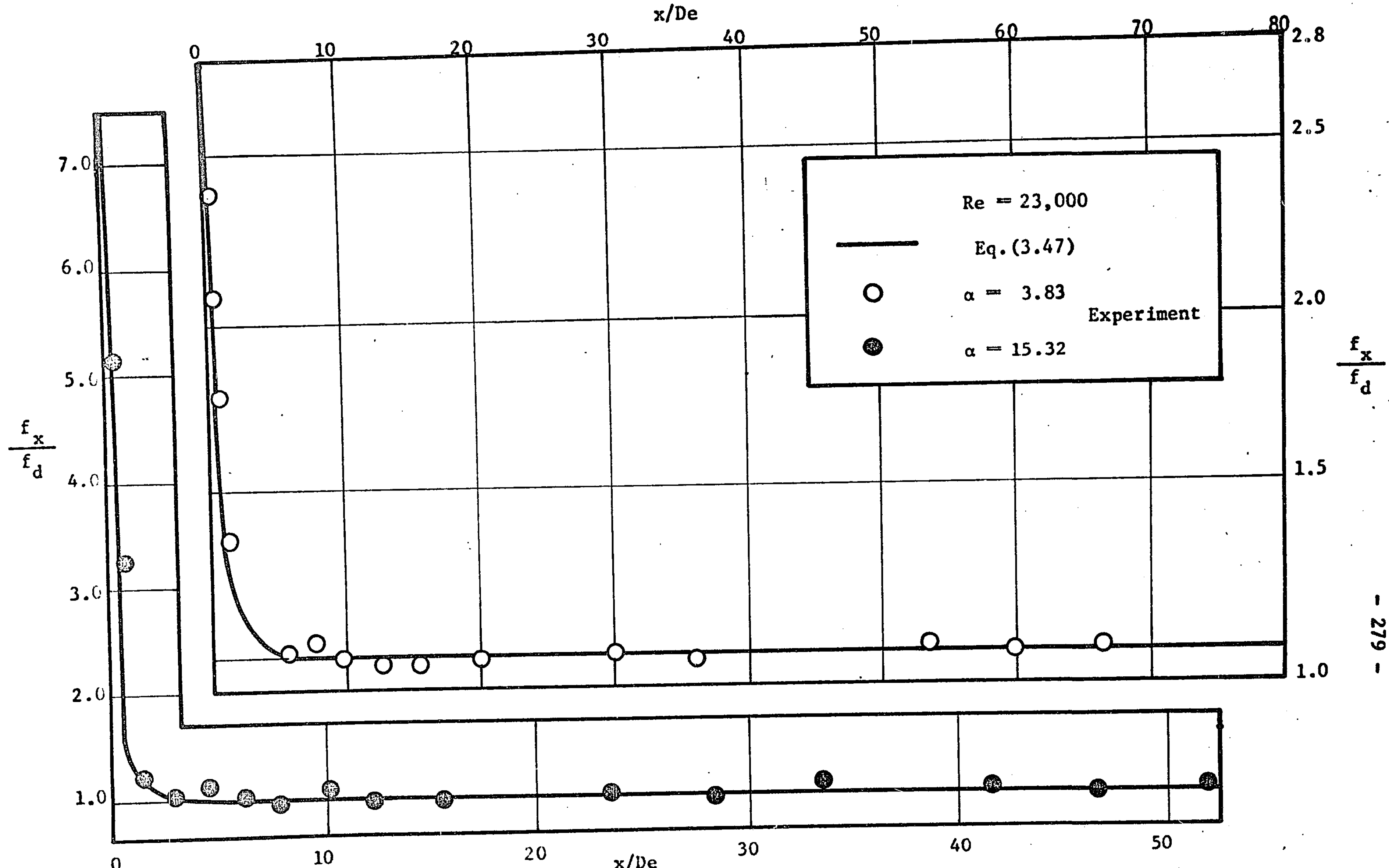

Fig. 5.30 Comparison of Experimental Results with Predicted Friction Factors, Entrance Regions, Concentric Annuli.

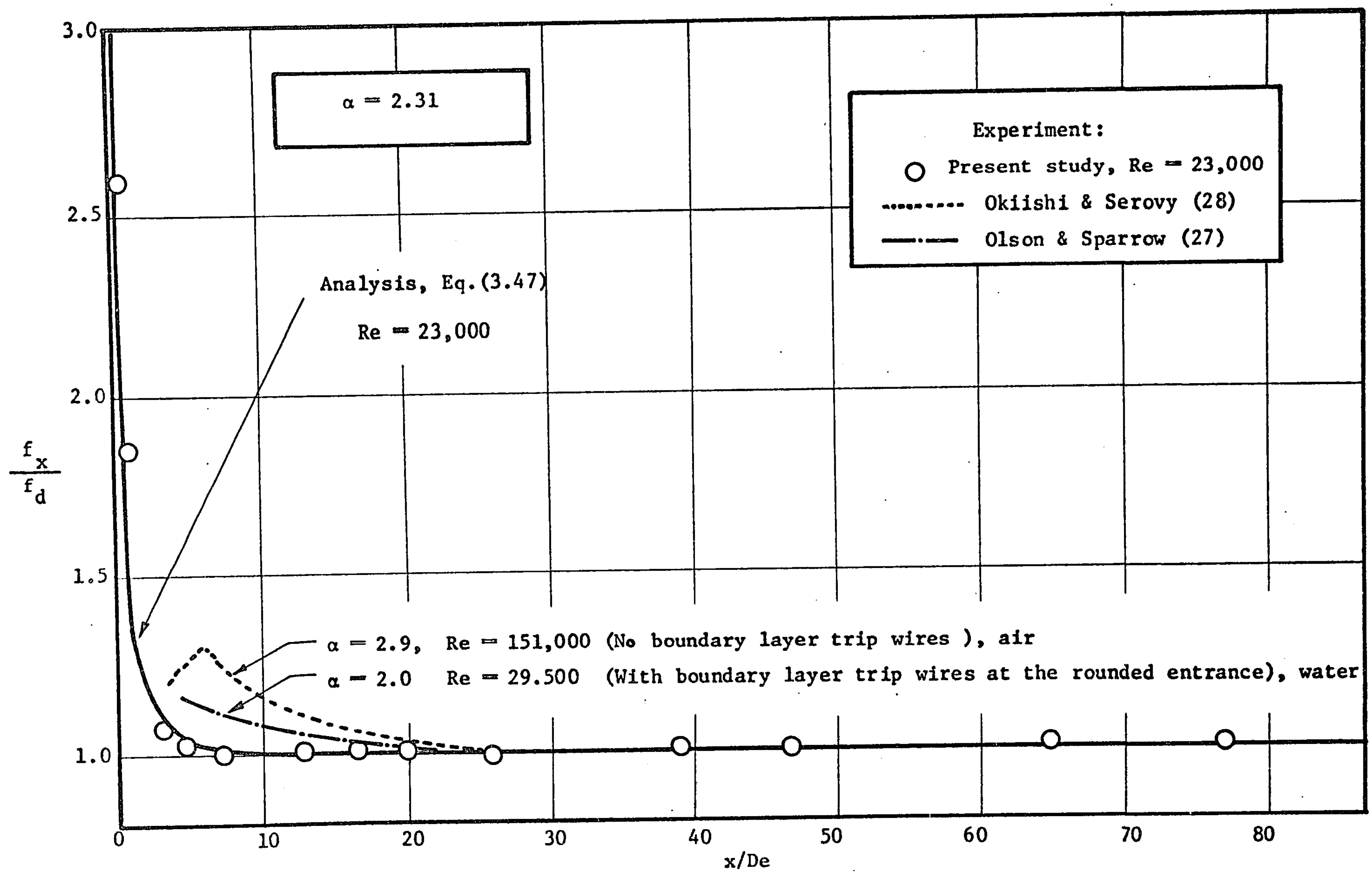

Fig. 5.31 Comparison of Experimental Results with Predicted Friction Factors, Entrance Region, Concentric Annulus.

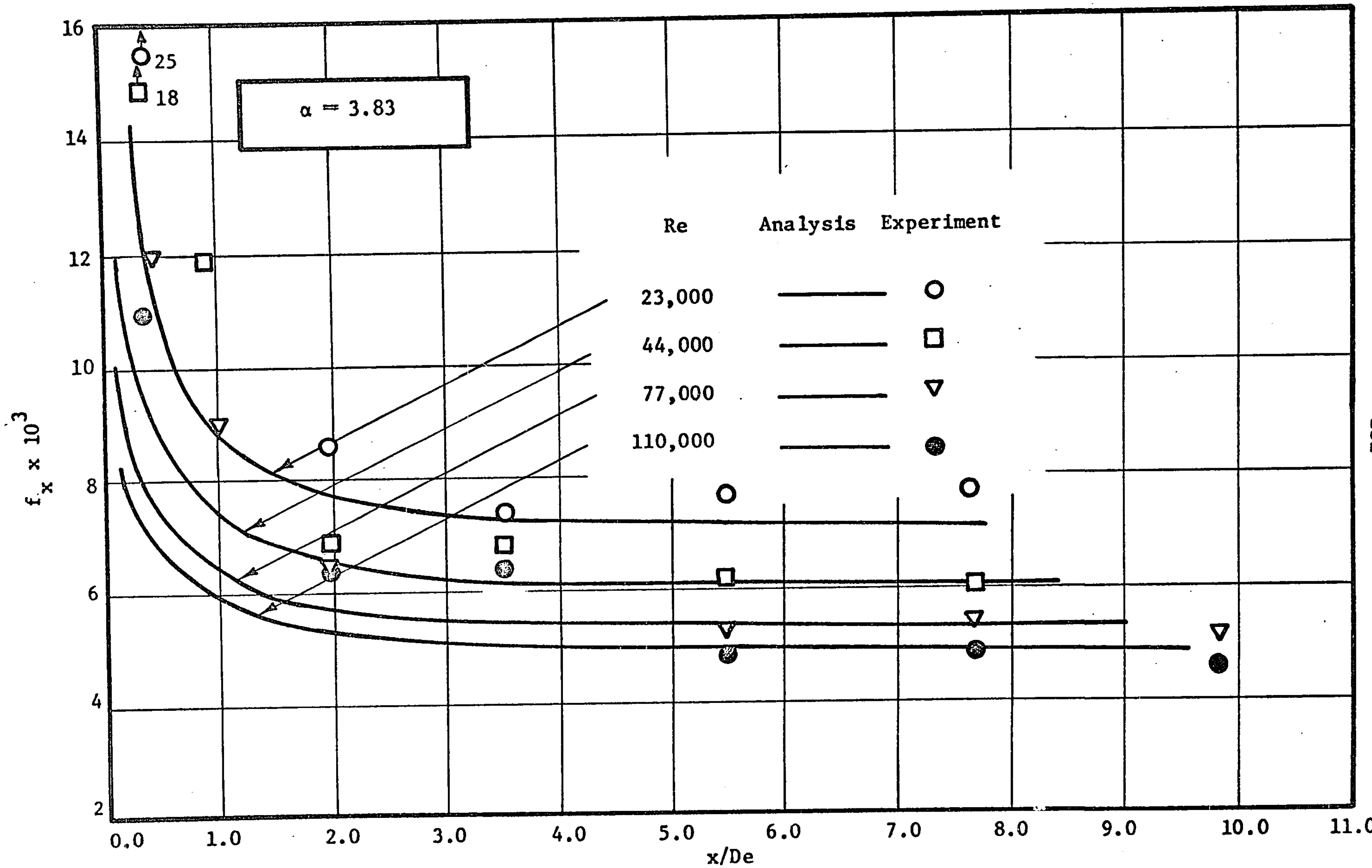

Fig. 5.32 Effect of Reynolds Number on the Variation of Friction Factors, Entrance Regions.

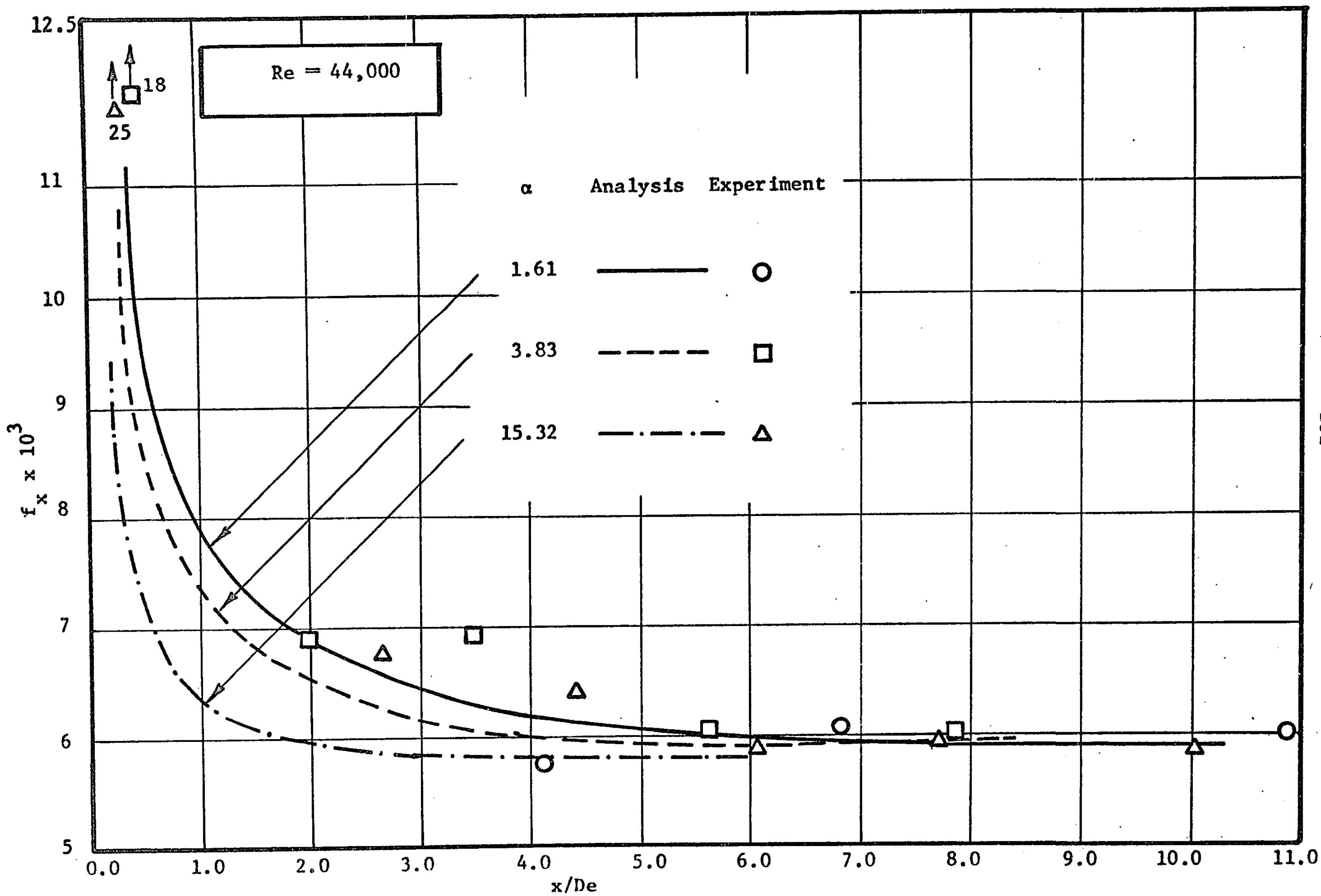

Fig. 5.33 Effect of Radius Ratio on the Variation of Friction Factors, Entrance Regions.

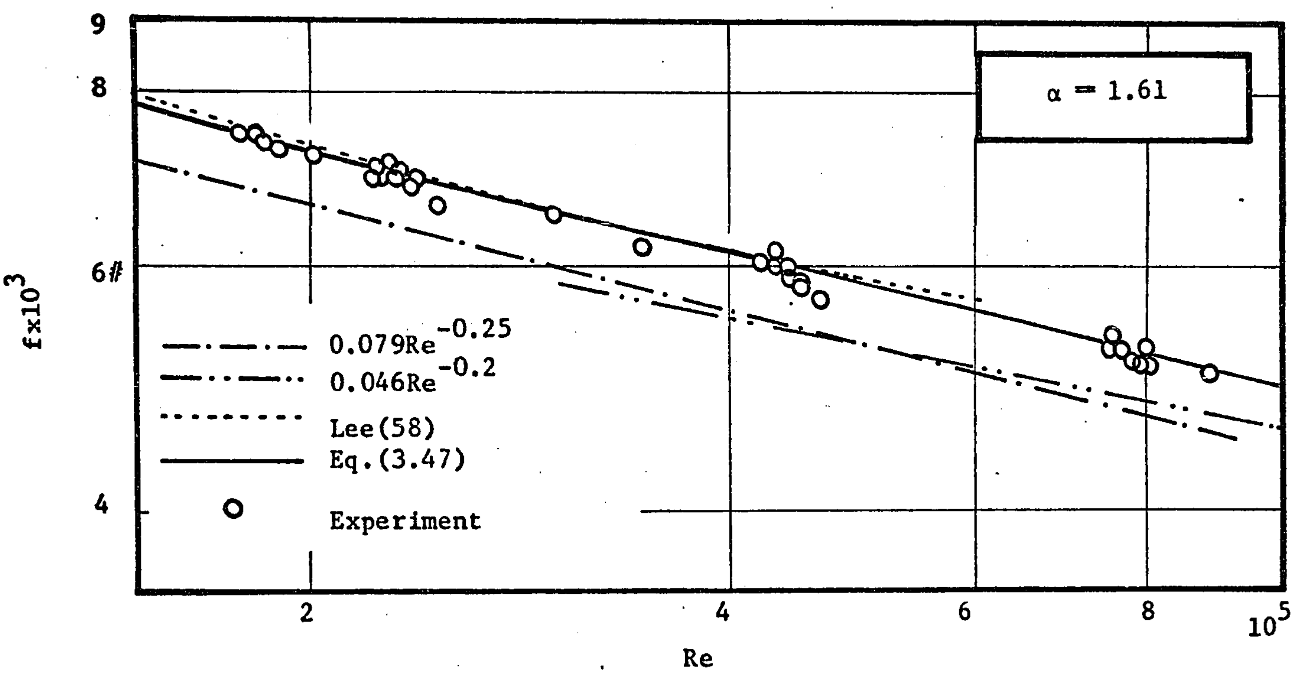

(a)

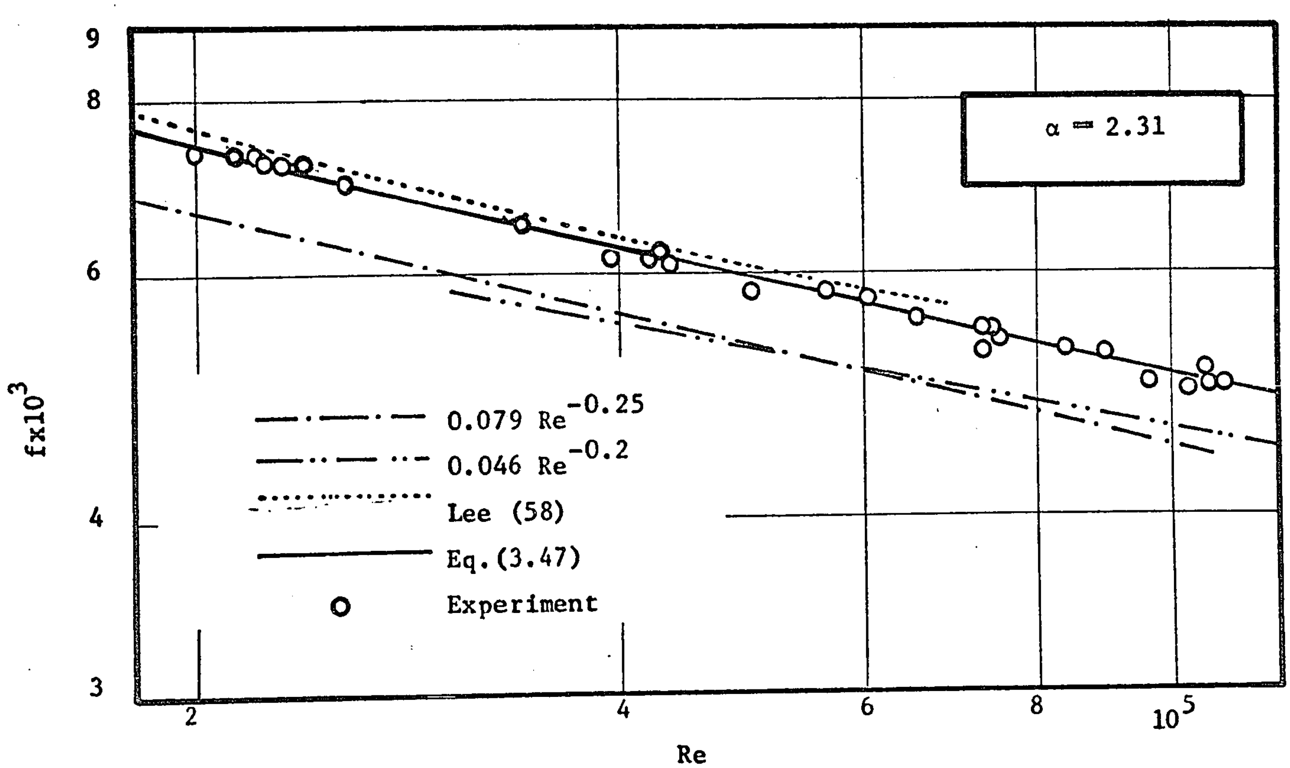

(b)

Fig. 5.34 Friction Factors, Fully Developed.

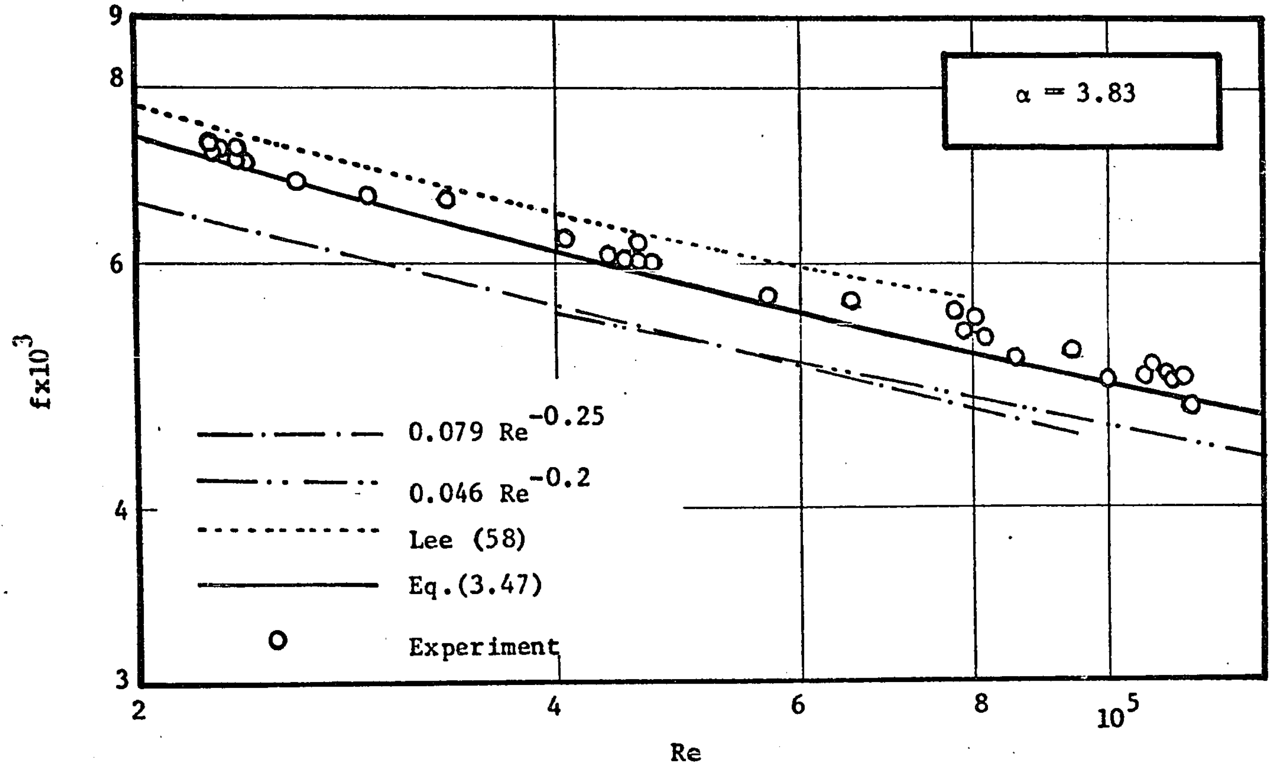

(a)

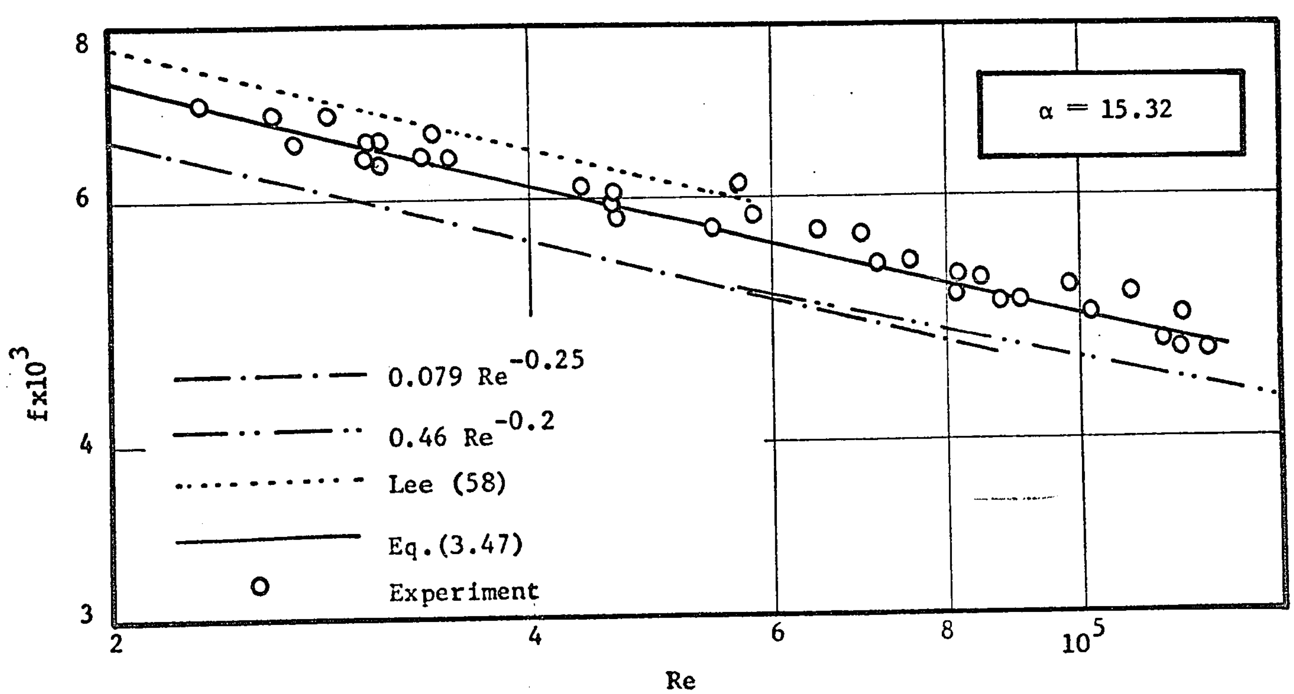

(b)

Fig, 5.35 Friction Factors, Fully Developed.

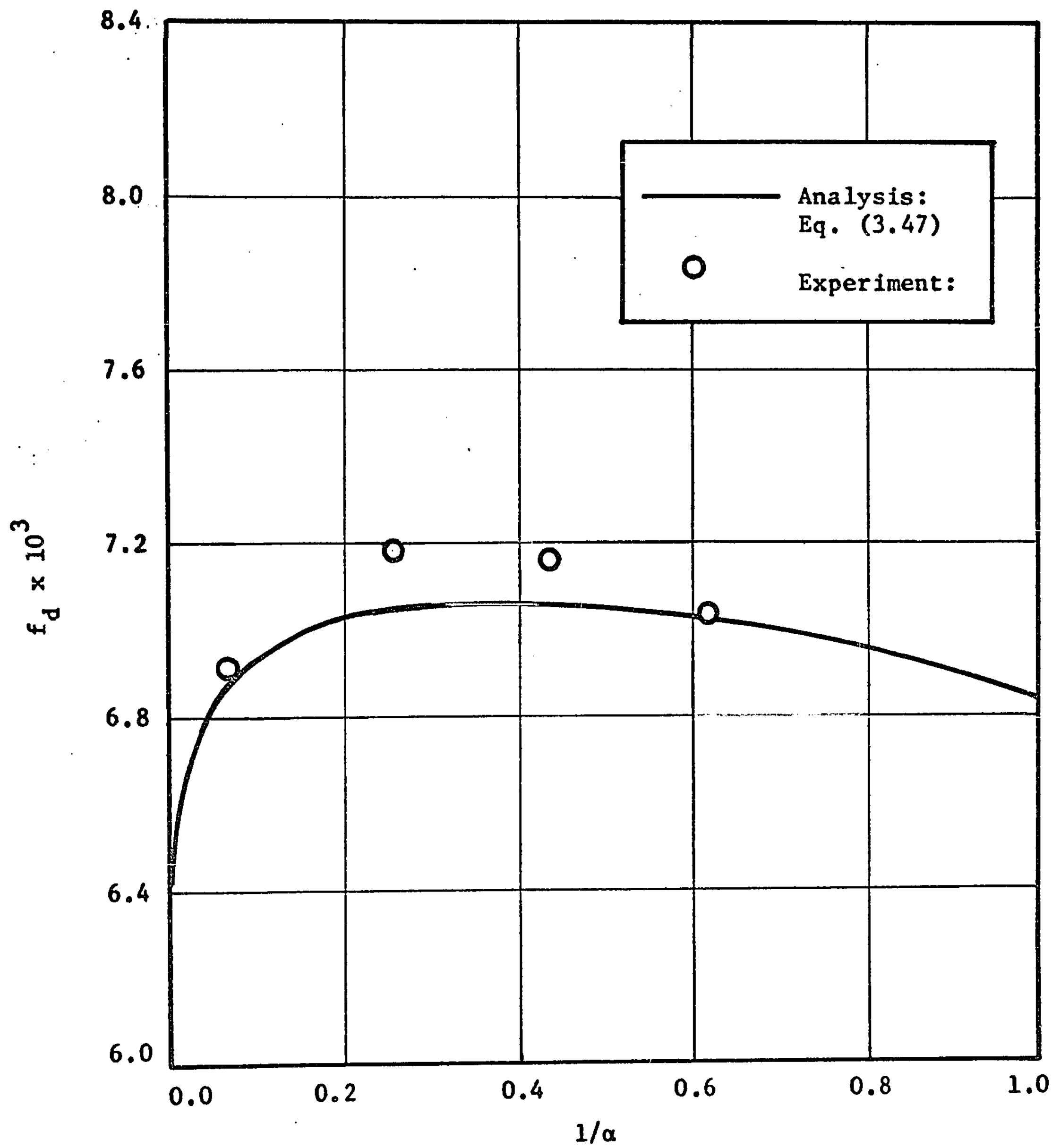

Fig. 5.36 Effect of Radius Ratio on Friction Factors, Fully Developed Region, Re = 23,000.

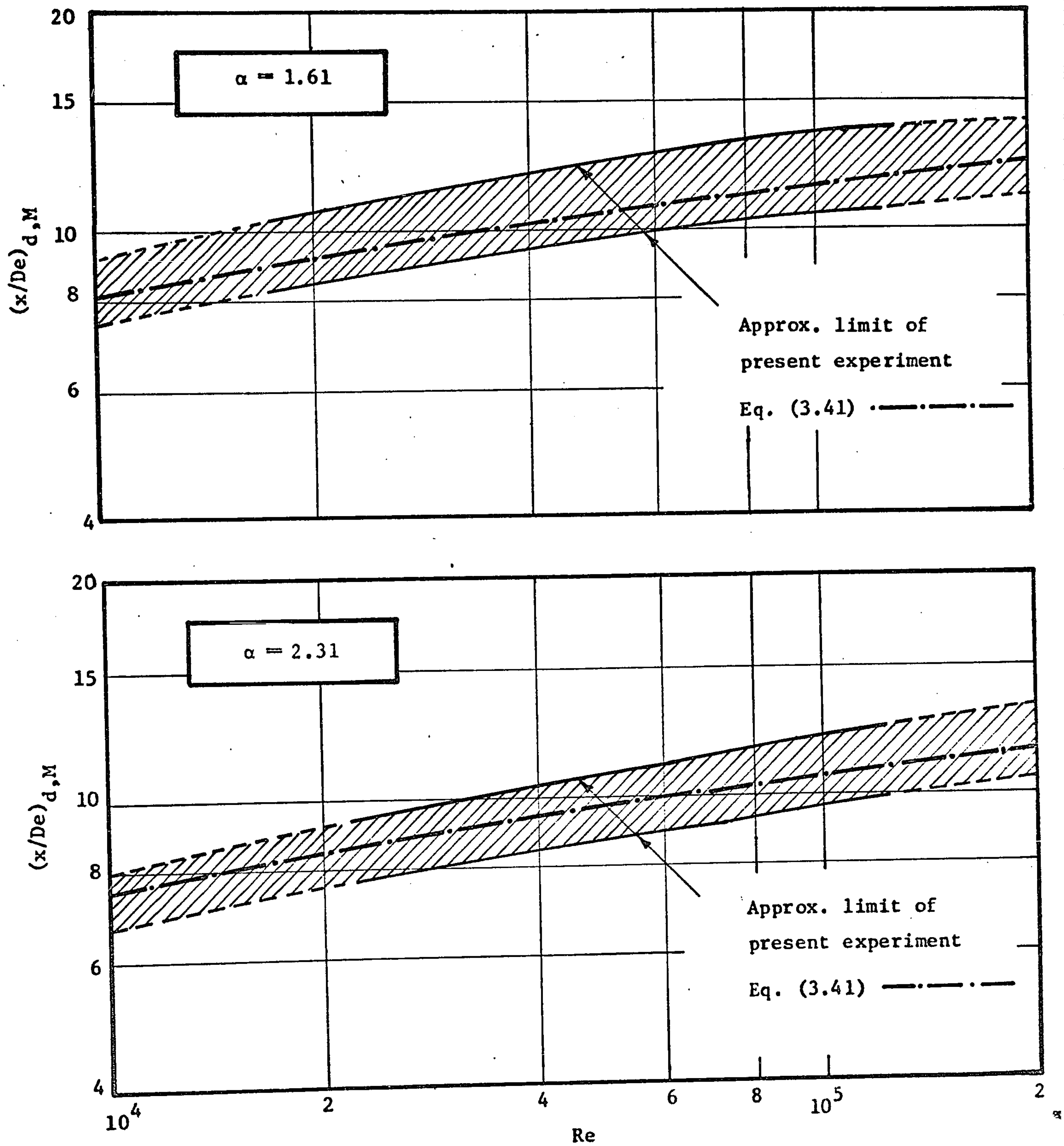

Fig. 5.37 Comparison of Experimental Results with Predicted Hydrodynamic Entry Lengths, Concentric Annuli.

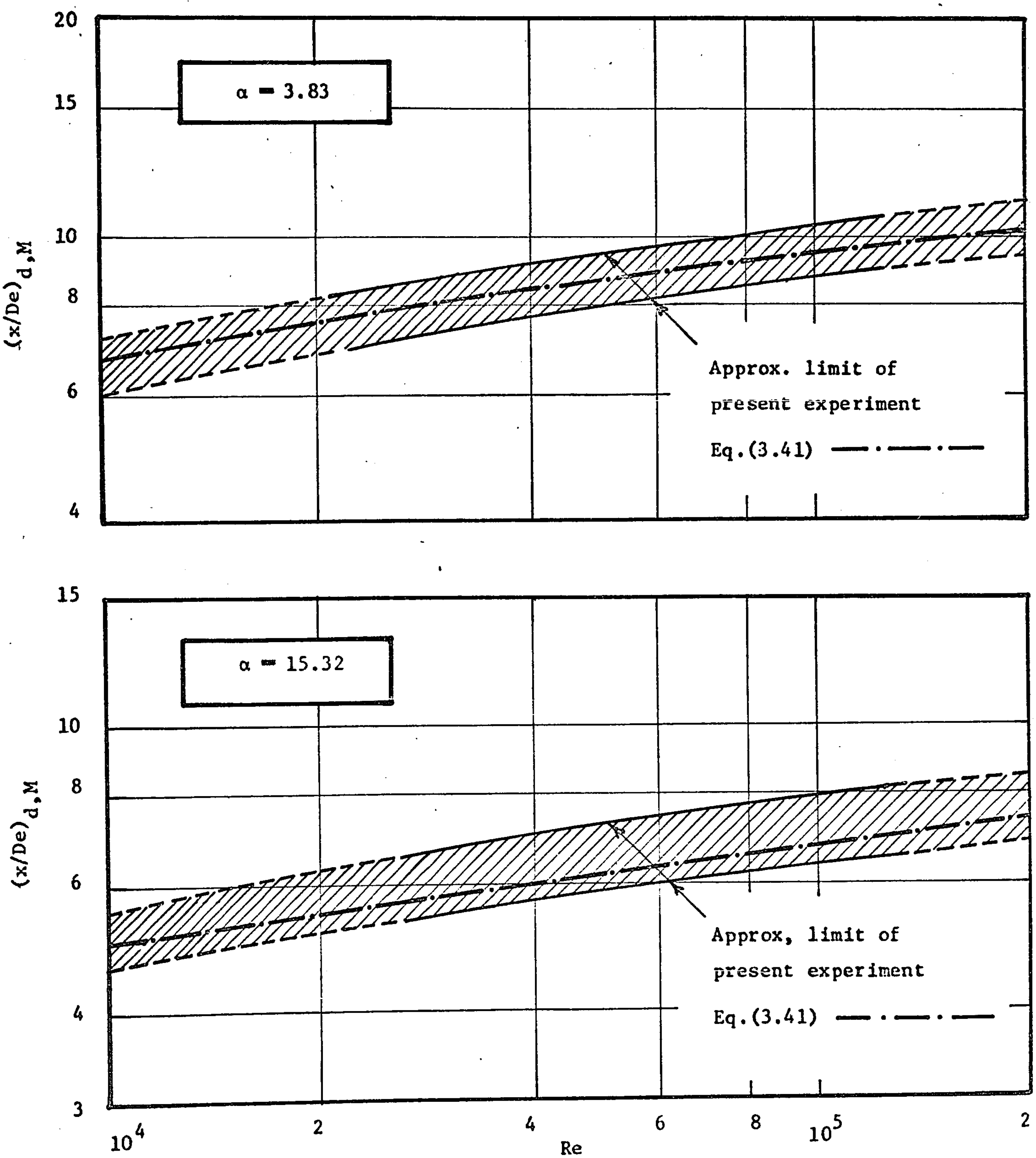

Fig. 5.38 Comparison of Experimental Results with Predicted Hydrodynamic Entry Lengths, Concentric Annuli.

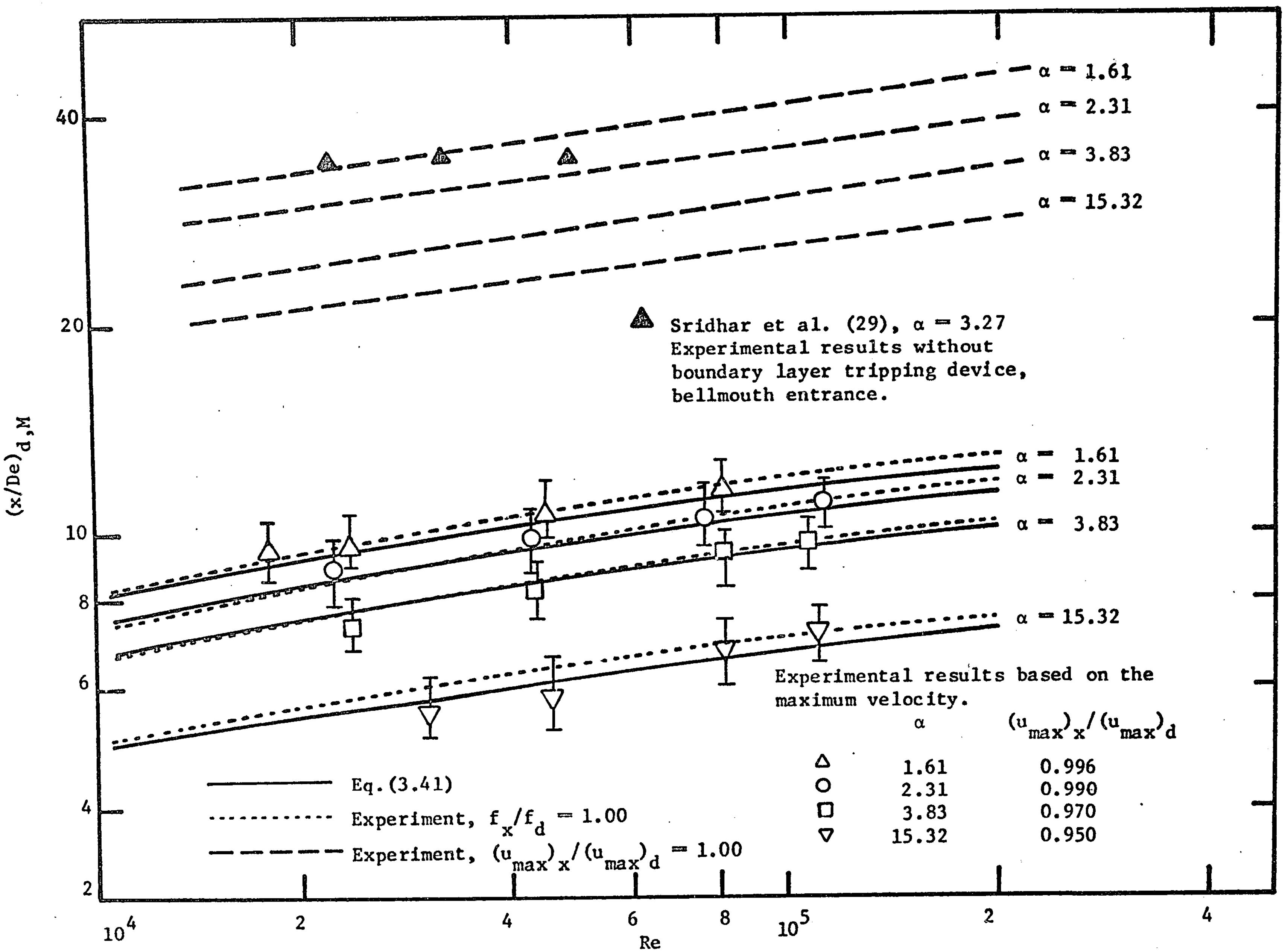

Fig. 5.39 Comparison of Experimental Results with Predicted Hydrodynamic Entry Lengths, Concentric Annuli.

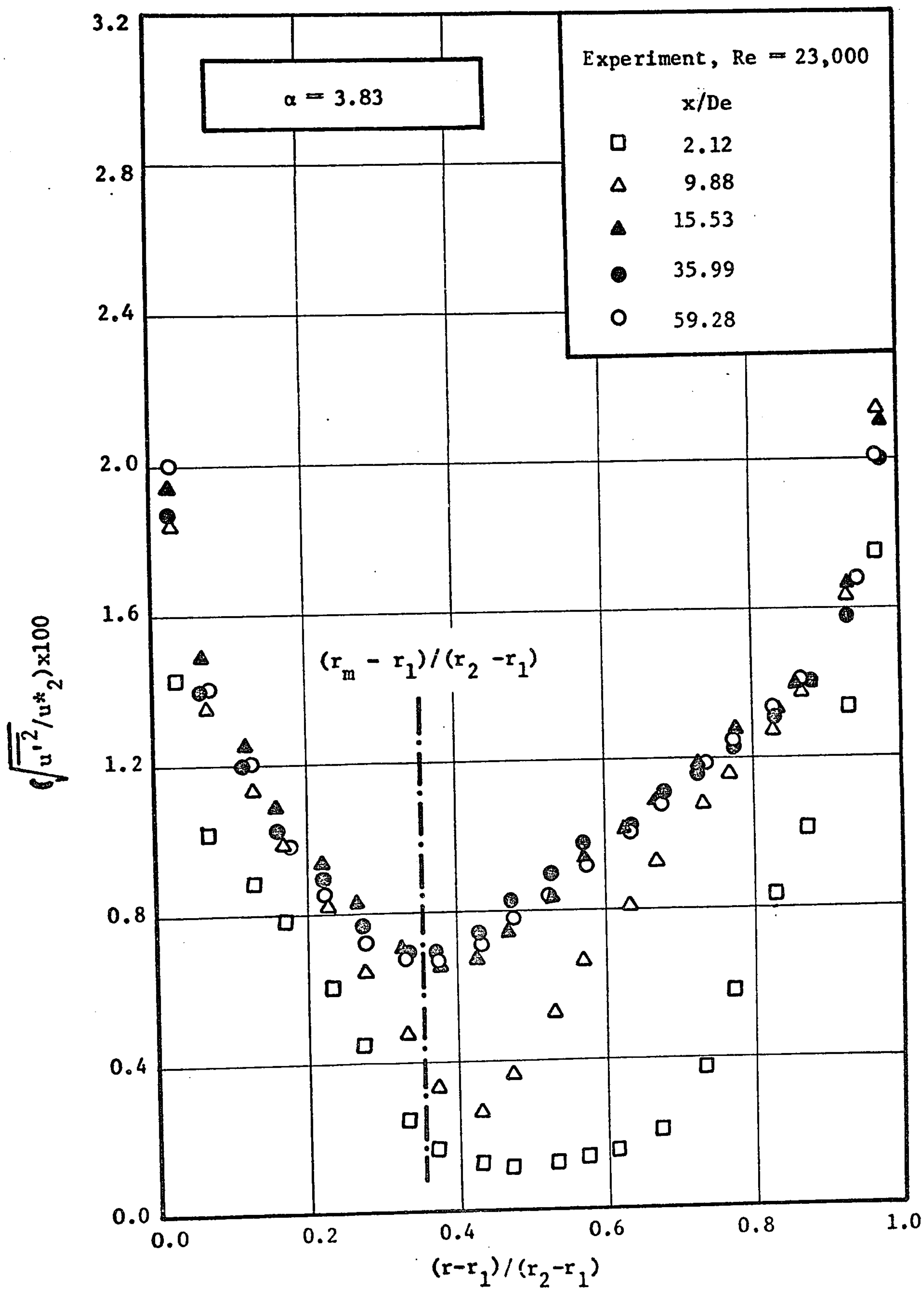

Fig. 5.40 Axial Turbulence Intensities, Entrance Regions.

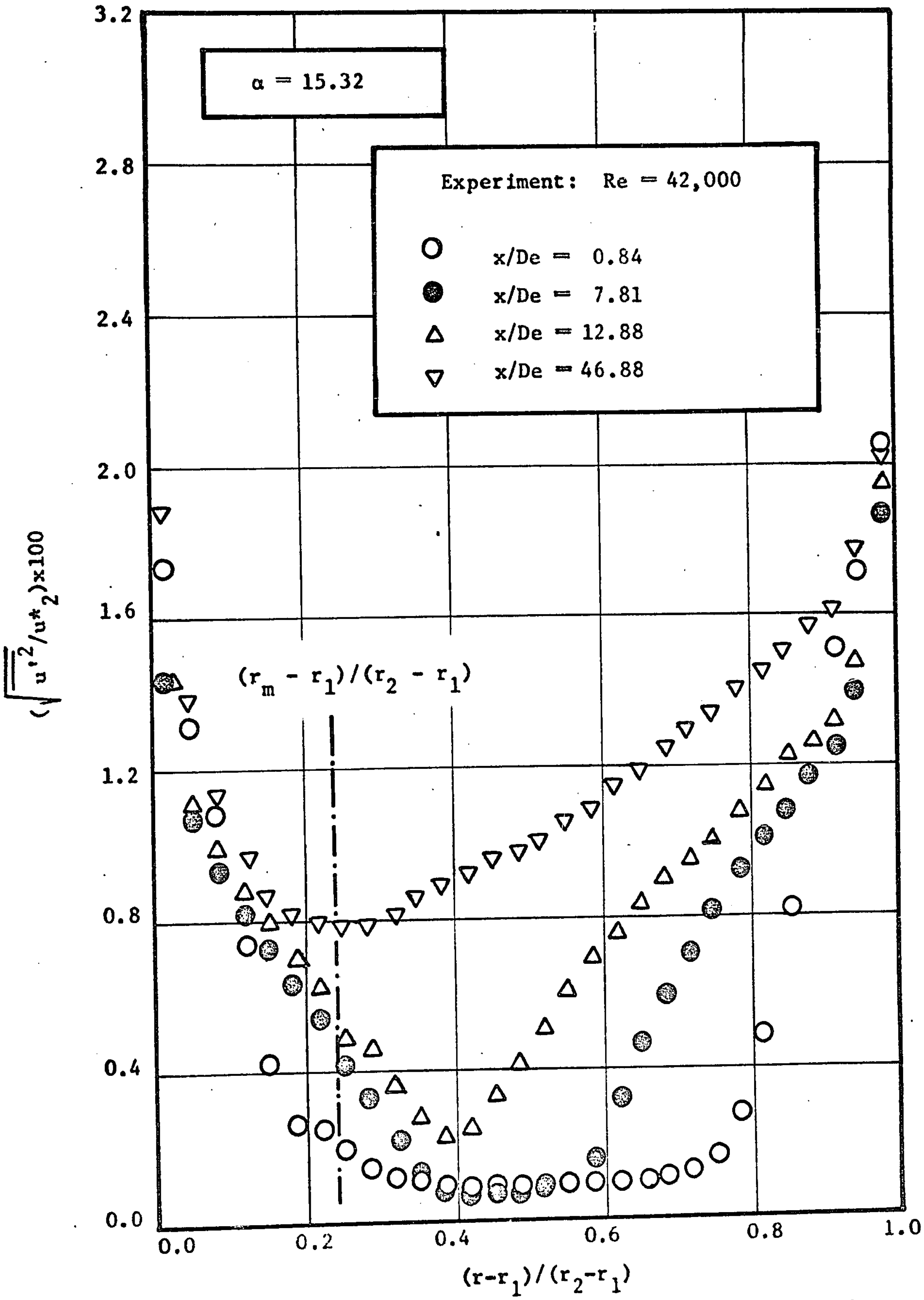

Fig. 5.41 Axial Turbulence Intensities, Entrance Regions.

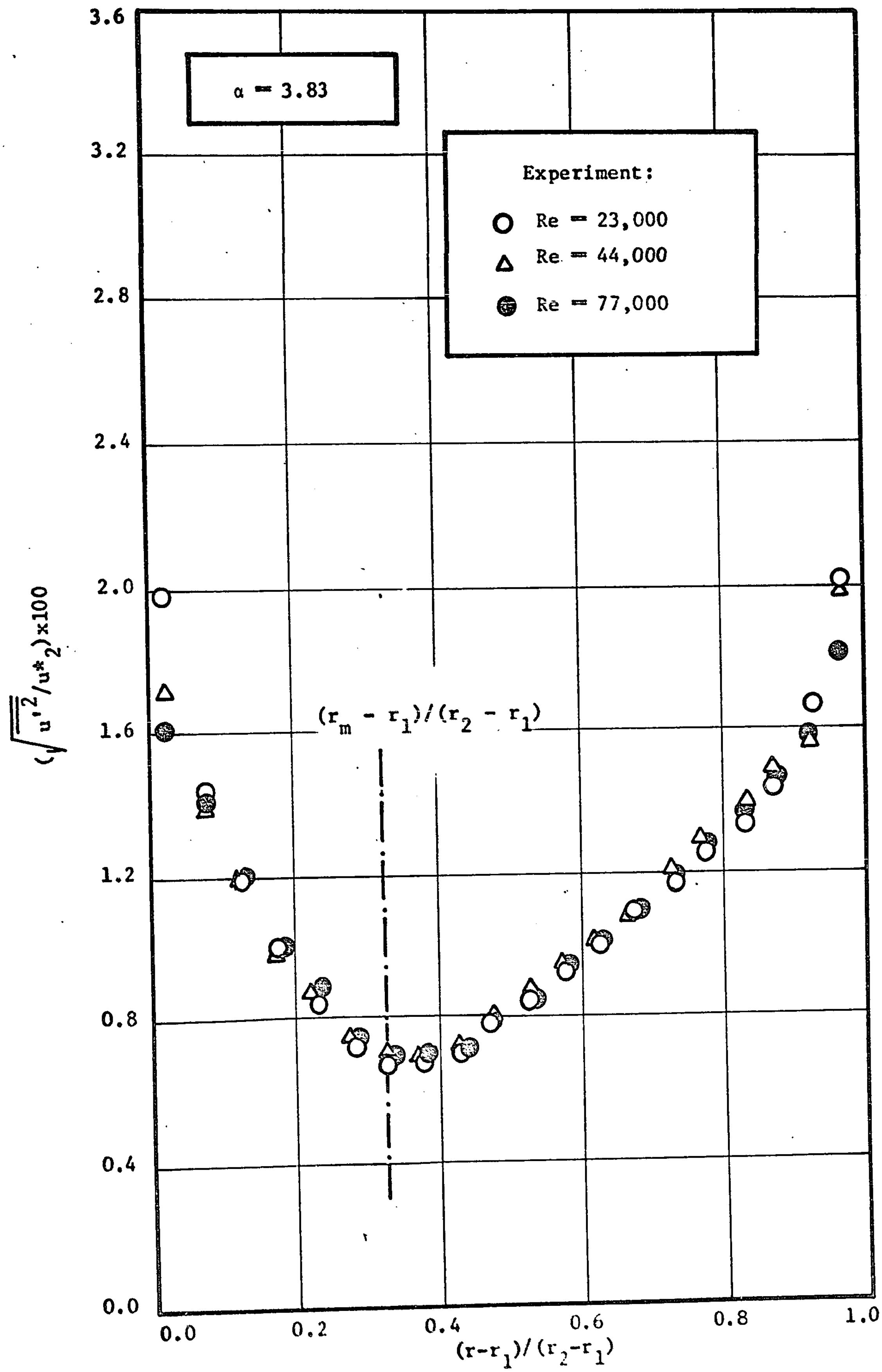

Fig. 5.42 Axial Turbulence Intensities, Fully Developed Regions.

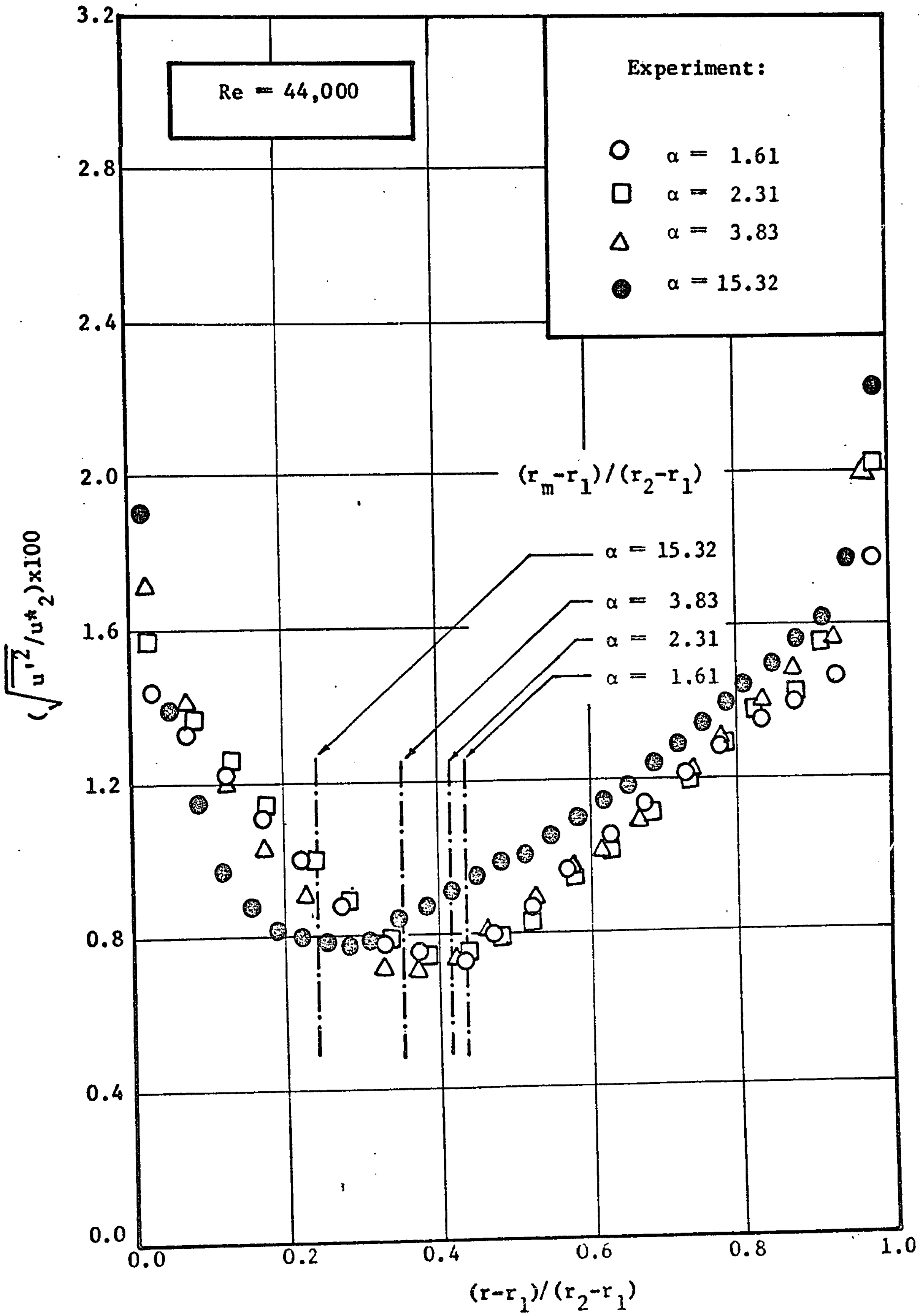

Fig. 5.43 Axial Turbulence Intensities, Fully Developed Regions.

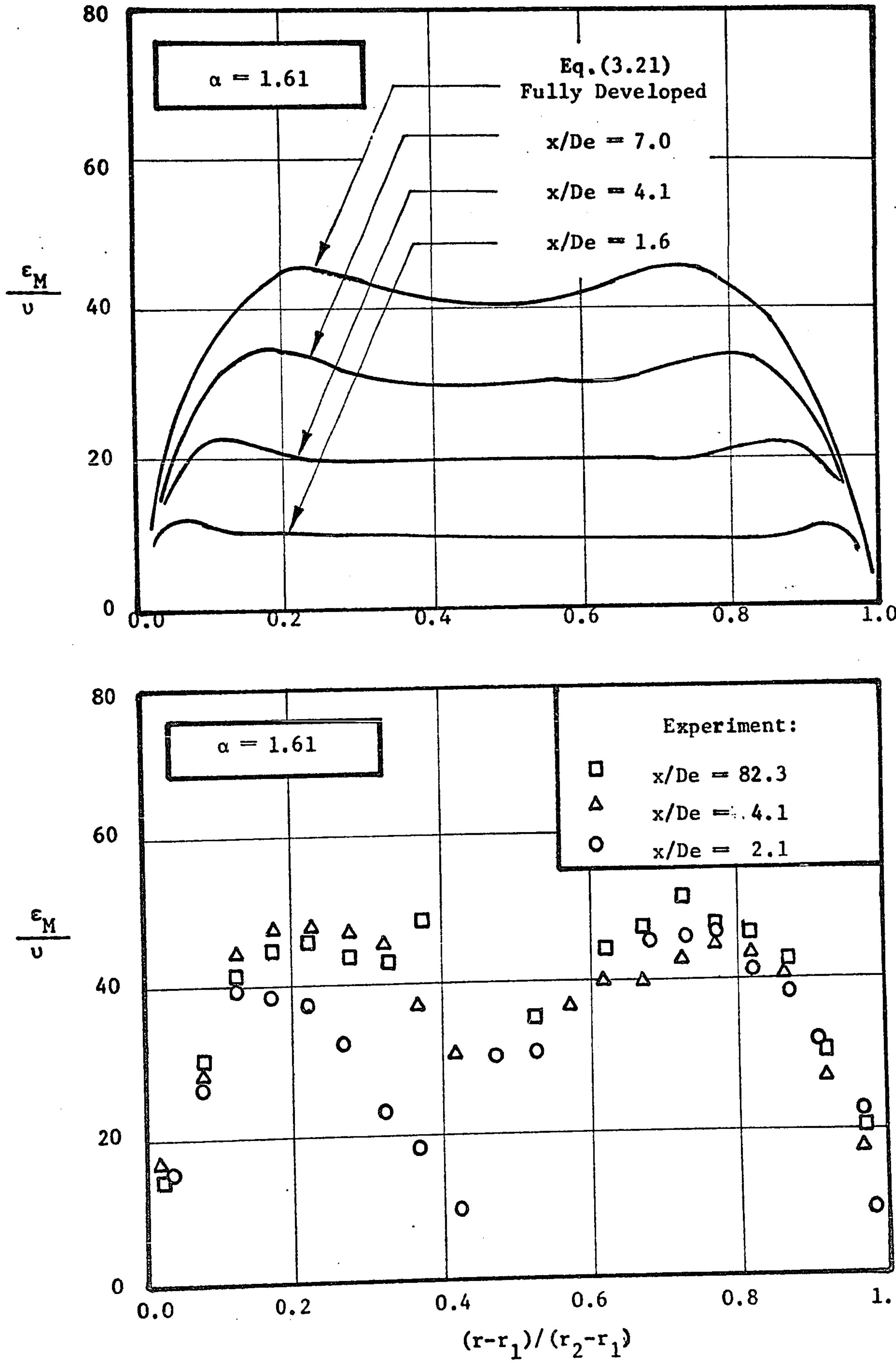

Fig. 5.44 Predicted and Experimental Eddy Diffusivity for Momentum, Entrance Regions, Re = 44,000.

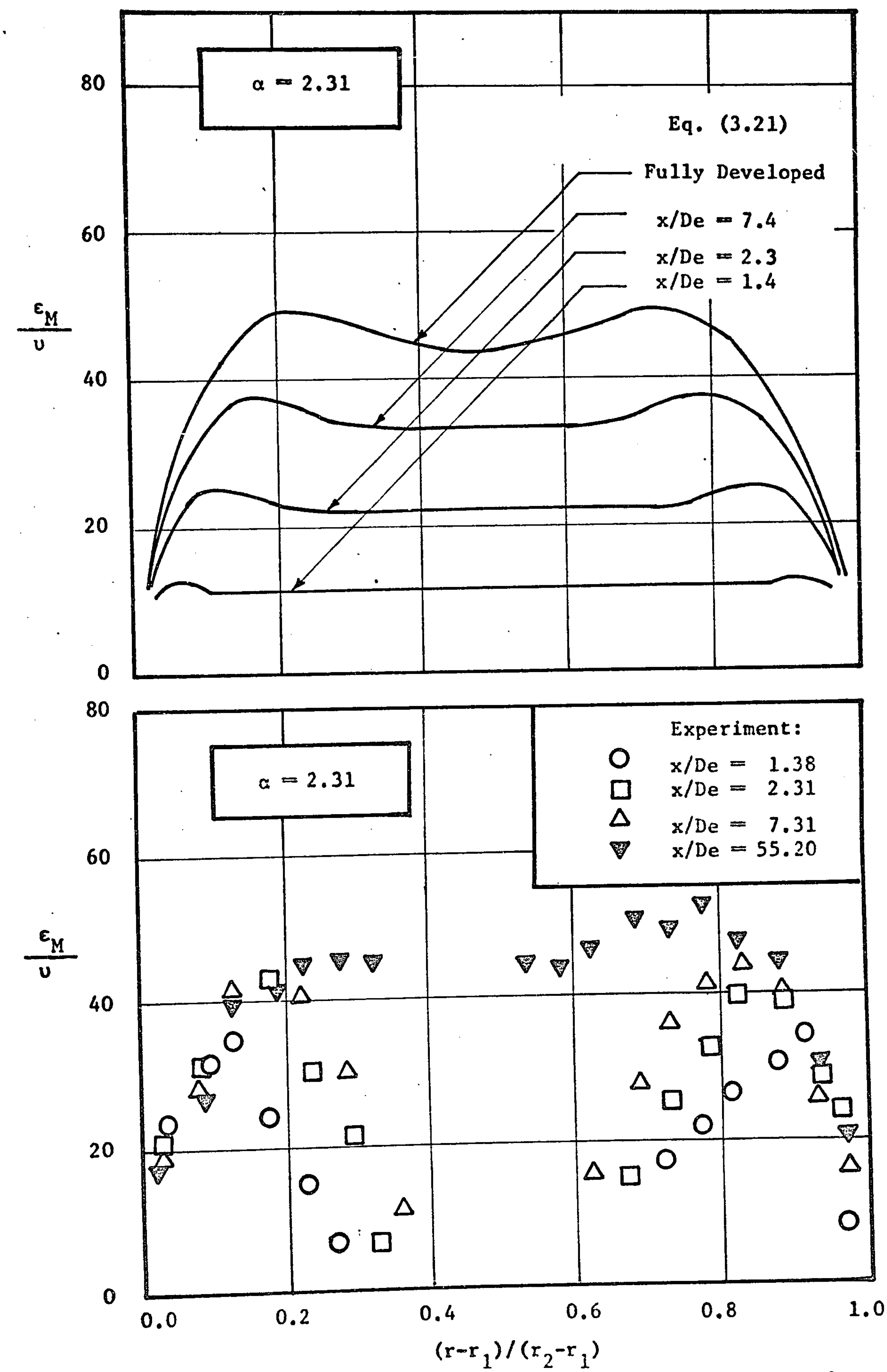

Fig. 5.45 Predicted and Experimental Eddy Diffusivity for Momentum, Entrance Regions, Re = 44,000.

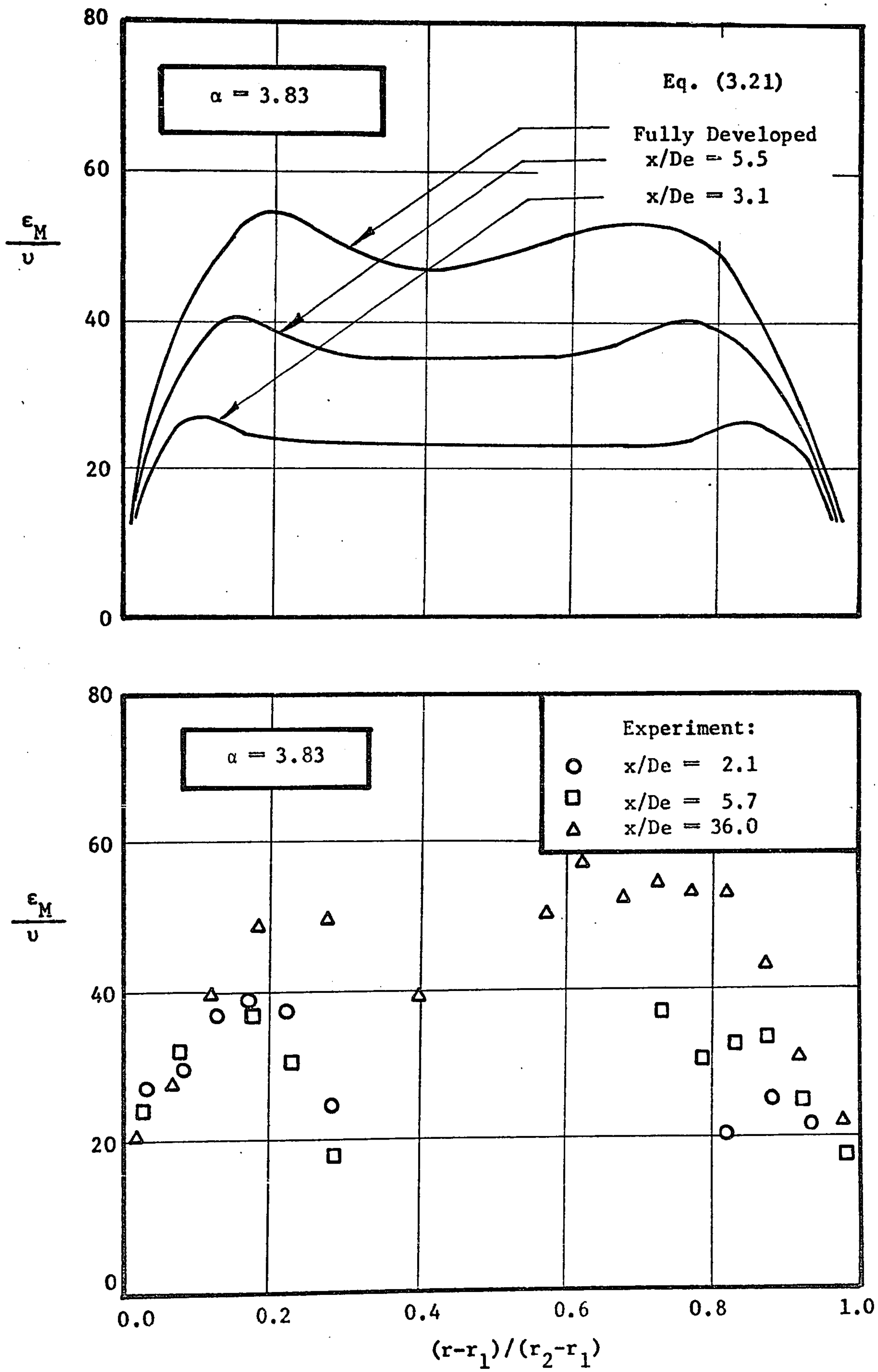

Fig. 5.46 Predicted and Experimental Eddy Diffusivity for Momentum, Entrance Regions, Re = 44,000.

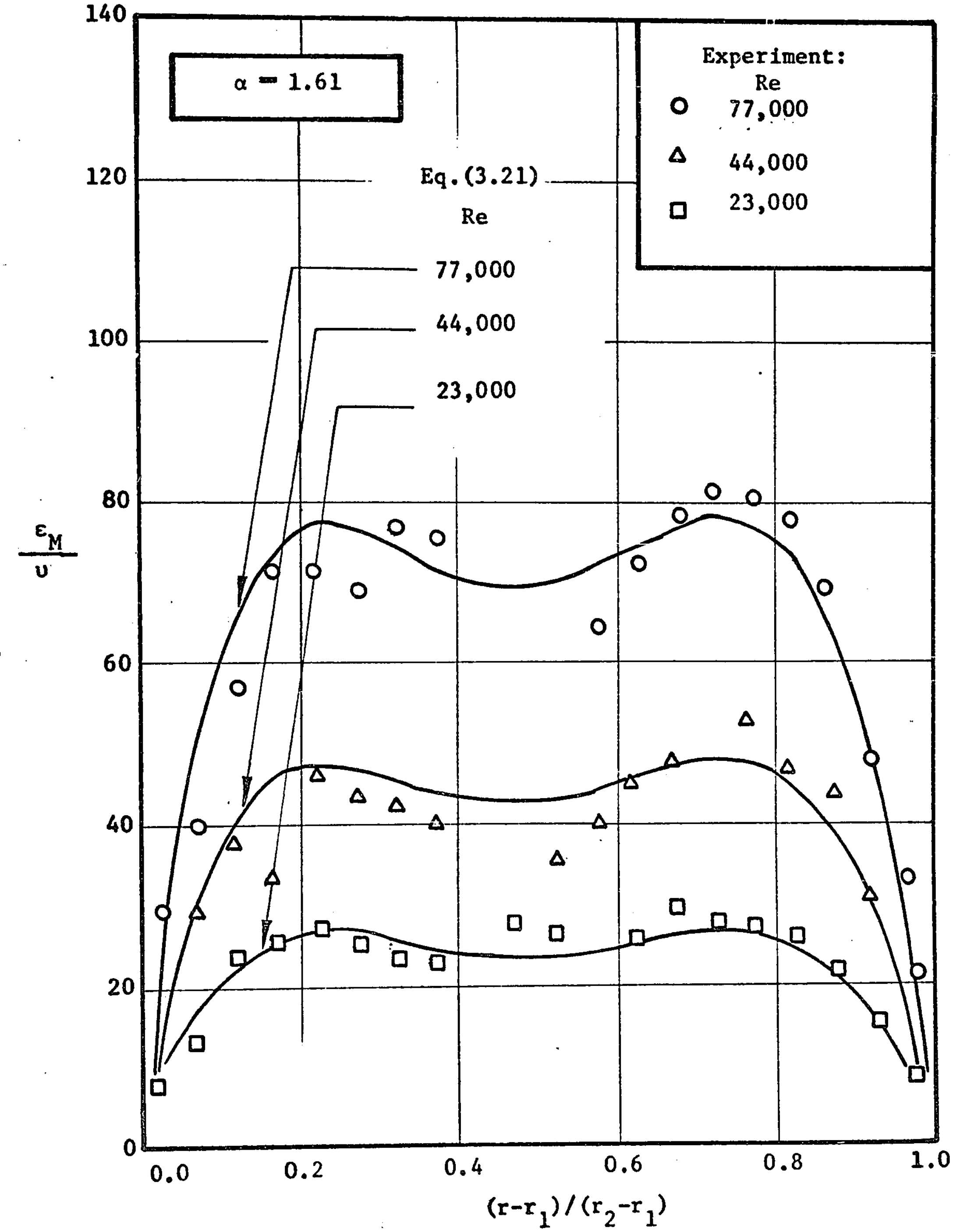

Fig. 5.47 Comparison of Experimental Results with Predicted Eddy Diffusivity, Fully Developed.

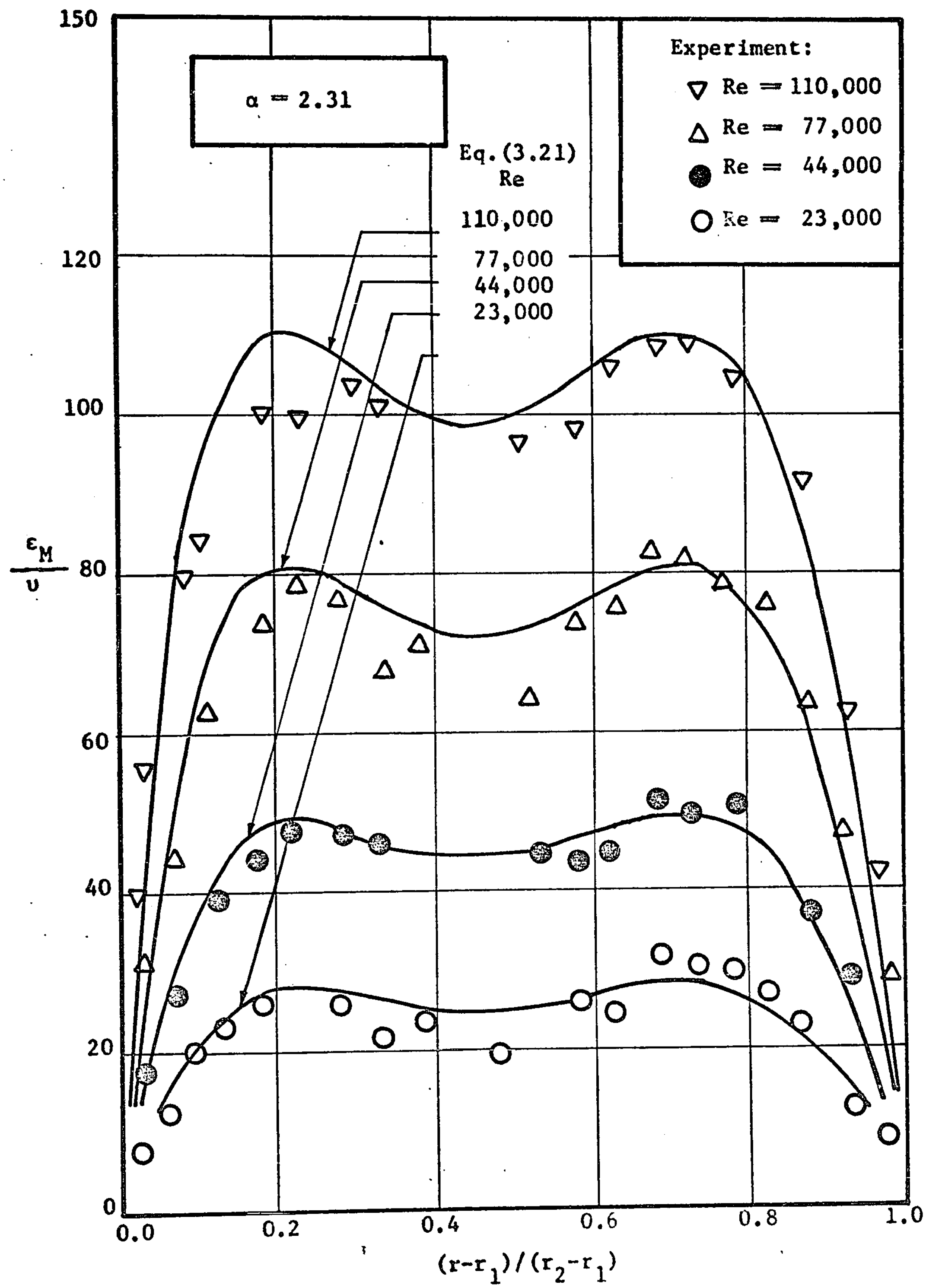

Fig. 5.48 Comparison of Experimental Results with Predicted Eddy Diffusivity, Fully Developed.

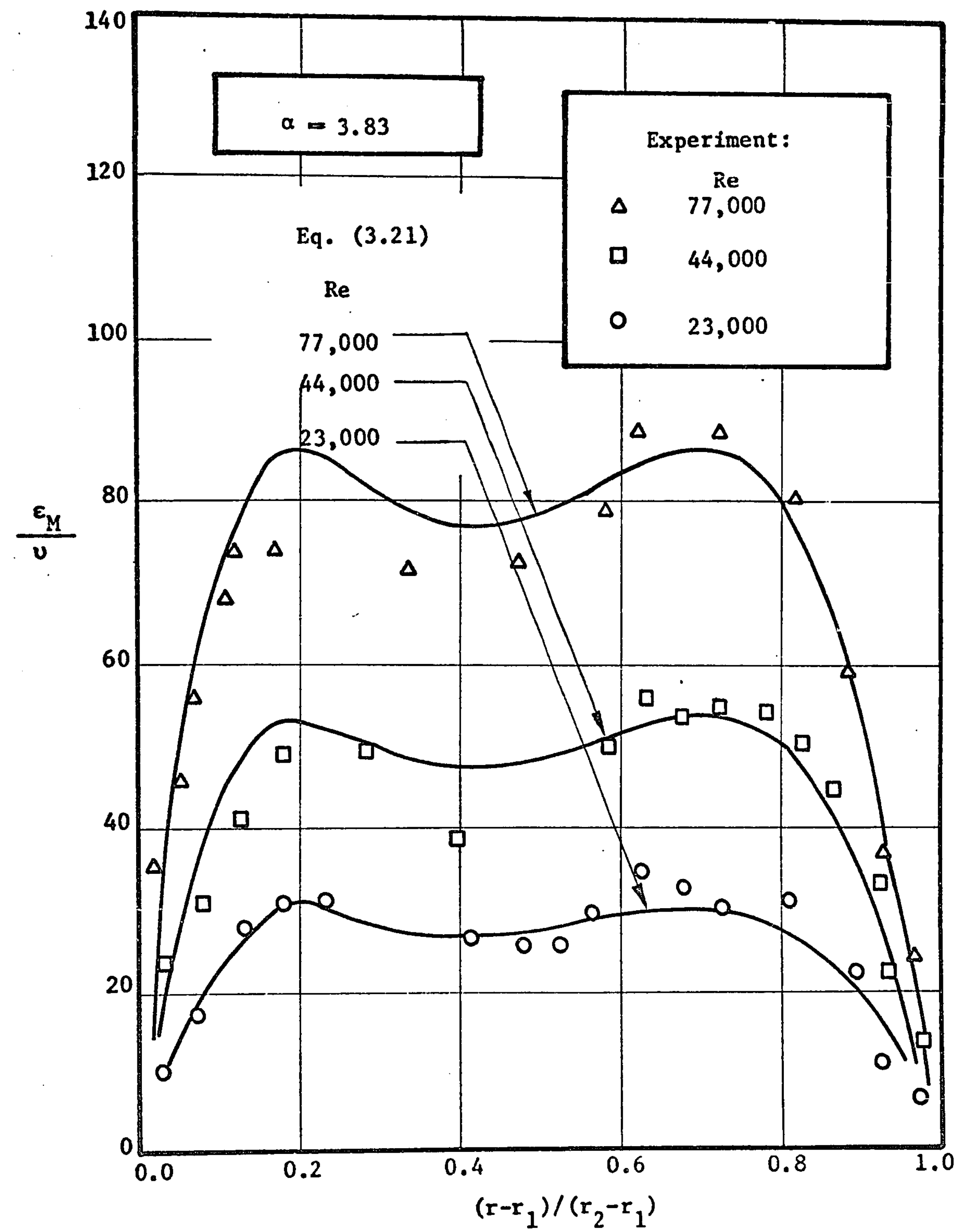

Fig. 5.49 Compaison of Experimental Results with Predicted Eddy Diffusivity, Fully Developed.

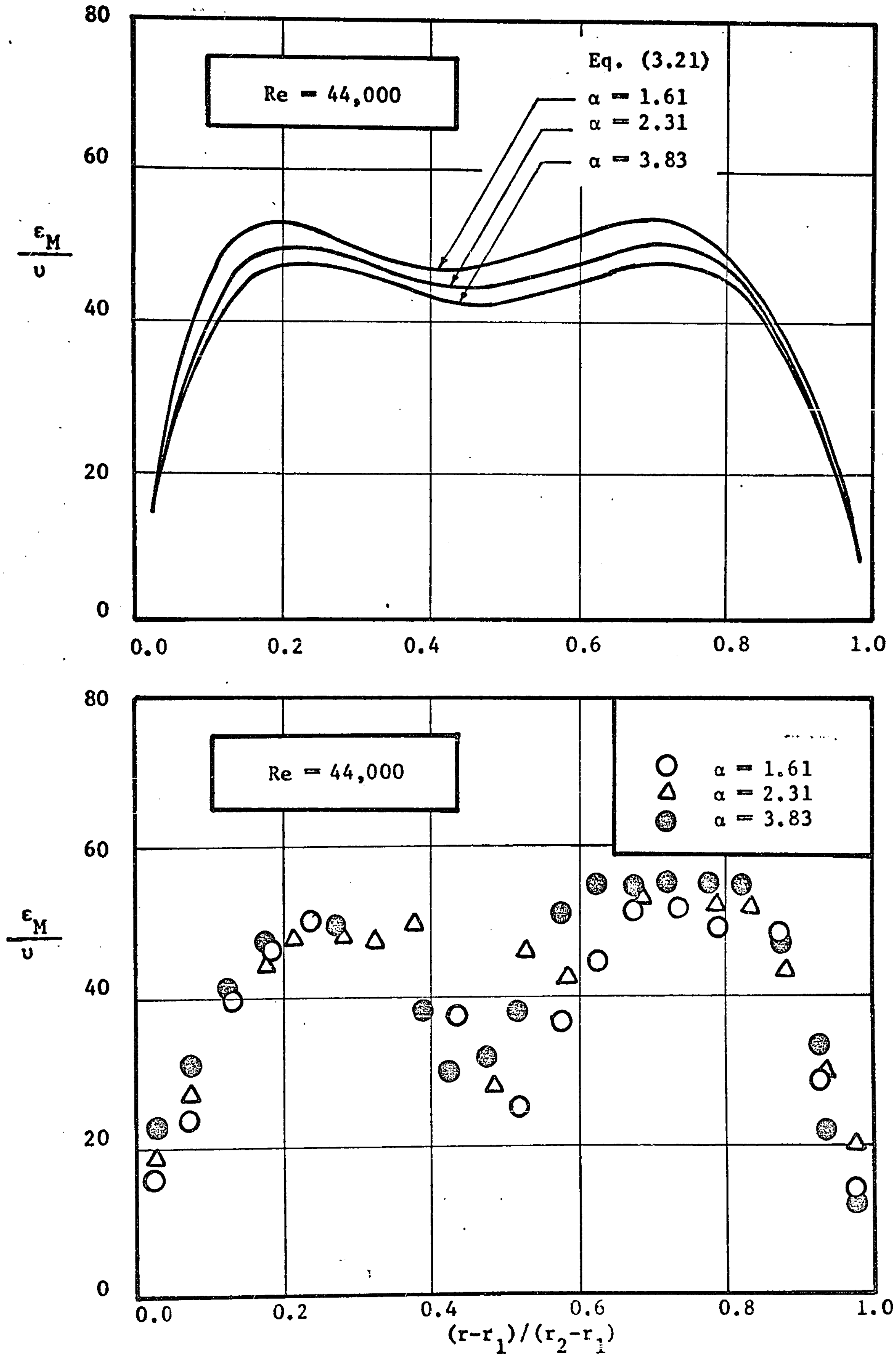

Fig. 5.50 Comparison of Experimental Results with Predicted Eddy Diffusivity, Fully Developed.

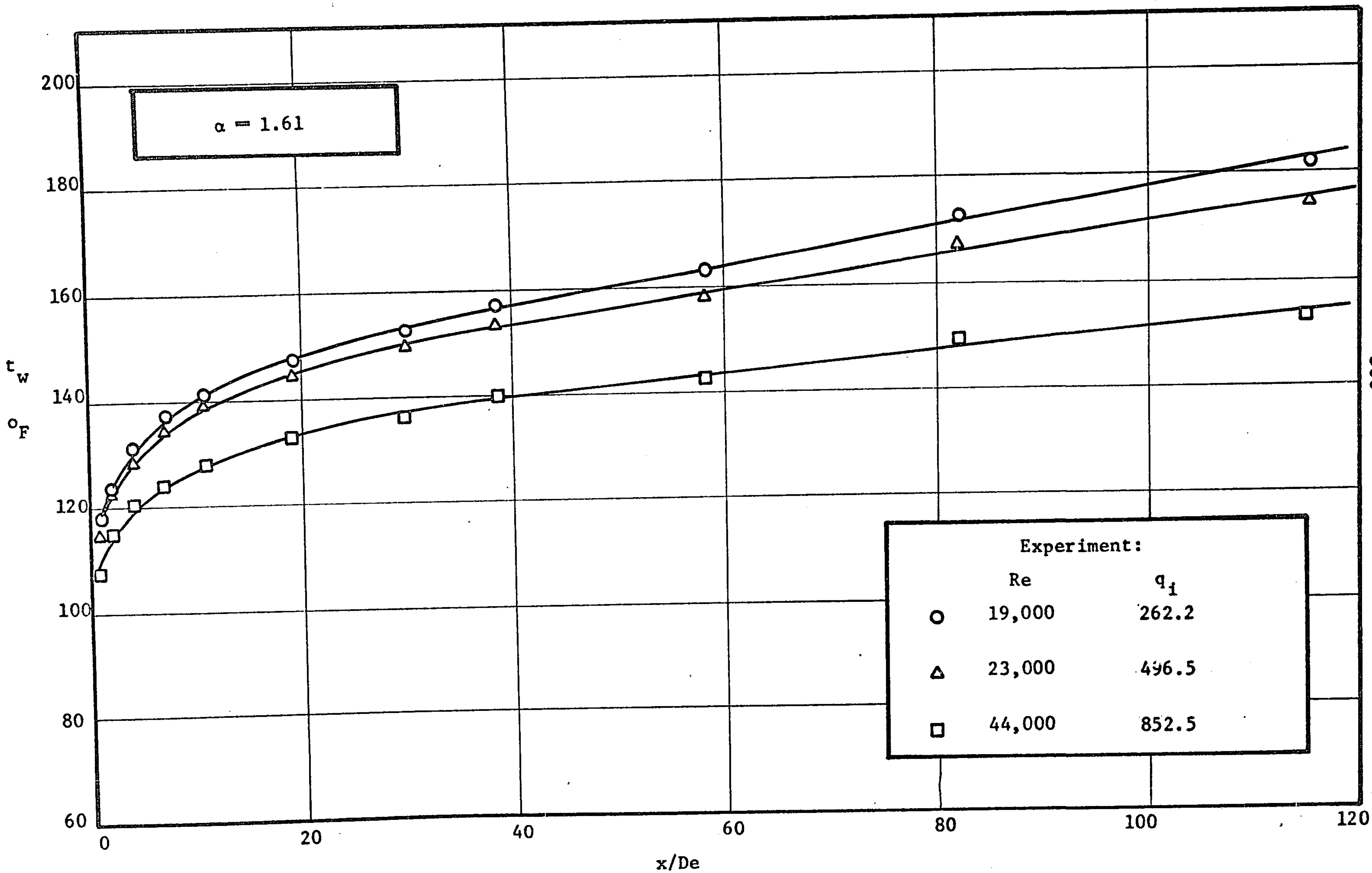

Fig. 5.51 Axial Wall Temperature Distribution, Constant Heat Flux at the Inner Core Tube, Pr = 0.71.

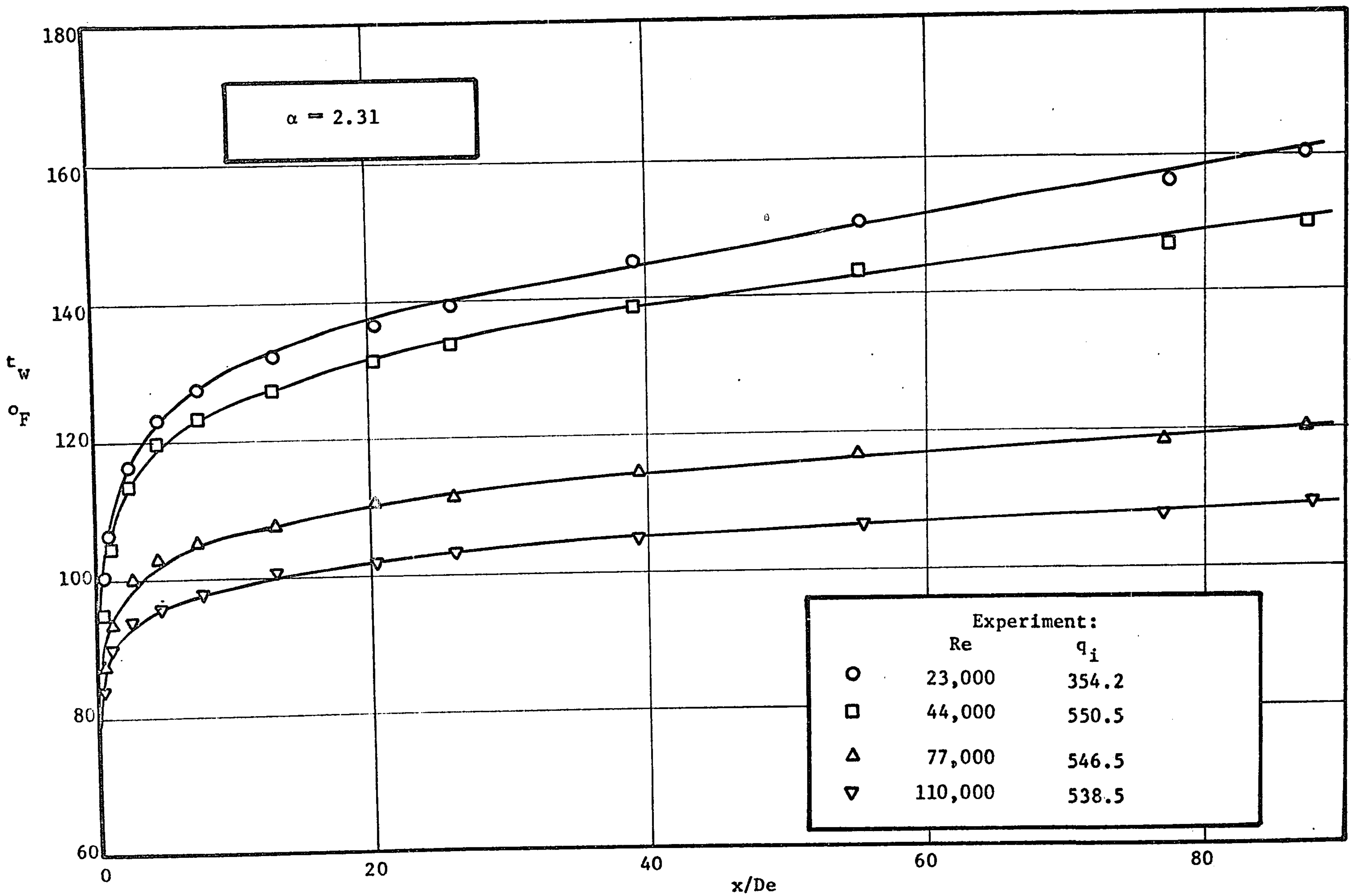

Fig. 5.52 Axial Wall Temperature Distribution, Constant Heat Flux at the Inner Core Tube, Pr = 0.71.

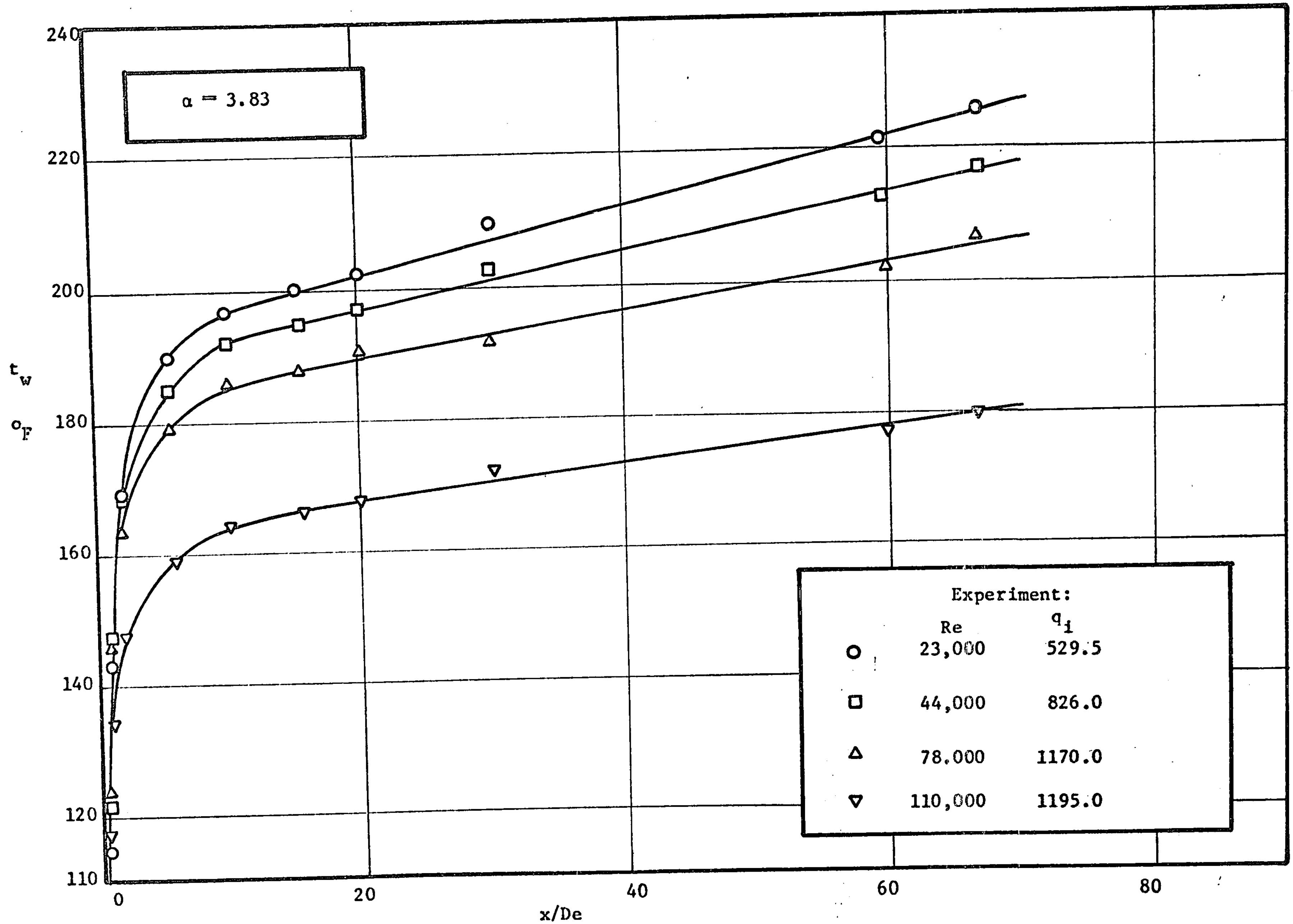

Fig. 5.53 Axial Wall Temperature Distribution, Constant Heat Flux at the Inner Core Tube, Pr = 0.71.

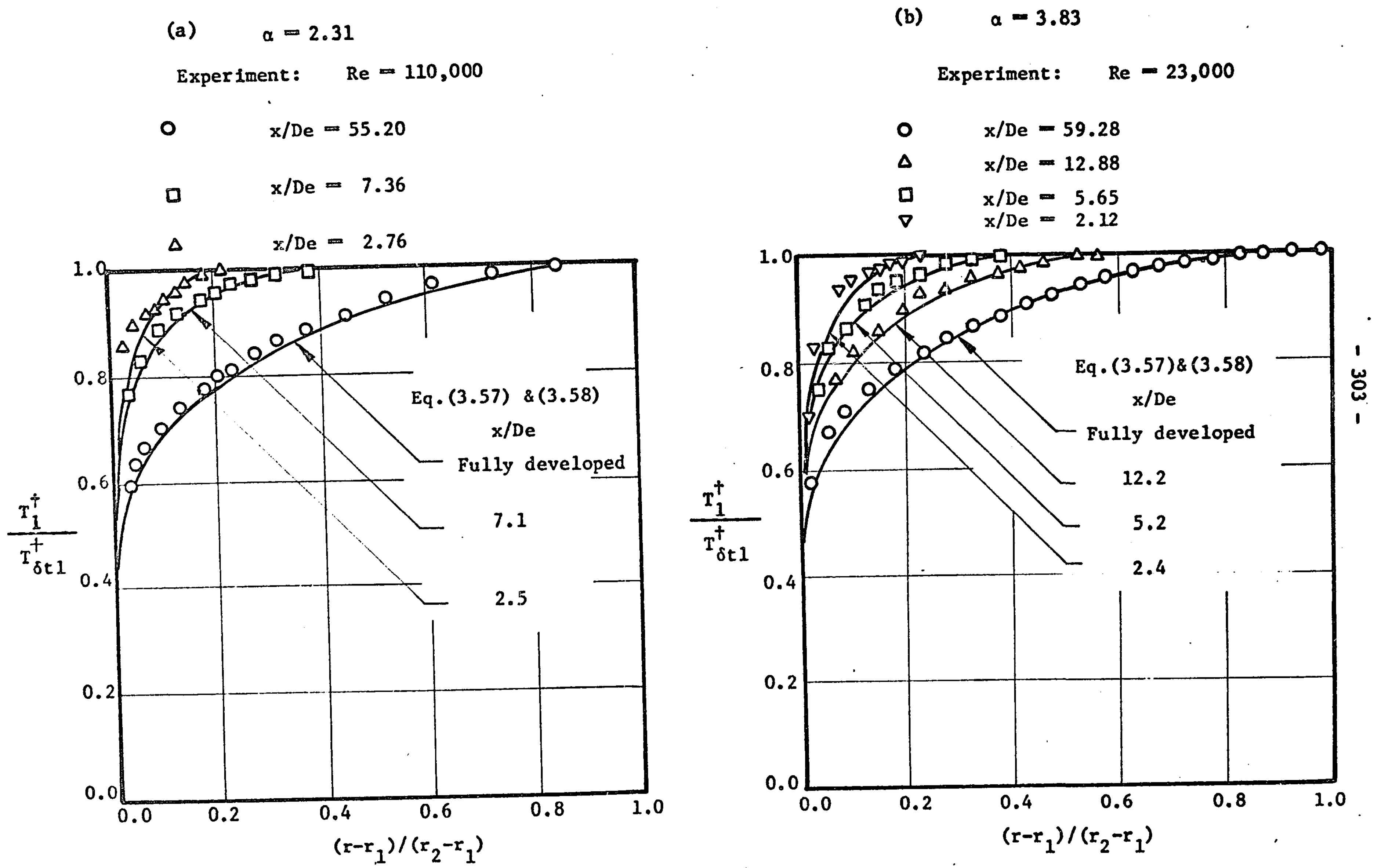

Fig. 5.54 Temperature Profiles, Entrance Regions, pr = 0.71.

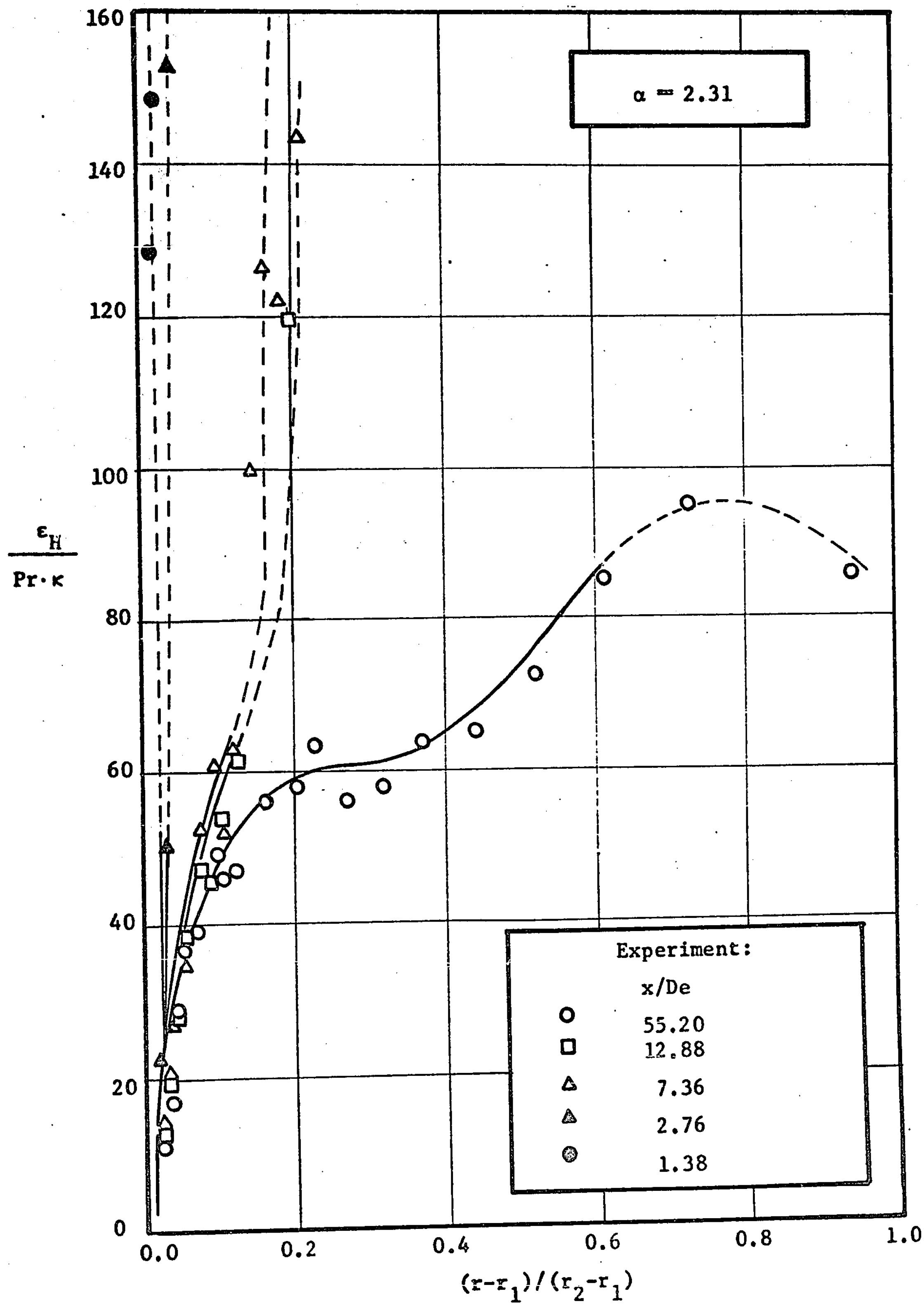

Fig. 5.55 Experimental Eddy Diffusivity for Heat, Entrance Region, Re = 44,000, Pr = 0.71.

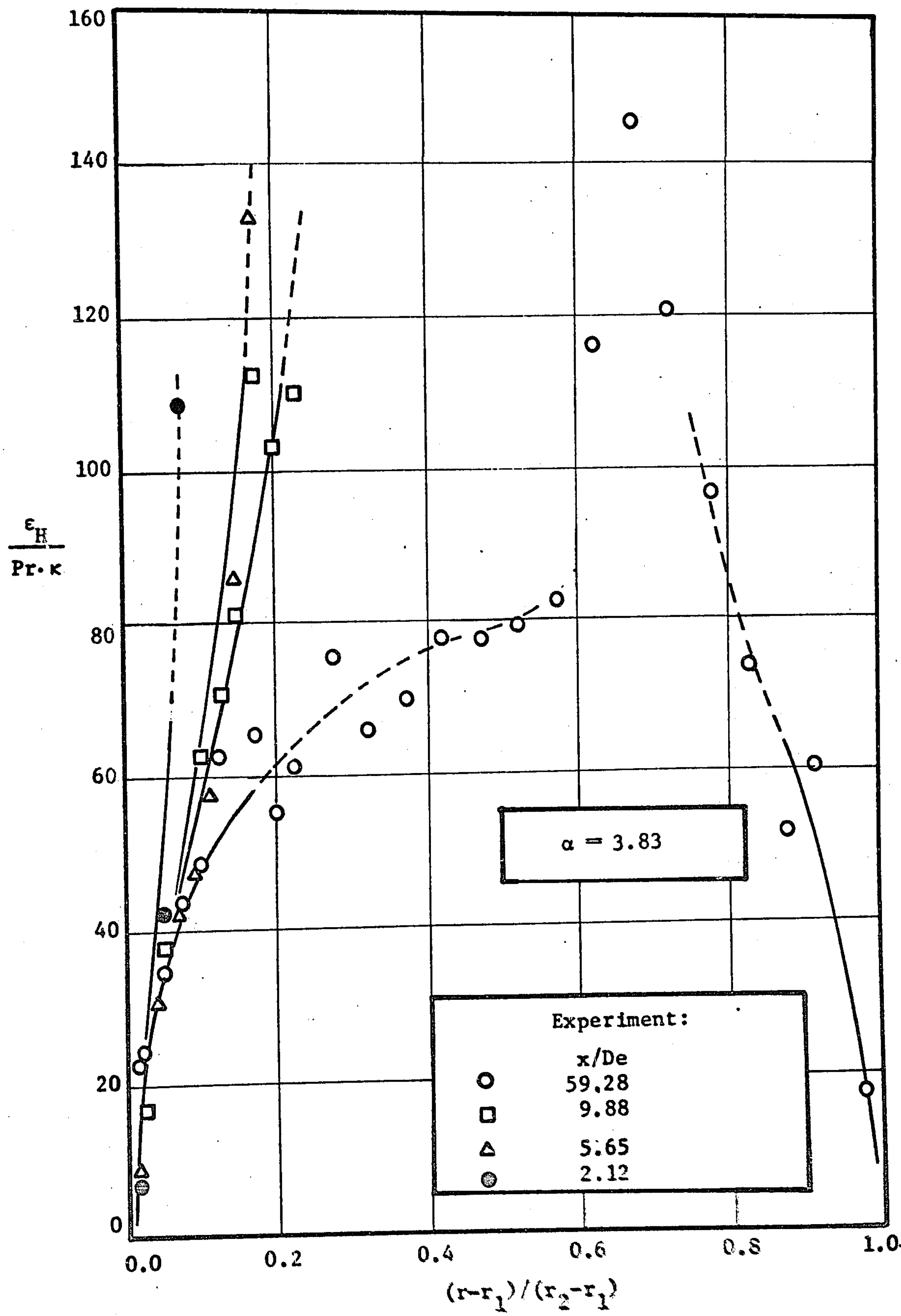

Fig. 5.56 Experimental Eddy Diffusivity for Heat, Entrance Region, Re = 44,000, Pr = 0.71.

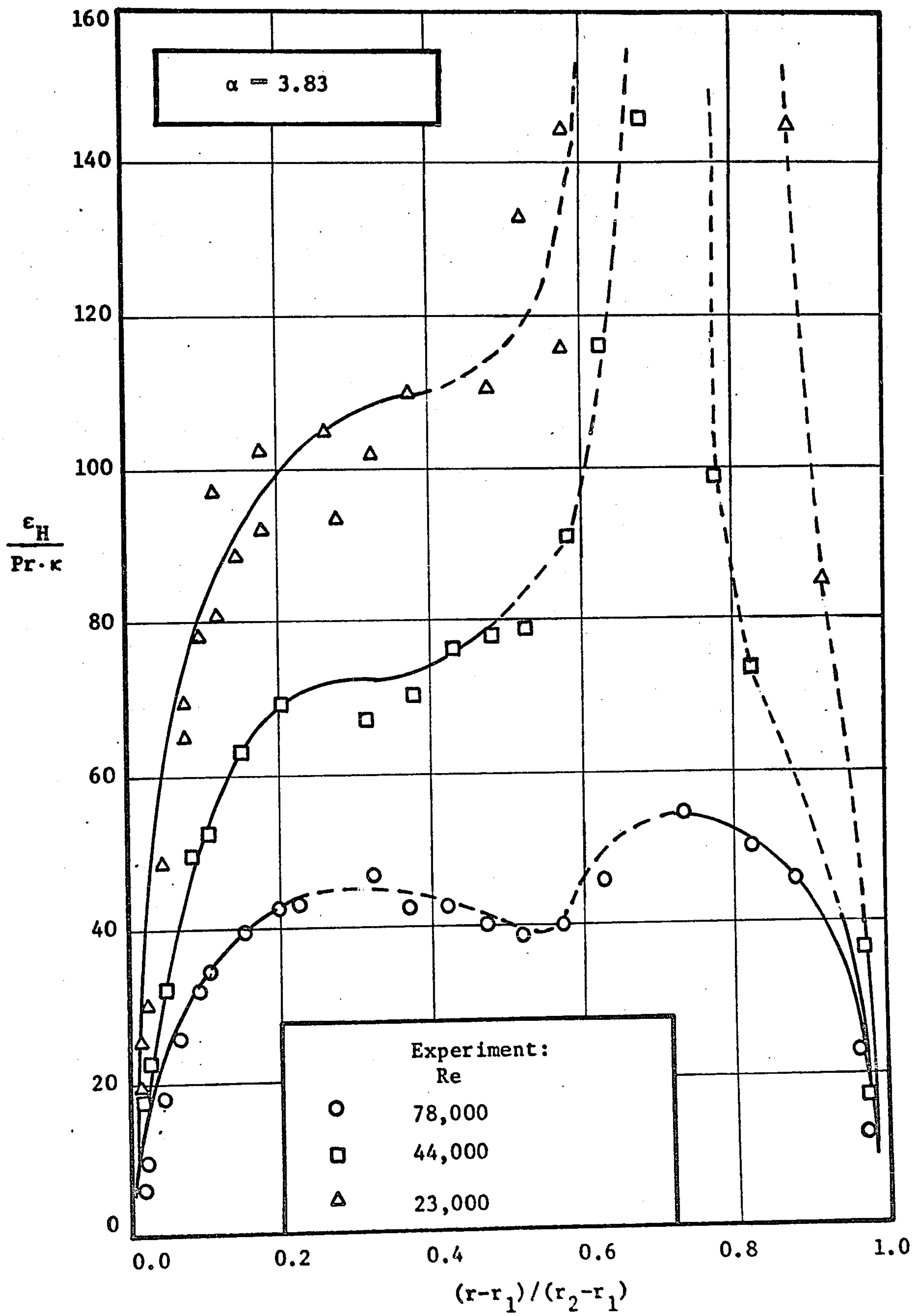

Fig. 5.57 Experimental Eddy Diffusivity for Heat, Fully Developed Region, Pr = 0.71.

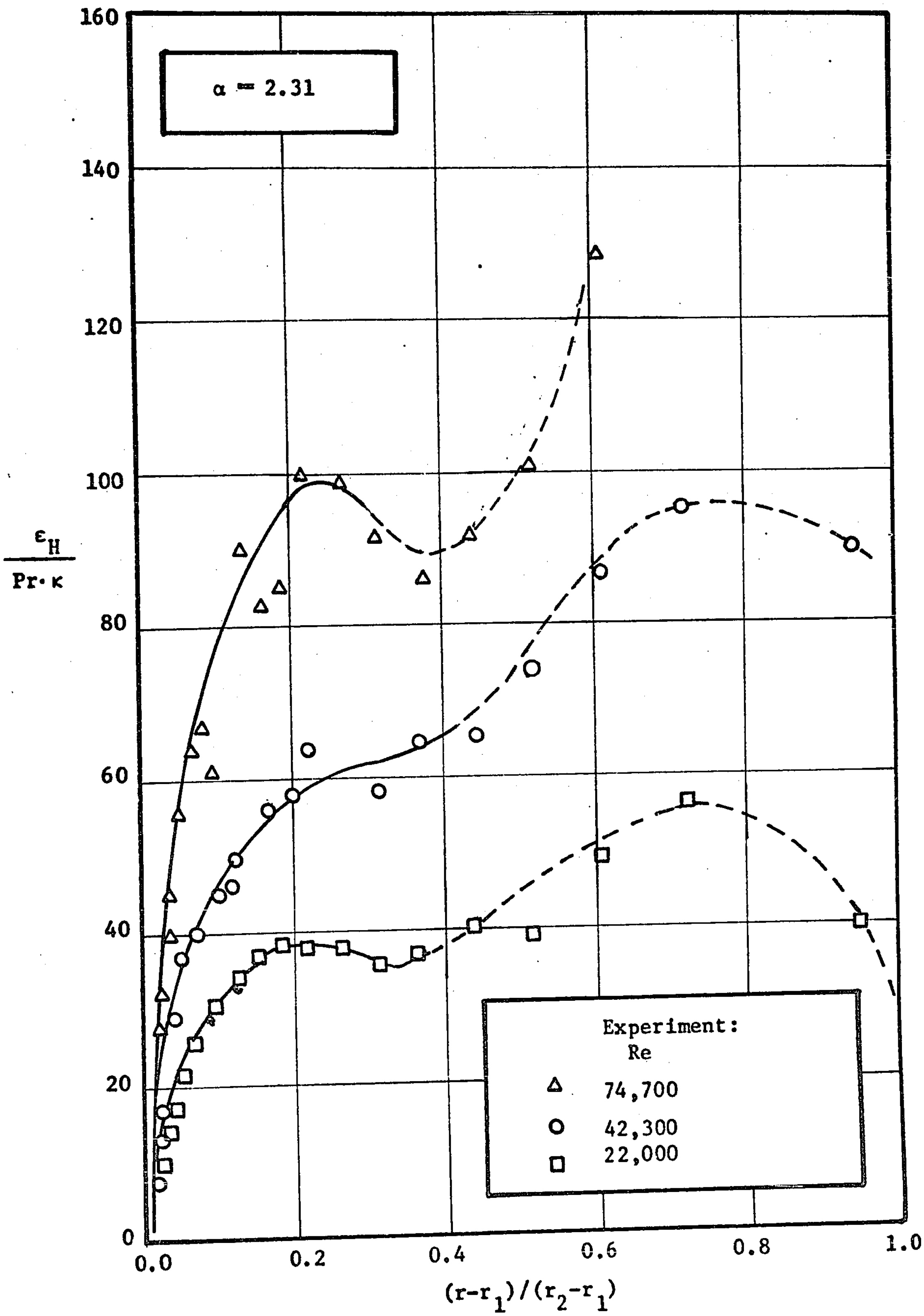

Fig. 5.58 Experimental Eddy Diffusivity for Heat, Fully Developed Region, Pr = 0.71.

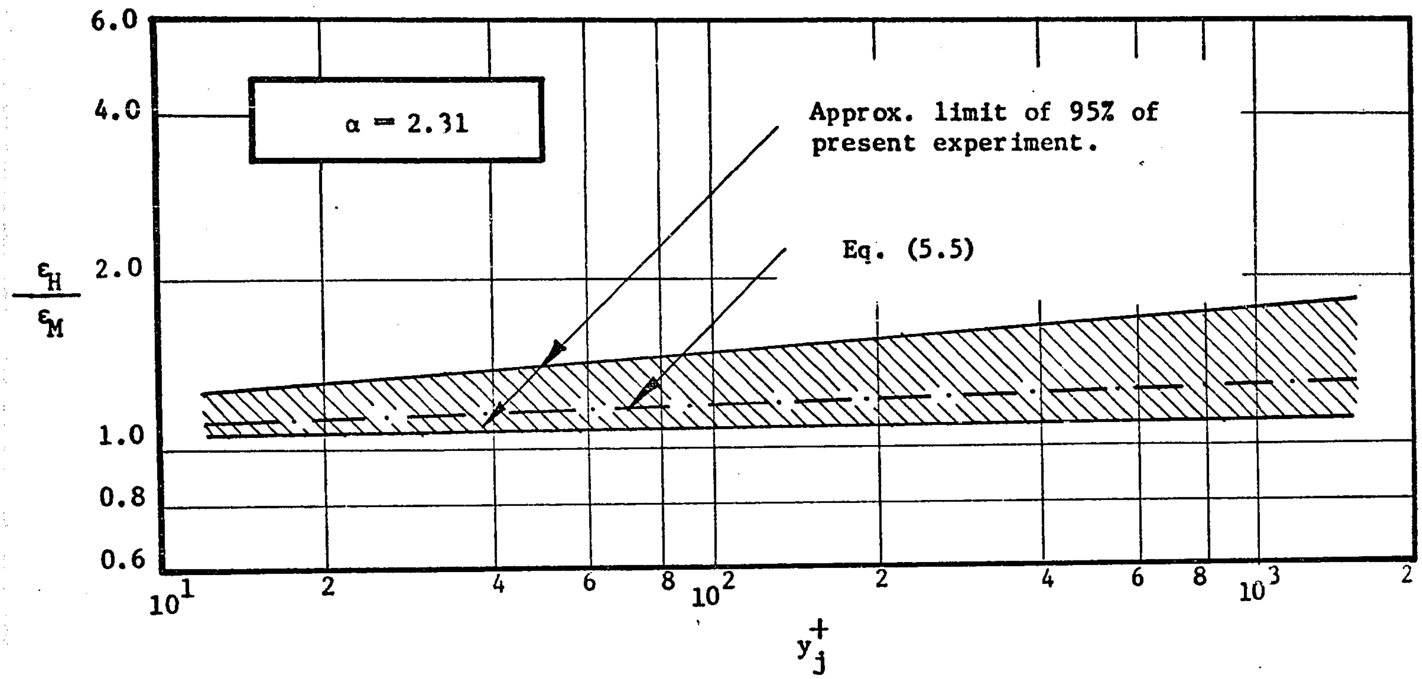

(a)

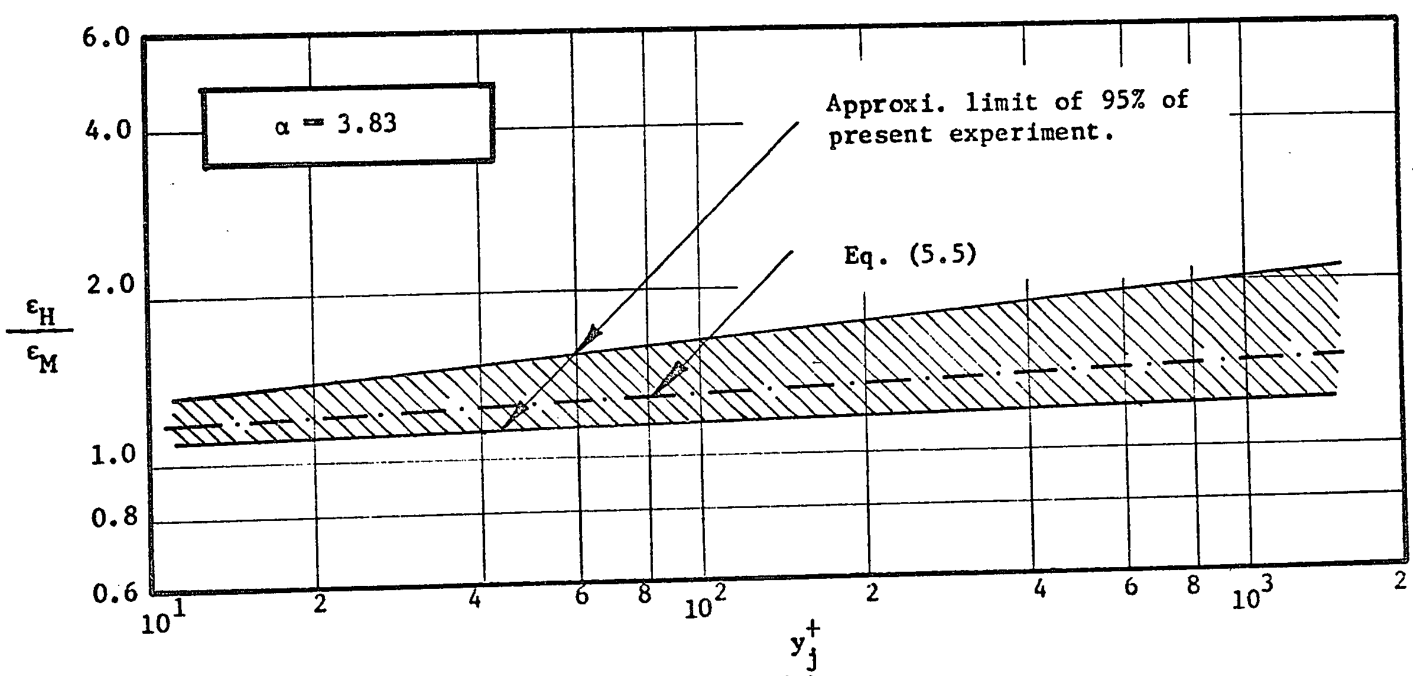

(b)

Fig. 5.59 Turbulent Prandtl Numbers, $\varepsilon_H/\varepsilon_M$, Fully Developed Regions, Constant Heat Flux at Inner Core Tube, Concentric Annuli, Pr = 0.71.

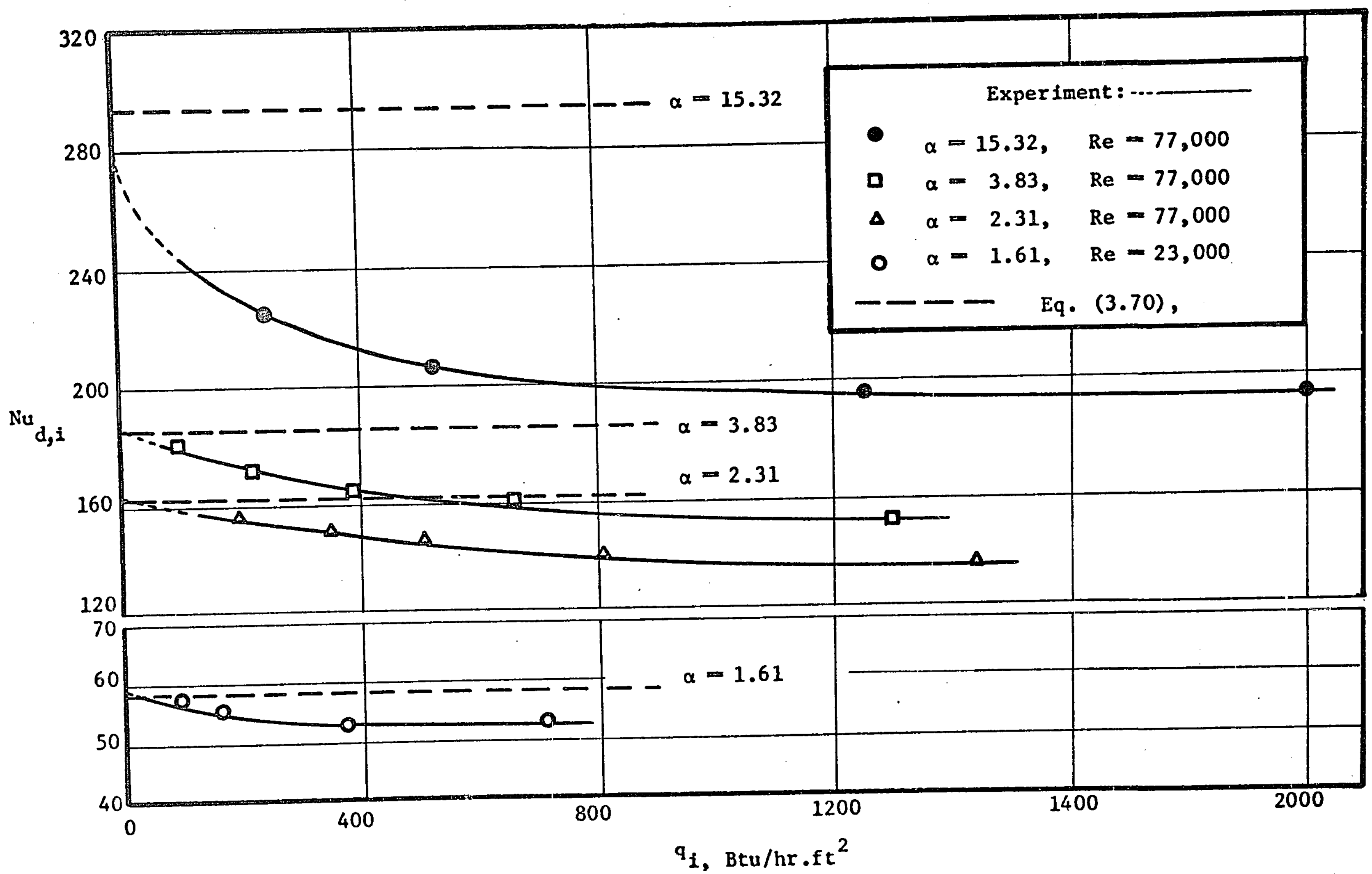

Fig. 5.60 Effect of Heat Flux on Nusselt Number, Fully Developed Region, Pr = 0.71.

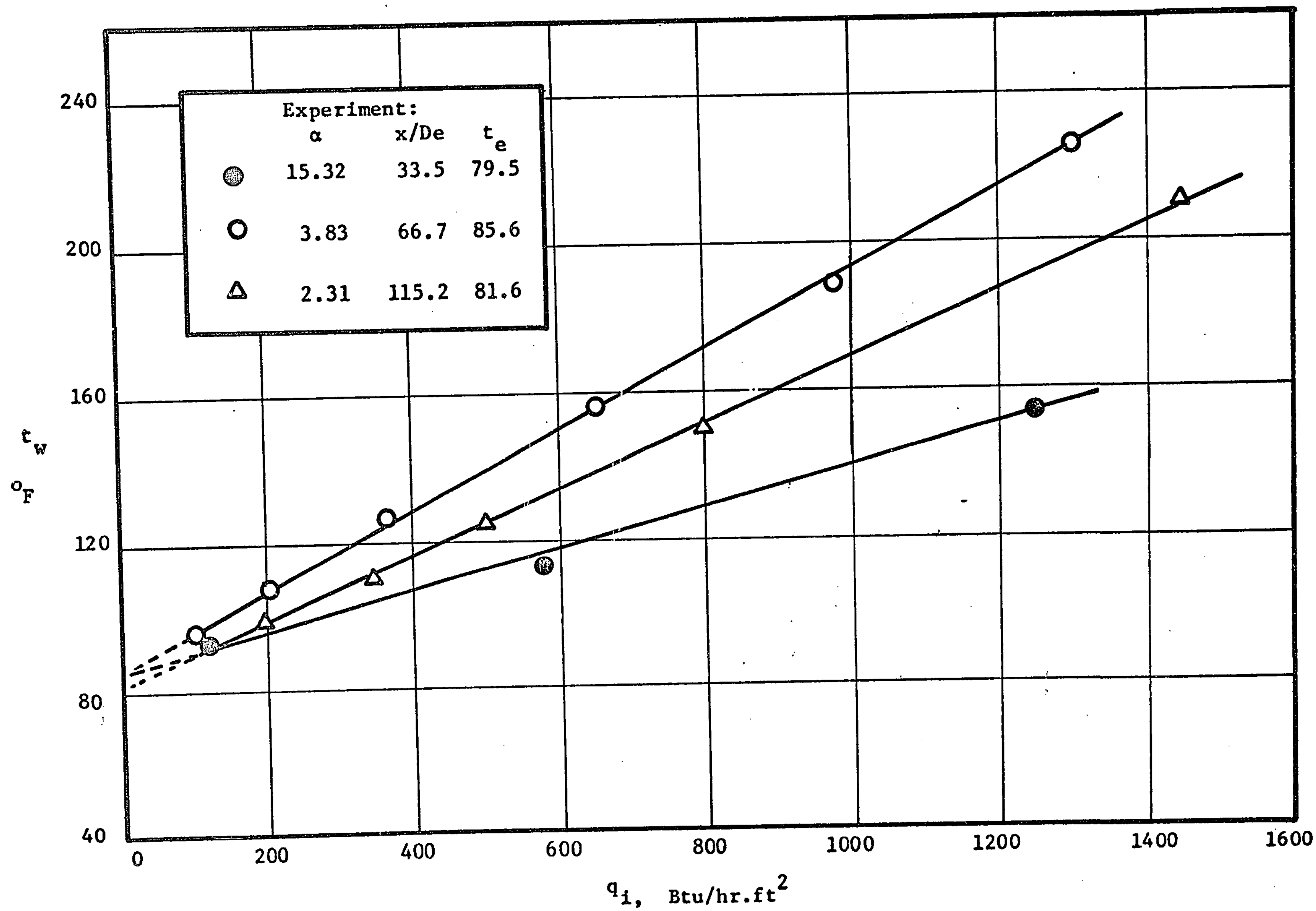

Fig. 5.61 Effect of Heat Flux on Wall Temperature, Re = 77,000.

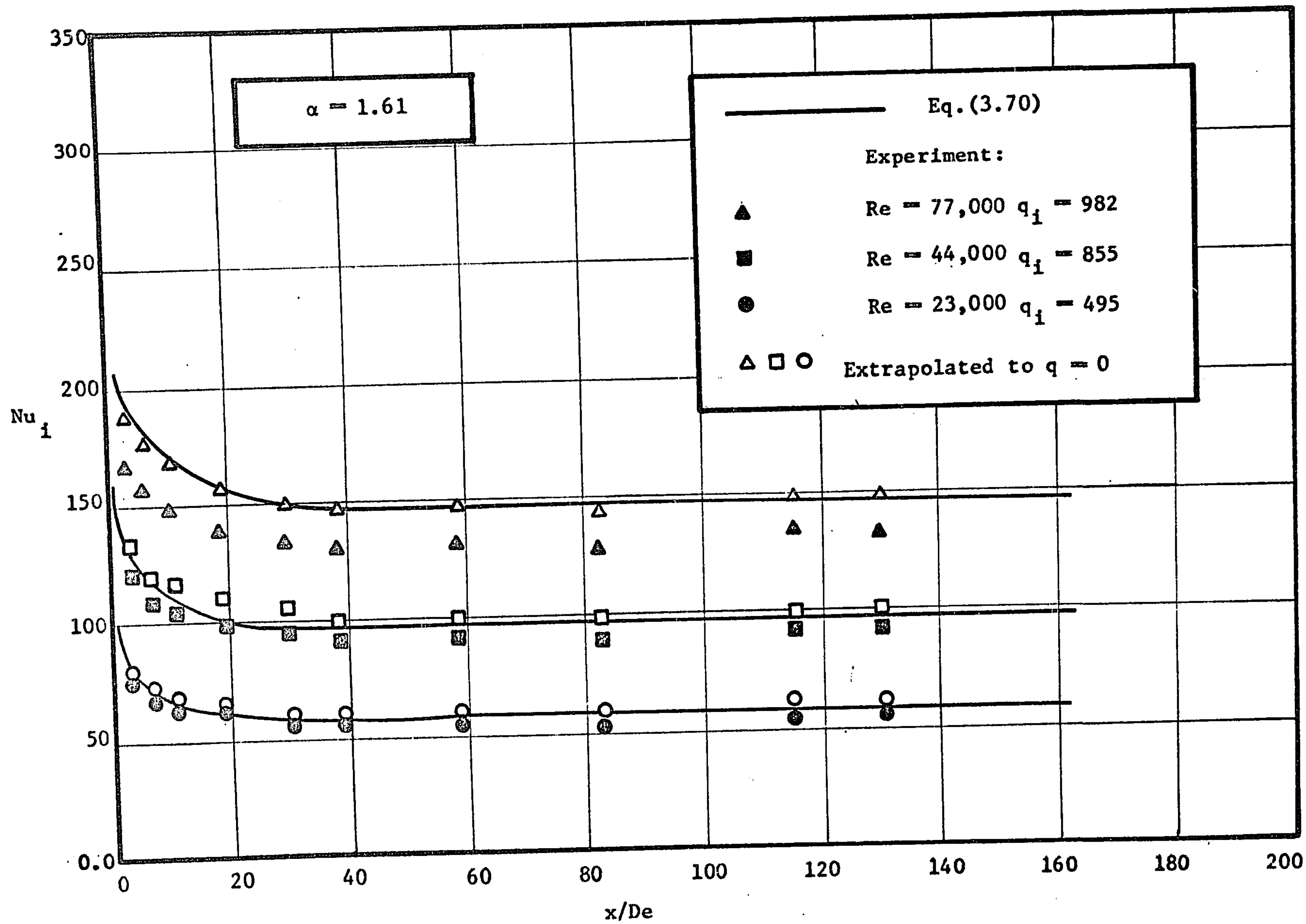

Fig. 5.62 Comparison between Prediction and Experiment, Entrance Region Nusselt Number, Pr = 0.71.

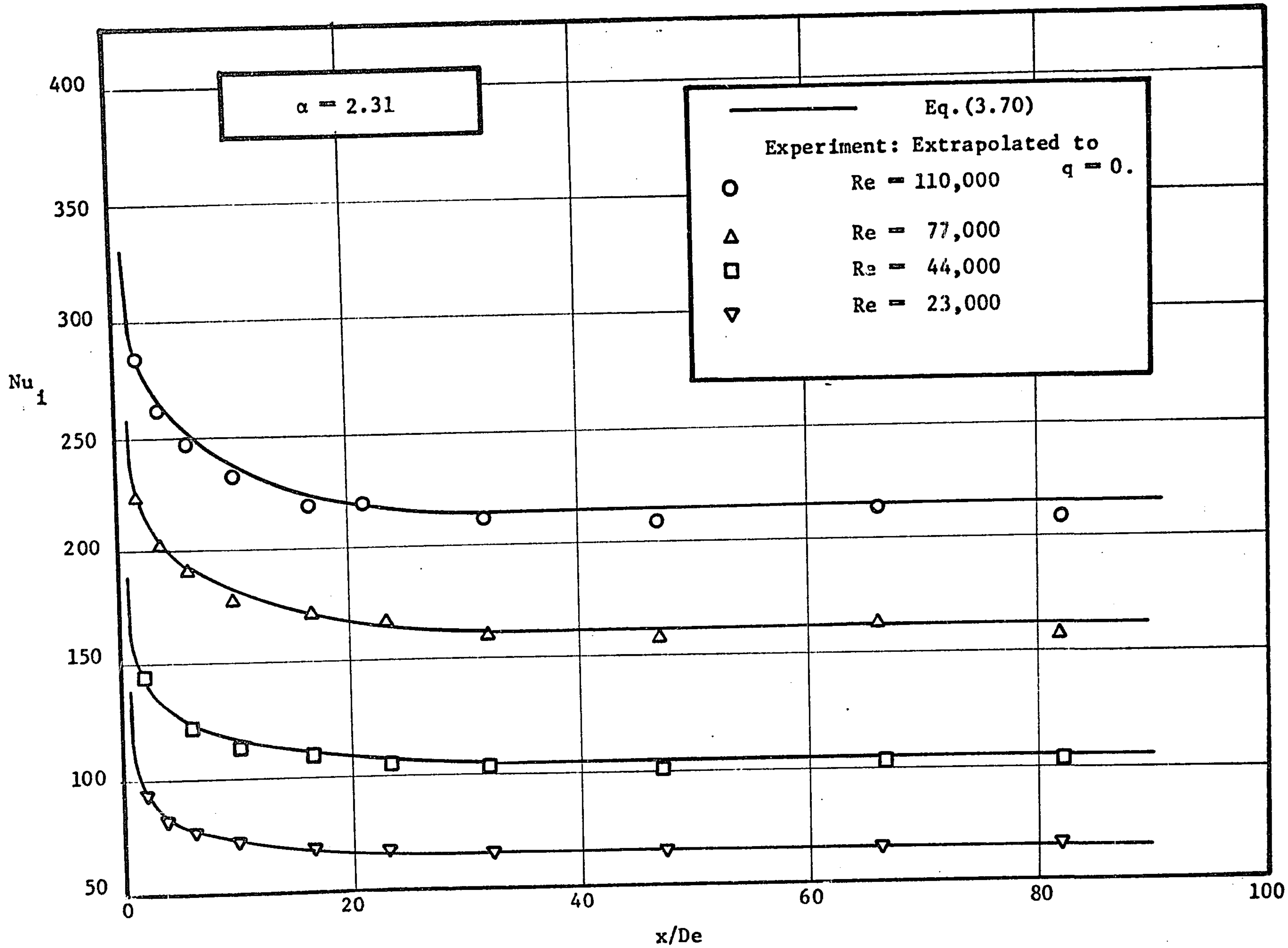

Fig. 5.63 Comparison between Prediction and Experiment, Entrance Region Nusselt Number, Pr = 0.71.

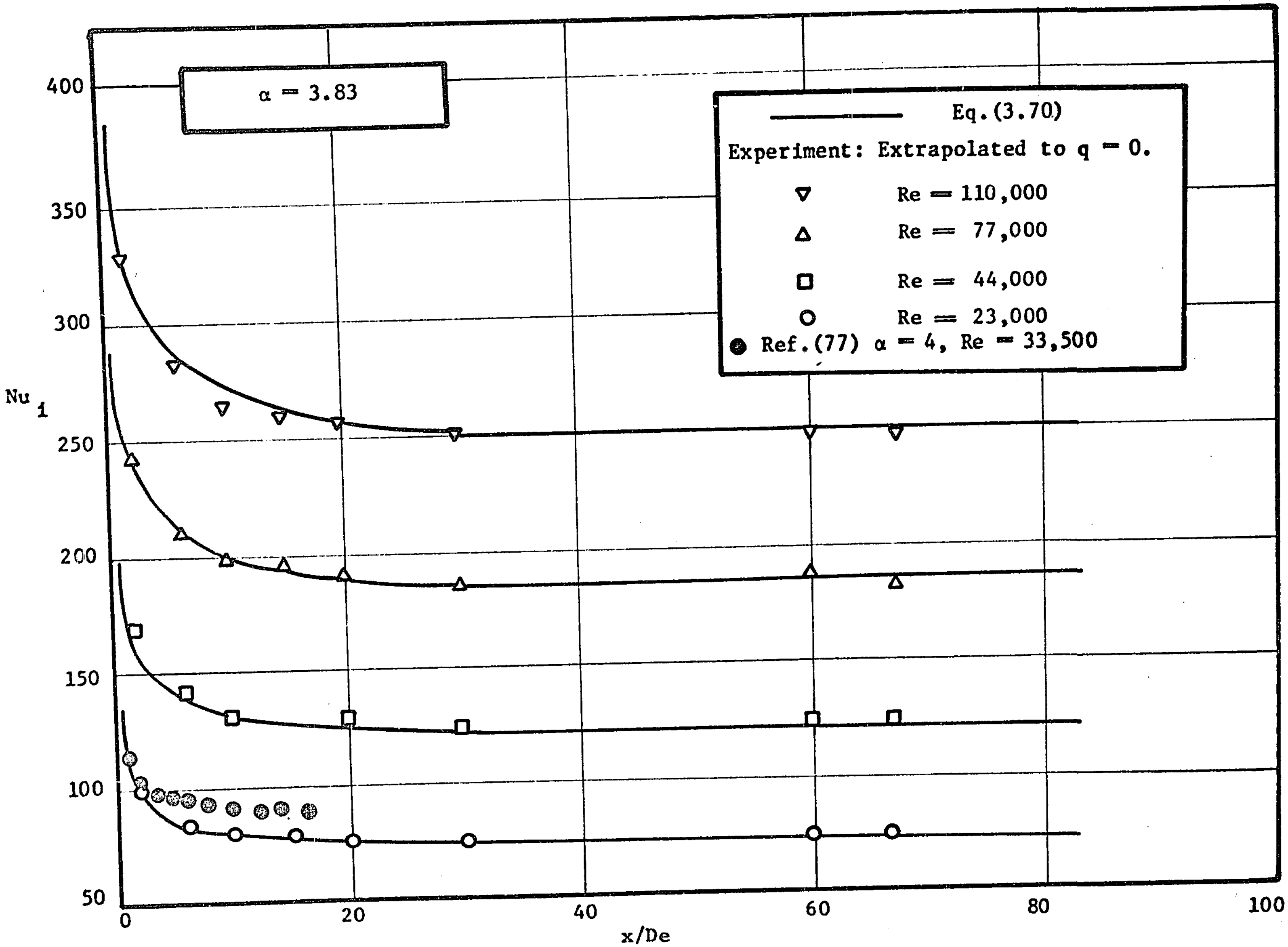

Fig. 5.64 Comparison between Prediction and Experiment, Entrance Region Nusselt Number, Pr = 0.71.

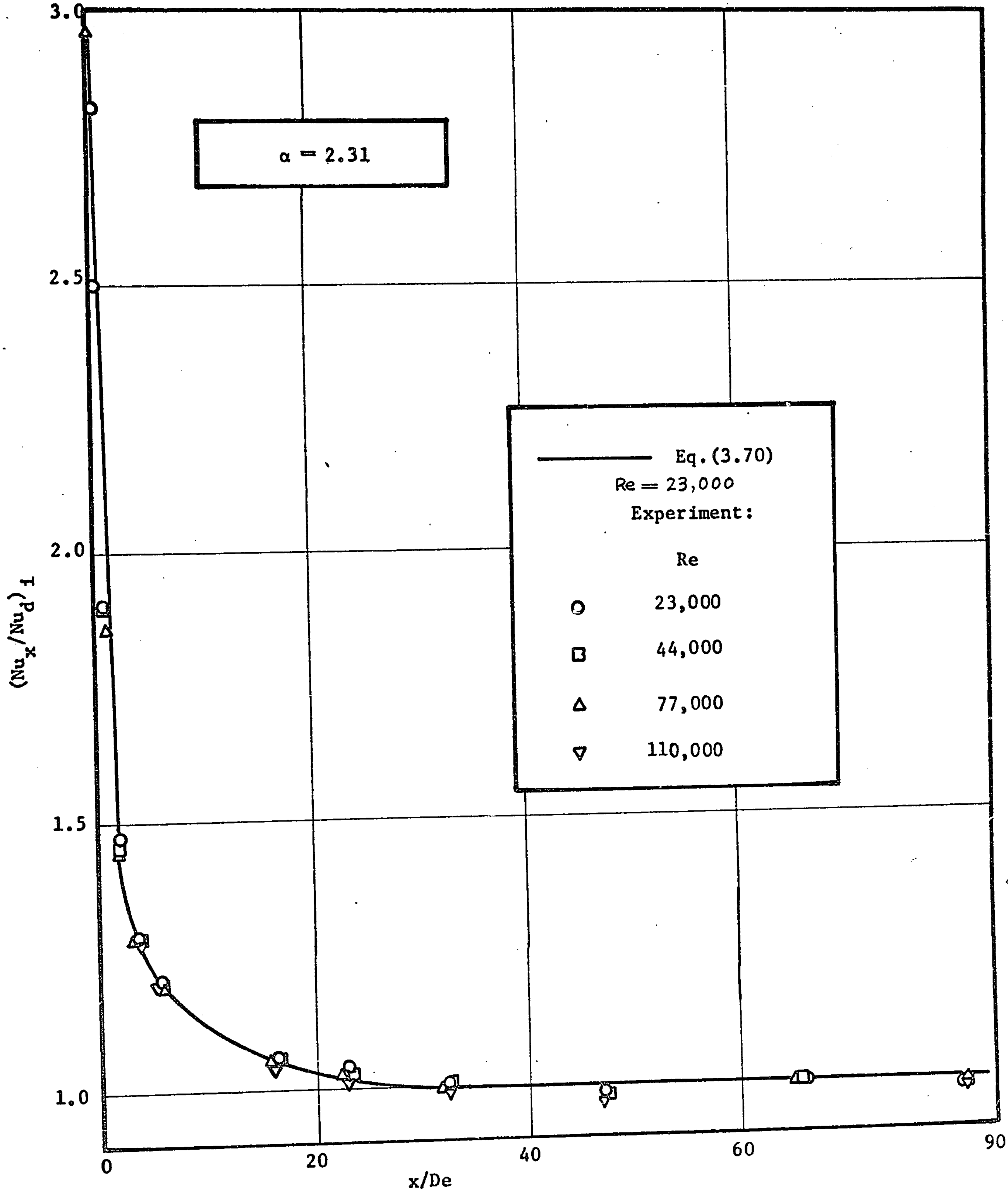

Fig. 5.65 Predicted and Experimental Nusselt Numbers, Entrance Region, Pr = 0.71.

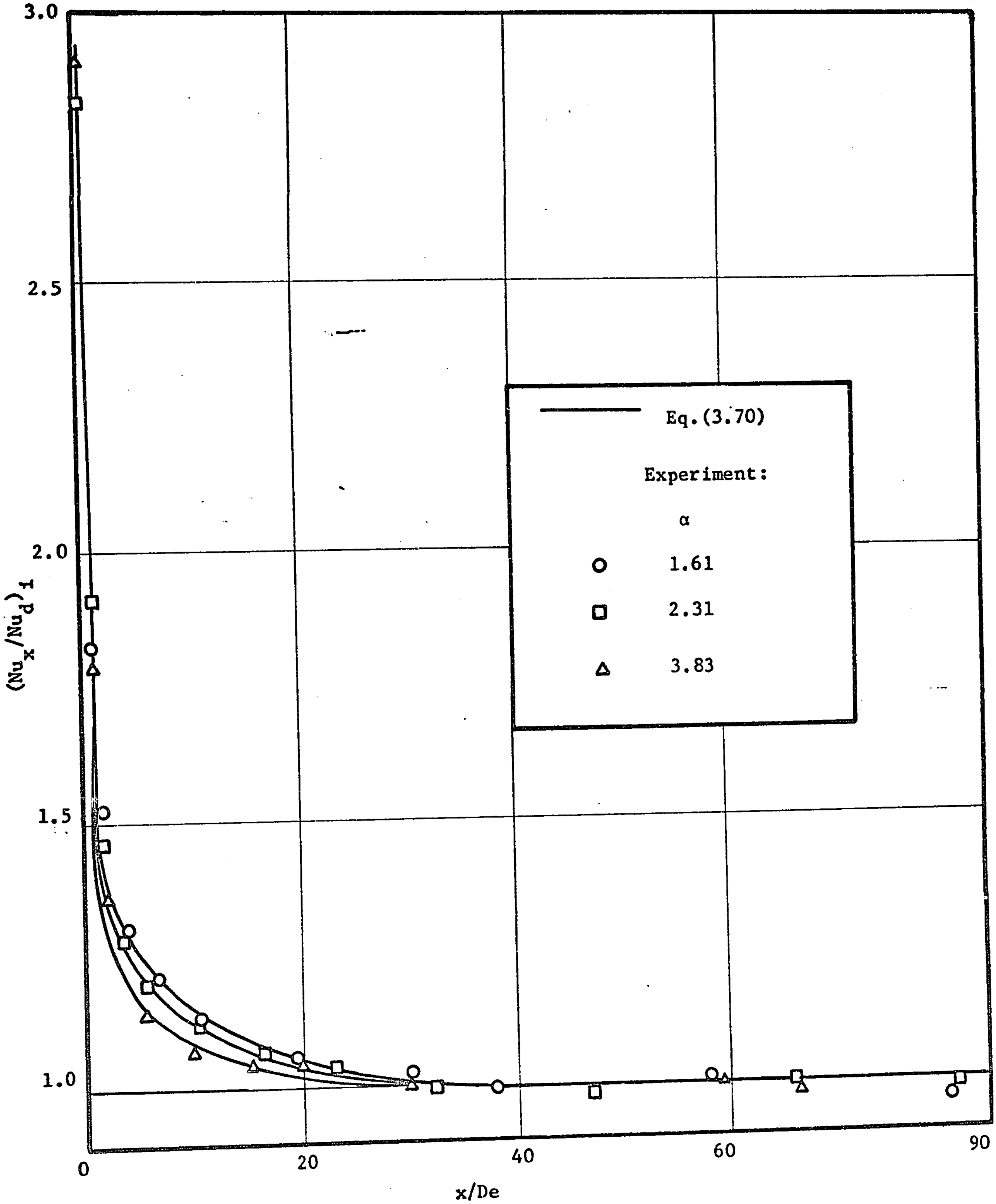

Fig. 5.66 Predicted and Experimental Nusselt Numbers, Entrance Region, Pr = 0.71.

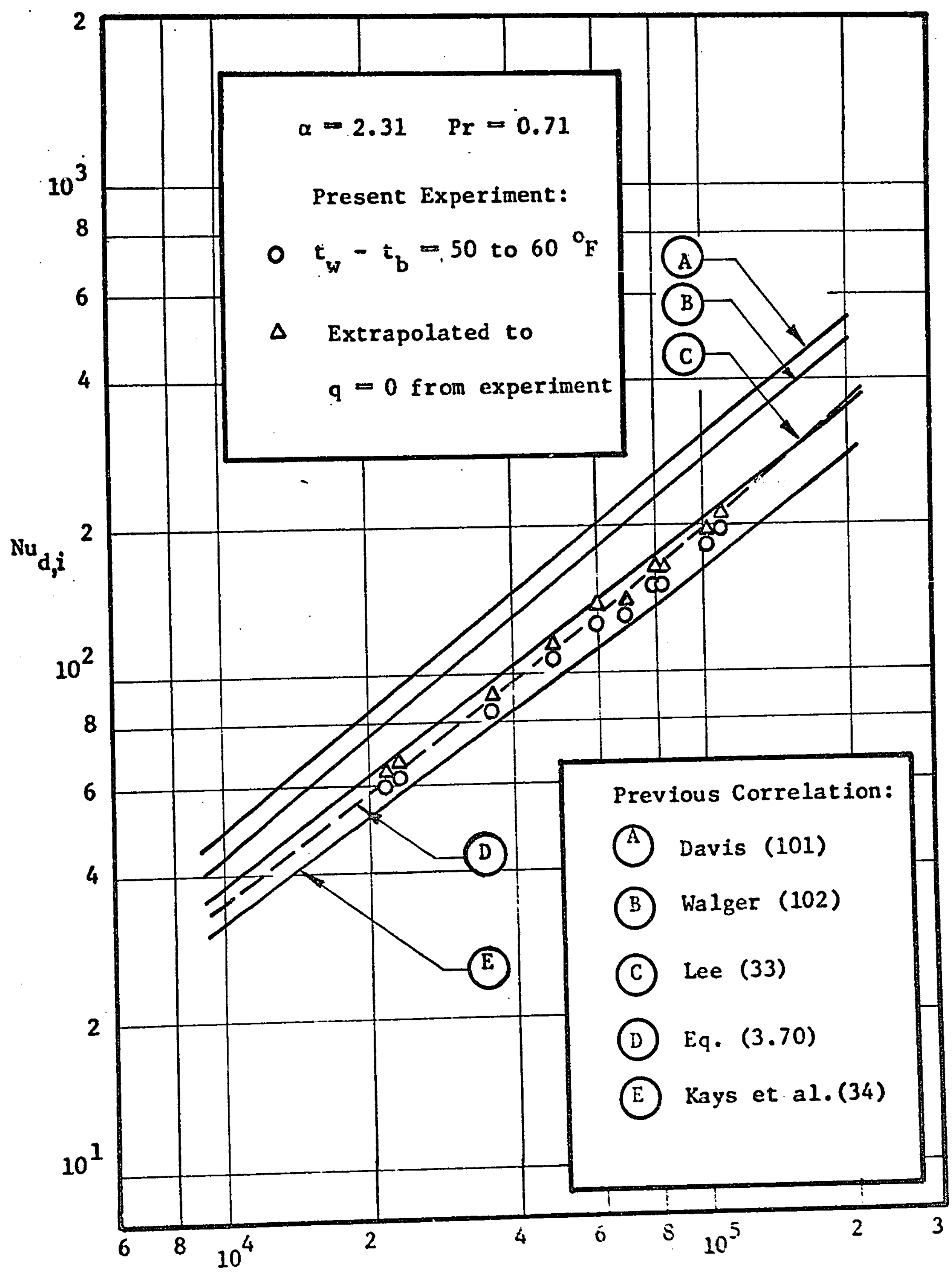

Fig. 5.67 Comparison of Fully Developed Nusselt Numbers with Previous Studies.

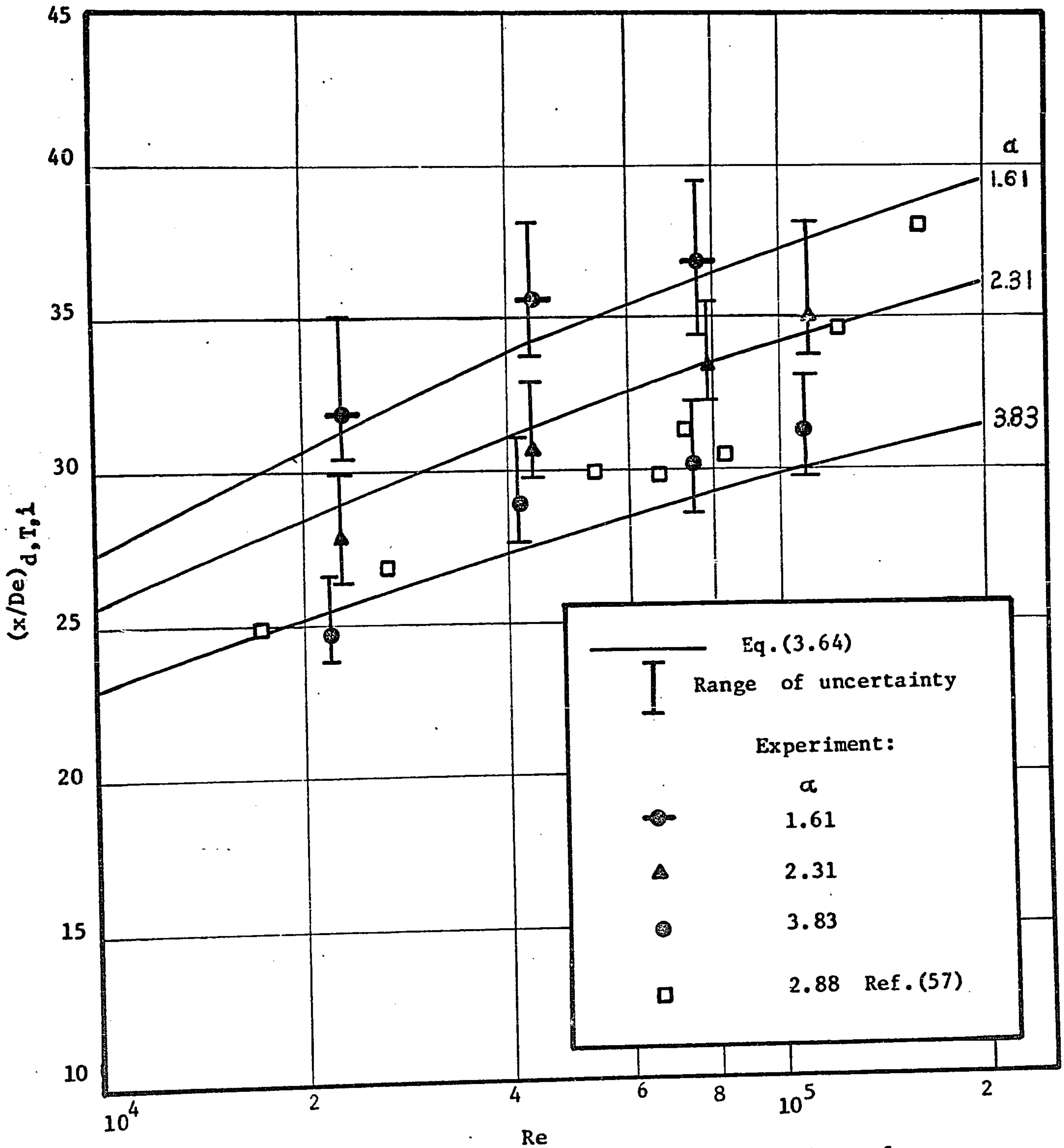

Fig, 5.68 Comparison between Prediction and Experiment for Thermal Entrance Length, Pr = 0.71.

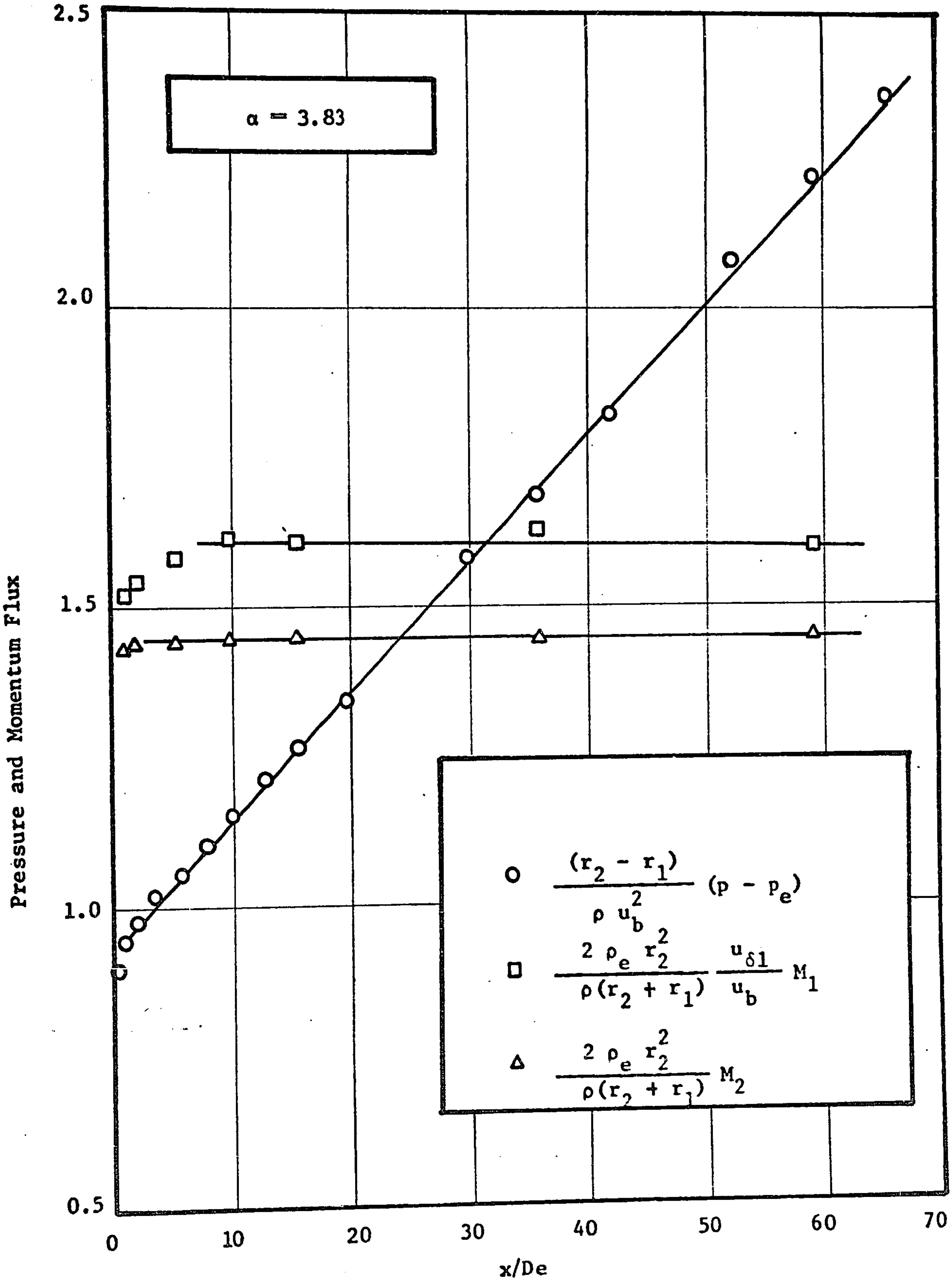

Fig. A.3.1 Variation of Static Pressure and Momentum Flux Parameters along Annulus.

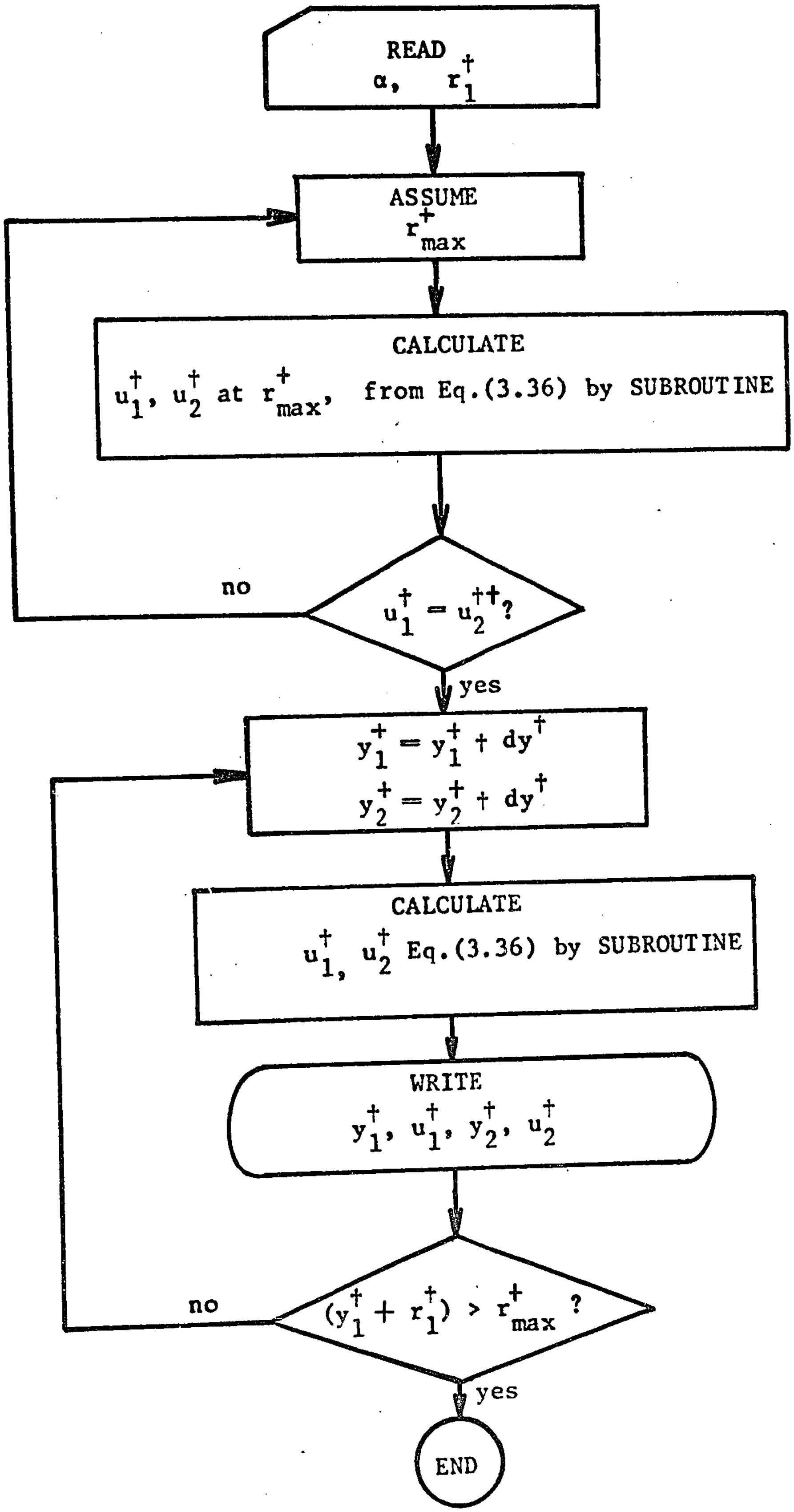

Fig. A.6.1 Simplified Flow Diagram of Velocity Profile Calculation.

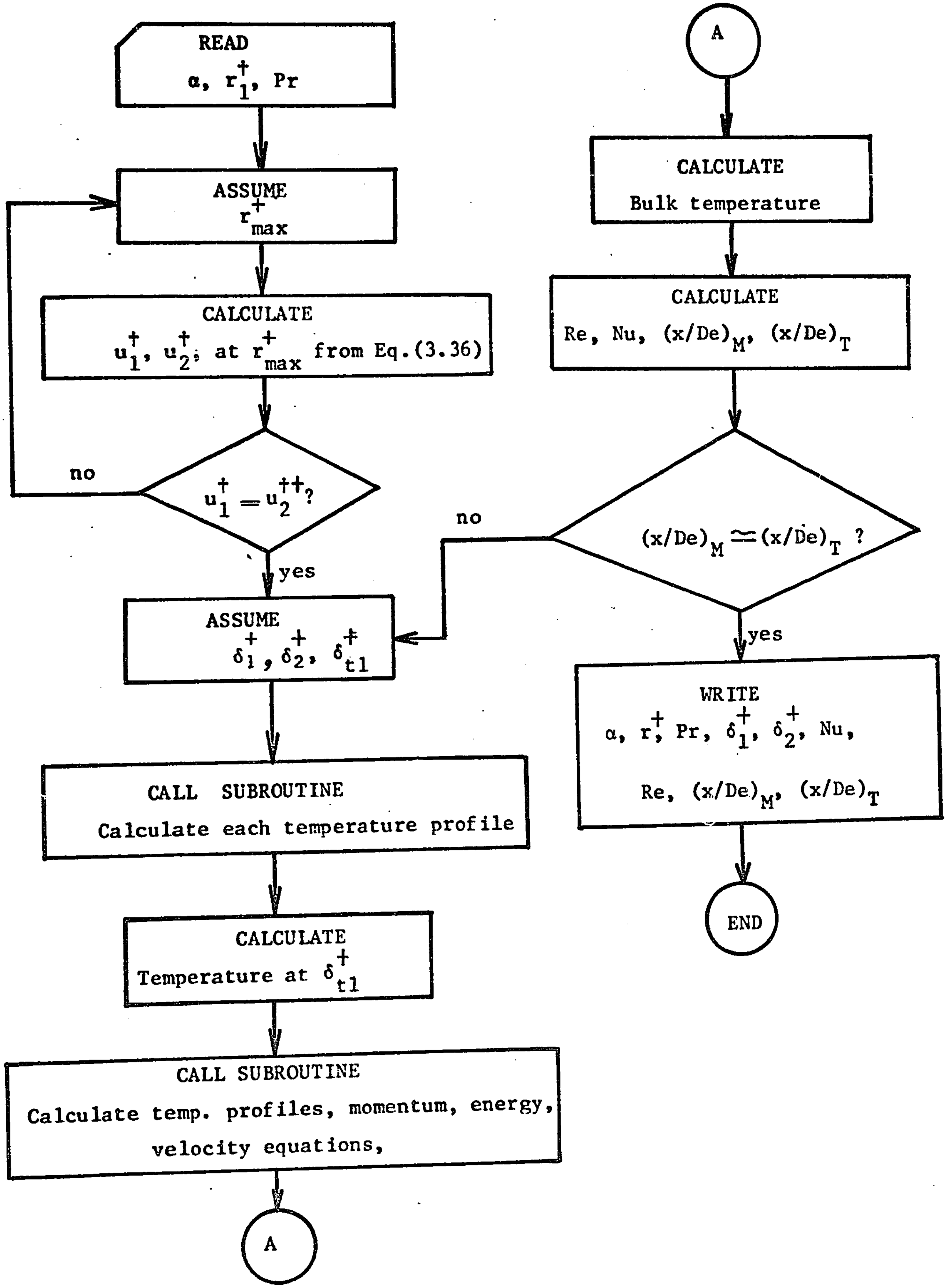

Fig. A.6.2 Simplified Flow Diagram of Nusselt Number and Entrance Length Caculation.

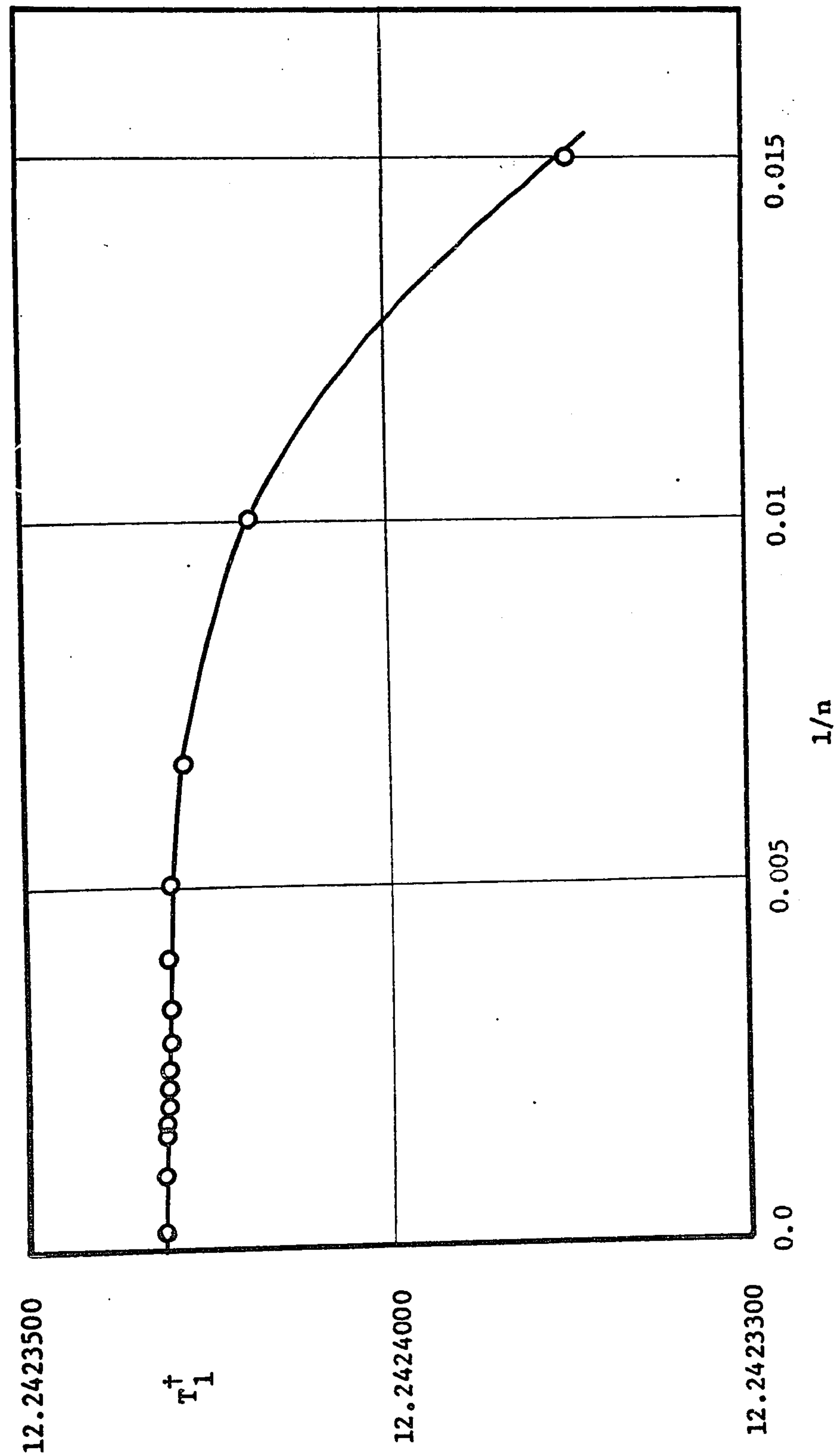

Fig. A.6.3 Accuracy Check of Integral , $\alpha = 2.31$, $r_1^+ = 951$, $y_1^+ = 104.0$.